An Experimental Study on the Infiltration Potential of Stormwater Ponds in Zeekoe Catchment, Cape Town, South Africa

By:

Paul Mavundla

Supervised by:

Prof. Denis Kalumba *PhD*

Co-Supervised by:

Prof. Neil Armitage *Pr Eng, PhD*

&

Dr John Okedi *Pr Eng, PhD*

A dissertation submitted in partial fulfilment of the requirements for a degree of Master of Science (M.Sc.) in Civil Engineering with Specialisation in Geotechnical Engineering

Department of Civil Engineering | University of Cape Town| South Africa

Plagiarism Declaration

1. I know that plagiarism is wrong. Plagiarism is to use another's work and pretend that it is one's own.

2. I have used the Harvard convention for citation and referencing. Each contribution to, and quotation in, this thesis from the work(s) of other people has been attributed and has been cited and referenced.

3. This dissertation is my own work.

4. I have not allowed and will not allow anyone to copy my work with the intention of passing it off as his or her own work.

Signature : Signed by candidate

Date : 25/01/2022

Dedication

Dedicated to my **FAMILY** for their endless love and support in all my undertakings.

Moeta-P, you are my leader.

Acknowledgements

Sincere gratitude to my supervisor, Professor Denis Kalumba for his guidance, motivation, patience, and invaluable contributions to making this work a successful project. I would also like to extend my appreciation to my co-supervisors Dr John Okedi and Professor Neil Armitage for their guidance and for allowing me to represent the Geotech Research Group in collaboration with the Future Water Committee of the University of Cape Town (UCT) for this study.

I acknowledge the constant National Research Foundation (NRF) funding received through the Future Water Committee of UCT as well as the sponsorship received from Zutari Pty (Ltd) towards this MSc degree.

I thank Fairbrother Geotechnical Engineering Pty (Ltd) for supplying borehole log data for this research.

A special thank you to the UCT Civil Engineering staff, particularly Charles Nicholas in the Workshop and Noor Hassen in the Geotechnical Laboratory. I would especially like to extend my thankfulness to my campus mother Ms Avril Courie for always looking out for me and sharing her uplifting knowledge and energy.

I thank all my Geotechnical Engineering colleagues (Mark, Steven, Prospect, Katlego, Charles, Monica, Tracey, Motheo, Lita, Shaina and Sane) for making my postgraduate years at UCT memorable.

A special thank you to my friend Yogendra Pudaruth for assisting with my field testing and sharing insightful moments.

My appreciation to Thambo Mthwalo, Tshegofatso Sehlapelo and Princess Caroline for their contributions towards the conclusion of this report.

Lastly, I would like to thank God for his favour throughout this project and for constantly surrounding me with the right people at the right time.

Glory to the almighty God.

One love.

Kgomoanwato Paul Mavundla

(MVNKGO001)

Abstract

In early 2018, the city of Cape Town, with a population of approximately 3.8 million, was at risk of running out of water from the six large reservoirs to the east of the city. This was due to the worst drought in almost a century, which occurred between 2015 – 2017, causing the city to be declared a disaster area. Although alternative water resources had been identified, they had not been developed. This has now become imperative as droughts are expected to recur in the future. This study investigated the prospect of using existing stormwater ponds in the Zeekoe catchment area as infiltration cells transferring detained stormwater into the underlying aquifer storage zone to enhance the available groundwater resource. The Zeekoe catchment is a 89 km^2 area within the 630 km^2 Cape Flats Aquifer (CFA). Based on hydrogeological data and aquifer parameter interpretation, it is considered to have good storage characteristics that can support groundwater development for water supply. Bouwer (2002) highlights how infiltration tests in the field can be useful for estimating desired volumetric recharge rates within a certain area. The hydraulic conductivity of the unsaturated layer is an essential non-linear function of soil-water content and has been generally recognised as the most important transport property to describe the ability of soil to permit water movement.

A series of in-situ infiltration experiments were conducted at three representative stormwater ponds using a Double Ring Infiltrometer (DRI) to determine the rate of water recharge. Infiltration data was interpreted using both the Green-Ampt and Horton methods to determine the hydraulic conductivity and infiltration decay constants. A total of 18 core samples retrieved from the in-situ infiltration test locations were analysed in the laboratory to determine the material's physical properties and the saturated hydraulic conductivity through constant-head permeability (CHP) tests. The physical and hydraulic soil parameters gathered from field and laboratory tests were used as inputs for a finite element numerical modelling software (HYDRUS 2-D) to estimate the range of recharge rates for the study area.

Based on field infiltration test results, the hydraulic conductivity was found to be 0.3 – 19.9 cm/hr; typical for silty sands to fine sands. Hydraulic conductivities estimated in the laboratory were greater than the field hydraulic conductivity by 103%. This could be attributed to entrapped air under field conditions which reduces the effective cross-sectional area available for water to flow. From the HYDRUS 2-D simulations, the period required for the wetting front movement from the pond surfaces to the water table (~5.5 m below the surface) was 15 – 140 hours. Hydraulic conductivities estimated using the pedotransfer function (PTF) of the built-in software, Rosetta-Lite, were also greater than the field hydraulic conductivity values by 118%. For an actual test pond, the infiltration rates would be expected to be slower, and recharge times would be greater because the HYDRUS 2-D simulations did not consider layers of low permeability within the alluvium or variations in the subsurface geology. Bouwer's (1969) suggestion that the field saturated hydraulic conductivity could be taken as roughly 0.5 times the laboratory hydraulic conductivity was thus considered reasonable. This means that ponds in the central area of the catchment would be suitable for artificial recharge with an estimated infiltration rate of around 20.6 cm/hr which could provide a mean annual groundwater yield of 29 – 33 Mm^3. A more extensive survey would aid in assessing local conditions that may impede groundwater flow.

Table of Contents

List of Figures

List of Tables

Symbols

Λ	Horton's decay coefficient (hr-1)
C_u	Soil coefficient of uniformity
C_c	Soil coefficient of curvature
d	Thickness of the soil layer (mm)
d_1	Depth of water in the surface layer (mm)
d_2	Thickness of the soil layer in the infiltration cell (mm)
d_3	Depth of water in the storage layer (mm)
dh	Change in hydraulic head (m)
dx and dy	Spatial steps in x and y-direction
d_{10}	Soil effective grain size
e	Soil void ratio
f	Infiltration rate at any time t (cm/hr)
F	Cumulative infiltration (cm)
fc	Final infiltration rate (after equilibrium at steady state) at t = t_c (cm/hr)
f_o	initial infiltration rate at t – 0 (cm/hr)
G_s	Soil specific gravity (g/cm^3)
g	Acceleration of gravity (m/s^2)
h	Vertical head difference
H	Hydraulic head of water in the conduit (m)
i	Precipitation rate falling directly on the surface
I_t	Inflow into the storage at current time t (m3)
$K_{T°C}$	Hydraulic conductivity when water temperature is

K	Darcy's hydraulic conductivity (cm/h)
$K(x, y)$	Hydraulic conductivity in 2-dimensions (cm/h)
η	Soil porosity (%)
n	Parameters of the Green & Ampt model determined as the slope
$\eta_{T°C}$	Viscosity of water at $T°C$
ρ_b	Soil bulk density (kg/m^3)
Q	Flow rate (m3/s)
S_c	Capillary suction at the wetting front (cm)
t	Simulation time (s)
T	Total number of time-steps in the simulation period
T_d	Factor of the derivative time (dimensionless)
T_i	Factor of the Integral time (dimensionless)
T_{max}	The mean daily maximum temperature (^{o}C)
T_{mean}	Daily mean temperature (^{o}C)
T_{min}	Mean daily minimum temperature (^{o}C)
t_{years}	Time (years)
V_{cap}	Maximum storage capacity (m^3)
Θ_2	Soil layer moisture content (fraction)

Acronyms and Abbreviations

CoCT	City of Cape Town
CFA	Cape Flat Aquifer
DWA	Department of Water Affairs
DWAF	Department of Water Affairs and Forestry
DWS	Department of Water and Sanitation
MAP	Mean Annual Precipitation (mm)
MAR	Managed Aquifer Recharge
MAR&R	Managed Aquifer Recharge and Recovery
PCSWMM	Personal Computer Storm Water Management Model
PHA	Philippi Horticulture Area
SAWS	South Africa Weather Services
StatsSA	Statistics South Africa
SWH	Stormwater Harvesting
SWMM	Storm Water Management Model
UCT	University of Cape Town
WHO	World Health Organisation
WRC	Water Research Commission
WTP	Water Treatment Plant
WWTW	Waste Water Treatment Plant
UWM	Urban Water Management
USCS	Unified Soil Classification System

1 Introduction

1.1 Background

The urban water cycle has been shifted to an unsustainable position characterized by water scarcity due to urbanization, rapid growth in population, and higher standards of living across most parts of the world (Gleick, 1998; Fletcher et al., 2016). The expansion of urban areas has also led to the replacement of natural landscapes by impervious surfaces. Furthermore, it has led to stormwater runoff being polluted despite the increase in overland runoff volumes and peak flow rates. Conventional drainage systems have intensified this problem by shortening the time of concentration and in turn raising flood peaks. This has consequently resulted in significant damage to downstream aquatic systems and infrastructure (Fletcher et al., 2007; Burns et al., 2012; Armitage et al., 2013). The hidden value of stormwater is increasingly becoming recognised as water security has become threatened since the potential resource had been traditionally viewed as a 'nuisance' by stormwater management stakeholders. This has led to various shortcomings of the conventional drainage systems (Fletcher et al., 2007; McArdle et al., 2011; Burns et al., 2012).

In 2007, Coombes and Barry (2007), Fletcher et.al. (2007) and Mitchel et. al. (2007) found that conventional water supplies needed to be leveraged to deal with increasing concerns around water security. Interest in making use of stormwater as an alternative water resource has grown over the years since it is a relatively abundant local source of water; thereby making it vital to enhance stormwater management's integration with other sectors of urban water management. Certain sustainable drainage system (SuDS) practices, particularly stormwater ponds, are well suited to incorporate the harvesting of stormwater (Mitchell et al., 2007).

Stormwater ponds are usually designed to reduce peak stormwater flows through the provision of temporary storage (Nascimento et al., 1999; Shamsudin et al., 2014). Stormwater ponds have the potential to be used as stormwater storage for water harvesting purposes. One of the key objectives of SuDS practices is to extend stormwater ponds' functionality beyond flood control, which can, inter alia, be achieved by their use as storage basins functioning as infiltration cells to promote groundwater recharge. Figure 1-1 illustrates the concept of groundwater recharge in an urban environment followed by the abstraction of groundwater for various end uses.

According to DWA (2004) and Pitman (2011), South Africa is known as a semi-arid and water-stressed country that relies mostly on surface water from unevenly distributed rainfall - the country's Mean Annual Precipitation (MAP) of 450 mm is about 50% of the world's MAP. Pitman (2011) further found that the streamflow to rivers is quite low with a Mean Annual Runoff (MAR) of 50 000 Mm^3. Unless there is a considerate change in water supply and use patterns, it is projected that by 2030 there could be a 17% deficit between water supply and demand owing to surface water resources being fully developed and utilized (DWA, 2008).

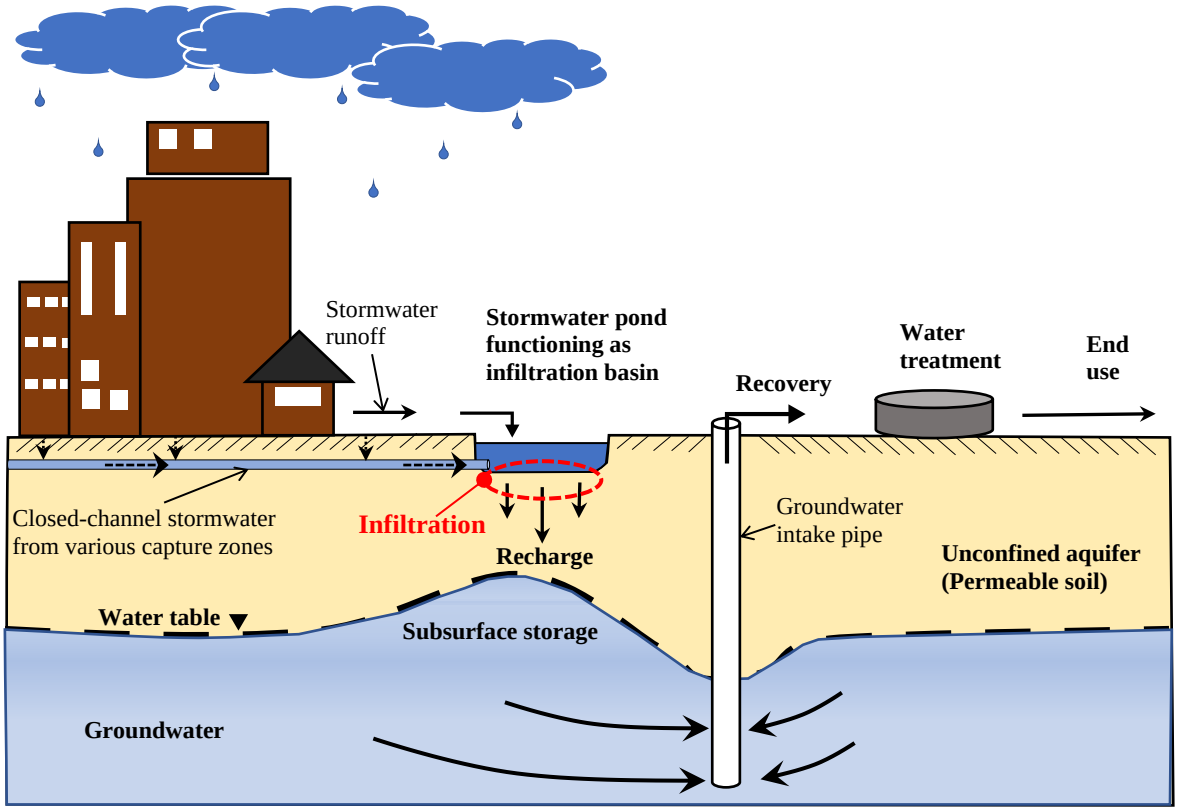

Figure 1-1: Conceptual schematic of how groundwater recharge and abstraction could be adapted with stormwater ponds in an urban area

1.2 Problem Statement and Justification of Study

DWS (2014) predicted that the six large reservoirs supplying the city of Cape Town with water will only be able to meet the water demands up to 2020 and 2023 based on the high annual demand growth of 3.4% and low annual demand of 2.3% respectively. The city has implemented various initiatives to alleviate the effect of limited surface water resources, which include pressure reduction and pipe replacement to minimize leakages, increasing block tariffs, installing water management meters to restrict excessive demand, and providing treated sewage to selected users as an alternative to potable water (Okedi, 2017).

The limitations of surface water resources were exposed by the prolonged drought of 2015 – 2017 as the water supply from the major reservoirs was severely tested, with the possibility of taps drying up by 2018. Alternative water resources such as seawater, wastewater effluent, augmentation of existing surface water systems, and groundwater need to be considered as droughts are expected to recur frequently in the future. Furthermore, population growth and rising living standards will add further pressure to the local water infrastructure.

Bouwer (2002) suggests that the adaptation of managed aquifer recharge (MAR) is one of the most effective methods that can be adapted to increase groundwater resources. The Cape Town

Metropolitan contains both primary and secondary aquifers, with the Cape Flats Aquifer (CFA) having the highest groundwater potential yet the most under-utilized (Wright & Conrad, 1995). Primary aquifers are made up of loose granular material like sand which enables water to move between the pores. Secondary aquifers form due to the development of fractures in hard rock material. The area between the interconnected fractures allows for the storage and flow of water (Mahed, 2018).

The Zeekoe catchment area is a region situated within the CFA. It is considered to have good storage characteristics to support its development for water supply according to hydrogeological data and aquifer parameter interpretation (Adelana et al., 2010).

Constructed ponds can be used for surface infiltration (Asano, 2006; Ferris et al., 1954). One drawback that has been identified with these ponds is possible clogging from fine particle material or bacteria, which can be mitigated by filtering water before infiltration, and periodically drying the pond basins to remove surface layers (Baveye et al., 1998; Bower, 2002; Reddy, 2008).

Studies on prospective sites have commonly been conducted to measure the infiltration rate before determining whether recharge of water through the unsaturated zone for storage in the underlying aquifer would be possible (Fatehnia, 2015; Teague, 2010; Gregory, 2004). Laboratory analysis of core material and other samples of unsaturated deposits overlying aquifers has additionally been used to determine other physical properties of the soil material in unsaturated zones (Izbicki et al., 2000; Bouwer, 2002).

Existing geological, geophysical, and hydrologic maps can provide information about the general geology and hydrogeology of the study area at a large scale (Greef, 1980; Theron, 1992; Wright & Conrad, 1995; Parsons, 2000). While useful, large-scale analyses cannot be used to draw substantive conclusions on the infiltration potential of a proposed recharge site. No physical test data has been found for soils within the existing stormwater ponds in the Zeekoe catchment area. To make an informed decision on the viability of adapting these ponds to function as infiltration cells, a more suitable representative of the hydraulic and physical properties of soil can be determined through field infiltration experiments and laboratory testing of retrieved samples.

1.3 Research Objectives

The focus of this study was therefore to evaluate the infiltration potential through the unsaturated surface deposits of selected existing stormwater ponds in the Zeekoe catchment area. This would indicate the feasibility of adopting these ponds to function as infiltration cells transferring detained stormwater into the underlying aquifer storage zone to enhance the available groundwater resource. To achieve this aim, a series of experiments were formulated through which specific objectives were met. The main objectives of this research were as follows:

- To study the infiltration potential of selected stormwater ponds through field experiments,
- Analysing and comparing physical and hydraulic properties of retrieved surface core samples through laboratory tests,
- Numerically modelling water flow through the unsaturated zone of the investigated stormwater ponds to obtain a better estimate of recharge through the unsaturated zone to the storage zone in the underlying aquifer.
- Providing recommendations for a suitable region within the Zeekoe catchment where existing stormwater ponds could be adapted to function as infiltration basins based on the investigated hydraulic properties.

1.4 Scope of Study

The scope of this research included a series of infiltration experiments conducted at strategically selected representative stormwater ponds within the Zeekoe catchment area following a detailed testing program described in Chapter 4. The infiltration tests were conducted using a standard Double-Ring Infiltrometer (DRI) apparatus. The adapted testing procedure was in accordance with the ASTM D3385-09 standard using the constant head method. This in-situ field testing procedure was chosen due to its relative simplicity and wide use in today's engineering projects (Hayden, 2010).

Soil core samples retrieved from the in-situ infiltration test locations were analysed in the laboratory to determine, inter alia., the saturated hydraulic conductivity through constant-head permeability (CHP) tests. The CHP test was the preferred method over the falling-head permeability (FHP) test due to its suitability to measure the saturated hydraulic conductivity of permeable granular soil in the laboratory (Braja, 2008). Other physical properties including bulk density, volumetric water content, porosity, effective porosity, saturation, effective saturation, residual water content, particle density, and particle-size distribution analysis were determined.

Borehole data was made available for this investigation, solely for research purposes, by two private geotechnical companies (i.e., Fairbrother and Core Geotechnical Consults) to understand the variation in soil conditions at greater depths within the study area.

A comparative study of all research results was also undertaken. This involved comparing the hydraulic conductivity values resulting from the field DRI tests and the laboratory CHP tests to assess apparent trends and correlations between various measured soil properties.

Lastly, surface infiltration data from the field and laboratory investigations of the selected representative ponds was input into HYDRUS-2D (a computer software used to simulate water movement through the thicker unsaturated zone) to firstly replicate and observe the DRI in-situ

test conditions and secondly, on a large-scale level, to estimate the time it would take before the wetting front would reach the water table from the ponds' surfaces.

1.5 Thesis Structure

Following this Introduction chapter, the thesis begins by providing a theoretical review on infiltration from the earth's hydrologic cycle to stormwater as an alternative water resource, infiltration processes using different models, and methods for the measurement of soil's hydraulic properties. An overview of the Zeekoe catchment area is presented in Chapter 3, where the chapter begins by introducing the study area's location and its various land uses before delving into the climate characteristics, geology, and regional hydrogeology of the land. A detail of the field infiltration investigation is laid out in Chapter 4. The analysis of the soil samples obtained during the field investigation as well as the experimental procedures adapted in the laboratory investigations are discussed in Chapter 5. The experimental results are analysed and discussed in Chapter 6 before infiltration simulations and applications are presented in Chapter 7. The research work concludes in Chapter 8 with a summary of the test results and recommendations for applications and future studies.

2 Infiltration Theory and Applications

2.1 Introduction

This chapter presents a summary of the literature which was reviewed and scrutinized to bring insightful knowledge and understanding of previously conducted research related to this study. The review was done to provide the reader with a firm theoretical and practical background of this investigation on the infiltration potential of stormwater ponds in the Zeekoe catchment area.

To provide context to the study, the chapter begins with an overview of the earth's hydrologic cycle. Following this is a definition and description of two main types of stormwater ponds, namely, detention ponds and retention ponds. The chapter then presents the theoretical background behind the movement of water through the unsaturated zone before discussing infiltration and artificial recharge processes. To describe the determination of infiltration potential, the in-situ, laboratory, and computational methods are discussed. The chapter concludes with a summary of previous similar studies which include projects surrounding the potential use of infiltration basins to promote groundwater recharge.

2.2 The Earth's Hydrologic Cycle

2.2.1 Components of the Hydrologic Cycle

Water on the earth occurs in three states (i.e., gaseous state, liquid state, and solid state) within a space called the hydrosphere. The hydrosphere is a region extending approximately 15 km radially from the surface of the earth into the atmosphere, and 1 km down into the lithosphere (earth's crust) (Fetter, 1988). Some examples of the various dynamic aspect of water include the evaporation of water from various water bodies such as ponds and oceans, the formation and movement of clouds, rain and snowfall, overland flow, infiltration, and groundwater flow. These various aspects of water constitute the hydrologic cycle.

The hydrologic cycle, shown schematically in Figure 2-1, is the fundamental focus of hydrology. The major components are depicted in relative units which relate to an annual land precipitation of 100 (Chow *et. al.* 1988). The cycle has no beginning or end as its processes occur continuously. A convenient starting point to describe the cycle is when water evaporates from the land surface and the oceans to become part of the atmosphere. When in the atmosphere, the vapour moves upwards to form clouds which, through condensation, precipitate largely onto the oceans (approximately 80%) and partly onto the land (roughly 20%).

A portion of precipitation that lands on the ground infiltrates the earth's surface, increases the soil's moisture content, and reaches the groundwater table. Some of the infiltrated water is absorbed by plant roots and transferred back into the atmosphere through transpiration.

The schematic in Figure 2-1 is a simplification of a more complicated process that has been in existence since the formation of the earth. Broadly speaking, the hydrological cycle can be broken down into two main components i.e., transport components and storage components, as summarised in Table 2-1.

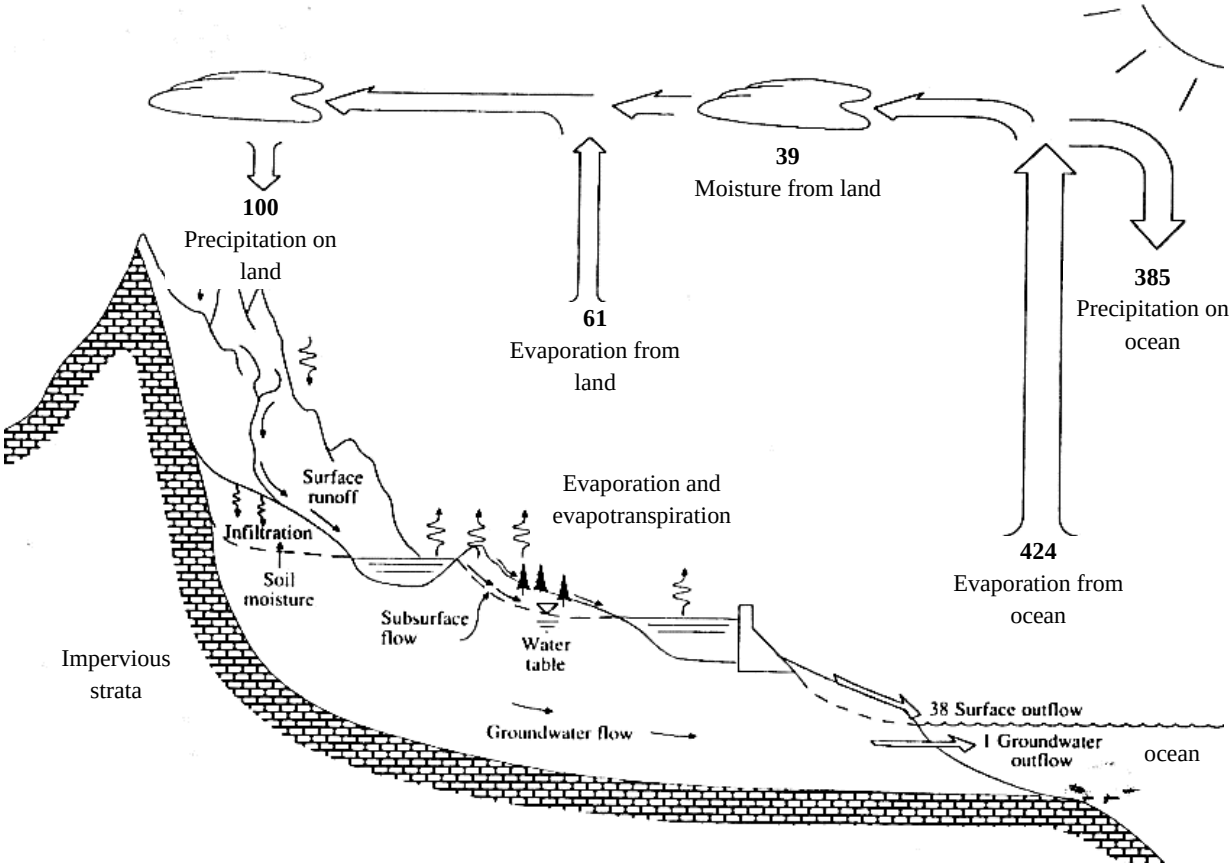

Figure 2-1: The earth's hydrologic cycle including average annual global water balance. Relative units are given as 100 for the annual precipitation
Adapted from: Chow et. al. (1988)

The interdependency of the transport components is represented schematically in Figure 2-2. A continuity principle referred to as 'water budget equation' or 'hydrologic equation' can be used to describe the quantity of water that flows through the various stages of the hydrological cycle. Of the various hydrological cycle components, this study focused primarily on infiltration; a component that was investigated through physical experiments and computational modelling discussed in the following chapters.

Table 2-1: Transport and Storage components of the earth's hydrological process
Adapted from Subramanya (2008)

Transport Components	Storage Components
• Precipitation • Evaporation • Transpiration • Infiltration • Runoff	• Storage on the land surface (Ponds, Reservoirs, Lakes, etc) • Soil moisture storage • Groundwater storage

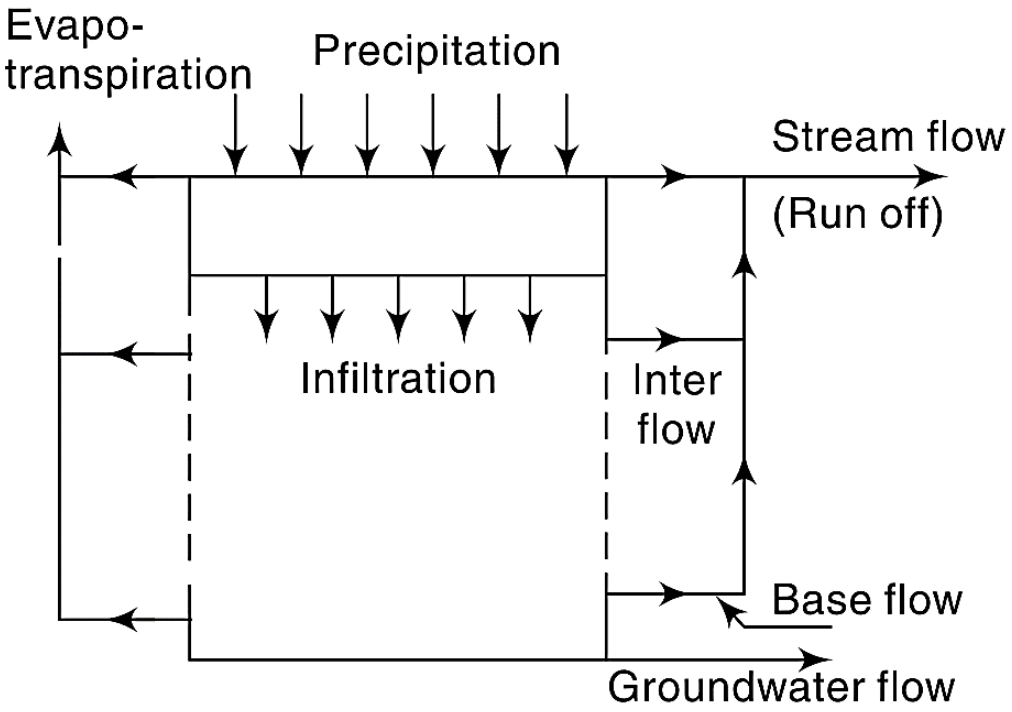

Figure 2-2: Transport components of the earth's hydrologic cycle
Source: Subramanya (2008)

According to UNESCO (1978), the total volume of water on the earth is approximately 1386 million cubic kilometres, of which 96.5% is in the oceans as saline water. Table 2-2 lists and quantifies the estimated distribution of water in its various forms on the earth. It can be noted that despite the substantial volumes of water on earth, only a small percentage of the world's total supply is available to humans as freshwater. Moreover, of the available freshwater, 98% is groundwater which significantly exceeds the volume of surface water.

Table 2-2: Estimated world water quantities
Source: UNESCO (1978)

Item	Area (10^6km^2)	Volume (Mkm^3)	Percentage of Total water	Percentage of Freshwater
1. Oceans	361.3	1 338 000	96.5	
2. Groundwater		-		
(a) Fresh	134.8	10 530	0.76	30.1
(b) Saline	134.8	12 870	0.93	
3. Soil Moisture	82	17	0.0012	0.05
4. Polar ice	16	24 024	1.7	68.6
5. Other ice and snow	0.3	35	0.025	1
6. Lakes		-		
(a) Fresh	1.2	91	0.007	0.26
(b) Saline	0.8	85	0.006	
7. Marshes	2.7	11	0.0008	0.03
8. Rivers	148.8	2	0.0002	0.006
9. Biological water	510	1	0.0001	0.003
10. Atmospheric water	510	13	0.001	0.04
Total (a) All water	510	1 385 985	100	
(b) Fresh water	148.8	35 029	2.5	100

2.2.2 Catchment Areas

A catchment area is a hydrological unit which can be defined as the area of land draining into a common watercourse or stream (Subramanya, 2008). A ridge called a 'divide' separates neighbouring catchment areas (Figure 2-3).

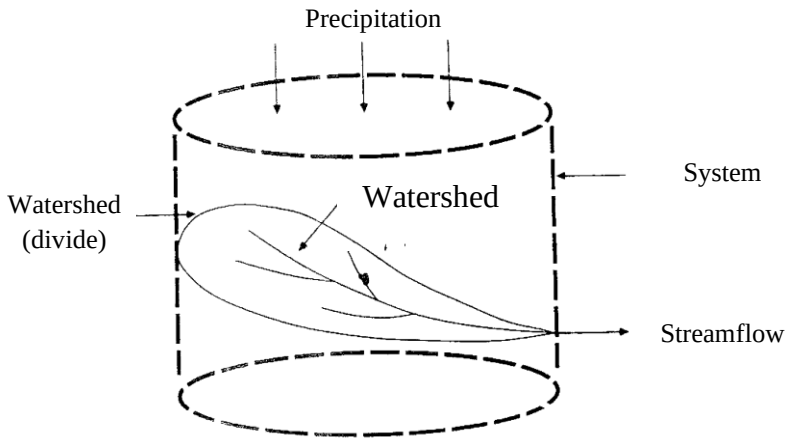

Figure 2-3: Schematic of a catchment area as a Hydrologic System
Source: Chow et. al. (1988)

To obtain an aerial extent of a catchment area, it is necessary to trace the ridge on a topographic map to delineate the catchment and measure the area by either making use of a planimeter or through computer software. A planimeter is a measuring apparatus used to determine the area of any two-dimensional shape. The groundwater divide is normally assumed to coincide with the surface divide. To study various aspects of hydrology and water resources of a region, the catchment area is the most logical and convenient unit of study that can be utilized. Furthermore, the catchment area is the most crucial drainage characteristic used for hydrology analysis and design (Subramanya, 2008).

2.2.3 Events During Precipitation

Some rainfall is intercepted by vegetation before it reaches the ground during a precipitation event, which may later fall to the ground or evaporate. In heavy forests, most of the precipitation is intercepted by leaves and twigs. During summer thunderstorms, the raindrops do not reach the forest floor, instead, the water will run down tree trunks and drip down once the storage capacity of the leaf surfaces is exhausted (Dunne & Leopold, 1978).

Rainfall can infiltrate pervious soil, which has finite and variable absorption capacity. The infiltration capacity varies depending on the soil conditions, material density and granularity. Moisture in the soil is drawn through capillary passages from the surface effects between soil particles and the tension exerted by water. The infiltration capacity drops as the capillary forces diminish with increased soil moisture content (Figure 2-4 (a)). As the moisture content increases, the colloidal particles in the soil swell leading to the infiltration capacity reaching almost a constant or equilibrium value. The infiltration curve can be described by Equation 5.1 (Horton 1933, 1940):

$$(f_p - f_c) = (f_0 - f_c)^{e^{-\lambda t}} \qquad 2.1$$

where

f_p is the infiltration capacity (m/s) at time t (s)

f_c is the equilibrium infiltration capacity (m/s)

f_0 is the initial infiltration capacity (m/s)

λ is a constant representing the rate of decreased infiltration capacity (l/s)

t is the time since the start of the infiltration (s)

All precipitation reaching the land surface will infiltrate if the precipitation rate is lower than the equilibrium infiltration capacity (Figure 2-4 (b)) whereas some water will remain on the land surface if the precipitation rate is greater (Figure 2-4 (c)). If the precipitation rate is greater

than the equilibrium infiltration capacity but less than the initial infiltration capacity, the precipitation will initially infiltrate until the infiltration drops below the precipitation rate when some of the precipitation will remain on the ground surface (Figure 2.8 (d)).

High infiltration is encouraged by coarse soils, well-vegetated land, low soil moisture, porous topsoil layer, and land-use practices that avoid soil compaction. Infiltrated water may move horizontally in the unsaturated zone if the underlying soil layer has a lower hydraulic conductivity as shown in Figure 2-5. The total runoff of some drainage basins may be significantly influenced by this interflow (Horton 1933, 1940).

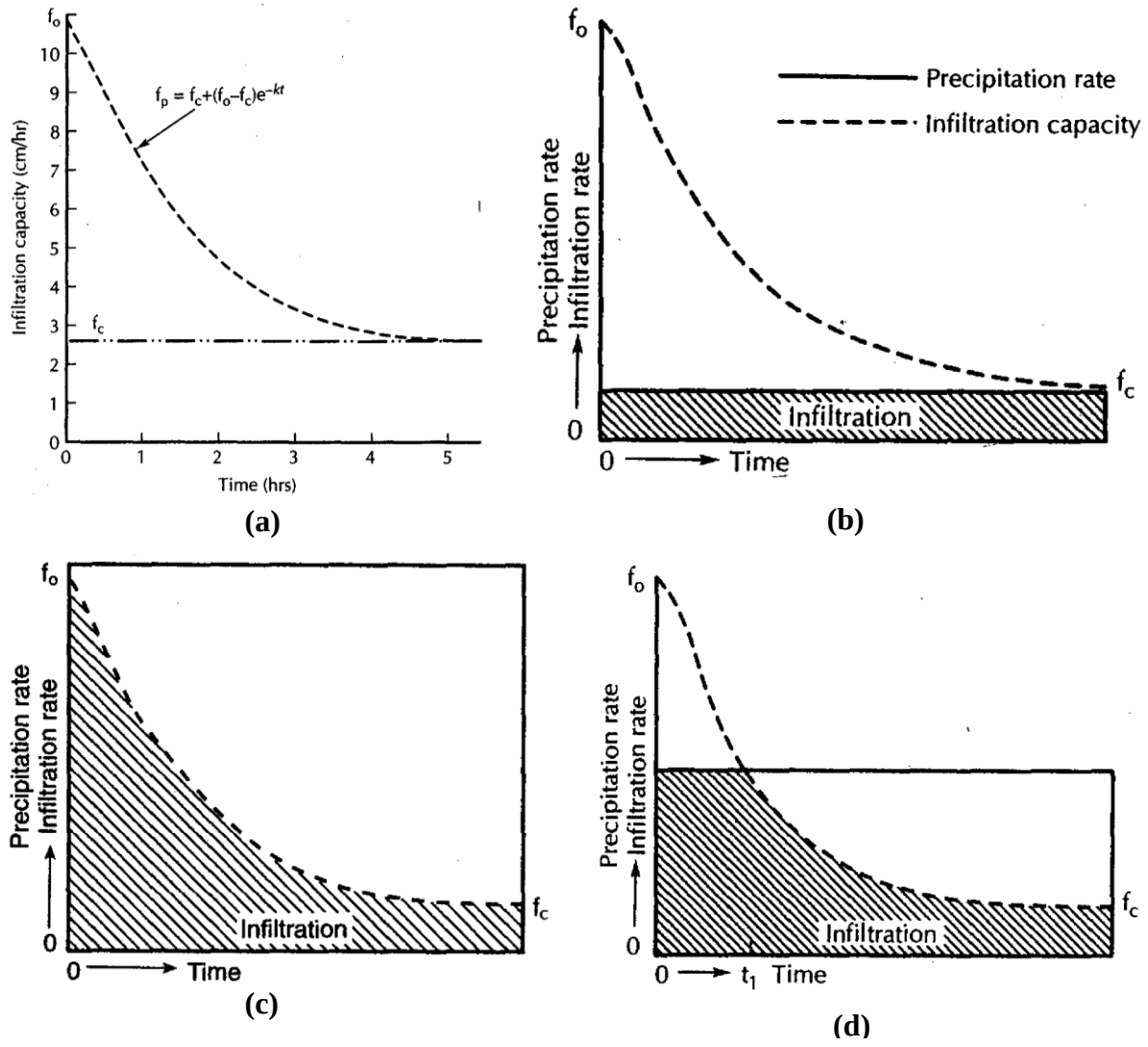

Figure 2-4:Relationships of infiltration capacity and precipitation (a) Decreasing infiltration capacity as soil-water content of soil increases (b) Precipitation rate less than equilibrium infiltration capacity (c) Precipitation rate greater than initial infiltration (d) Precipitation rate greater than equilibrium infiltration capacity but less than the initial infiltration capacity
Adapted from: Fetter (1988)

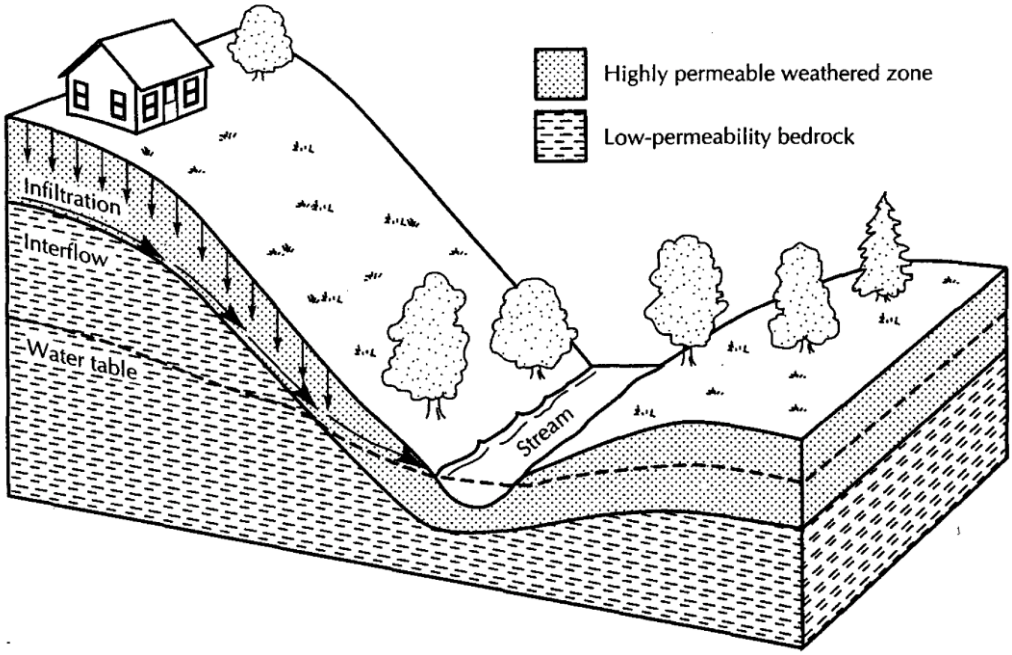

Figure 2-5: Development of interflow where a thin and highly permeable layer of weathered rock overlies a bedrock of lower permeability
Source: Fetter (1988)

2.3 The Threat of Water Scarcity

Water is a crucial need for human health and the successful functioning of ecology, economies, and communities (Gleck.1998, Rockstrom et al., 2014). According to Oki and Kanae (2006), freshwater may be in abundance, however, readily available freshwater only accounts for 1% of the total volume of water present on Earth's surface. The water scarcity issue is further escalated by the continued increase in population and higher standards of living, thereby decreasing the already limited water supply (Gleick, 1998; Walsh et al., 2012).

Water scarcity is a concern for the world at large, however, the issue is quite prevalent in the South African climate. (DWAF, 2004; Noemdoe et al., 2006). South Africa is situated in a semi-arid climate and is ranked as the 30th driest country in the world with an estimated annual rainfall of 450 mm, which is below the world's average annual rainfall of 860mm (Hedden & Ciliers, 2014).

According to Muller et al (2009), South Africa's potable water demand will surpass the available water sources by 2025 as per the analysis on the current water demand. This has been evidenced by the 2015 drought which left five provinces declared as 'drought disaster areas', whilst the other areas had to implement severe water restrictions (Hawker, 2015; Ngoepe, 2015; Singh, 2015). To ensure water security, Muller et al. (2009) and Armitage et al. (2014) suggest that existing water systems require more effective management than at present.

2.4 Stormwater as an Alternative Water Resource

Urban stormwater has historically been managed by promptly collecting and conveying runoff from a storm event away from locations of rainfall incidences to mitigate flooding. Cities have been identified by Wong (2007), Brown et al. (2008), and Dotto et al. (2014) as potential catchment areas, which when well-managed, may yield valuable water resources which can substantially meet water demands in urban areas.

In South Africa, stormwater management infrastructure has been mainly utilized for flood control with limited application for other purposes. The recent Cape Town drought that commenced in 2015 encouraged the city needs to seek alternative sources such as stormwater rather than solely relying on conventional surface water schemes (Fisher-Jeffes et al., 2017).

The stormwater systems which can be used as storage include closed underground tanks (typically used for rainwater harvesting) or open stormwater ponds (used to collect & store rainwater from roof and paving) (Hatt et al., 2006; Begum et al., 2008; Armitage et al., 2013).

2.5 A Description of Stormwater Ponds

Stormwater ponds are man-made basins constructed with the primary purpose of attenuating peak storm discharges and high volumes of surface water runoff generated from urban areas by providing temporary storage (Nascimento *et a*l., 1999; Shamsudin *et al*., 2014). This periodic function, however, often leaves them underutilized. For this reason, the introduction of stormwater ponds as multifunctional devices could provide a solution to the storage concerns faced by stormwater harvesting developers (Rezende *et al*., 2011). In areas with pervious soils, deliberate recharge of aquifers from stored stormwater can potentially enhance groundwater augmentation through infiltration to increase groundwater as a resource (Okedi, 2019).

Because this research focused on the infiltration potential of existing stormwater ponds, knowledge of the study area's subsoil conditions would need to be attained before considering their functioning as suitable multifunctional devices serving the key functions of attenuating stormwater and promoting groundwater recharge. This principle aligns with that of Managed Aquifer Recharge (MAR); a strategy that provides a storage option for areas that experience high evaporation rates, have limited space, and possess a suitable aquifer (Philip et al., 2008). By extending retention times in ponds, not only can infiltration be promoted, but stored water may additionally be treated through natural filtration and removal of pathogens (Dillon et al., 2009; Fisher-Jeffes, 2015).

There are two main types of stormwater ponds, namely: detention ponds and retention ponds. Despite their different characteristics, each type serves the key objective of managing stormwater runoff in different environments.

2.5.1 Detention Ponds

A detention pond is a dry basin that temporarily stores stormwater (Figure 2-6). Depending on the design, detention ponds reduce peak stormwater flows by capturing and detaining runoff for a maximum time of 72 hours (Clare et al., 2004). The captured runoff is simultaneously released at a controlled flow rate, leaving them usually empty unless immediately after a storm event. Table 2-3 lists several significant advantages and disadvantages of these ponds.

Table 2-3: Advantages and disadvantages of detention ponds
Adapted from: (Armitage et al., 2015):

Advantages	Disadvantages
• Able to handle a wide range of storm events by providing temporary storage and attenuating downstream flow rates. • Simple and relatively cheap to design. • Easy to maintain. • Potential for multiple functions.	• Water treatment benefits are minimal. • Minimal ability to reduce flood volumes. • During storm events, settled sediments become resuspended. • Require large surface areas, thus not suitable for high-density residential areas.

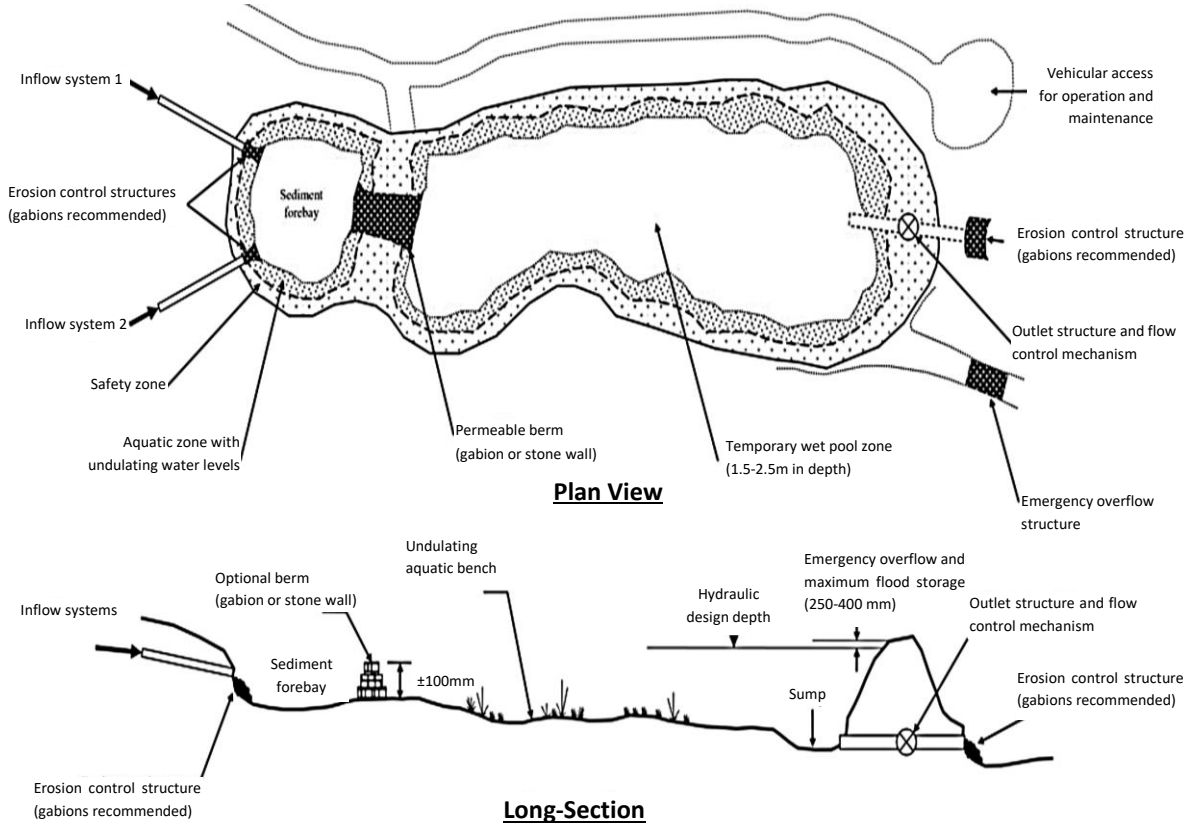

Figure 2-6: General schematic of a detention pond
Adapted from: (Armitage et al., 2013)

2.5.2 Retention Ponds

Retention ponds are stormwater attenuation devices that include a permanent volume of water within their total storage capacity. The permanent volume of water serves to provide water treatment benefits, whilst the remaining storage volume is designed to manage stormwater flows during a variety of storm events (Woods-Ballard *et al.*, 2007; Hancock *et al.*, 2010). Table 2-4 summarises some key advantages and disadvantages of retention ponds whilst Figure 2-7 illustrates a general design of these types of ponds.

Table 2-4: Advantages and disadvantages of retention ponds
Adapted from: (Woods-Ballard et al., 2007):

Advantages	Disadvantages
• Ability to accommodate a variety of storm events and reduce peak flows. • Provision of water treatment benefits and removal of pollutants. • Enhancement of aesthetic and ecological value to local areas and communities.	• Unable to remove pathogens and fine particles from stormwater. • Pose as a potential health hazard such as drowning. • If the permanent water body is not aerated, it poses a risk for anaerobic conditions, water stagnation, and mosquito breeding.

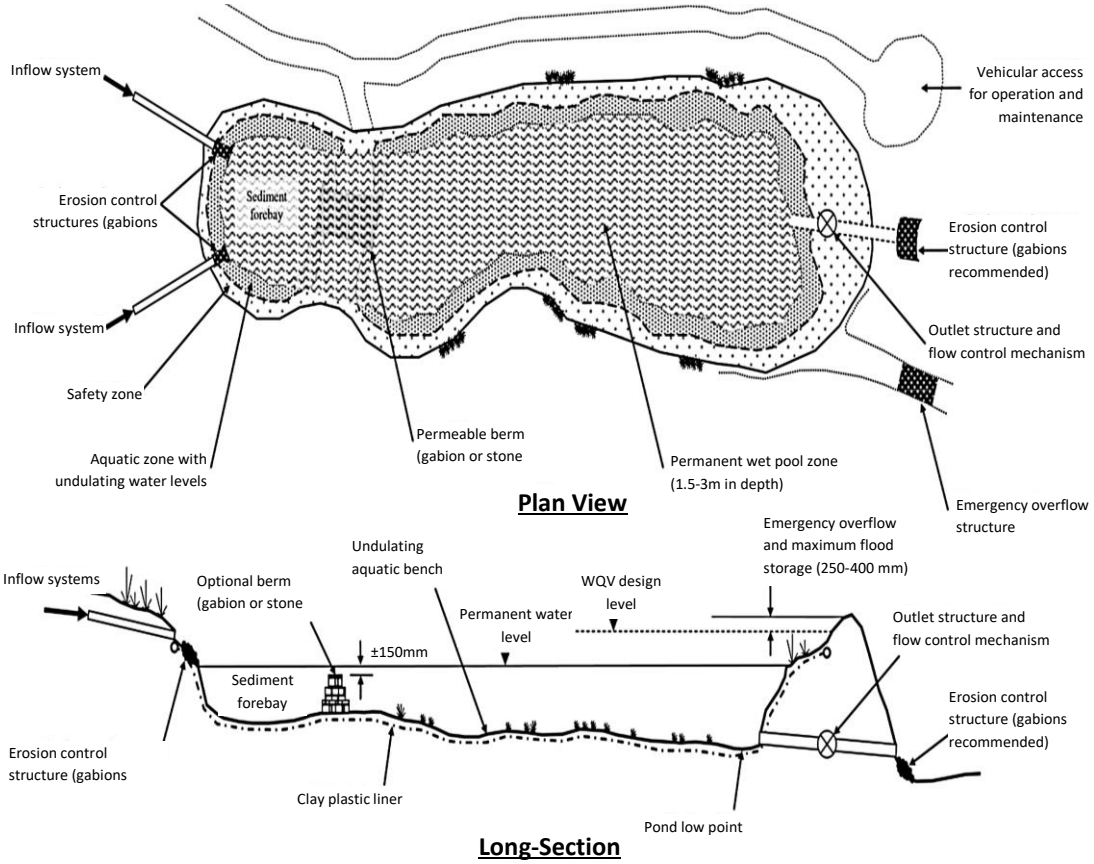

Figure 2-7: General schematic of a retention pond
Adapted from: (Armitage et al., 2013)

2.6 Different Models of Water Infiltration into Soil

The infiltration process is governed by two primary forces, namely gravity, and capillary action, and is the component of the general mass balance hydrologic budget. Extremely small pores pull water through capillary action in addition to and against the force of gravity, even though small pores also offer great resistance to gravity.

The infiltration rate is described as the velocity or speed at which water enters the soil and is measured by the depth of the water layer that can enter the soil in a unit of time.

Several models are used to estimate the volume and/ or rate of infiltration of water into the soil. These models are categorized as summarised in Table 2-5 and briefly discussed in this section.

Table 2-5: Summary of soil-water infiltration models

Model Description	Equation	Year
Steady Flow in Saturated Soils	Poiseuille Equation	1842
	Darcy Equation	1856
Steady Flow in Unsaturated Soils	Buckingham-Darcy Equation	1907
Transient Flow in Unsaturated Soils	Green-Amp Equations	1911
	Richards Equation	1931
	Phillips Model	1957
	Kostiakov Model	1932
	Horton Model	1940
	Holtan Model	1961

2.6.1 Steady Flow in Saturated Soils

Two prevalent models which describe steady flow in saturated conditions were developed by Poiseuille (1842) and Darcy (1856).

2.6.1.1 Poiseuille Equation

The formula was developed by Poiseuille in 1842 to describe the blood flow in arteries, which applies to steady flow at the pore scale. The volumetric flow rate (Q) [L^3T^{-1}] approximated as a water-filled cylinder at a microscopic scale of an individual pore, can be measured using Equation 4.1 as follows:

$$Q = \frac{\pi R^4 \rho_W g \Delta H}{8 \eta L} \quad 2.2$$

where ρ_W is the water density [ML^{-3}], η is the coefficient of liquid viscosity [$ML^{-1}T^{-1}$], L is the distance between two points along the cylinder [L], g is the gravitational acceleration [LT^{-2}] and ΔH is the head difference [L].

2.6.1.2 Darcy Equation

The Darcy (1856) equation can be used to measure steady flow in saturated soils at a macroscopic scale. Darcy found that the volumetric flow rate (Q) [L^3T^{-1}] per unit cross-sectional area (A) through a sand filter of a given thickness (L) [L] was proportional to the soil water potential head gradient across the sand ($\Delta H/L$). The proportionality constant was called the saturated hydraulic conductivity K_s [LT^{-1}]. Darcy's Law is described by Equation 2.3:

$$i(t) = \frac{Q}{A} = -K_s \frac{\Delta H}{L} \quad 2.3$$

where $i(t)$ [LT^{-1}] represents the *water flux* which is defined as the volumetric flow rate of water per unit cross-sectional area.

2.6.2 Steady Flow in Unsaturated Soils

The Buckingham-Darcy model is the only model that describes the steady flow in unsaturated soils. Other unsaturated soil models relate rather to transient flow and are discussed in section 2.6.3.

2.6.2.1 Buckingham-Darcy Equation

Larger pores drain more readily than smaller ones in unsaturated zones. In unsaturated conditions, the hydraulic conductivity is much less as the water moves through smaller pores or as films along the walls of large pores. The unsaturated hydraulic conductivity is measured as a function of negative pressure head [$K(h)$)] or as a function of water content [$K(\theta)$)]. Buckingham modified Darcy's equation expressed in Equation 2.4:

$$i(t) = \frac{Q}{A} = -K(h)\frac{\partial H}{\partial z} = -K(h)\left(\frac{\partial H}{\partial z} + 1\right) \quad 2.4$$

where the sums of the pressure and gravitational heads equate to the total head, $H = h + z$.

2.6.3 Transient Flow in Unsaturated Soil

2.6.3.1 Green-Amp Equations

The simplified mechanistic equation was developed by Green and Amp in 1911 for infiltration by assuming that the wetting front in soil was a square wave or sharp front. If the amount of water behind the predicted square front is equal to the amount of new water behind the true wetting front, the infiltration rate can be predicted although this is only true in coarse-textured soils. With the inclusion of gravity effects, the Green-Ampt formula for cumulative infiltration in a uniform soil (Equation 2.5) is as follows:

$$I(t) = -K(h_0)t + \Delta h \Delta\theta \; ln\left(1 + \frac{I(t)}{\Delta h \Delta\theta}\right) \qquad 2.5$$

where $\Delta\theta = \theta_0 - \theta_i$ and $\Delta h = h_0 - h_f$. The initial water content is expressed as θ_i and the water content at the surface extending to the wetting front is denoted by θ_0. The pressure head at the water content θ_0 is expressed as h_0 whilst h_f is symbolizes the pressure head at the wetting front.

2.6.3.2 Richards Equation

The Richards equation was developed by Richards in 1931. The conservation equation considers the representative elementary volume to develop the non-steady vertical water flow. The water fluxes into this volume during a small-time interval, Δt, must be equal to the water flux out of the volume, plus the change in water stored within the volume and any sources or sinks. The resultant conservation equation is referred to as the *mass conservation equation* or the *continuity equation* shown in Equation 2.6 as follows:

$$\frac{\partial\theta}{\partial t} = \frac{-\partial J_w}{\partial z} - S(h) \qquad 2.6$$

where J_w denotes the volumetric flux density, θ, is the volumetric water content [L^3L^{-3}], $S(h)$ is a sink function [$L^3L^{-3}T^{-1}$] (a negative $S(h)$ represents a source), and t is time [T].

To produce the governing equation for variably saturated water flow, the conversational equation must be combined with one or several equations describing volumetric flux density, J_w. By substituting the Buckingham-Darcy equation for J_w in the continuity equation (Equation 2.6), the Richards equation can be obtained (Equation 2.7).

$$\frac{\partial \theta(h)}{\partial t} = \frac{\partial}{\partial z}\left(K(h)\frac{\partial h}{\partial z}\right) + \frac{\partial K(h)}{\partial z} - S(h) \quad 2.7$$

In the Richards equation, capillary and water movement are accounted for by the first term on the right-hand side of the equation while effects of gravity and water movement are represented by the second term.

2.6.3.3 Phillips Model

The Phillip equation makes use of mathematical approximation for infiltration processes in a soil matrix. The Philip model has two forms, namely, horizontal and vertical infiltration.

Philip modified the Richards equation and expressed the infiltration rate as per Equation 2.8 for the horizontal infiltration rate:

$$i(t) = \frac{1}{2}St^{-0.5} \quad 2.8$$

where S is a function of θ_0 and θ_i which are boundary and initial moisture content, respectively. S is soil-water sorptivity [$LT^{-0.5}$]

For the vertical infiltration, the equation consists of two parts i.e., one for a short duration and the other for a long time after infiltration has commenced. The solution describes the time dependence of cumulative infiltration using an infinite power series which can be estimated by two-parameter models as per Equation 2.9:

$$I(t) = St^{0.5} + At \quad 2.9$$

whereby differentiating this equation with respect to time results in a solution for the infiltration rate (Equation 2.10). A is a constant representing the soil-water transmissivity [LT^{-1}] which approaches the saturated hydraulic conductivity K_s of the soil material's profile as the time approaches infinity i.e., $t \to \infty$.

$$i(t) = \frac{1}{2}St^{-0.5} + A \quad 2.10$$

2.6.3.4 Kostiakov Model

The equations were developed by Kostiakov in 1932 to explain horizontal cumulative infiltration (I) an infiltration rate (i) as expressed in Equations 2.11:

$$I = Bt^{-n}$$
$$i = B't^{-n-1} \quad (2.11)$$

where the parameters n, B and B' are constants without any physical meaning. By fitting Equations 2.11 to data obtained from experiments, the values of these constants can be determined. From the cumulative infiltration equation, it can be deduced that as t approaches 0, I approaches ∞. Contrastingly, as t approaches ∞, I approaches 0.

To account for vertical infiltration, Kostiakov (1932) limited the applicable time range by proposing a maximum time $t_{max} = (B/K_s)^{1/n}$. Additionally, another coefficient, i_c, was included by Mezencev (1948) which effectively moves the axis of the infiltration rate equations. The modified formulas are expressed in Equations 2.12 where it can be inferred that a finite steady-state rate of infiltration is approached as $t \to \infty$.

$$I = i_c t + Bt^{-n}$$
$$i = i_c + B't^{-n-1} \quad (2.12)$$

2.6.3.5 Horton Model

Horton (1940) equations for cumulative infiltration (I) and infiltration rate (i) are as per Equations 2.13:

$$I = i_c t + \frac{i_0 - i_c}{k}[1 - e^{-kt}]$$
$$i = i_c t + (i_0 - i_c)e^{-kt} \quad (2.13)$$

where i_0 represents the initial infiltration rate (i.e., when $t = 0$), and i_c steady-state infiltration rate. The rate at which i_c is approached by i_0 is determined by the constant k. The three constants in the equation need to be evaluated through experiments, which makes the results more reliable however cumbersome to evaluate. The decrease in infiltration rate with time can be described by several factors, such as the closure of solid pores by a swelling soil or erosional deposit, compaction due to raindrop impact, etc. (Horton, 1940).

2.6.3.6 Holtan Model

The Holtan equation for infiltration rate in soil matrix is again a two-form mathematical formula expressed firstly by Equation 2.14:

$$i = i_c + af'_a \qquad 2.14$$

where i_c is the steady-state infiltration rate and f'_a represents the available porosity, which is reduced by infiltration volumes and expressed by Equation 2.15:

$$f'_a = M - I \qquad 2.15$$

where the moisture storage capacity of the soil overlaying the first intercepting stratum (also known as the control layer) is represented by the M.The cumulative infiltration at a specific time is denoted by I. For the infiltration equation to remain consistent, the following criteria need to be upheld: $0 \leq I \leq M$. In the equation, it is assumed that $i = i_c$ for $M \leq I$.

2.7 Models for Determining Soil Hydraulic Properties

The water retention curve depicts the relationship between the water content, θ, and the soil potential, ψ . The curve is also known as the *soil moisture characteristic*. In unsaturated soil studies, it is crucial to predict the soil hydraulic properties in different water ratios. Several solid hydraulic models (summarised in Table 2-6) try to approximate the soil moisture characteristic curve, which will be introduced in this section.

Table 2-6: Summary of models for determining soil hydraulic properties

Model Description	Year
Brooks and Corey Model	1964
van Genuchten-Mualem Model	1980
Modified van Genuchten Model	1988
Kosugi Lognormal Distribution Model	1996
Durner Dual-Porosity Model	1999

2.7.1 Brooks and Corey Model

The soil water retention function, also known as the capillary pressure function, was proposed by Brooks and Corey (1964) as described in Equation 2.16

$$S_e = \begin{cases} |\alpha h|^{-n} & h < -1/\alpha \\ 1 & h \geq -1/\alpha \end{cases} \qquad 2.16$$

where S_e is the effective water content [-], n and α represent empirical constants with units [-] and [1/L] respectively, and h is the pressure head [L].

The corresponding hydraulic conductivity function represented by the Brooks-Corey retention function is represented by Equation 2.17

$$K(S_e) = K_s S_e^{\frac{2}{n}+l+2} \qquad 2.17$$

where l is an empirical parameter, $K(S_e)$ denotes the unsaturated hydraulic conductivity and K_s is the saturated hydraulic conductivity [L/T].

2.7.2 van Genuchten-Mualem Model

The water retention function given in the model by van Ganuchten (1980) is defined in Equation 2.18

$$S_e(h) = \frac{\theta(h) - \theta_r}{\theta_s - \theta_r} = \begin{cases} \dfrac{1}{(1 + |\alpha h|^n)^m} & h < 0 \\ 1 & h < 0 \end{cases} \qquad 2.18$$

$$K(S_e) = K_s {S_e}^{1/2} \left[1 - \left(1 - S_e^{1/m}\right)^m\right]^2$$

where θ_s and θ_r are the saturated and residual water contents, respectively, with units [-]. The empirical parameters in this equation are symbolized by α , m and n [1/L], [-], [-]. Like the Brooks and Corey (1964) model, K_s represents the saturated hydraulic conductivity and $K(S_e)$ is the unsaturated hydraulic conductivity [L/T] at a pressure head h [L].

2.7.3 Modified van Genuchten Model

Vogel and Cislerova (1988) modified the van Genuchten model to differentiate between various descriptions to give the user allowance to specify conditions linked with either the main wetting curve or main drying retention curve (Equation 2.19). Three descriptions can be specified, namely, a hysteric description inclusive of both the retention and hydraulic conductivity curves, a non-hysteric description, or a hysteric description which is only in the retention curve as defined below:

$$\theta(h) = \begin{cases} \theta_r + \dfrac{\theta_m - \theta_r}{(1 + |\alpha h|^n)^m} & h < h_s \\ \theta_s & h \geq h_s \end{cases} \qquad 2.19$$

where h_s is a value representing the air entry [L], θ_m is defined by Equation 2.20

$$\theta_m = \theta_r + (\theta_s - \theta_r)(1 + |\alpha h|^n)^m, \qquad 2.20$$

and the unsaturated hydraulic conductivity $K(S_e)$ is expressed in Equation 2.21

$$K(S_e) = \begin{cases} K_0 S_e^L + \left[\dfrac{1 - F(S_e)}{1 - F(1)}\right]^2 & h < h_s \\ K_0 & h \geq h_s \end{cases} \qquad 2.21$$

whereby K_0 denotes a matching point when the soil is saturated [L/T], L is an empirical parameter representing pore-connectivity and $F(S_e)$ the effective saturation defined in Equation 2.22

$$F(S_e) = \left[1 - (S_e)^{\frac{1}{m}}\right]^m. \qquad 2.22$$

in which $S_e(h) = \frac{\theta_s - \theta_r}{\theta_m - \theta_r} = \frac{\theta(h) - \theta_r}{\theta_m - \theta_r}$.

2.7.4 Kosugi Lognormal Distribution Model

A lognormal distribution model was suggested by Kosugi (1996) for the effective water content S_e as expressed in Equation 2.23

$$S_e = \frac{\theta - \theta_r}{\theta_s - \theta_r} = \begin{cases} \frac{1}{2} erfc\left\{\frac{ln(h/\alpha)}{\sqrt{2n}}\right\} & h < 0 \\ 1 & h < 0 \end{cases} \qquad 2.23$$

where n and α are empirical parameters, θ_s is the saturated water content [-], and θ_r is the residual water content [-]. By applying the van Genuchten (1980) model, the function for hydraulic conductivity K [L/T] can be expressed by Equation 2.24

$$K = \begin{cases} \frac{1}{2} erfc\left\{\frac{ln(h/\alpha)}{\sqrt{2n}} + \frac{n}{\sqrt{2n}}\right\}^2 & h < 0 \\ 1 & h < 0 \end{cases} \qquad 2.24$$

2.7.5 Durner Dual-Porosity Model

The porous medium was divided into a minimum of two overlapping regions by Durner (1994) who suggested describing each region as a van Genuchten (1980) type function for soil hydraulic properties. Durner et al, (1999) proposed for the functions to be superimposed linearly for each region to give the function for the multimodal pore system defined by Equation 2.25.

$$S_e = w_1[1 + (\alpha_1 h)^{n_1}]^{-m_1} + w_2[1 + (\alpha_2 h)^{n_2}]^{-m_2}$$

$$K(S_e) = K_s \frac{(w_1 S_{e1} + w_2 S_{e2})^l \left(w_1 \alpha_1 \left[1 - \left(1 - S_{e1}^{\frac{1}{m_1}}\right)^{m_1}\right] + w_2 \alpha_2 \left[1 - \left(1 - S_{e2}^{\frac{1}{m_2}}\right)^{m_2}\right]\right)^2}{(w_1 \alpha_1 + w_2 \alpha_2)^2} \qquad 2.25$$

where l, α_i, n_i, and $m_i (= 0 - 1/n_i)$ represent empirical parameters of individual hydraulic functions ($i = 1,2$), and w_i denotes factors for weighting of the two (or more) coinciding regions.

2.8 Measurement of Infiltration and Soil Hydraulic Properties

The infiltration rate of soil can be determined by measuring the volume of water, at regular time intervals, as it infiltrates the soil. The hydraulic conductivity of soil is a key factor to consider when it comes to infiltration. It is a measure of the soil's ability to transmit water when it is subjected to a hydraulic gradient (Fatehnia, 2015). This parameter is commonly symbolized as K_S under saturated conditions. Knowledge of the saturated hydraulic conductivity for a specific soil is crucial in various geotechnical, environmental, and agricultural applications. The soil surface governs the quantity of runoff for catchment areas during storm events, and the ability for infiltration and groundwater recharge to take place. These factors, *inter alia*, are important to environmental health and the determination of flood hazards. Infiltration measurements are also useful for understanding the efficiency of irrigation systems, plant rooting preferences, infiltration rates, and knowledge of where runoff to channels can be expected.

In a given space and time, K_S is assumed to be constant and can be used to compute the velocity in which water moves toward and into drain lines below the water table (Amoozegar and Wilson, 1999). Values determined from laboratory methods seldomly agree with those obtained through field experiments. Because field measurements are conducted closer to natural conditions, they are often found to be more reliable than laboratory methods (Scott, 2000). Computational software can be used, often with input data from field and laboratory test results to model and estimate long-term effects which in reality would be limited by time; for example, the amount of time it would take before the wetting front reaches the water table (Radcliffe and Šimůnek, 2010).

2.8.1 Field Methods

Infiltration tests in the field can aid in estimating the surface area required to archive desired volumetric recharge rates within a specific area of interest (Bouwer, 2002). Knowledge of recharge volumes is helpful in designing, *inter alia*, stormwater ponds, and infiltration basins.

Some common infiltration test methods and apparatus have been investigated (Fatehnia, 2015; Dixon 1975; Reynolds and Elrick (1985); ASTM, 2009) and are broadly discussed below:

2.8.1.1 Pressure Infiltrometer

The Pressure Infiltrometer is a Mariotte-type infiltrometer commonly used to evaluate the integrity of soil barriers such as clay liners. The apparatus, Figure 2-9 (a), is normally constructed from non-corrosive materials (i.e., PVC, Plexiglas, and Teflon). It does not require an external energy supply as it uses the principle of mechanical-hydraulic energy (Fatehnia, 2015). The cumulative infiltration of ponded water can be measured from the device's metal infiltration ring which has an inner diameter of 15 cm. The ring comes ready with a built-in water gauge for measuring the constant water level within the infiltration ring at regular time

intervals during the infiltration experiment. The penetration depth of the metal ring into the soil can be up to 10 cm. According to Matula and Kozáková (1997), the infiltrometer can supply an amount of water corresponding to a K_S value of 77 metres per day.

2.8.1.2 Mini-Disk Infiltrometer

Unlike other common infiltration test methods, the Mini-Disk Infiltrometer does not measure water flow under saturated conditions. The underlying issue with those methods is their inability to represent infiltration under sprinkle or rainfall conditions. Consequently, several authors made an effort to create negative potential (tension) on the water flow to eliminate the effect of macropores in the flow process, thus only measuring the matrix flow of the soil. One of the earliest investigations was conducted by Dixon (1975) who established a closed-top infiltrometer to measure and quantify macropores. Various researchers suggested several methods which can be applied to measure the saturated hydraulic conductivity using test results from the Mini-Disk Infiltrometer. Some of which were Fatehnia *et al*., (2014), who explained and compared eight similar methods before comparing their degree of accuracy in the predicting of K_S.

The mini-Disk Infiltrometer, Figure 2-9 (b), measures tensions ranging between -0.5 and -6.0 cm. The upper and lower chambers of the apparatus are both filled with water to obtain readings. The upper chamber, commonly referred to as the bubble chamber, serves to control the suction whereas the lower chamber contains the volume of water that infiltrates into the soil at a preselected rate governed by the chosen suction in the bubble chamber. Like a graduated cylinder, the lower chamber contains labels indicating volumes in millilitres. To limit water leakage into the open air, the infiltrometer contains a porous sintered stainless-steel disk. Due to the small inner diameter of the device, undisturbed measurements can be obtained on relatively level soil surfaces, however, the small-scale nature of this infiltrometer only allows for a small portion of the soil to be measured, thus limiting the requirements of a representative volume.

2.8.1.3 Guelph Permeameter

The Guelph Permeameter, shown in Figure 2-9 (c), is a field apparatus used to measure in-situ saturated hydraulic conductivity by applying a constant pressure head within a shallow hole or borehole. The apparatus is quick and easy to assemble and provides relatively accurate measurements. The instrument applies a constant head using a Mariotte cylinder allowing water to infiltrate into unsaturated soil. Once steady-state flow conditions are achieved, the measurements can be used to calculate saturated hydraulic conductivity values. Apart from soil hydraulic conductivity, other parameters such as soil sorptivity and matrix flux potential can be accurately evaluated in all soil types using this instrument Fatehnia (2015). Depending on the soil type, measurements can be made within a depth range of 15 to 75 cm below the surface within a period of 0.5 to 2.0 hours using approximately 2.5 litres of water.

The test set-up is light and easy to assemble. It consists of a permeameter, a well auger, a tripod, a portable water container, and a vacuum test hand pump. Optional depth attachments are available which can increase the operation depth by 80 cm. According to Reynolds and Elrick (1985), the apparatus has a maximum applicable operation depth of 315 cm.

2.8.1.4 Ring Infiltrometer

The Ring Infiltrometer apparatus is used to measure the saturated hydraulic conductivity, K_S, of soil surface layers under ponded (saturated) conditions. There are two distinct types: the Single-Ring Infiltrometer (SRI), and the Double-Ring Infiltrometer (DRI). Each of the devices requires rings to be driven 10 to 15 cm into the ground. According to Hayden (2010) when comparing the two, the DRI is a relatively better test for measuring soil permeability because the outer rings assist in reducing errors associated with lateral flows. The presence of the outer ring turns a three-dimensional system into a one-dimensional model which simplifies calculations by alleviating the need to account for lateral flows (ASTM, 2009). The typical flow patterns below each of these infiltrometers are depicted in Figure 2-8.

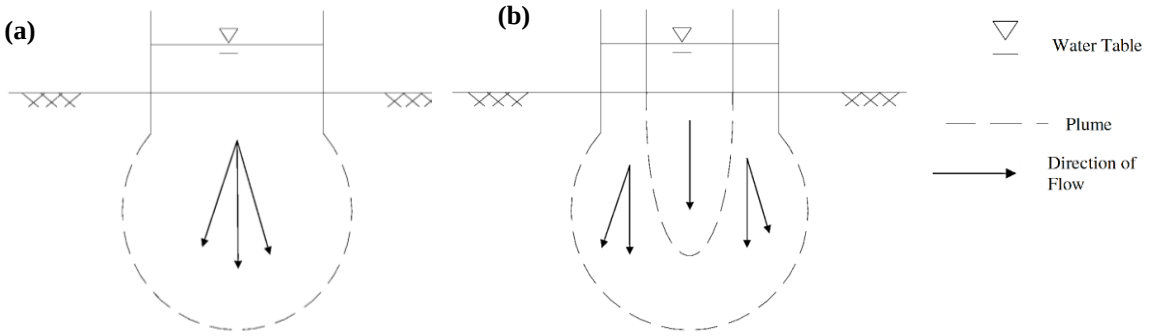

Figure 2-8: General flow direction beneath (a) Single-Ring Infiltrometer and (b) Double-Ring Infiltrometer
Adapted from: Hayden (2010)

Two operational techniques can be used with the double-ring infiltrometer to measure the flow of water into the soil (i.e., constant-head, and falling-head test). In the constant-head test (suitable for relatively coarse-grained soils), the water level in the inner ring is maintained at a fixed level by manually controlling the flow of liquid, using constant-level float valves, or by using a Mariotte tube. In this method, the volume of water used to maintain this water level is measured. In the falling head test (suitable for fine-grained soils), the time that the water level takes to decrease in the inner ring is measured. In both constant and falling head tests, the water level in the outer ring should be kept at a constant level to prevent leakage between rings and to force vertical infiltration from the inner ring. DRI is the main test method applied for infiltration measurement of detention/retention ponds for stormwater management purposes.

For the DRI test procedure, both the inner and outer rings are supplied with a constant head of water and the hydraulic conductivity of the soil is estimated once the flow rate of water in the

inner ring reaches a steady state. The infiltration rate is determined by the volume of water that infiltrates the surface area of the inner disk in a specific amount of time. The recorded data is plotted on a graph illustrating the relationship of infiltration vs time. The stead-steady infiltration rate will, theoretically, be reached once the soil becomes saturated. That becomes evident on the plotted graph once the relationship between cumulative infiltration and time becomes linear. The slope of the best fit line on the linear section of the plot (excluding any outlying data points) represents the steady-state infiltration rate. Figure 2-9(d) illustrates the experimental setup of the DRI.

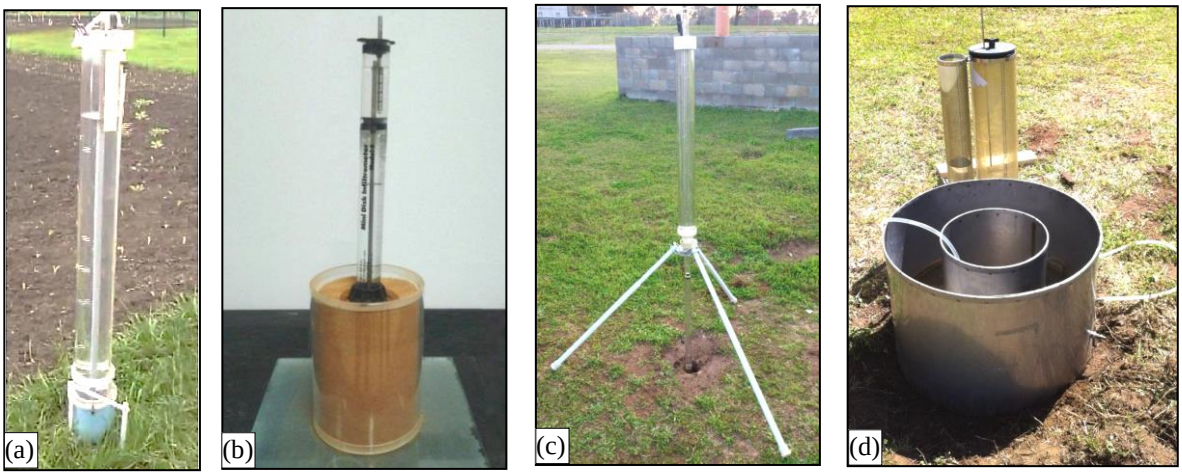

(a) Pressure Infiltrometer; (b) Mini Disk Infiltrometer; (c) Guelph Permeameter; (d) Double-Ring Infiltrometer

Figure 2-9: Various field methods for measuring hydraulic conductivity of topsoil. (a) Pressure Infiltrometer; (b) Mini-Disk Infiltrometer; (c) Guelph Permeameter; (d) Double-Ring Infiltrometer

Adapted from: Fatehnia (2015)

2.8.2 Laboratory Methods

Investigating soil hydraulic properties in the field may not always be possible due to limitations such as long required testing periods; availability of testing equipment and skilled labour, safety concerns, and accessibility to sites of interest. Consequently, soil samples retrieved from an area of interest are often tested in the laboratory to determine certain soil properties such as, *inter alia*, the hydraulic conductivity.

The saturated hydraulic conductivity of soil, K_S, can be measured in the laboratory through permeability tests which measure the soil's capacity to permit the flow of water through pore spaces between solid particles. Permeability of soil depends on void ratio, density, particle size, and degree of saturation. The degree of permeability can be determined by measuring the rate of water flow under a specific hydraulic pressure gradient. In engineering problems, knowledge of the soil permeability can aid in determining, for example, the rate of leakage through an earth dam or the quantity of seepage under hydraulic structures (Braja, 2002).

Two standard laboratory tests for determining hydraulic conductivity of soil are the constant-head test and the falling-head test. The two testing methods are briefly discussed as follows:

2.8.2.1 Constant-Head Test

The constant-head permeameter is an apparatus best used to measure the saturated hydraulic conductivity of permeable granular soil in the laboratory (Braja, 2008). For the test procedure, the soil specimen is placed inside a cylindrical specimen tube and a constant-head loss of water h flowing through the sample is maintained by adjusting the water supply. Water flowing out from the sample is collected in a measuring cylinder and the collection period is recorded.

By rearranging Darcy's law in Equation 2.3, the total volume of flow Q at time t can be determined using Equation 2.26

$$Q = Avt = A(ki)t \tag{2.26}$$

and because the water flux $i = h/L$, where L is the specimen length, h/L can be substituted into Equation 2.26 to yield Equation 2.27 for determining the saturated hydraulic conductivity

$$k = \frac{QL}{Aht} \tag{2.27}$$

The general arrangement for the test is illustrated in Figure 2-10(a).

2.8.2.2 Falling-Head Test

The falling-head permeameter is a suitable laboratory apparatus for measuring the saturated hydraulic conductivity of fine-grained soils such as silty and clay-like soils. A typical arrangement of the testing apparatus is shown in Figure 2-10(b).

The investigated soil specimen of length L is placed inside a cylinder with a water supply tube attached to the top of the specimen. Water is allowed to flow through a standpipe into the soil sample at time $t = 0$ and the initial head difference h_1 is logged. The final head difference h_2 at time $t = t_2$ is subsequently recorded.

The flowrate of water q at any given time t can be computed using Equation 2.28

$$q = k\frac{h}{L}A = -a\left(\frac{dh}{dt}\right) \tag{2.28}$$

where a is the cross-sectional area of the standpipe and A is that of the soil sample. Equation 2.29 can be obtained by rearranging and making the rate of change of time, dt, as the subject, which when integrated on the left side, with time limits from $0 - t$, and the right side with head difference limits from h_1 to h_2

$$t = \frac{aL}{Ak} log_e \frac{h_1}{h_2} \qquad 2.29$$

which when k is made the subject of the formula Equation 2.30, allows for the computation of the soil material's hydraulic conductivity

$$k = 2.303 \frac{aL}{At} log_{10} \frac{h_1}{h_2} \qquad 2.30$$

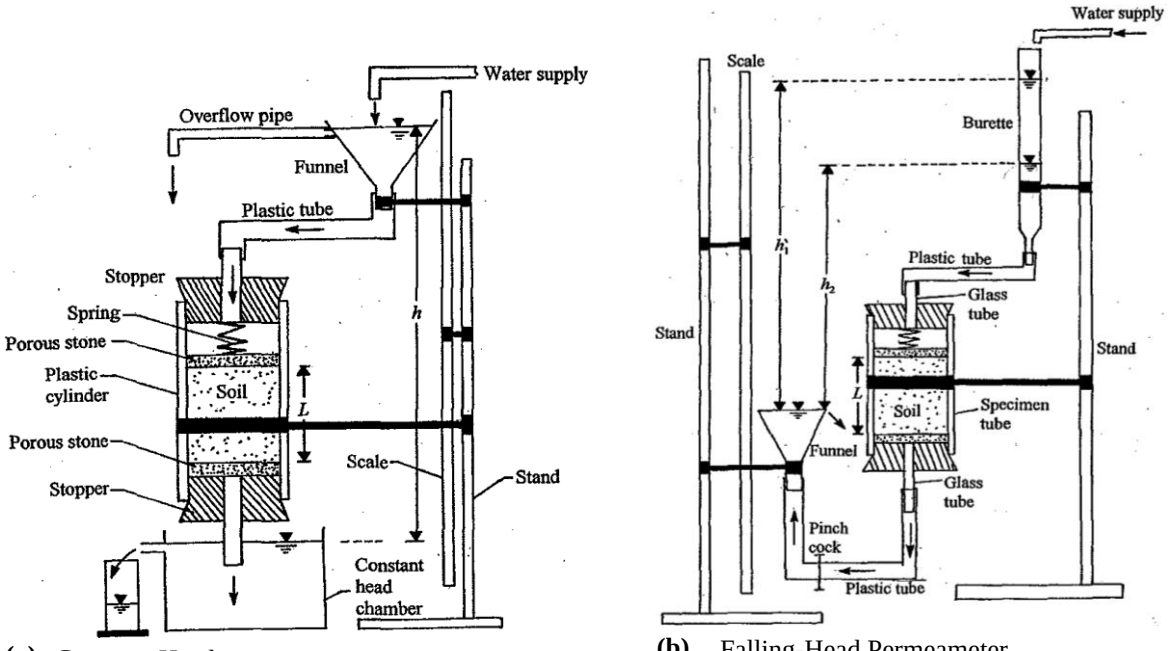

(a) Constant-Head **(b)** Falling-Head Permeameter

Figure 2-10: Schematic diagrams of (a) Constant-head and (b) Falling-head Permeameter apparatus

Adapted from: Braja (2002)

2.8.3 Laboratory Versus Field Methods

Test results may vary with the method of testing used due to their nature and limitations present in the environment in which the test is performed. The advantages and disadvantages are summarised in Table 2-7 and Table 2-8 the laboratory and the field methods respectively.

Table 2-7:Advantages and disadvantages of laboratory infiltration tests

Advantages	Disadvantages
• Especially relevant for compacted soil • Can efficiently perform tests under different boundary conditions. • Cost-effective to perform. • Different tests can be performed concurrently	• Limited specimen size • Sample selection tends to be subjective as 'good' samples are selected. • The sample may be disturbed. • Flow may not be in the most crucial direction (Figure 2-11)

Table 2-8: Advantages and disadvantages of field infiltration tests

Advantages	Disadvantages
• Large volumes of soil can be tested. • Minor disturbances in samples • Produces more relevant results as the proper flow direction is followed (Figure 2-11).	• Costly to perform. • Time-consuming • Data reduction may be an issue if the test procedures are ill-defined.

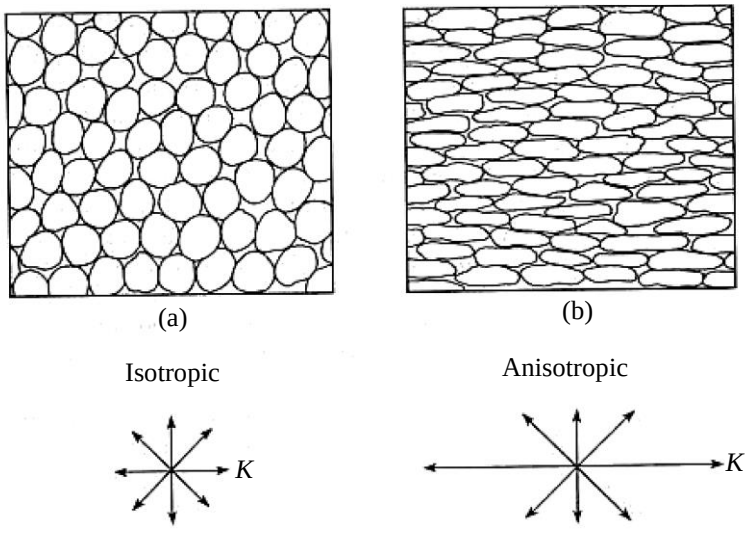

Figure 2-11: Difference in grain shape and orientation (a) Isotropic and (b) Anisotropic
Adapted from: Shan (n.d.)

2.9 Equivalent Hydraulic Conductivity in Stratified Soil

To simplify computations for stratified soil deposits where the hydraulic conductivity for flow in a given direction changes from layer to layer, an equivalent hydraulic conductivity can be calculated from Equation 2.31 adapted from Darcy's (1856) law used to determine steady flow in saturated soils. Figure 2-12 illustrates n layers of soil with flow in the horizontal direction. Assuming that k_{H_1}, k_{H_2}, $k_{H_3}\ldots k_{H_n}$ are hydraulic conductivities of the individual layers in the horizontal direction and $k_{H_{(eq)}}$ is the equivalent hydraulic conductivity in the horizontal direction.

$$k_{H_{(eq)}} = \frac{1}{H}\left(k_{H_1}H_1 + k_{H_2}H_2 + k_{H_3}H_3 + \cdots + k_{H_n}H_n\right) \qquad 2.31$$

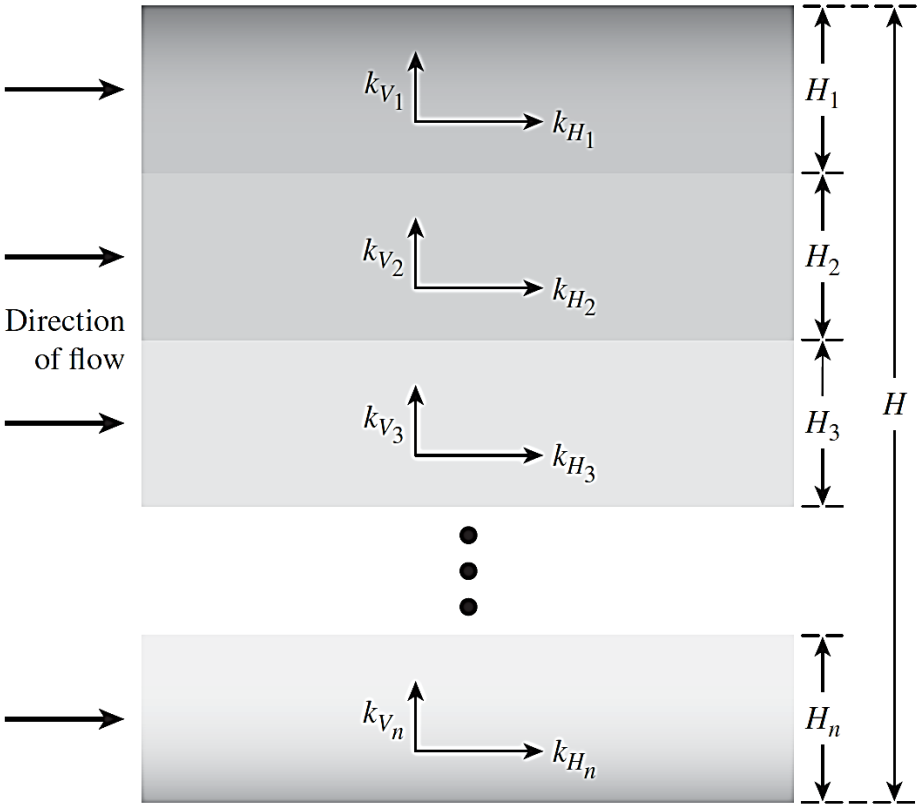

Figure 2-12: Equivalent hydraulic conductivity determination in stratified soil – horizontal flow
Source: Braja (2013)

In the case of flow in the vertical direction, the *n* layers of soil are depicted in Figure 2-13. The velocity of flow through all layers is the same whereas the total head loss h is equal to the sum of head losses in all layers.

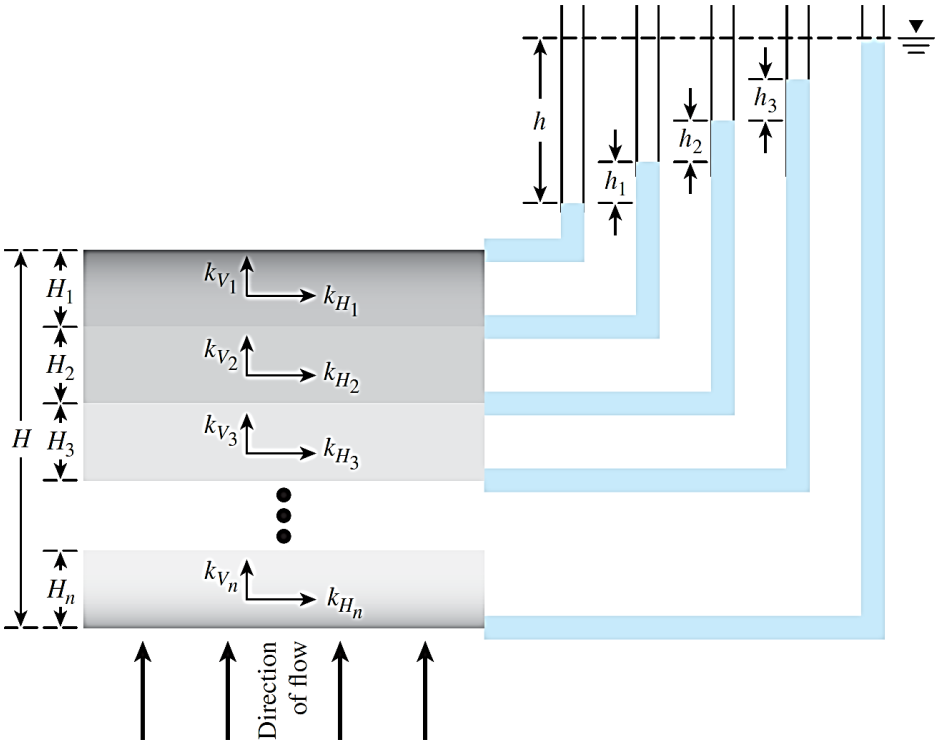

Figure 2-13: Equivalent hydraulic conductivity determination in stratified soil – vertical flow
Source: Braja (2013)

Again, from Darcy's (1856) law, the equivalent vertical hydraulic conductivity $k_{V_{(eq)}}$ could be expressed by Equation 2.32 where $k_{V_1}, k_{V_2}, k_{V_3} \ldots k_{V_n}$ represent the hydraulic conductivities of individual layers in the vertical direction

$$k_{V_{(eq)}} = \frac{H}{\left(\frac{H_1}{k_{V_1}}\right) + \left(\frac{H_2}{k_{V_2}}\right) + \left(\frac{H_3}{k_{V_3}}\right) + \cdots + \left(\frac{H_n}{k_{V_n}}\right)} \qquad 2.32$$

2.10 Infiltration Modelling Using Computer Software

Due to the limitations of conducting many in-situ infiltration tests, computer simulations can be an alternative to physical tests for data collection (Fatehnia, 2012). Numerical modelling programs can be used to estimate soil hydraulic properties as well as evaluate the wetting front arrival time from the surface to the water table. Furthermore, adjustments of required parameters can be made to observe their respective effects on measured infiltration rates. Various software is available to simulate infiltration; some reliable ones used by other authors (Lappala, 1981) Fatehnia, 2012; Teague, 2021) are briefly discussed in the following sections.

2.10.1 VS-2D Software

VS2D can be used to simulate isothermal, two-dimensional movement of water in variably saturated porous media. Lapalla (1981) performed an extensive review of the literature on numerical modelling of variably saturated flow during the development of VS2D. The program was developed to include the following capabilities:

- Handling problems where part of the mathematical solution domain is saturated and partly unsaturated.
- Solving difficult non-linear problems
- Analysing problems in one and two dimensions with planar or cylindrical geometries.
- Forming a modular structure to enable simple program modification.

2.10.2 Rosetta Software

Rosetta V1.0 is a program used to estimate unsaturated hydraulic properties from surrogate soil data. This model is also called pedotranfers (PTF) and can be used to estimate the following properties: water retention parameters, saturated & unsaturated hydraulic conductivity according to Mualem (1976) and van Genuchten (1980).

The software offers five PTFs that are used to predict hydraulic properties with limited data or extended sets of input data. The model uses a hierarchical sequence to input data as listed below (Schaap et al., (2001):

1. Soil textural class
2. Sand, silt, and clay percentage
3. Sand, silt and clay percentage and bulky density
4. Sand, silt and clay percentage and bulky density and water retention point at 330 cm
5. Sand, silt and clay percentage and bulky density and water retention point at 330 and 1500 cm

2.10.3 HYDRUS Software

The HYDRUS suite of modelling software uses a finite element code to simulate the and three-dimensional water flow, heat, and solute transport in soils of various degrees of saturation. To simulate variably saturated flow, the program applies Richard's (1931) equation (Šimůnek et al., 2007).

The software is supported by a graphic user interphase (GUI) able to display results interactively. With the capability of accommodating irregular boundary shapes and conditions, the software also supports flow regions comprising of nonuniform soils with some degree of local anisotropy. The user can refine the degree of accuracy in a model domain by varying the size of the discretized triangular finite elements.

2.11 Previous Similar Studies

Gregory (2004) investigated lot-level stormwater infiltration in North Central Florida. To quantify soil infiltration rates, he compared a small DRI (15 cm inner diameter and 30 cm outer diameter) to several other double-ring methodologies and found that this was a suitable methodology for measuring soil infiltration rates in the sandy soils found in North Central Florida. Gregory further highlighted how the use of the small DRI allowed for infiltration tests to be conducted in areas where a methodology such as that specified by the ASTM would not be suitable due to insufficient spacing between trees or because the volumes of water required to maintain a constant head in the larger diameter double-ring infiltrometers were unable to be transported to remote sites.

Hayden (2010) investigated how permeability most accurately predicted a stormwater pond's actual infiltration rate by conducting field DRI tests, taking subsurface samples for laboratory analysis, and utilizing the Modret computer program. She concluded that the DRI test was a better field test to measure the permeability of an in-situ soil compared to a single ring infiltration test, and also the saturated permeability value obtained from a laboratory falling head permeability test was approximately equal to the unsaturated rate measured in the field using a single ring infiltration test.

Hayden (2010) conducted two DRI tests following the ASTM D3385-03 standard. The results of this DRI test are shown graphically in Figure 2-14. The infiltration rate began at 12.0 feet per day (3.7 metres per day) and slowly dropped and levelled off at approximately 1.6 feet per day (0.5 metres per day). The infiltration rate varied significantly from the beginning to the end of both tests. Hayden concluded that if the beginning infiltration values of either 5.7 feet per day (1.7 metres per day), or 12.0 feet per day were used for the design of a stormwater management facility, it would grossly overestimate the infiltration rate of the subsoils.

As part of the study, Hayden (2010) further conducted two field infiltration tests using only the inner ring of the DRI setup. This test was performed because some geotechnical engineers believed that a single ring infiltration test produced results that were similar to that of a double ring infiltration test and the method was less confusing to their field technicians. Results of this single-ring test are shown in Figure 2-15. The infiltration rates encountered in both single-ring tests were noticeably higher than those measured in the double-ring infiltration tests. This was expected because water flow in a single ring infiltrometer is three-dimensional compared with the two-dimensional flow in the inner ring of a DRI. It appeared that the infiltration rate from the single-ring infiltration test was approximately 48 % higher than that obtained from the double-ring infiltration test.

Teague (2010) conducted several DRI tests at eight sites in alluvial deposits near Joshua Tree, California to measure surface infiltration rates and aid in evaluating the study area for potential construction of infiltration ponds to recharge groundwater. A summary of the hydraulic properties obtained by Teague is presented in Table 2-9. He estimated the hydraulic

conductivity of alluvium from infiltration data using the computer program VS2D and concluded that the study site was suitable for artificial recharge.

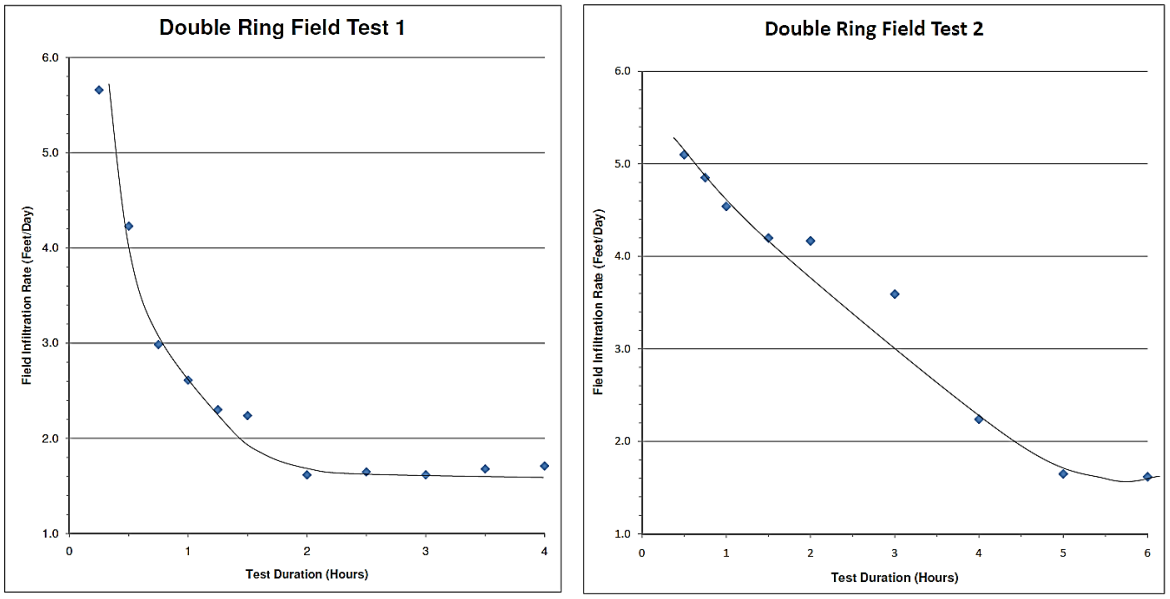

Figure 2-14: Infiltration rate versus time from Double-Ring Infiltrometer test
Adapted from: Hayden, 2010

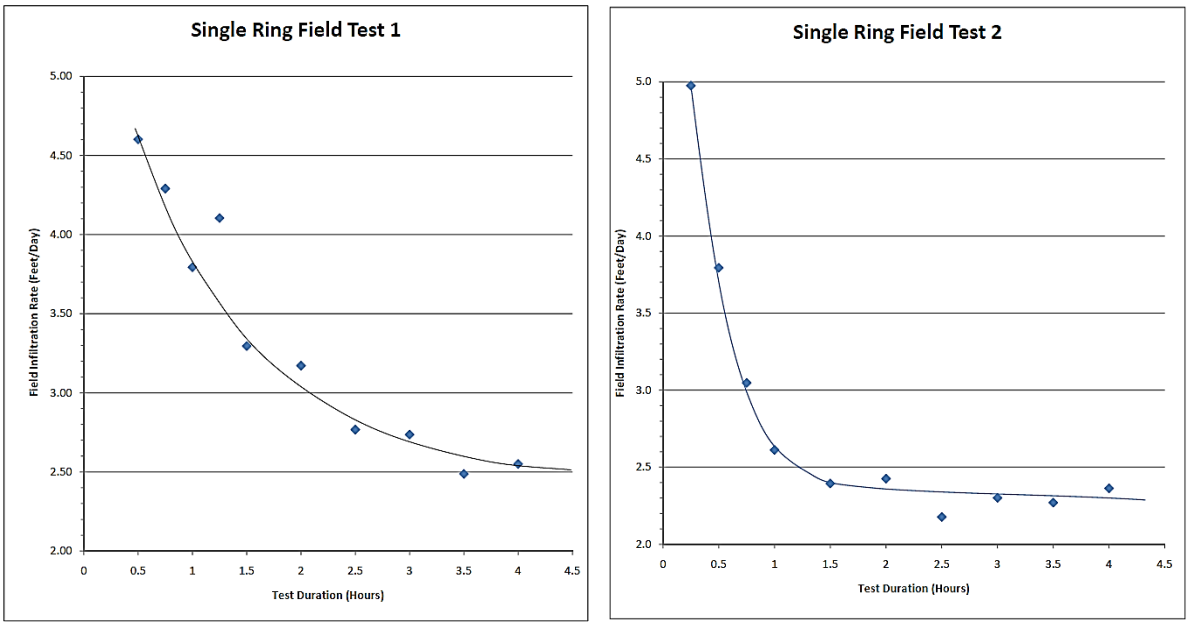

Figure 2-15: Infiltration rate versus time results from Single-Ring Infiltrometer test
Adapted from: Hayden, 2010

From laboratory testing of surface cores from the eight tested sites, Teague (2010) further found that the hydraulic conductivity data ranged from $4.33x10^{-5}$ ft/s ($13.2x10^{-6}$ m/s) to $7.59x10^{-5}$ ft/s ($23.1x10^{-6}$ m/s) (see Figure 2-9). These values of hydraulic conductivities are within the range for fine sands to silty sand (Table 2-10). Hydraulic conductivity values were expected to be within the range for medium to fine sands based on visual inspection of the surficial materials at the study area. Lower calculated values were anticipated due to compaction of the core material during collection or the presence of a fine-grained dominated surficial crust. Unlike the infiltrometer data, the hydraulic conductivities did not show a good correlation with location to Yucca Wash (the study area).

Table 2-9: Laboratory hydraulic properties data of the eight tested sites
Adapted from: Teague (2010)

Site ID	Bulk Density	Porosity	Volumetric Water Content	Saturation	Residual Water Content	Hydraulic Conductivity
	(g/cm^3)	(m^3/m^3)	(m^3/m^3)	(m^3/m^3)	(m^3/m^3)	(m^3/m^3)
Site 1	1.80	0.341	0.015	0.044	0.011	$6.65x10^{-5}$
Site 2	1.79	0.372	0.018	0.047		$5.27x10^{-5}$
Site 3	1.73	0.346	0.033	0.097	0.022	$5.62x10^{-5}$
Site 4	1.65	0.341	0.02	0.058		$7.54x10^{-5}$
Site 5	1.77	0.334	0.03	0.09	0.007	$6.47x10^{-5}$
Site 6	1.80	0.325	0.039	0.119		$6.76x10^{-5}$
Site 7	1.73	0.351	0.027	0.077		$4.33x10^{-5}$
Site 8	1.65	0.39	0.039	0.1		$7.59x10^{-5}$

Studies conducted by Fatehnia (2015) on small-scale DRI tests revealed that the ring diameter was the most influential parameter affecting the infiltration rate. To further corroborate these findings, Fatehnia (2015) conducted large-scale field tests using various inner ring diameters and the results agreed with those that were found in the laboratory. The DRI field test results are shown in Figure 2-16.

Fatehnia (2015) further used the HYDRUS-2D software to develop a total of 864 2D-axisymmetric model domains which represented Double-Ring Infiltrometer (DRI) test conditions. Because of limitations in conducting a large number of in-situ DRI tests, Fatehnia selected computer simulations as an alternative to physical test data allowing him to generate 864 numeral simulations with varying parameters.

Another study by Chowdary et al. (2006) and Reynolds et al. (2002) considered the ring insertion depth as one of the aspects affecting infiltration rates from DRI field test results.

Table 2-10: Soil classification table based on values of saturated hydraulic conductivity
Adapted: Formerly valid Czech standard (CSN 721020)

Soil (according to the Relative Permeability)	Approximate Range of Saturated Hydraulic Conductivity (m s^{-1})	Examples of Soil Types
Highly impermeable	< 10^{-10}	Clays with low and medium plasticity, clays with high and extremely high plasticity
Impermeable	from 10^{-8} to 10^{-10}	Gravel loams, gravel clays, and sandy clays, loams with low and medium plasticity
Lowly (poorly) permeable	from 10^{-6} to 10^{-8}	Sandy loams, loamy sands and clayey sands, loamy gravels and clayey gravels
Permeable	from 10^{-4} to 10^{-6}	Sands and gravels, containing fine-grained fraction (5 – 15 %)
Highly permeable	> 10^{-4}	Sands and gravels without or with a very low fine-grained fraction (<5%)

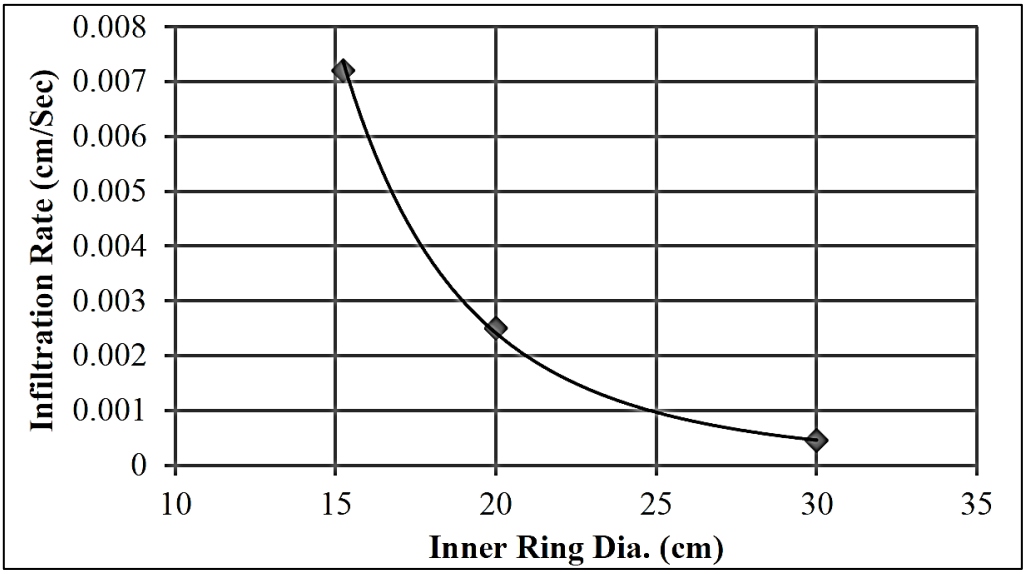

Figure 2-16: Field test results indicating a reduction in infiltration rate due to an increase in inner-ring diameter
Source: Fatehnia (2015)

ASTM (2009) recommends ring insertion depths of approximately 150 mm, however, Chowdary et al. (2006) recommend that, for adequate accuracy in infiltration measurements to be achieved, rings should be embedded between depths of 190 mm to 220 mm. Difficulties may arise in driving the rings into the ground when dealing with stiff soil materials which is why further studies on the effects of this parameter have been recommended.

One of the ways that municipalities can conserve water is by making use of treated wastewater and stormwater that is diverted from large basins where it infiltrates into the sandy aquifer from where it is abstracted and reused. Atlantis is a perfect example of this, where the groundwater supplies have been augmented by approximately 25% to 30% by transferring water into aquifers; a process known as artificial recharge (DWA, 2010).

Atlantis is a town located 50km north of Cape Town's city centre and has a population of approximately 57 000 people. Two infiltration basins are currently in use and are recharged from treated domestic effluent, domestic and industrial stormwater. The water scheme is referred to as the Atlantis Water Resource Management Scheme (AWRMS). AWRMS has successfully supplied water to both residential and industrial areas for over 30 years, proving itself as a cost-effective artificial recharge solution. Water sources and aquifers need to be meticulously managed to ensure future sustainability. Figure 5.1 reflects the layout of the AWRMS including the location of the recharge basins and wellfields.

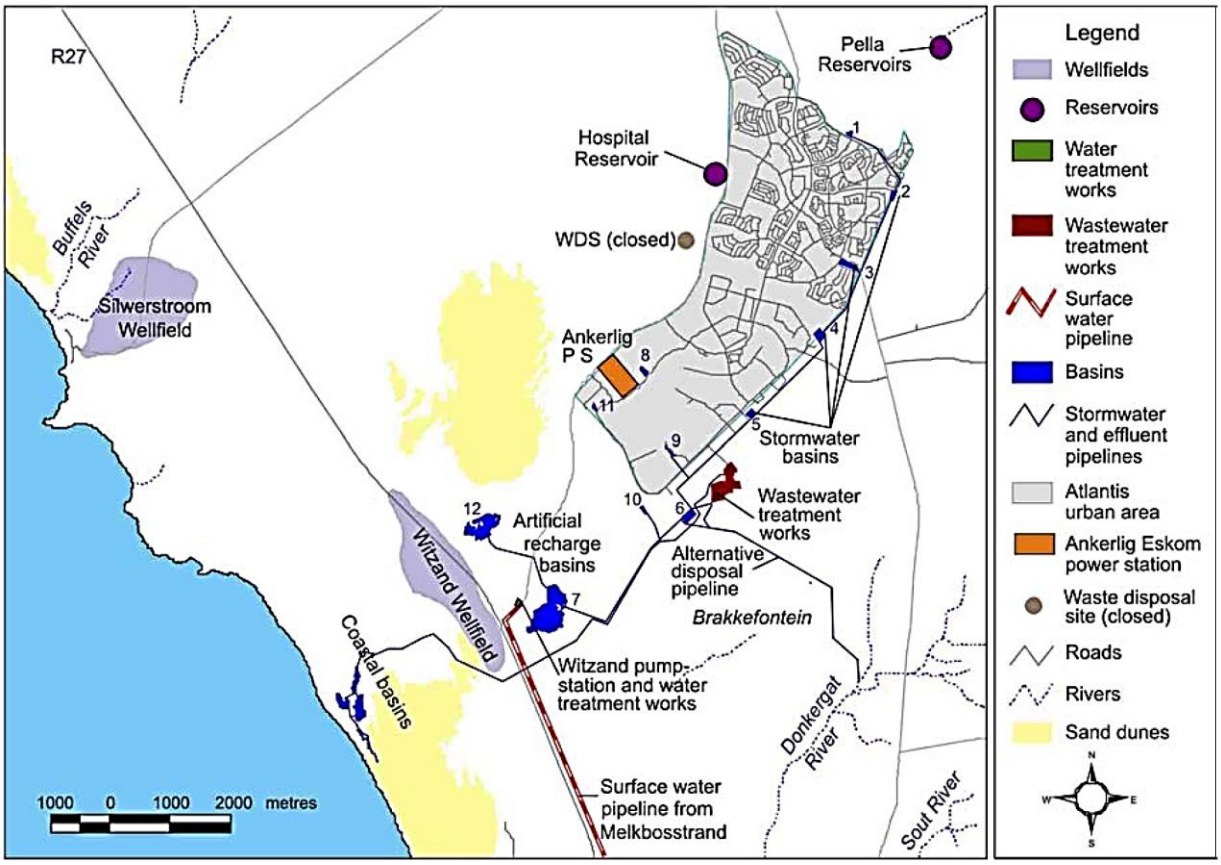

Figure 2-17: Layout of Atlantis Water Resource Management Scheme
Source: Bugan et al. (2016)

The map reflects the following aspects of the scheme: residential and industrial areas, the stormwater system as well as stormwater retention basins, the artificial recharge basins that

recharge the aquifer centrally (no 7 & 12), the coastal basins by the sea, industrial and domestic wastewater treatment works, water softening plant, Silwerstroom, and Witsand wellfields; and alternative discharge route to the Donkergat River. Table 2-11 presents the area, unsaturated zone depth, and infiltration rates of the facility's three main recharge ponds.

Table 2-11: Average values for characteristics of main recharge facilities
Adapted from: (DWA, 2010

Facility	Area (ha)*	Unsaturated Zone (m)	Infiltration Rate (m/day)**
Basin 7	28.3	1.5	0.01
Basin 12	16.8	4.5	0.16
Coastal Basins	12.5	10.5	0.11
*Total basin area when full; Basin 12 mostly dry. **Rate based on basin area			

3 The Zeekoe Catchment Area

3.1 Introduction and Background

The Zeekoe Catchment's footprint (Figure 3-1) is situated within the Cape Flats aquifer (CFA) which, according to Burman (1962), was stripped of its vegetation by slaves in search of firewood during the eighteenth century. This soon resulted in the Cape Flats becoming a massive desert encompassing growing dunes driven by south-easterly winds. It was not until 1936 that the Cape Town City Council initiated activities to reclaim and stabilize the sand dunes by introducing and promoting vegetation growth (Heydorn & Grinley, 1982).

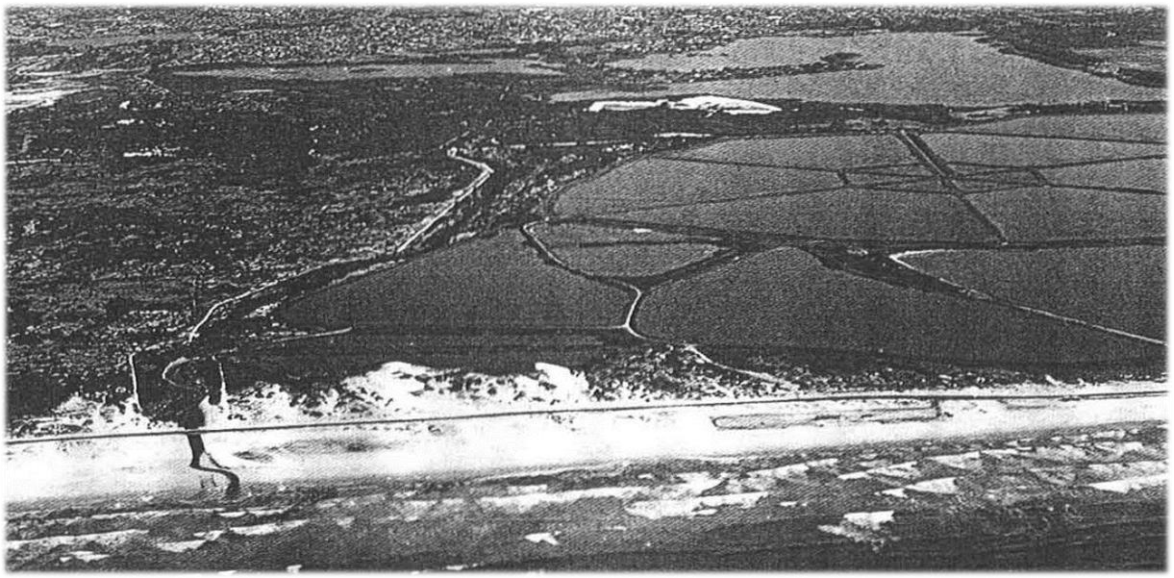

Figure 3-1: Aerial view of Zeekoe canal and components of the drainage system
Source: Heydorn & Grinley (1982), after NRIO 82-12-20

Primary aquifers of the south-western Cape, comprising of unconsolidated sediments of Cenozoic age (i.e. not older than 65 million years of age (Brumer, 1981)), were initially explored in the late 1960s (Vandoolaeghe, 1984). The first of these explorations was a hydrogeological study of sand deposits near the Cape Flats, and between Melkbosstrand and Atlantis along the West Coast. The purpose of these investigations varied with time as different projects' objectives changed. However, they were ultimately related to either the development of an alternative urban or municipal water supply, or to assess the storage potential of the aquifer for treated wastewater and surface water, or stormwater runoff (Vandoolaeghe, 1984).

Rigorous hydraulic explorations in the Cape Flats aquifer have been driven by the National Institute of Water Research (NIWR) of the Council for Scientific and Industrial Research (CSIR), with the objectives of reviewing the feasibility of reclamation, storage, and abstraction of purified wastewater in the CFA (Henzen, 1973; Gerber, 1976). In one such study, research facilities for the pre-treatment, artificial recharge, and post-treatment of sewage effluent were

designed and constructed according to the sequences illustrated in Figure 3-2. In their paper, Tredoux et al. (1980) describe how an experimental site in the Cape Flats, comprising of the components demonstrated in Figure 3-2, was established to obtain geophysical data, particularly regarding the transmissivity, storage capacity and extent of saturation of the deposits. Results from initial abstraction studies indicated that the aquifer was potentially suitable for artificial recharge and groundwater abstraction (Tredoux et al. 1980).

More recently, a study by Okedi (2017), to determine the viability of stormwater ponds in the Zeekoe catchment as a water resource, has produced findings (through hydrogeologic models developed using PCSWM software) that suggested stormwater harvesting as a feasible approach. Moreover, the existing stormwater ponds in the catchment have been proposed to function as infiltration basins promoting groundwater recharge.

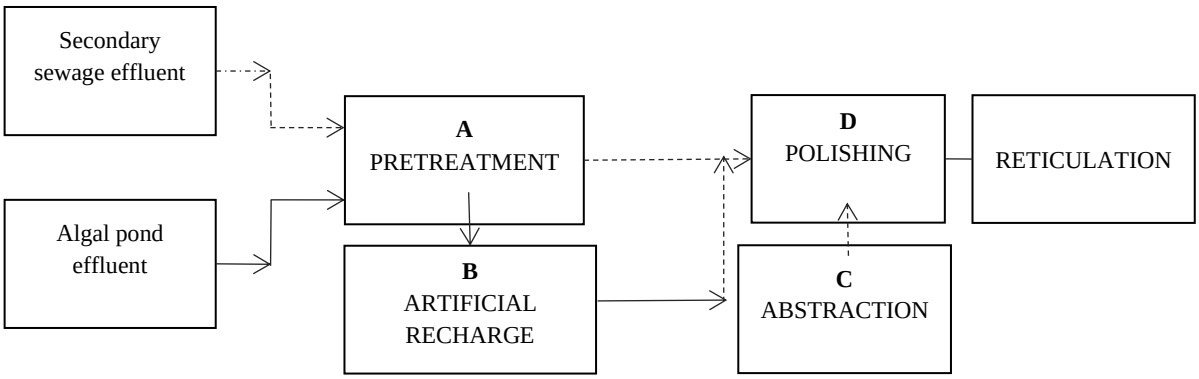

Figure 3-2: Components of research test facilities
Adapted from: Tredoux et al. (1980)

Existing information of groundwater conditions within and around the Cape Flats aquifer is relatively vast as it has been accumulated over approximately 60 years (Henzen, 1973; Gerber, 1976; Wessels and Greeff, 1980; Tredoux, 1981; Adelana et al., 2010; Okedi, 2017). However, the heterogeneous and anisotropic nature of the layered Cenozoic deposits results in variability of hydraulic properties from one area to another – even within the same aquifer unit. It is thus difficult to simply generalize reliable hydraulic parameters of an area. Vandoolaeghe (1984) refers to the knowledge of the Cenozoic deposits as being, “rather patchy” and the averages, “quite superficial”.

Local aquifer characteristics are crucial, particularly in the design phase of any artificial recharge project. Because this study focuses on groundwater recharge through infiltration basins, it was thus considered imperative to conduct in-situ tests within the stormwater ponds of interest to attain reliable estimations of local hydraulic properties.

This chapter presents an overview of Zeekoe catchment as the study area for this investigation. It follows with a description of the catchment’s geographical location, land use, and the climate

conditions around the region. Before concluding with a description of the stormwater ponds within the study area, the geology and geohydrological features of the catchment are described.

3.2 Geographical Location

The Zeekoe catchment is situated approximately 20 km south of Cape Town's central business district; its mouth lies between 34°06' South and 18°30' East (Figure 3-3(a)). The study area is sited within a section of the Cape Flats Aquifer (CFA) (Figure 3-3(b)), a region possessing good groundwater storage characteristics which support its potential development for water supply (Adelana et al., 2010). This being an urban area, the catchment delineation was based on the urban drainage system (i.e., pipe network) that channels water downward by gravity.

The CFA surface sands cover an area of between 630 km^2 (Hartnady &Rogers, 1990) and 765 km^2 (Maclear, 1995), with a topography that is mostly dominated by sandy soils and dunes (Tredoux et al. 1980). The region extends from the False Bay coastline in the south, expanding to Milnerton and Tygerberg in the northwest and north-east directions, respectfully (Hay et. al., 2015). Within the CFA, the Zeekoe catchment occupies approximately 177 km^2 and is amongst one of 22 major catchments in the city of Cape Town (Rohrer, 2014). A delineation of the city's major catchments and Zeekoe's position is mapped in Figure 3-4.

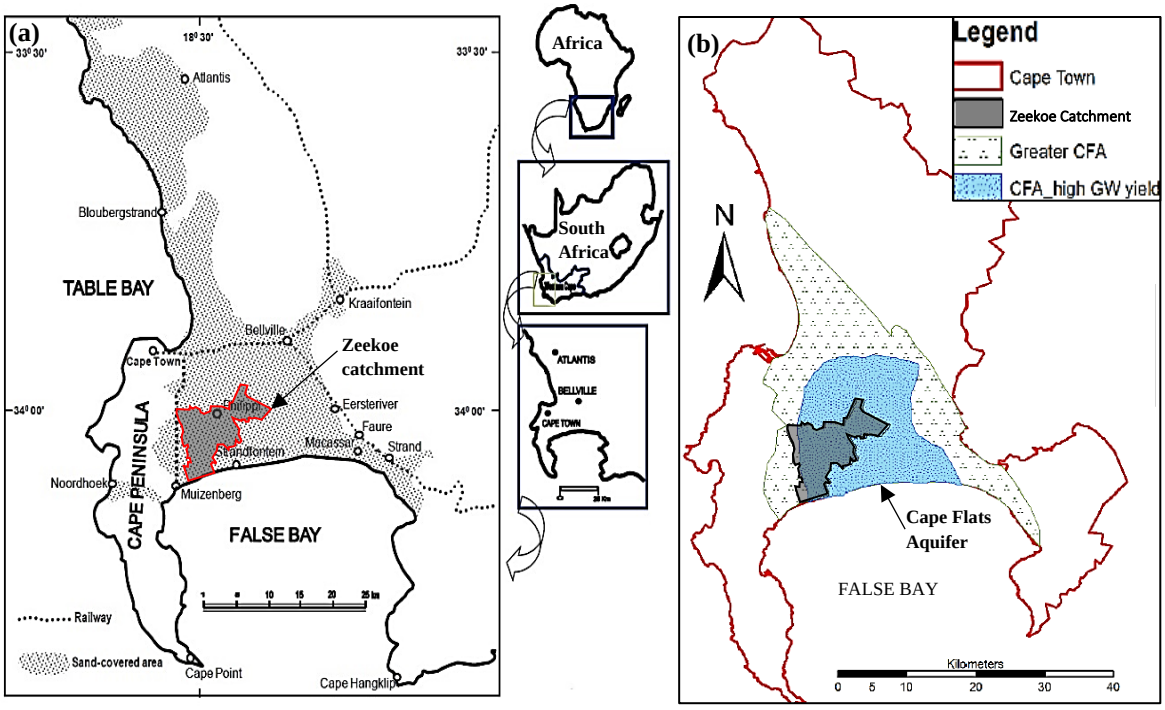

Figure 3-3: (a) Map of Zeekoe catchment, and its position in relation to the rest of South Africa and, (b) in relation to the Cape Flats Aquifer (CFA)
Adapted from: (a) Adelana et al. (2010), & (b) Okedi (2017)

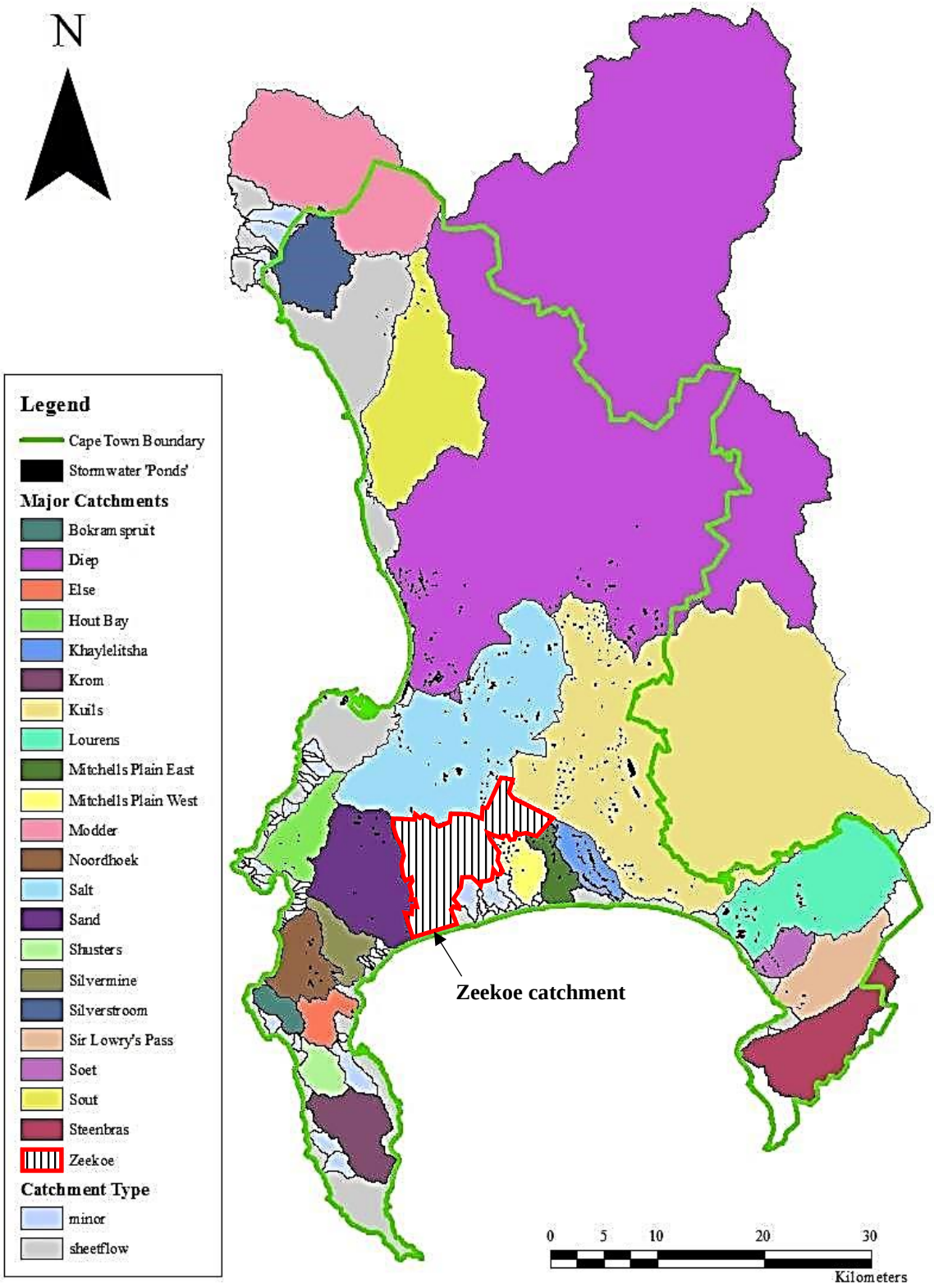

Figure 3-4: Map depicting the location of Zeekoe catchment in relative to all major catchments in the city of Cape Town
Adapted from: Rohrer (2014)

3.3 Land Ownership / Uses

Like many urbanized areas, the Zeekoe catchment is highly impacted by various land uses, socioeconomic variations, and different affluence areas. Moreover, the catchment's abiotic characteristics have been altered extensively by stormwater drainage as well as input from the Cape Flats Wastewater Treatment Works (WWTW) (Bickerton, 1982). Additionally, urbanization has resulted in a subsequent hardening of previously pervious surfaces as well as canalization of main watercourses, particularly the Lotus River. For instance, Cape Town International airport is located on the high north-eastern area of the catchment whereas the central-eastern part is predominantly the Philippi Horticultural Area (PHA), owned by small plot holders and used mainly for urban agriculture. Industrial areas are distributed in regions near the airport, to the west, as well as south-west portions of the catchment. The remainder of the catchment is occupied by residential areas varying in affluence levels generally from very low (i.e. high-density informal settlements with mass unemployment, poverty-related problems, and basic communal services), to medium-high (i.e. medium to low density, formal settlements which are well serviced; some with medium-sized gardens). Figure 3-5 shows a map of the different land uses in Zeekoe the catchment.

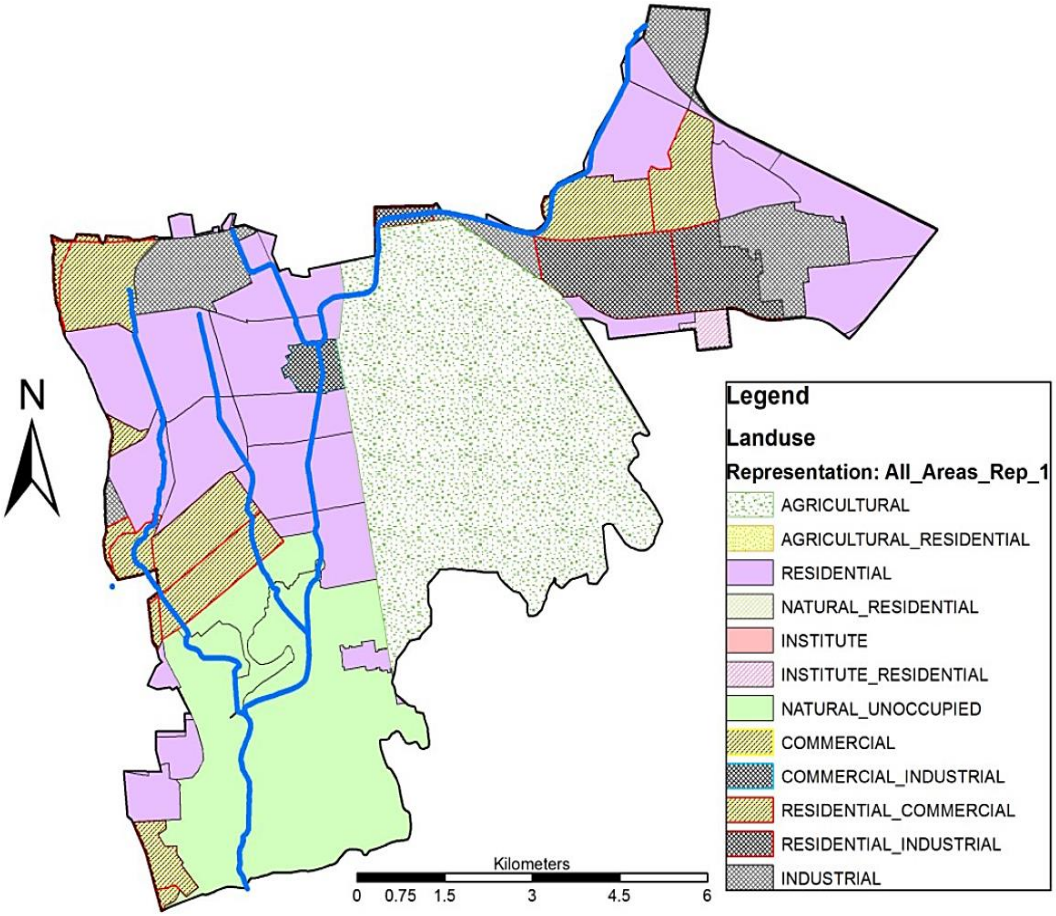

Figure 3-5: Land use within Zeekoe catchment
Source: Okedi (2017) after CoCT (2012)

3.4 Climate

Cape Town's climate is characterised by wet cool winter months between May and August (with average rainfalls below 80 mm/month) and dry warm summer months between September and April (with average rainfall from 80 – 295 mm/month). Significant variations in the region's climate exist due to the mountainous nature of the Cape Fold Mountain range which stretches along the southern and western coastlines of South Africa Adelana (2010). To provide a reasonable description of the Zeekoe catchment's climate, only data recorded at the Cape Town International Airport's (CTIA) weather station was considered in this research because of its proximity to the study area

Historical temperature records (Figure 3-6-a and b) over 73 years (1933 to 2006) reveal a general increase in temperature over the years, with a mean of approximately 17.5 °C. Rainfall data from the years 1841 to 2016 demonstrates large variations in the annual rainfall throughout the 175 years (Figure 3-7). No distinct trend is notable; however, the rainfall generally lies within a range of 400 to 800 mm/a, with a minimum of 230 mm recorded in the year 1935.

Wind statistics based on data collected over seven years (i.e., 2000 to 2017) at the airport indicate that the wind direction in the study area changes seasonally (Windfinder, 2017). During the summer months, the wind blows in the northeast direction at speeds ranging between 41 to 71 km/h., while in winter months, it blows towards the southeast at lower velocities between 33 to 41 km/h (Windfinder, 2017).

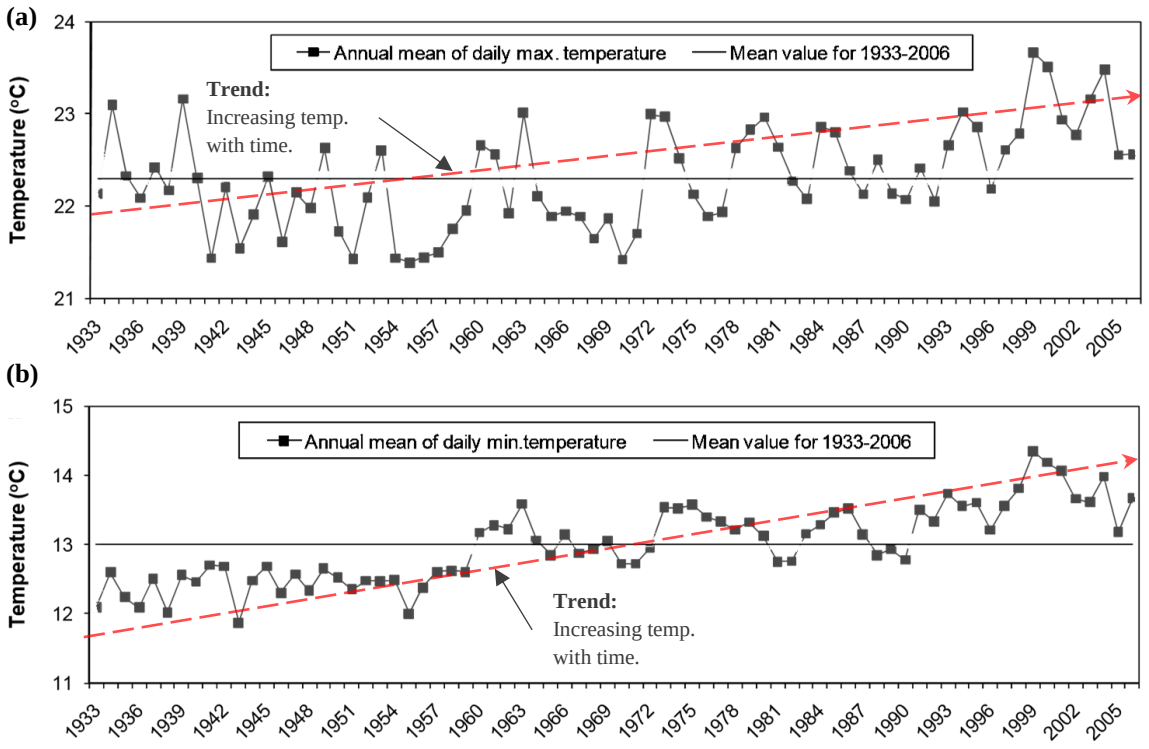

Figure 3-6: Historical climate data (a) Maximum temperature, (b) Minimum temperature
Adapted from: Adelana et al. (2010)

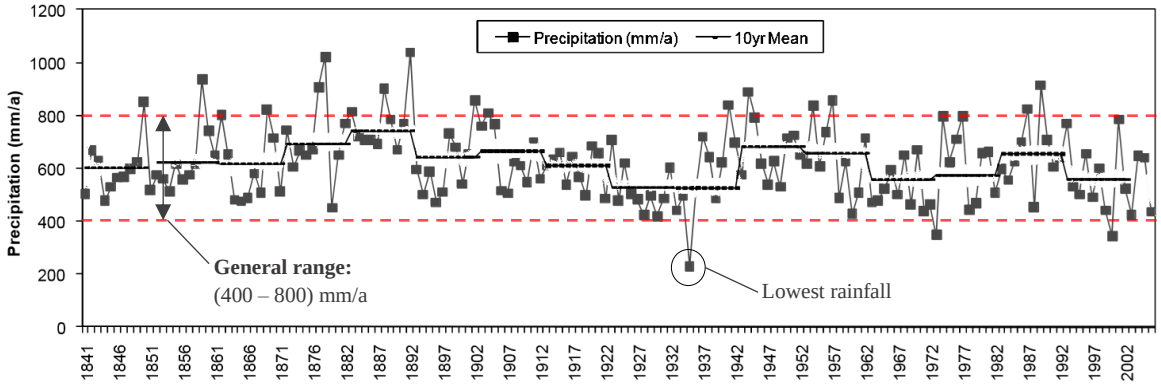

Figure 3-7: Historical climate data - rainfall
Modified from: Adelana et al. (2010)

Average monthly evaporation and rainfall data around the catchment area is presented in Figure 3-8. The evaporation data was recorded at three stations in the Zeekoe catchment managed by the Department of Water and Sanitation (DWS) using a Class A Evaporation Pan (Okedi, 2017). Cumulatively, the evaporation, based on the data presented, is 586 mm with an annual average of approximately 49 mm/a (i.e., 586/12).

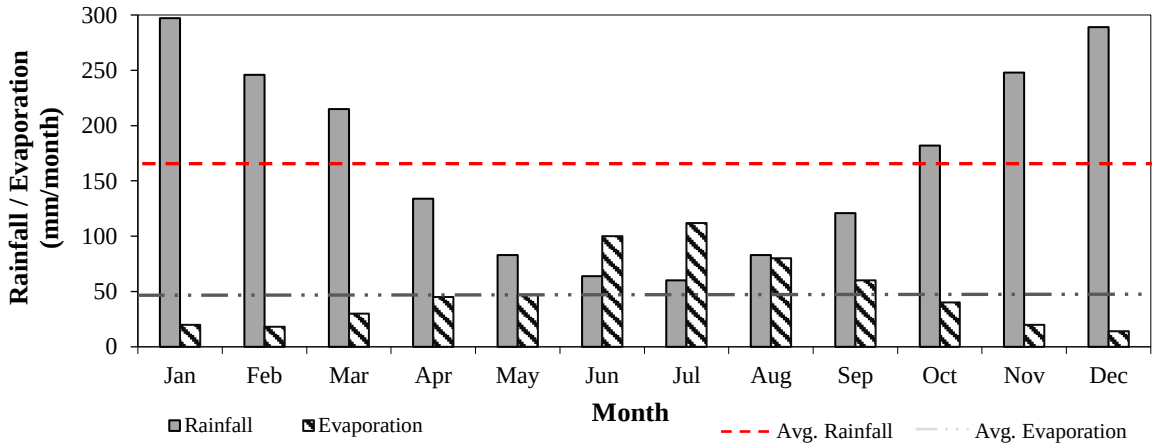

Figure 3-8: Average monthly rainfall and evaporation in the study area
Modified from: Okedi (2017) after DWS (2015)

From the rainfall and evaporation data presented, it is evident that this study's field infiltration investigation carried out during April 2017 (described in Chapter 4) was completed during a relatively high rainfall period with low evaporation. Consequently, groundwater recharge during this season was expected to be significant as the rainfall occurs during a period of low evaporation. The observed reduction in average rainfall, over time, emphasizes the need for alternative water resources in the city.

Figure 3-9 shows the negative impact of reduced rainfall on the city's main dams during the prolonged drought of 2015 – 2018. Furthermore, because evaporation is a function of temperature, and the observed historical trend is a general increase in temperature (Figure 3-6),

storing water underground as opposed to on the surface will, not only act as an alternative water resource but mitigate water losses associated with high-temperature conditions.

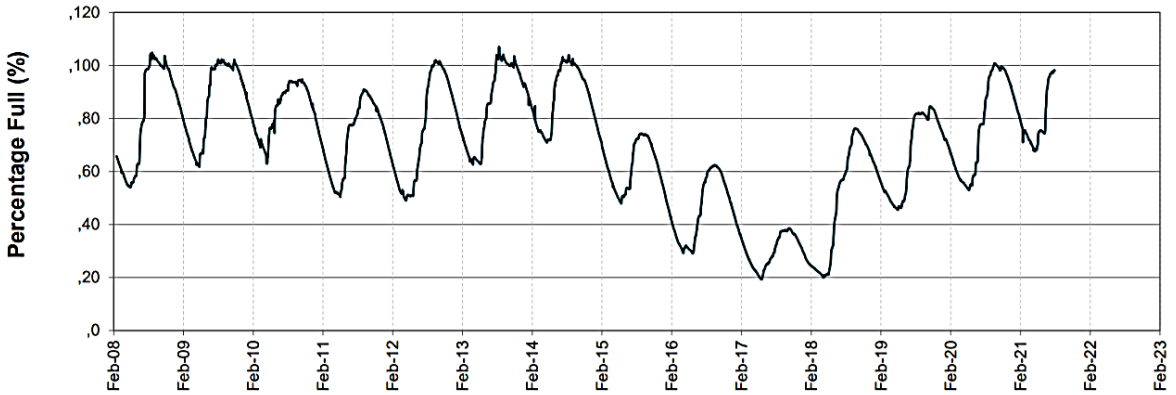

Figure 3-9: Western Cape water supply system storage record (2018 – 2021)
Source: City of Cape Town; Weekly Water Dashboard (2021)

3.5 Regional Geology

3.5.1 General Description

The Cape Flats Aquifer's (CFA) topography is characterized by mostly low-lying flat plains between the Cape Peninsular Mountain Range (west) and the Hottentots-Holland Mountain Range (east). Historically, the mountains were off-shore islands, divided from the mainland by a shallow channel. This division was integrated by the formation of enlarged reinforced sandbars (or tombolas) formed by the recent stabilization of sea levels and an accumulation of sands (Brumer, 1981).

The geology of the area is characterized by Quaternary-age (i.e. earlier than 2.58 million years) sediments of the Sandveld Group underlain essentially by the residual bedrock of the Malmesbury Group (Wright & Conrad, 1995; Giljam, 2002). The Cenozoic deposits consist of formations from different periods. From the Middle and Late Miocene: the Elandsfontein and Saldanha formations respectively; from the Pliocene: the Varswater formation; from the Pleistocene: the Milnerton, Velddrift, Langebaan and Witzand formations. The geology underlying this area gives rise to soil with minor variations across the plain. A brief description of the Cenozoic formations of Cape Town is presented in Table 3-1.

A prominent characteristic of the sediments in the study area is the dominant presence of shelly material. Consequently, the groundwater has a high calcium carbonate content resulting in the formation of calcrete deposits near the water table. Calcareous deposits, however, are more concentrated nearer to the sea, along the Falsebay coastline (Tredoux et al. 1980).

Table 3-1: Cenozoic formations of Cape Town
Adapted from: Adelana et al. (2010) after Theron et al. (1992)

Group	Formation	Description	Epoch		Age in Myr
Sandveld	Witzand	Aeolian, calcareous, quartzose sand	Holocene		1.7
	Langebaan (Wolfgat)	Aeolian, calcrete-capped, calcareous sandstone	Pleistocene		
	Velddrif	Littoral, calcrete-capped coquina			
	Milnerton	Fluvial gravel, marine clay, and littoral sand			
	Springfontyn (Philippi)	Aeolian, quartzose sand with intermittent peaty clays			
	Varswater	Quartzose and muddy sand, and shelly gravel, phosphate-rich	Pliocene		5.2
	Saldanha	Conglomeratic sandy phosphorite	Late	Miocene	22
	Elandsfontyn	Angular quartzose gravely sand and peaty clays	Middle		

Of the various formations which make up Cape Town's geology, the Zeekoe catchment area is predominantly underlain by deposits of the Witzand and the Springfontyn Formations (Condrad, 2014). An expanded description of these two formations is presented below:

1. Witzand Formation

The Witzand Formation is the earliest formation consisting of calcareous coastal dunes occurring towards the east of Swartklip between the suburbs of Wolfgat and Muizenberg. The dunes are unconsolidated and partially vegetated comprising of very coarse calcareous sands with an abundance of shells and shell fragments (Write & Conrad, 1995; Conrad, 2014).

2. Springfontyn Formation

According to Hartnady & Rogers (1990), the Springfontyn Formation is generally an aeolian formation (i.e. the sediments are wind-deposited materials) comprising of fine to medium-fine quartzose sands, increasing in grain size with depth. The formation is relatively uniform with occasional localized calcareous and peat lenses discovered within most of the central regions of the aquifer (Wright & Conrad, 1995; Vandoolaeghe, 1989). Because of the relatively pure nature of sands (i.e. 99.5% silica) in the Philippi area, they have been mined and used to produce high-quality glass (Wright & Conrad, 1995). Another area that possesses sands of similar characteristics is Atlantis on the west coast; an area used for managed aquifer recharge (MAR) and groundwater and abstraction (Hartnady & Rogers, 1990).

Vandoolaeghe (1989) proposes the Springfontyn Formation to be some decalcified facies of the Witzand formation because whenever one formation is dominant in an area, the presence of the other is insignificant. He adds by suggesting that this decalcification can be owed to the

high surface and subsurface permeability of the deposits which are conducive to groundwater recharge and subsurface flow.

The underlying basement rock of the study area is made up of Precambrian metasediments belonging to the Malmesbury Group which form part of the Tygerberg Formation (Vandoolaeghe, 1984). Sediments of the Malmesbury Group comprise mainly of schists, grey to green phyllites, greywackes (impure sandstone), and shales (Conrad, 2014). The sediments are mostly heavily weathered except for those present less than ten metres below sea level (Vandoolaeghe, 1984). Because the gradient of the bedrock slopes towards the south-west direction, its depth varies substantially at different locations, rising to 80 metres above sea level (masl) in Belville, dropping down to 20 metres below mean sea level at the airport, and below 40 masl at Zeekoevlei) (Wright & Conrad, 1995; Conrad, 2014).

3.5.2 Geological Cross Sections

The variability of subsoil material increases with depth (Shreurs, 2001). An example of this can be seen from a typical subsurface geological cross-section (Figure 3-10(a)). Seven types of sedimentary deposits have been observed to a depth of 10 km. For design and modelling purposes, simplified cross-sections (Figure 3-10 (b)) are often produced to ease the analysis of models and to compute speedy preliminary estimations.

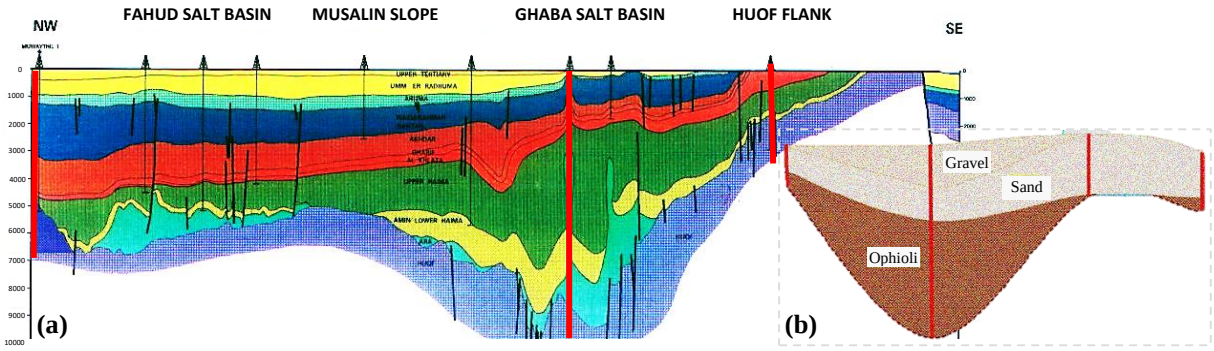

Figure 3-10: (a) Typical subsurface geological cross-section up to 10 m and, (b) simplified cross-section
Adapted from: Schreurs (2001)

The main geological features of the Cape Flats have been mapped by Tredoux et al. (1980) as illustrated in Figure 3-11-a. A cross-section, line A-B-C, spanning towards the west (line A-B) and north-eastern directions (line B-C) of the Zeekoe catchment clearly shows the low-lying topography of the study area (Figure 3-11-b). The relative heights of the Cape Peninsular and the Hottentots-Holland Mountain Ranges on the west and east, respectfully, of the study area, can be seen from the cross-section. Similar horizontal sandstone formations have been discovered within these mountain ranges' peaks. In between the mountains, post-Palaeozoic erosion of sandstone has, over time, resulted in the consequent formation of Cape Flats (Reid et al., 1993; Hartnady & Rogers, 1990).

More locally, a geological map of the area around the Zeekoe catchment is illustrated in Figure 3-12, with seven section lines drawn around the region, labelled: L-L', H-H', G-G', F-F', E-E', D-D', and A-B-C.

Geological cross-sections (Figure 3-13) associated with each of the abovementioned section lines were suggested based on a conglomerate of previous and current regional studies (Henzen, 1973; Gerber, 1981; Vandoolaeghe, 1989; Adelana and Xu, 2008).

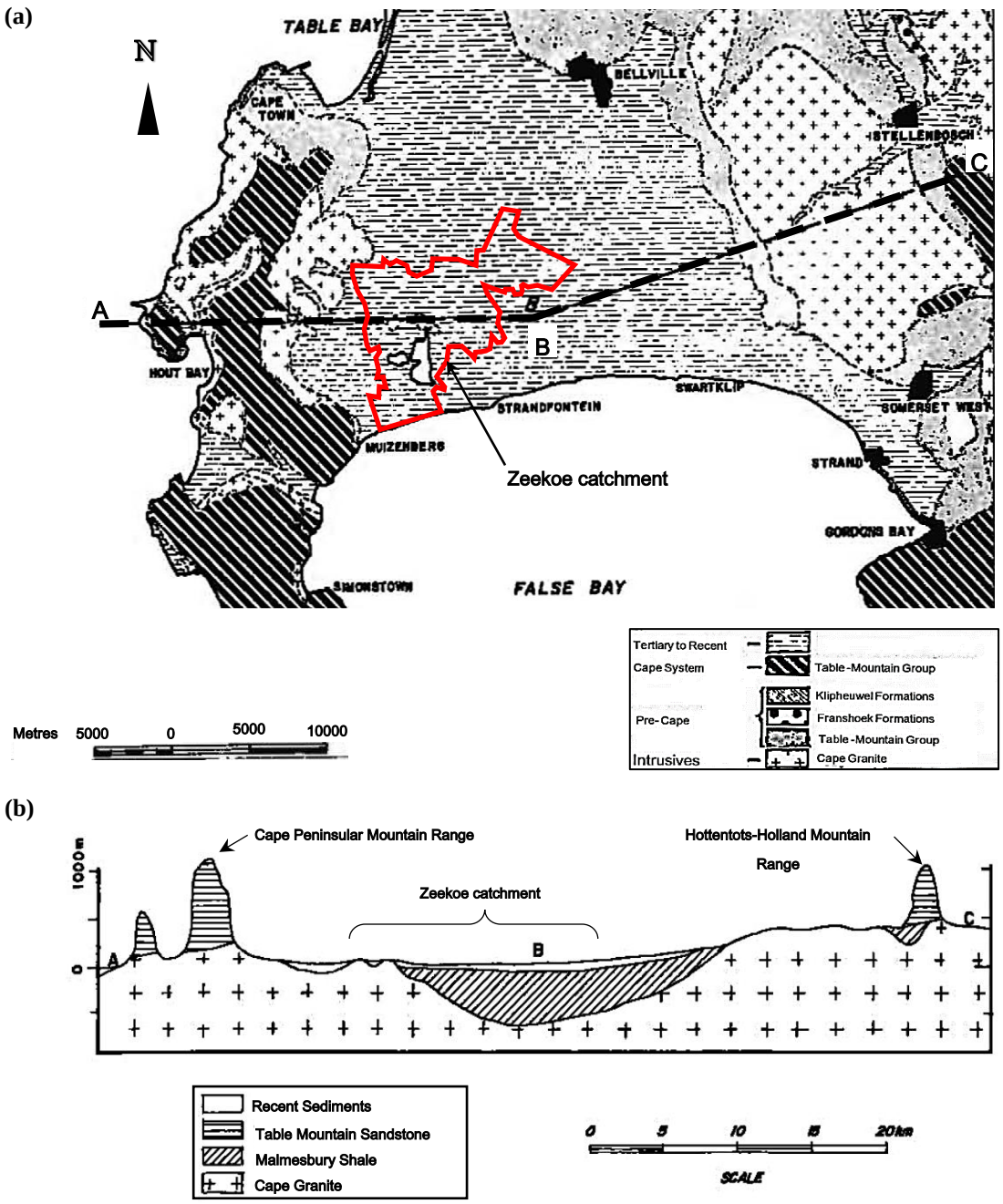

Figure 3-11: (a) Geological map and (b) Section ABC along the CFA
Modified from: Tredoux et al. (1980)

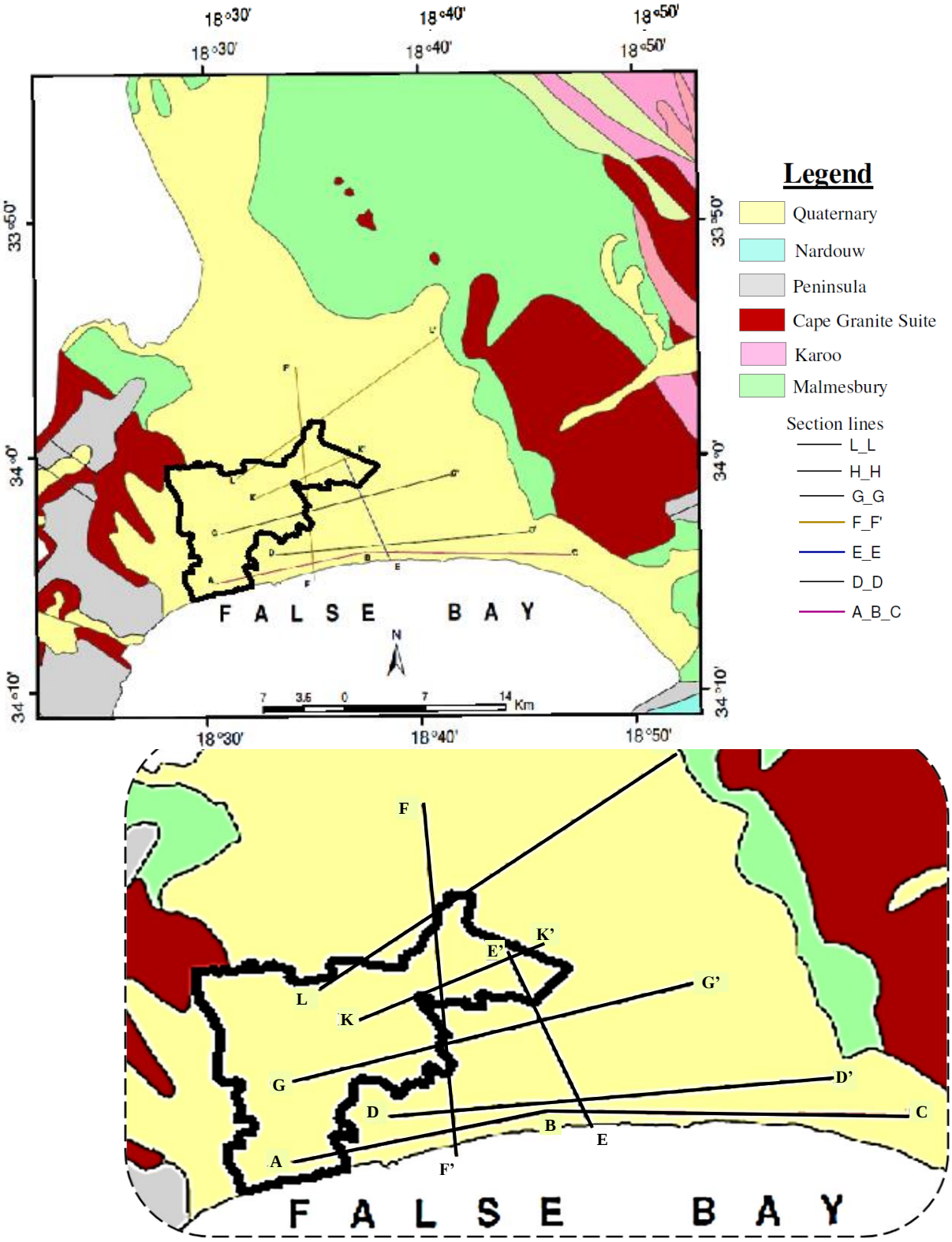

Figure 3-12: Geological map of the area around the Zeekoe catchment
Modified from: Adelana et al. (2010)

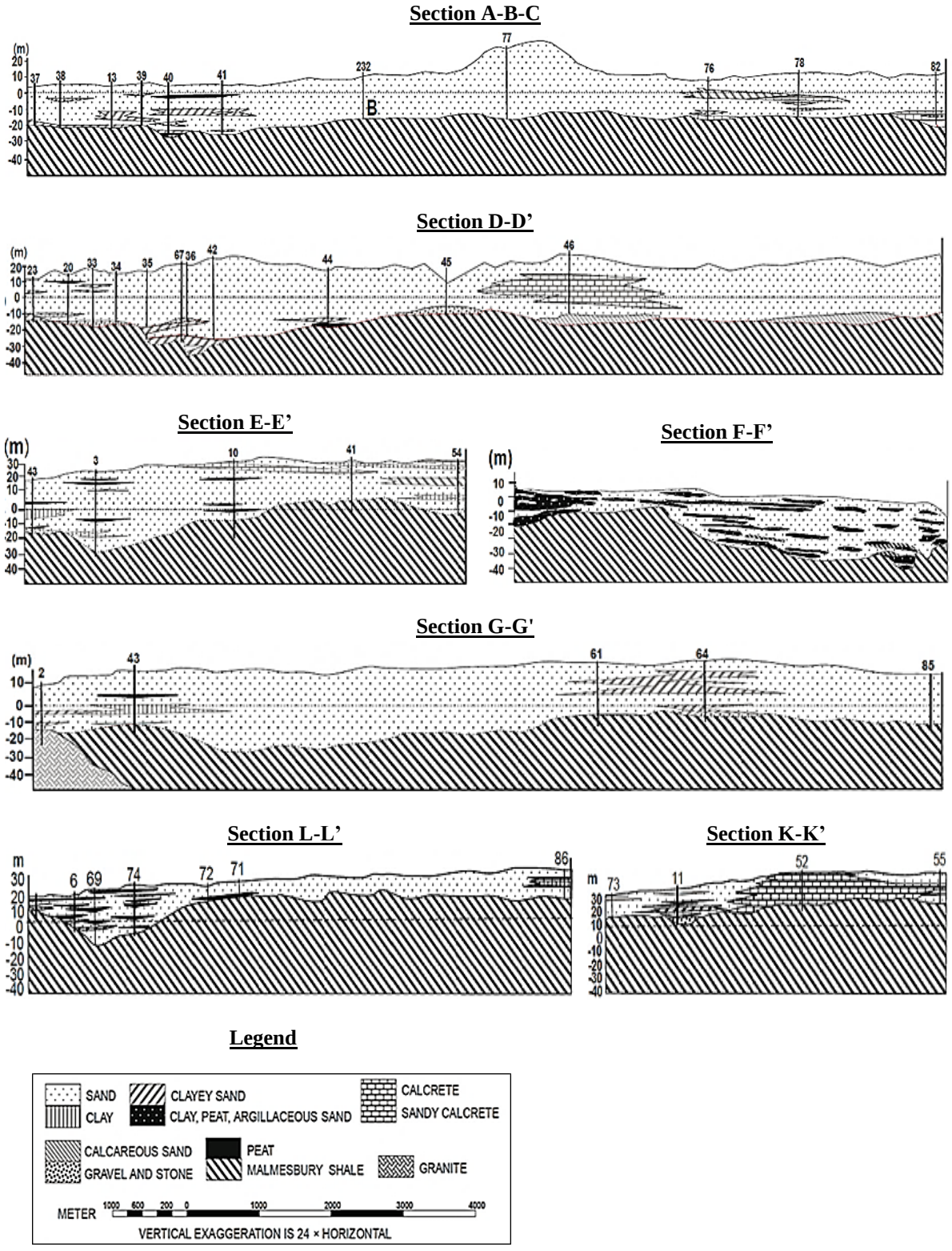

Figure 3-13: Geological cross-sections (lines indicated in Figure 3-12) illustrating the inter-relationships of sediments around the study area
Modified from: Adelana et al. (2010)

Non-intrusive field investigations have also been carried out within and adjacent to the study area by Mayer and De Beer (1981) and Smith (1982). They conducted various forms of geophysical explorations at wellfields located near the study area; the closest ones being at Punt Road in Philippi, and Mitchell's Plain (Figure 3-14-a). A comparison was done between the performance of the various geophysical methods, namely: gravimetric, refraction seismic, and the electrical resistivity method. The resistivity technique was found to not only be the most cost-effective of the three, but it also depicted a reasonably accurate and useful picture of the thickness and lithologies of the stratum formed during the Cenozoic era (Vandoolaeghe, 1984).

From the geological profile established using the resistivity method (Figure 3-14-b), a clear similarity in lithology, and layer thicknesses can be observed when compared to the geological sections in Figure 3-13. Both profiles generally indicate the presence of a thick calcrete and (or) sand layer on the surface, underlined by Malmesbury shale discoverable approximately 20 m above mean sea level.

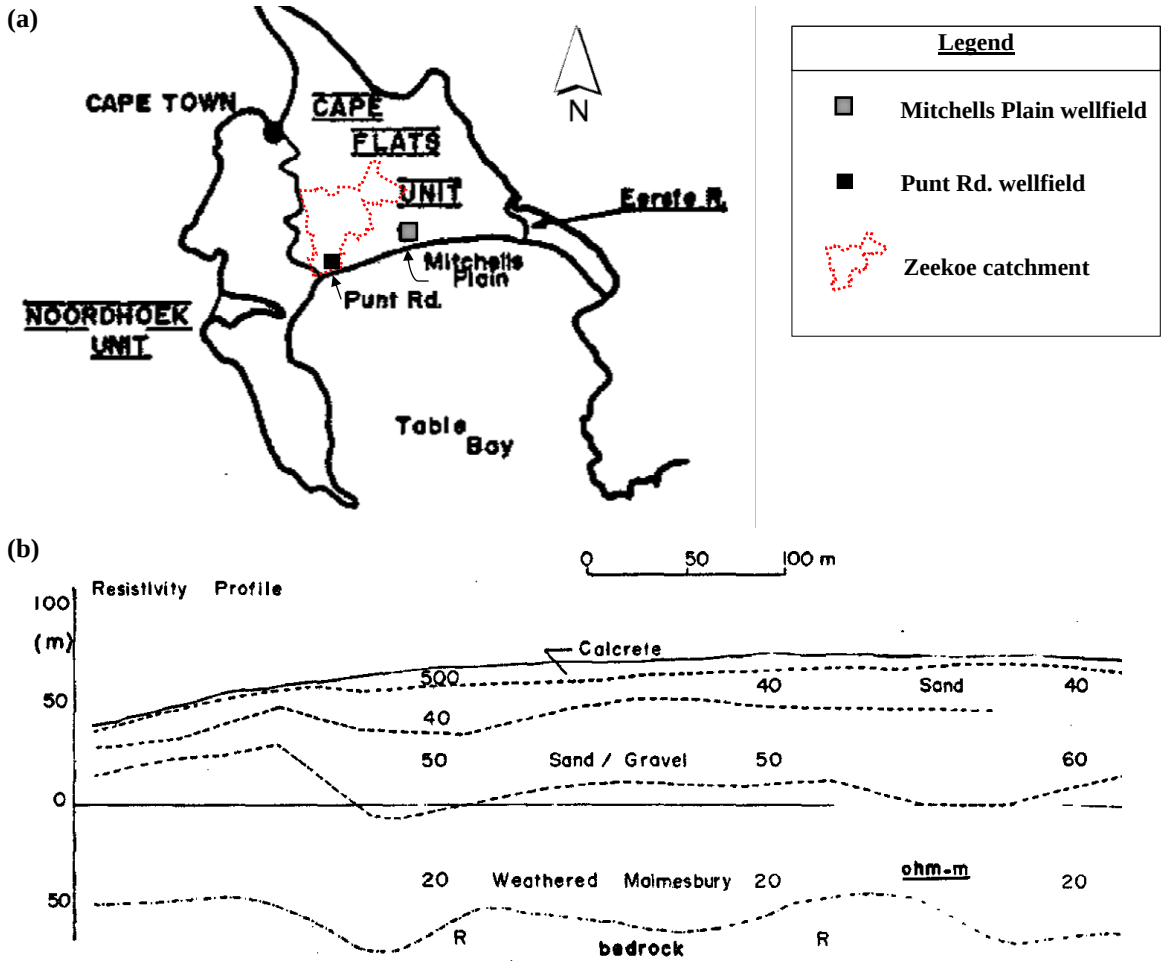

Figure 3-14: (a) Map indicating the location of Mitchells Plain and Punt Road wellfields and, (b) Resistivity profiles
Modified from: Vandoolaeghe (1984)

3.5.3 Borehole data

This study also looked into past project-related borehole logging data of sites situated within and around the Zeekoe catchment. The approximate drilling locations of the attained borehole logs are shown on the map in Figure 3-15.

The borehole data used for this study was provided by two private geotechnical companies (i.e., Fairbrother and Core Geotechnical Consults) solely for research purposes. Furthermore, six borehole logs (i.e., UWC1 -UWC-6) from the University of Western Cape (UWC) test site, obtained from Adelana et al. (2010), were also considered because of t their proximity to the Zeekoe catchment.

The soil interpretations in the borehole drill-log reports from private contractors (Figure 3-16) were relatively crude compared to those in the reviewed literature. Extracted soil specimens were visually classified by competent drill loggers without laboratory tests being conducted on them. Soil colours and general material types were described in the borehole logs. Because of the sensitive nature of some projects as well as intellectual property rights, some project details were omitted, however, the overall data about the general location and soil descriptions were included in this investigation. A description of the borehole locations and their associated sources is summarised in Table 3-2.

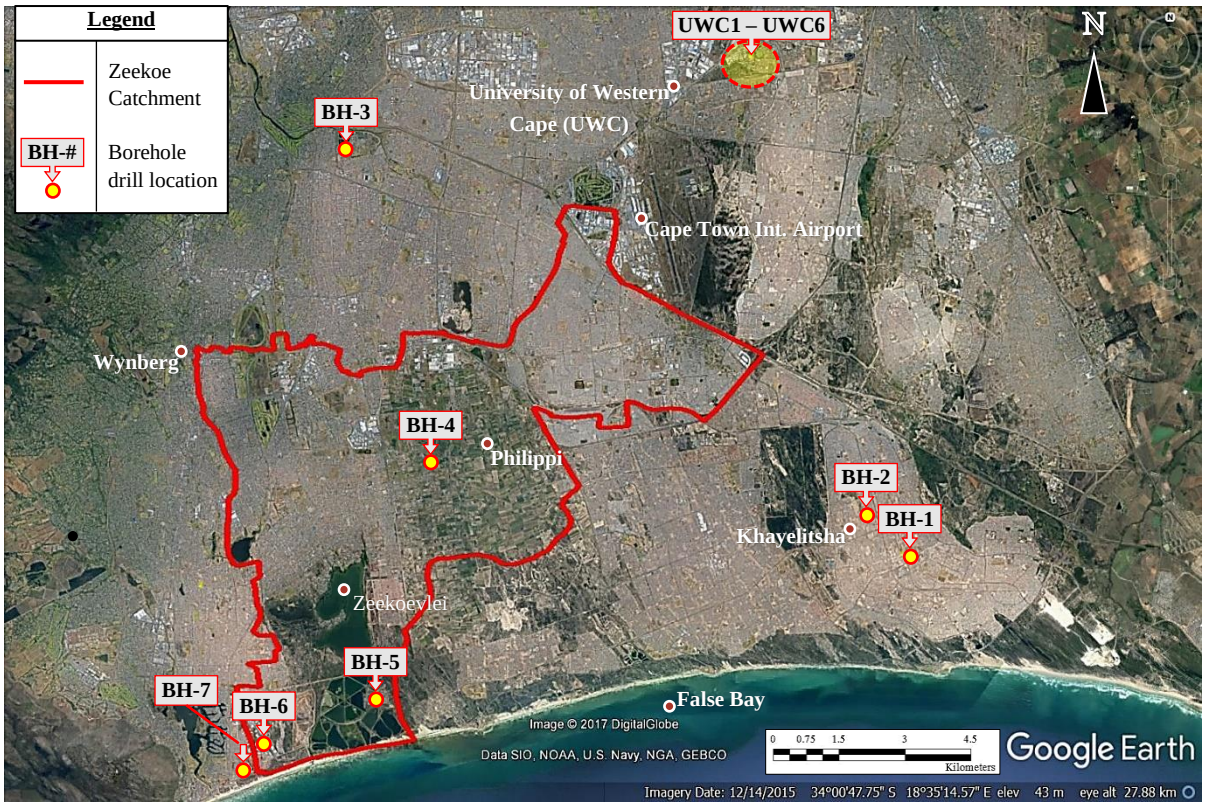

Figure 3-15: Map indicating borehole drill locations within and around Zeekoe catchment
Modified from: Google Earth (2017)

Table 3-2: Description of General Location and Source of Borehole Data

Borehole ID	Location / Area Description	Source
UWC1 – UWC6	Bellville	University of Western Cape
BH-1	Khayelitsha	Core Geotechnical Consultants
BH-2	Khayelitsha	Fairbrother Drill Company
BH-3	Athlone	Fairbrother Drill Company
BH-4	Philippi	Fairbrother Drill Company
BH-5	Muizenberg	Fairbrother Drill Company
BH-6	Muizenberg	Fairbrother Drill Company
BH-7	Muizenberg	Fairbrother Drill Company

Borehole drillings carried out at the UWC test sites reached depths ranging between 10 m and 105 m below ground level (Figure 3-17), whilst those conducted by private contractors were much shallower with minimum and maximum drill depths of 2 m and 25 m respectively (Figure 3-18). The borehole logs presented in Figure 3-18 were produced with the aid of six drill-log datasheets from Fairbrother, and a Geotechnical Investigation Report from Core Geotechnical Consultants totalling seven simplified graphical representations of the local soil strata. Because the terrain within and around the Zeekoe catchment area is relatively flat (Reid et al., 1993; Hartnady & Rogers, 1990), the ground level of each borehole does not vary significantly.

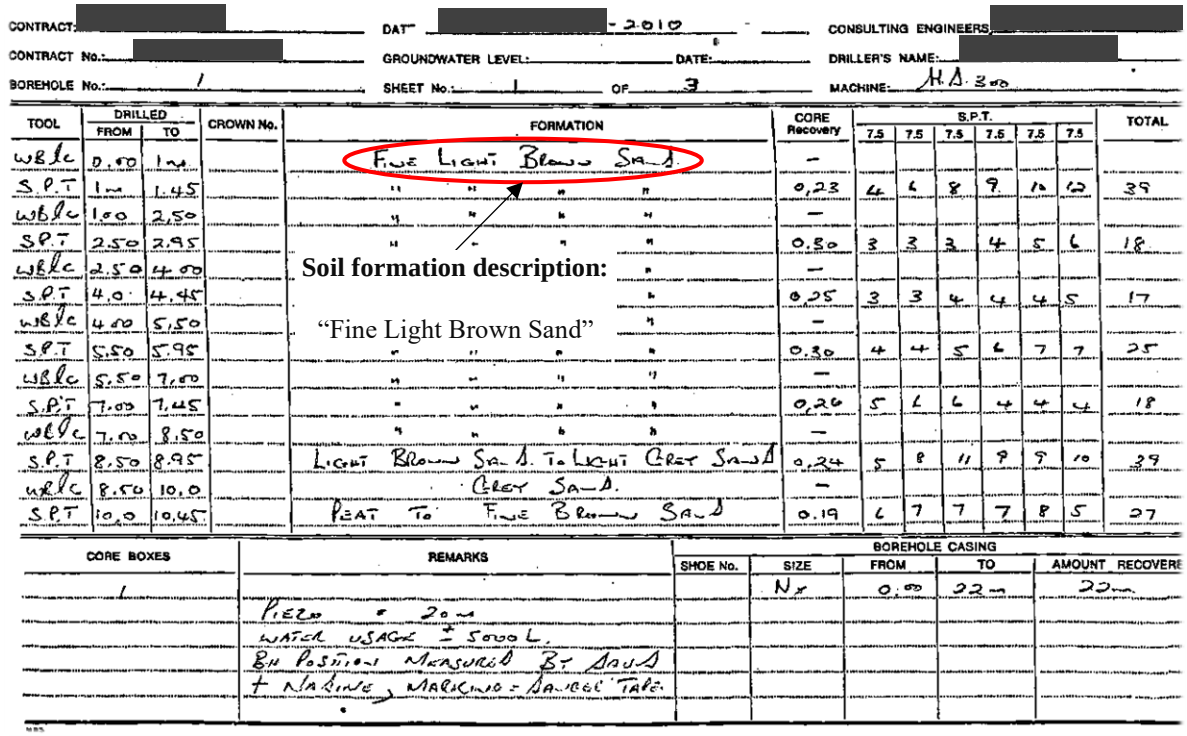

Figure 3-16: Sample page of borehole drill-log datasheet
Source: Fairbrother Drill Company (Pty) Ltd Drilling Report (2010)

Despite the shallow drill depths and limited soil classification from the drill reports, the defined materials were consistent with those from the UWC Test Site, as well as literary descriptions of the region's geology. A noteworthy consistency between the cross-sections shown in section 3.5.2 earlier, and the borehole log data, is the thick (30 – 40 m) overlying sandy layer (better described as 'Calcareous sand') consisting of occasional impervious clay or peat lenses which reach up to 15 m in thickness. Underlying the sandy layer, basement Malmesbury shale was discoverable from depths varying between 35 m and 105 m below natural ground level.

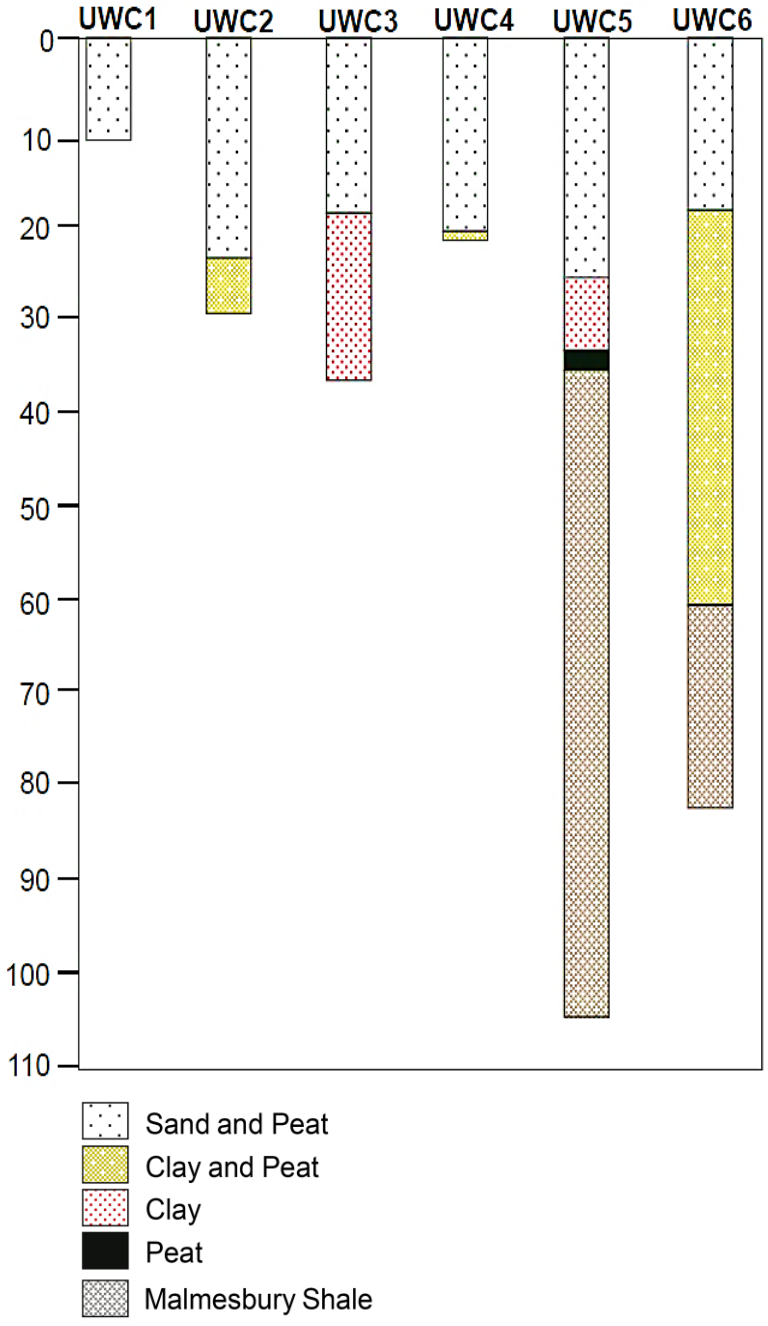

Figure 3-17: Litho-logs of monitoring wells drilled at UWC test site
Adapted from: Adelana et al. (2010)

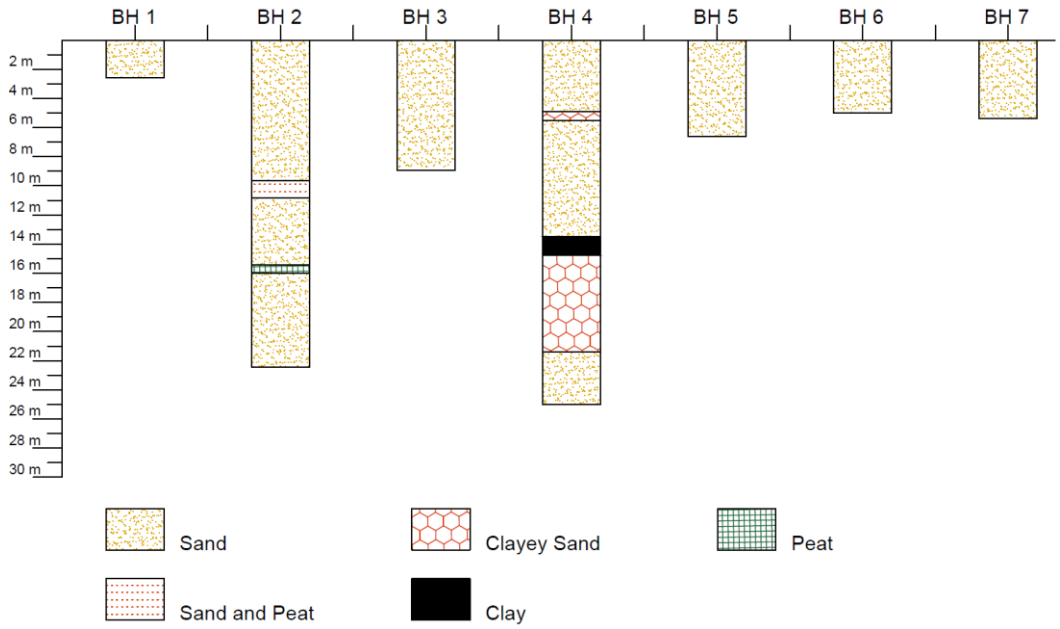

Figure 3-18: Borehole logs summarised from drill-log datasheets
Data from: Fairbrother Drill Company Drilling Reports

From the borehole logs in Figure 3-18, a three-dimensional perspective of the borehole locations and depths, in relation to the study area, was developed using Civil 3D AutoCAD software (see Figure 3-19). The key information required to generate the 3-D model was: the boreholes' coordinates (Table 3-3), and the depths and descriptions of each deposit. A vertical to horizontal scale ratio (i.e., V: H) of 1H:1000V was adapted to add emphasis on the vertical variation in sedimentary deposits in each borehole.

Table 3-3: Coordinates of borehole drill locations

Borehole ID	Location / Area Description	Latitude	Longitude
UWC1 – UWC6	Bellville	33°56'0.67"S	18°37'40.65"E
BH-1	Khayelitsha	34° 2'52.01"S	18°40'27.36"E
BH-2	Khayelitsha	34° 2'20.62"S	18°39'51.21"E
BH-3	Athlone	33°57'21.18"S	18°30'38.13"E
BH-4	Philippi	34° 1'38.57"S	18°32'11.35"E
BH-5	Muizenberg	34° 4'56.61"S	18°31'19.05"E
BH-6	Muizenberg	34° 5'36.13"S	18°29'21.48"E
BH-7	Muizenberg	34° 5'59.50"S	18°29'0.77"E

The inclusion of more borehole data for a given area can significantly increase the accuracy of a 3-D subsurface profile because less area would need to be interpolated. Based on available borehole log data, this investigation was limited to developing a foundation on which larger and more detailed subsurface geological maps can be generated further. Vandoolaeghe (1984)

stressed that to obtain an accurate reliable regional management model, “many more boreholes would be required to reach these objectives”.

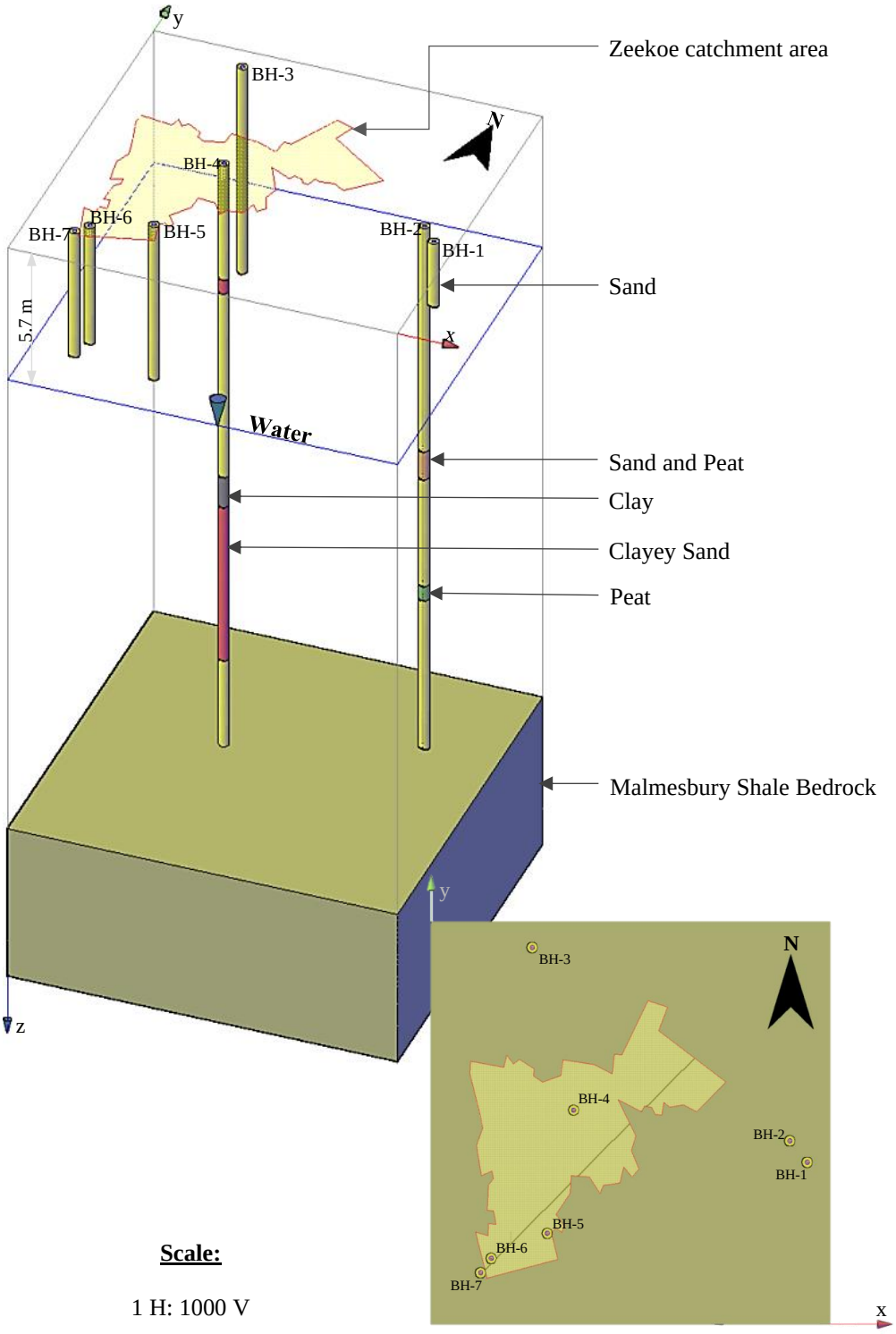

Figure 3-19: Plan-and 3D-view of borehole logs around the Zeekoe catchment

3.6 Regional Hydrogeology

3.6.1 Surface Water

Four main water bodies form part of the stormwater, and wastewater drainage systems in the Zeekoe catchment area, these are Princessvlei, Rondevlei, Zeekoevlei, and the Cape Flats WWTW (Figure 3-20). Using Google Earth's (2017) Path function, the total drainage length (along the channel) from the Cape Town Internal Airport (CTIA) to the mouth of the Zeekoe canal, was traced and measured to approximately 20 km which is comparable to the 18 km approximated by Heydorn & Grinley (1982) from the Cape Town City Council Map TPX 8770.

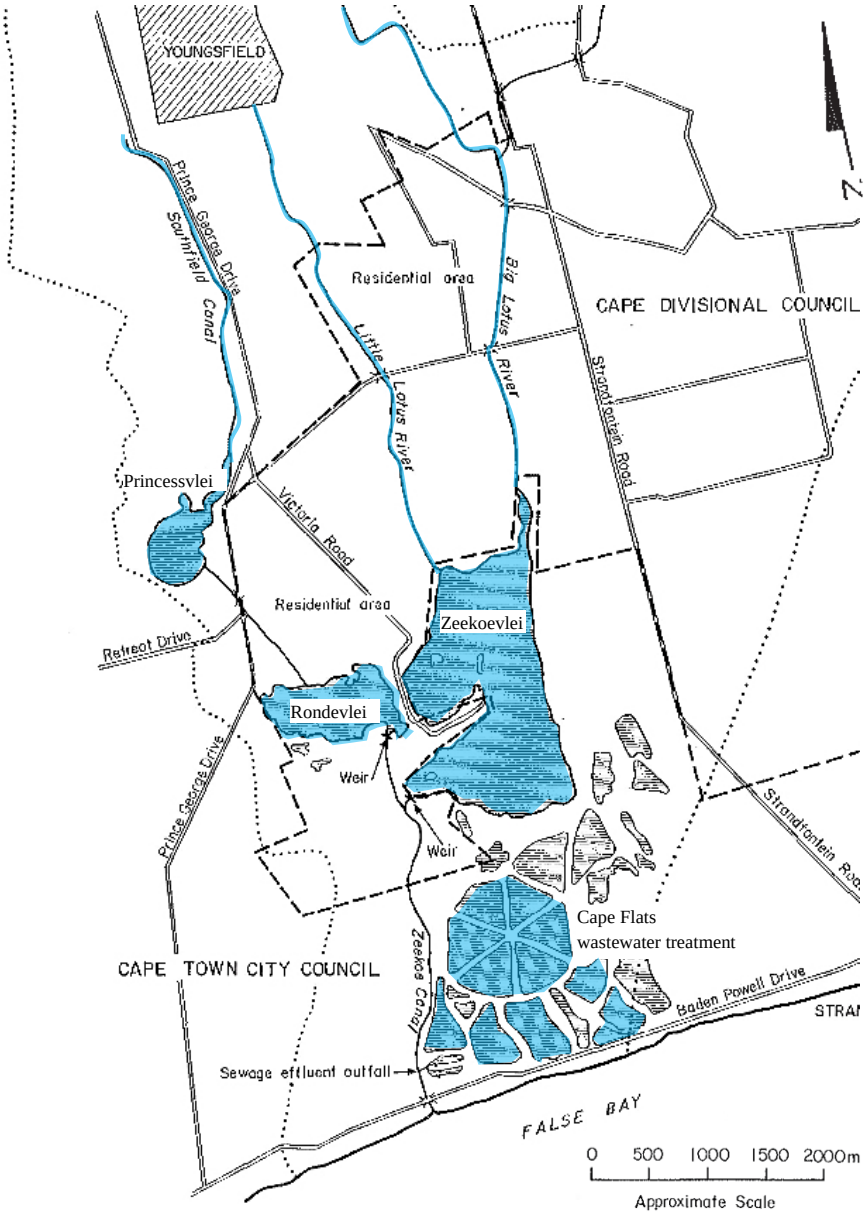

Figure 3-20: Major components of the Zeekoe drainage system
Modified from: Heydorn & Grinley (1982)

The current stream systems flowing on the Cape Flats Aquifer's surface are Lotus River, and Kuils-Eerste River System (Giljam, 2002). A summarised description of each river system is presented in Table 3-4.

Table 3-4: Stream systems on the Cape Flats
Source: Giljam (2002) after Hartnady & Rogers (1990)

Stream System	Description
Lotus River	This River begins from the far north of the Zeekoe catchment area, at Cape Town International Airport, and enters the Zeekoevlei complex.
Kuils-Eerste River System	Ascending from the northeast of the Cape Flats, the river has been limited from entering the sea due to the Late Pleistocene aeolianites of the Langebaan formation. Consequently, it flows east joining the Eerste River

3.6.2 Ground Water Table and Aquifer Depth

The Cape Flats Aquifer is generally unconfined with a maximum thickness of 45 – 50 m along the False Bay coastline, spreading in the northward direction to a thickness of 5 – 10 m (Figure 3-21 (a)). Relative to the average sea level, the water table's head elevation increases towards the northeast from nearly zero at the coast, to a maximum of 40 m as shown in Figure 3-21-b.

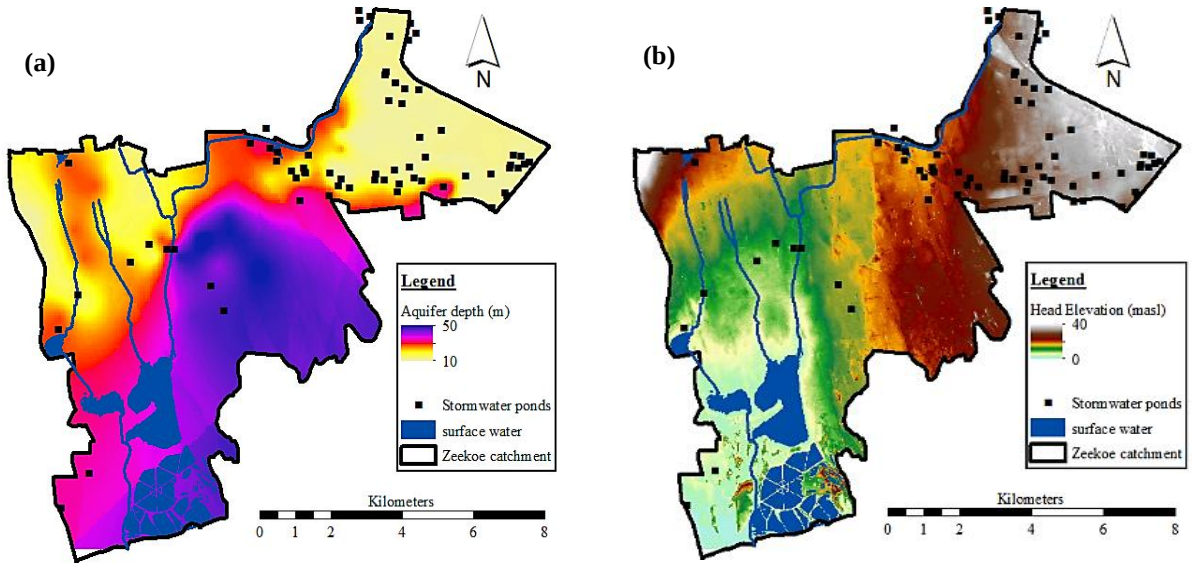

Figure 3-21: (a) Aquifer depth and (b) Water table head elevation of Zeekoe catchment
Adapted from: Adelana et al. (2010) & Okedi (2017)

Data on long-term fluctuations of groundwater levels within the Cape Flats Aquifer is very limited. The University of Western Cape (UWC) however, has conducted continuous monitoring of groundwater levels by drilling several research boreholes equipped with water-level sensors and data loggers (Conrad, 2014). No reports were attainable, yet it was possible to obtain continuous groundwater level data from two of the research boreholes situated

approximately 2.8 km southeast of the Cape Town International Airport. Plotted in Figure 3-22 are the long-term groundwater level graphs throughout four to five years.

Between the years 2002 – 2006, a seasonal groundwater table fluctuation of around 0.7 m, with minimum and maximum levels of 4.9 meters below ground level (mbgl) and 5.6 mbgl, respectively, were observed from the UWC Logger 02 borehole data in Figure 3-22 (a). From Figure 3-22 (b), the natural groundwater fluctuation recorded in the UWC Logger 06 borehole was approximately 0.9 m, whilst the water table depth ranged between 5.2 and 6.1 mbgl, with an average of about 5.7 m. It has been assumed that barometric pressure corrections were taken into account.

Another hydrological study was conducted by Geohydrological and Spatial Solutions (GEOSS) International during the year 2013, from summer to winter, at a proposed development site in Belhar. The Belhar study area is situated about 3 km northeast of the airport. Groundwater levels measured from six installed piezometers revealed greater fluctuations in the groundwater level than at the UWC Test Sites. The greatest variation in the groundwater level was recorded to be 1.7 m with the lowest being approximately 1.6 m (Conrad, 2014 after GEOS, 2013).

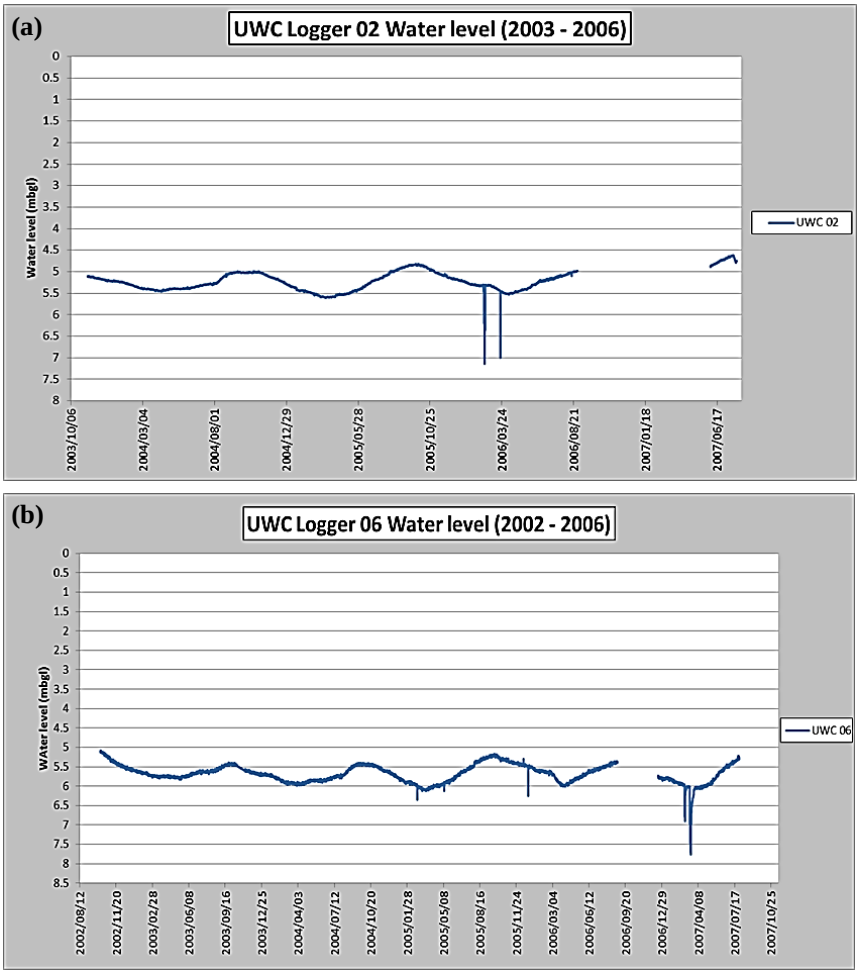

Figure 3-22: Long term groundwater level graphs from UWC research boreholes
Source: Conrad (2014)

3.6.3 Groundwater Movement

The hydrology of Cape Flats Aquifer was dominated by preferential flow paths originating from paleochannels (i.e. ancient river channels) of the Kuils, Lotus, and Elisieskraal Rivers (Hay et. al., 2015). Often infilled with granular or coarse fluvial deposits, paleochannels possess considerable water storage and transmission characteristics. Moreover, when below the water table, these ancient river channels are often targeted as water resources by farmers and households with abstraction pumps (DWA, 2017).

The flow path of the regional groundwater is comparable to that of the river courses. Groundwater movement around the study area is towards the south, descending from Belville to False Bay (Figure 3-23). Additionally, the groundwater paths appear to be directed towards regions of great aquifer thickness like the Zeekoe catchment area.

Because the CFA is regionally unconfined and free of lateral or geological boundaries, its proximity to the sea could have a substantial influence on groundwater discharge into the sea. This discharge may occur through permeable bottom sands where the aquifer is hydrologically connected to the sea (Swarzenski et al., 2001).

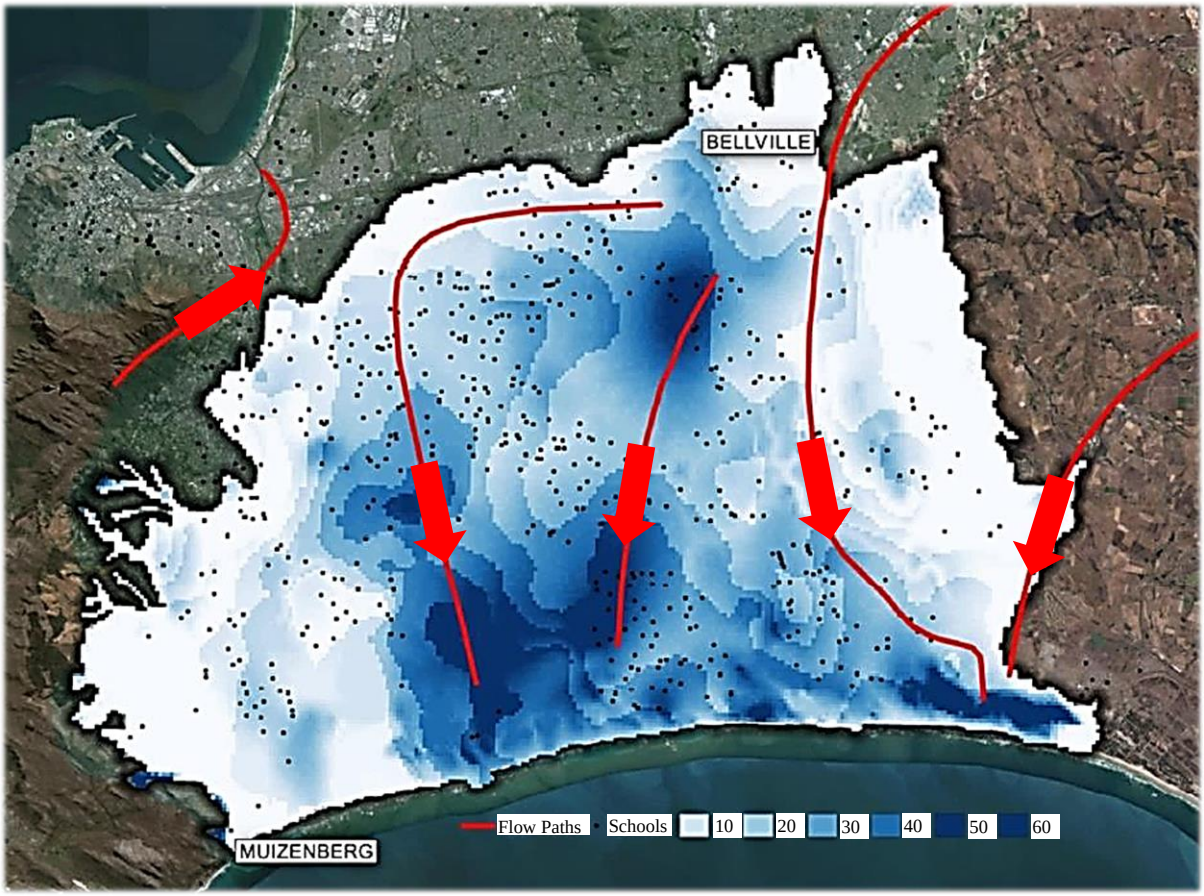

Figure 3-23: Groundwater flow path and aquifer thickness around the Zeekoe catchment
Modified from: Hay et. al (2015)

3.6.4 Hydraulic Parameters of Aquifer

Numerous hydrological investigations have been conducted in the CFA to determine the district's hydraulic properties. Okedi (2017) undertook a study that carried out a water-demand and stormwater resource assessment for Cape Town, with a focus on the Zeekoe catchment. Based on modelled results, he proposed that groundwater yields were greatest (above 5 l/s) on the south-eastern edges of the catchment area (Figure 3-24). This can be attributable to the increasing aquifer depth and soil characteristics towards the sea. Most of the region's groundwater yield was estimated to range between 2.0 – 5.0 l/s, with the lowest yields (0 – 0.5 l/s) towards the north-western region of the catchment. Another study discussed by Meyer (2001) observed, from a total of approximately 500 boreholes drilled around the Zeekoe catchment area, groundwater abstraction yields ranging between 0.5 and 2 l/s.

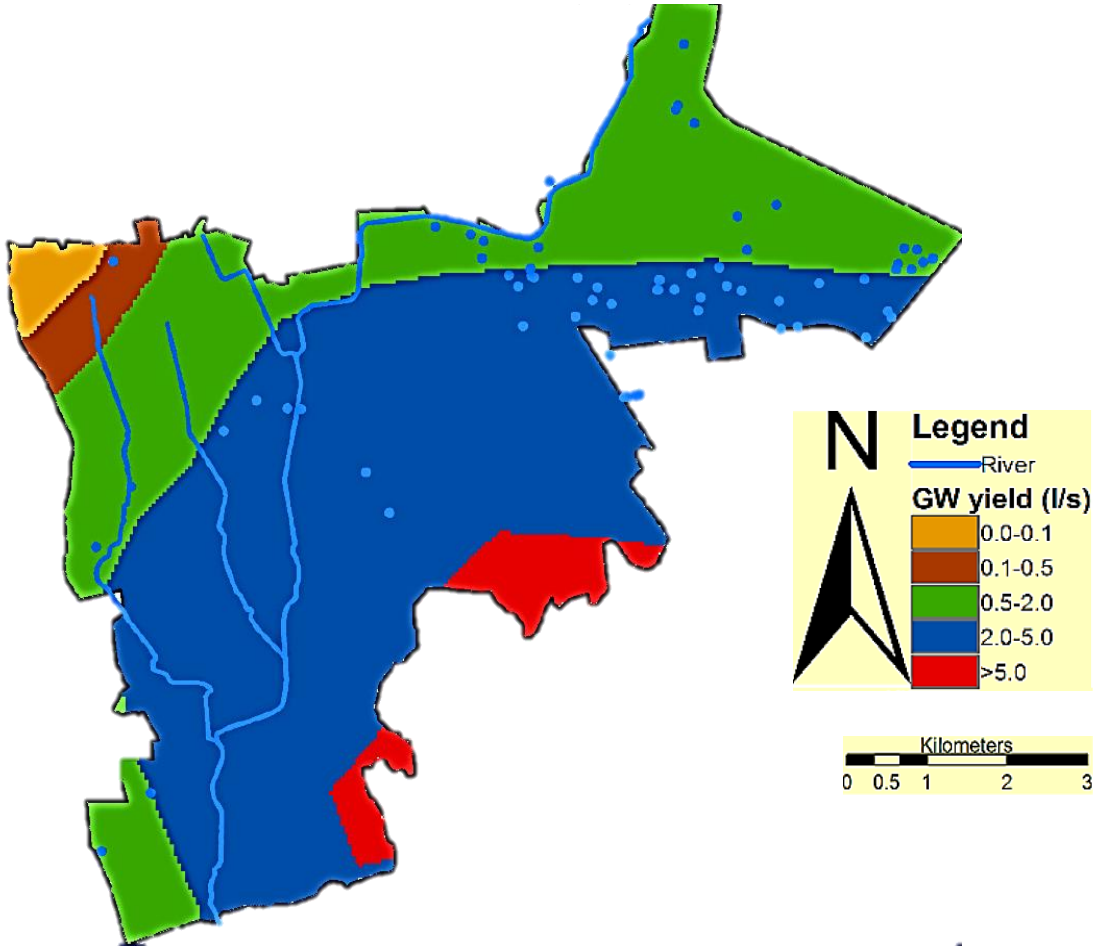

Figure 3-24: Map depicting groundwater yield in the Zeekoe catchment
Source: Okedi (2017)

A transmissivity distribution map (Figure 3-25) was produced by Gerber (1976) and Vandoolaeghe (1989) through their evaluation of the hydraulic conductivity of the Cape Flats aquifer. Gerber's (1976) findings suggested transmissivity values ranging between 50 – 650 m^2/d; these results corroborate a study by Adelana et al. (2010) which estimated average transmissivity values from 32.6 to 618.8 m^2/d. Because of the anisotropic nature of the deposits

in the study area, Gerber (1976) found, from a series of 26 abstraction and recovery tests (each lasting 20 days), the vertical permeability to be smaller by up to 100 times when compared to the horizontal permeability.

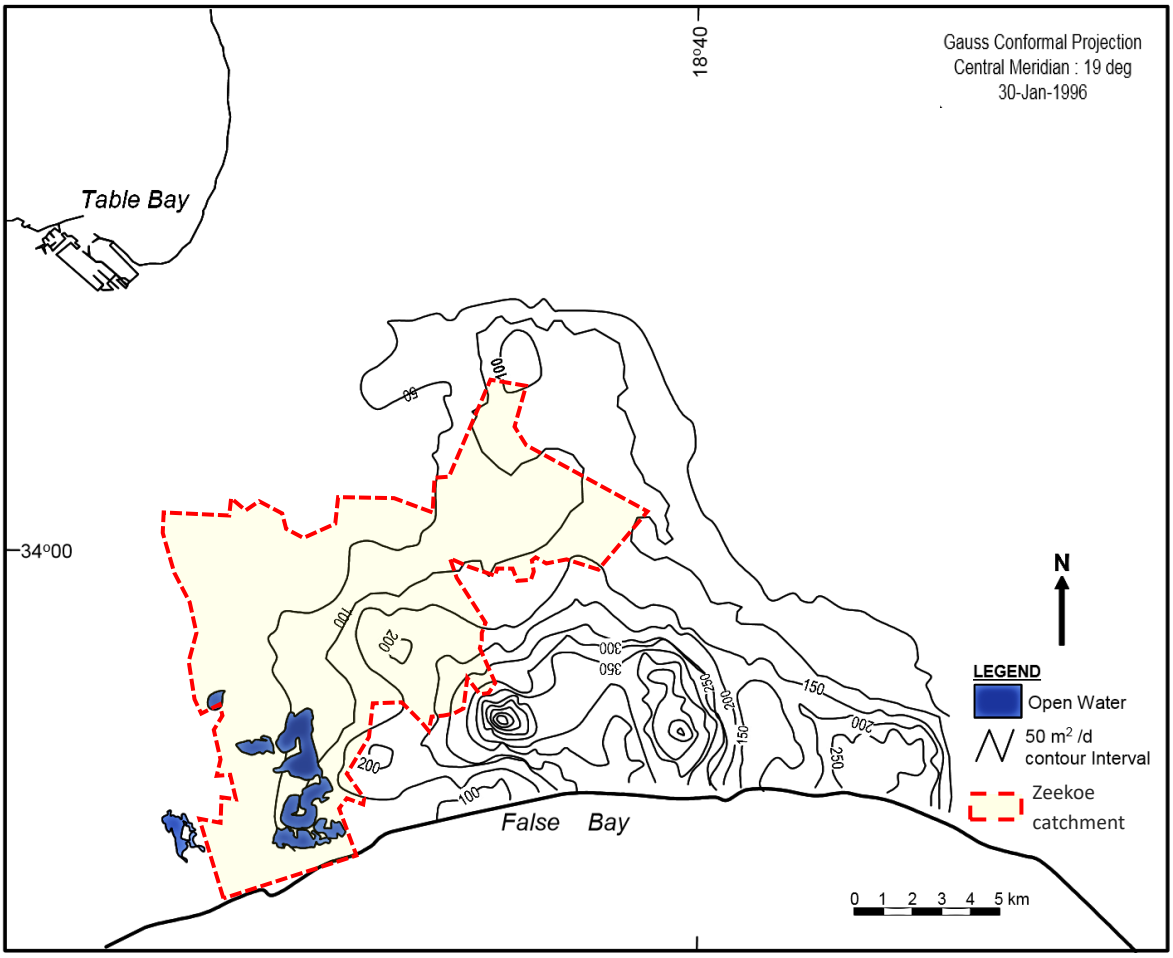

Figure 3-25: Transmissivity distribution map
Modified from: Adelana et al. (2010) after Wright and Conrad (1995): original data from Gerber (1981)

Tredoux et al (1980) assessed the suitability of the Cape Flats aquifer for artificial recharge and abstraction by extensive investigations into the geohydrological properties of the district. Their investigation included the drilling of several hundred exploratory wells and the acquisition of core samples according to the encountered strata. Particle-size distribution curves were determined through standard screening procedures on soil particles in the retrieved core samples.

Despite the presence of occasional localized impervious peat layers underlying the sand deposits of the study area, good filtration properties were supported by the soil material's average effective grain size (0.1 to 0.2 mm) and uniformity coefficient (2.5 to 4.0) (Tredoux et al 1980). Detailed in Figure 3-26 is a typical cross-section through the soil deposits of the CFA,

including associated details of grain size and distribution (i.e. Effective Size and Uniformity Coefficient).

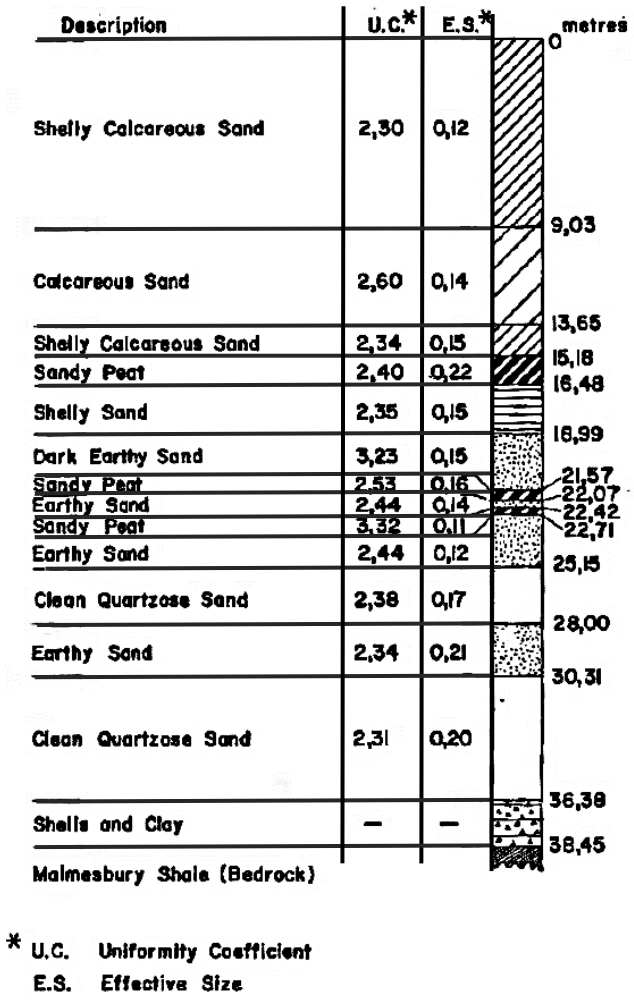

Figure 3-26: Typical cross-section of the deposits encountered around the Zeekoe catchment
Adapted from: Tredoux et al (1980)

Correlations between hydraulic conductivity and soil physical properties have been recognised by various authors succeeding the pioneering Green and Ampt (1911) who noticed a direct proportionality between the in-situ material's porosity, and the hydraulic conductivity. Vandoolaeghe (1984) adds to this by suggesting the probable link between hydraulic conductivity and sediment facies. Facies describe the characteristics of a rock or sedimentary deposit. They reflect the environment of deposition and serve to distinguish sediments deposited in adjacent environments (Geology.com, 2017).

With the knowledge of relative positions and geological variations in different aquifer units, it is evident that areas with high groundwater yields are limited in extent as demonstrated by numerous drillings in the Cape Flats and Atlantis districts Vandoolaeghe (1984). High-yielding boreholes have generally been owed to two primary factors: aquifer thickness and available hydraulic head (Vandoolaeghe (1984).

Recharge in the aquifer is mainly governed by the precipitation falling within the catchment. The recharge rates in the CFA have been proposed as a percentage of the mean annual precipitation (MAP) by Gerber (1981) and Vandoolaeghe (1989) to be approximately 40% and 15 – 37% respectively. The approach of estimating groundwater recharge rates as a percentage of the MAP is considered by Parsons (2000) to be rather simplistic and crude because it overlooks other relevant factors including rainfall intensity, the ground slope, the hydraulic conductivity, and the moisture conditions of the soil. Parsons (2000) further states that for an unconfined system such as the CFA, recharge is unlikely to transpire should the rainfall intensity be below 10 mm over 5 consecutive days.

Despite the CFA's geology being relatively uniform, variations in the aquifer's hydraulic parameters are significant. Region-specific in-situ tests are vital for assessing the suitability of a proposed area's infiltration potential. A summary of Cape Flats' general hydraulic properties sourced, from various authors, is presented in Table 3-5.

Table 3-5: Summary of Cape Flats Aquifer hydraulic parameters from various authors

Parameter / Property	Units	Magnitude	Source / Author	Year
Aquifer transmissivity	**m^2/d**	50 - 650	Gerber	1976
		32 - 620	Meyer	2001
Soil effective porosity	**-**	0.10 – 0.15	Wessels & Greeff	1980
		0.02 – 0.25	Gerber	1980
		0.10 – 0.25	Tredoux et al.	1980
		20 – 25	Henzen	1973
Borehole groundwater yield	**l/s**	0 - 5	Okedi	2017
		17	Tredoux et al.	1980
		80	Vandoolaeghe	1984
		0.5 - 2.0	Meyer	2001
Horizontal hydraulic conductivity	**m/d**	1.5 – 17.5	Gerber	1980
		15 – 30	Wessels & Greeff	1980
		20 – 25	Henzen	1973
		3.4 - 36	Tredoux	1981
Vertical Hydraulic conductivity	**m/d**	0.01 -1	Gerber	1980
		3.5 - 17	Wessels & Greeff	1980
Aquifer storage capacity	**$m^3 \times 10^6$**	1500	Vandoolaeghe	1984
		1500	Tredoux et al.	1980
		1500	Meyer	2001
Soil effective grain size, D_{10}	**mm**	0.1 – 0.2	Tredoux et al.	1980
Soil Uniformity Coefficient, C_U	**-**	2.5 -4.0	Tredoux et al.	1980
Mean Annual Precipitation, MAP	**mm/yr**	619	Adelana	2010
		500 - 700	Henzen	1973
Recharge	**%***	16 - 47	Adelana	2010
		40	Gerber	1981
		15 - 37	Vandoolaeghe	1989

%* Percentage of MAP

3.6.5 Groundwater Quality

The Cape Flats area is not only characterized by its productivity of groundwater resources but also dense human settlements as well as industrial and agricultural activities that are all sources of pollutants (Adelana & Xu, 2006). Sources of pollution include, among others: highway run-off, urban residential wastewater entering canals through stormwater networks, nutrients from agricultural areas, and direct dumping of waste and grey / black water from informal settlements with poor sanitation services. The Lotus River (both Great and Little) comprises of portions that are lined with concrete to manage increased runoff due to urbanization. The highly polluted water from upstream in the Great Lotus River is diverted to the Cape Flats WWTW thus resulting in clearer downstream water in the Little Lotus (Figure 3-27).

Figure 3-27: Water pollution in Zeekoe catchment river streams

Polluted surface water infiltrates the ground and contaminates the aquifer from various locations, mainly along the natural river courses. The chemical quality of the indigenous groundwater of the aquifer is presented in Table 3-6. The water is generally of low salinity with relatively high hardness (i.e., high concentration of dissolved Calcium and Magnesium) (Tredoux et al.,1980). The abundant presence of shelly material throughout the aquifer results

in the occurrence of calcrete horizons (caused by calcium carbonate) observable near the water table (Wright & Conrad, 1995).

Using the classification system set out by the National Water Act (NWA), the Cape Flats precinct has been delineated to indicate different levels of recourse protection (Figure 3-28). The quality of groundwater in the Zeekoe catchment area was mostly good, aside from the central Philippi area which had a high salt, Potassium, and Nitrate content due to the 400 tons of fertilizer used annually for irrigation (Wright & Conrad, 1995).

Table 3-6: Indigenous groundwater quality in the Cape Flats Aquifer
Source: Tredoux et al (1980)

Chemical Parameters	Units	Concentrations		
		Median	Medium	Maximum
Sodium	mg/*l*	57	20	760
Potassium	mg/*l*	1,5	0,9	120
Calcium	mg/*l*	95	36	150
Magnesium	mg/*l*	11	3,9	93
Ammonia (as N)	mg/*l*	<0,5	<0,5	1,2
Sulphate	mg/*l*	30	4	166
Chloride	mg/*l*	99	35	1317
Total Alkalinity (as CaCO3)	mg/*l*	248	80	391
Nitrate (as N)	mg/*l*	<0,1	<0,1	2,6
Nitrite (as N)	mg/*l*	<0,05	<0,05	0,1
Total phosphate (as P)	mg/*l*	<0,1	<0,1	0,35
pH	mg/*l*	7,7	7	8,2
Electroconductivity	mg/*l*	78	43	499

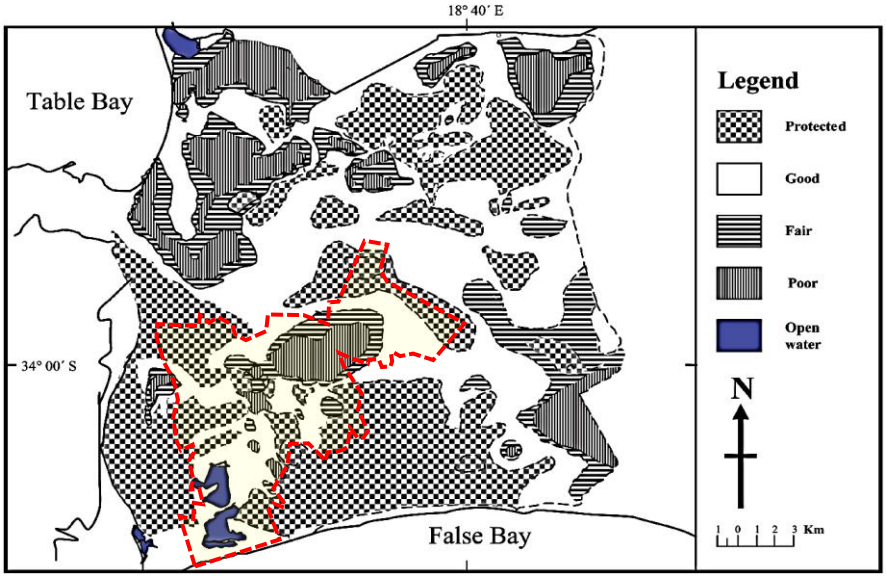

Figure 3-28: Cape Flats Aquifer protection zoning based on the groundwater quality and resource directed measure concept
Source: Adelana & Xu (2006)

3.7 Stormwater Ponds in Zeekoe Catchment

The City of Cape Town (CoCT) has approximately 800 stormwater ponds in its various catchment areas for the management of stormwater runoff. Roughly 8% of these ponds can be found in the Zeekoe catchment. Because most of these ponds were constructed rapidly over the past 40 odd years, the city has not managed to timeously record as-built data which has resulted in gaps in the geographic information systems (GIS) records of actual pond locations (Rohrer, 2016 after Austin 2014).

Rohrer (2014) undertook a study that aimed at creating a database containing the locations, types, and sizes of all the stormwater ponds in the CoCT. In his investigation, Rohrer observed a total of 61 ponds in the Zeekoe catchment, of which most were detention ponds (84%), some retention ponds (14%), and very limited wetlands (2%) (Table 3-7).

Table 3-7: Number of each type of pond in the Zeekoe catchment
Source: Rohrer (2014)

Catchment Area	Total Area of Ponds	Total No. of Ponds	No. of Detention Ponds	No, of Retention Ponds	No. of Wetlands	No. of Ponds Per km^2
(km^2)	(km^2)	-	-	-	-	-
177	0.763	61	51	9	1	0.34

The ponds are situated at various elevations above the water table, with surface areas ranging between 156 and 410 m^2. The shape of the ponds is typically rectangular or oval in plan with depths from 0.9 to 2.0 m (Figure 3-29). The distribution of the ponds throughout the catchment area is uneven as they are largely concentrated in the north-eastern region with a few towards the south and west of the study area (Figure 3-30).

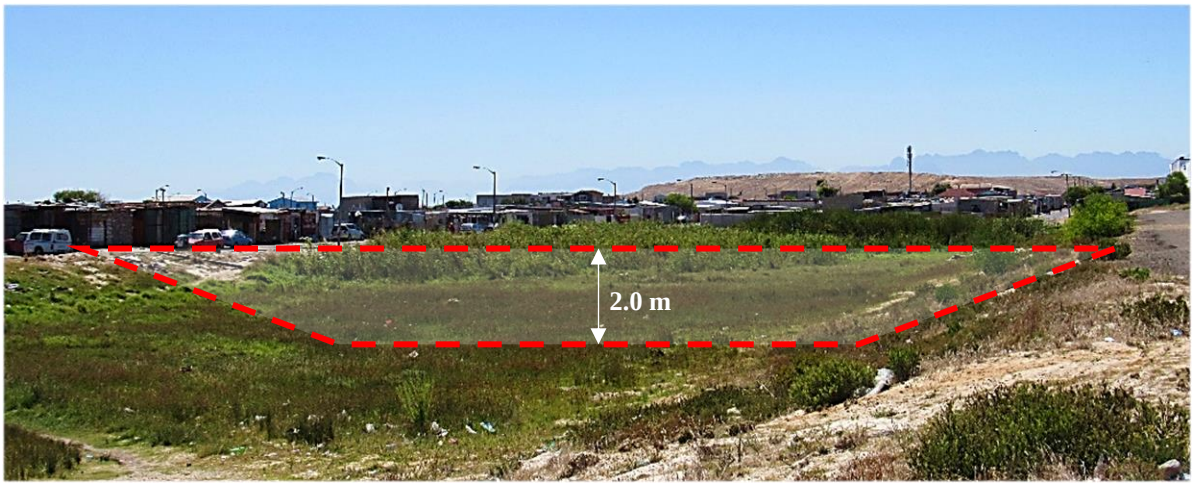

Figure 3-29: General shape and depth of stormwater ponds in the Zeekoe catchment

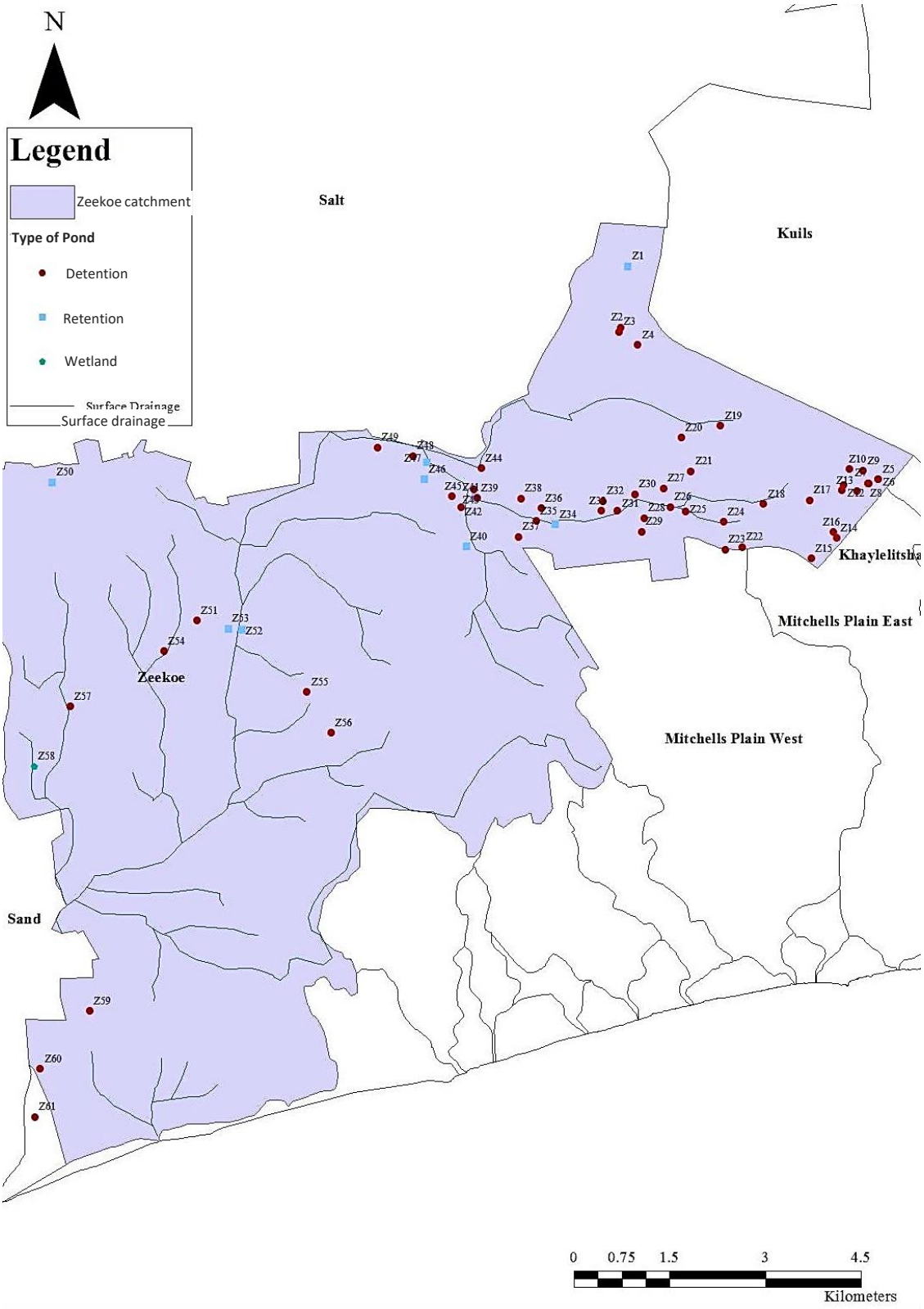

Figure 3-30: Location of stormwater ponds in the Zeekoe catchment
Source: Rohrer (2014)

4 Field Infiltration Investigation

4.1 Introduction

The main apparatus use in this study for in-situ infiltration measurements was the Double-Ring Infiltrometer (DRI). This field test method was employed to measure the steady-state infiltration rate of water through the surface of the selected stormwater ponds. The chapter begins with a presentation of the preliminary site investigation undertaken before the selection of the investigated ponds, followed by an outlook into the criteria used to select representative samples. The chapter proceeds with a presentation of the established infiltration test program and the DRI apparatus used to conduct the field tests before concluding with a description of how quality was ensured throughout the investigations. The chapter details the test procedure and Preliminary Site Investigation

4.1.1 Access to Ponds

Before conducting a preliminary site investigation, a desktop study was undertaken with the aid of Google Earth software and the City of Cape Town's (CoCT) pond database generated by Rohrer (2016). The desktop study involved the preselection of potential ponds to be investigated based on their location within the catchment area.

One of the main purposes of the preliminary site investigation was to not only physically validate the existence of the preselected ponds but to also determine the accessibility of the ponds and the practicability of conducting infiltration tests in them. Some of the initially preselected ponds were omitted after the preliminary site investigation because of access constraints such as the ponds being within a graveyard, or the ponds being fenced off. An overview of the ponds and study area is shown in Figure 4-1.

4.1.2 The Function of Stormwater Ponds

More than 80% of the investigated stormwater ponds were originally designed as detention ponds because of their proximity to residential areas. Designing them as retention ponds would have posed potential health and safety hazards related to stagnant open water bodies such as algal blooms, mosquito breeding, and risk of children drowning (Åstebøl et al., 2004; Clar et al., 2004; Woods-Ballard et al., 2007).

The ponds were observed to serve the primary purpose of detaining stormwater during rainy seasons however, in dry seasons, the ponds were used for multiple purposes such as playgrounds for children; football fields; grazing for cattle, sheep and horses; and general pathways for pedestrians (Figure 4-1-f).

Figure 4-1: Images of study area captured during preliminary site investigation of SW ponds

4.2 Selection Criteria for Representative Sample

Three representative stormwater ponds were selected across the Zeekoe catchment for this investigation. The ponds were selected based on their distribution across the study area; each pond represented a group of ponds within a region of the catchment area (Figure 4-2). The locations and surface areas of the three sites are given in Table 4-1.

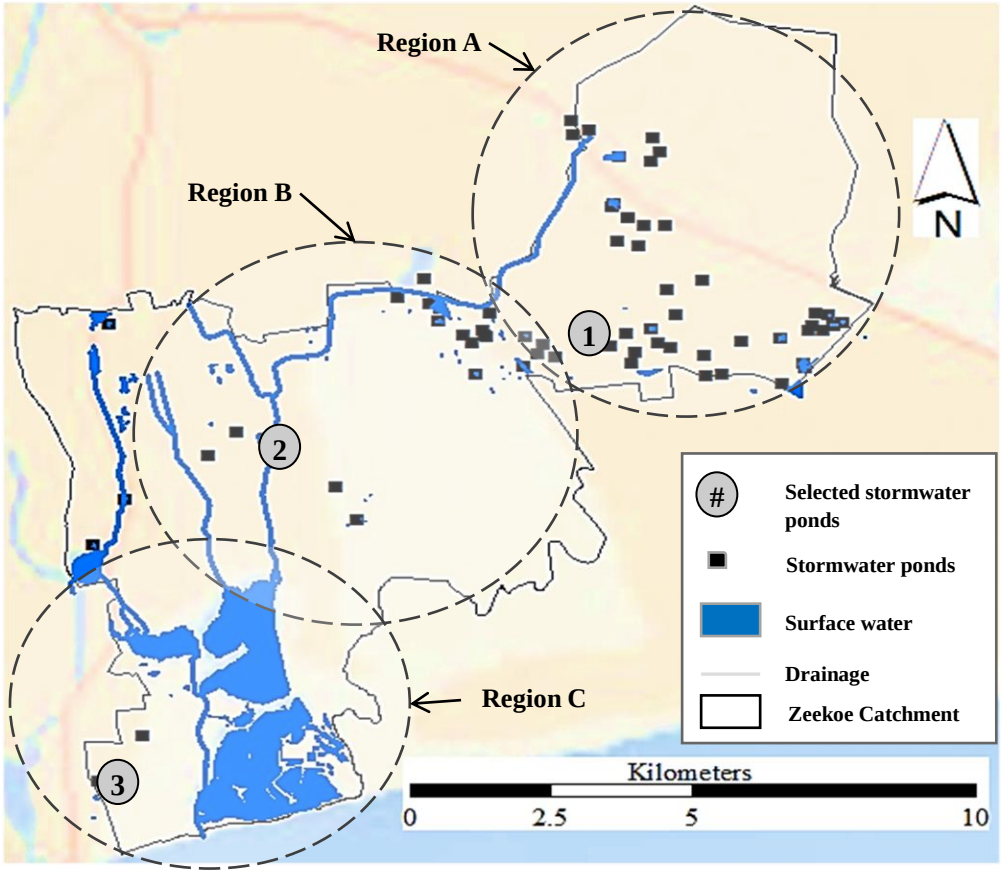

Figure 4-2: Locations of investigated stormwater ponds
Modified from: Okedi (2017)

Table 4-1: Selected pond locations

Pond No.	Pond Type	Surface Area (m^2)	Suburb Name	Road Name	Latitude	Longitude
1	Detention	32,000.0	Browns Farms	2309 Msingizane Street	-34.009	18.581
2	Retention	10,000.0	Lotus River	7 Eric Way	-34.025	18.519
3	Detention	9,000.0	Vrygrond	86 Drury Road	-34.087	18.484

The determination of the number of Double-Ring Infiltrometer (DRI) tests to be undertaken was based on the following:

a) From preliminary site visits, it was observed that soil texture, soil type, and vegetation in ponds varied considerably across the catchment. Thus, it was decided to conduct DRI tests on selected representative ponds distributed across the catchment to determine the general infiltration parameters (i.e. *inter alia* infiltration rates and porosity) of the study area and to observe differences in infiltration potential owing to regional effects.

b) From site visits, it was also observed that soil texture and type varied within ponds. Accordingly, it was decided to conduct three DRI tests on different positions within each of the selected ponds to determine the general infiltration parameters of each pond.

c) Since stormwater runoff contains fine soil particles which can alter properties of the top layer of the stormwater pond surface over time, it was decided that on each tested position, another test be conducted after excavating at least 200 mm of topsoil (Figure 4-3). This would indicate the change in infiltration rates with depth i.e., on the surface and sub-surface (200 mm below the surface). Furthermore, the effects of vegetation and top organic soil on infiltration would be mitigated since the soil deposits were observed to remain relatively uniform below a depth of 200 mm.

d) Thus, a total of 18 DRI tests were conducted i.e., 6 tests per stormwater pond, three on the surface and three on the sub-surface (Figure 4-4).

Figure 4-3: Surface strata observation pit in a pond from surface to 20cm depth

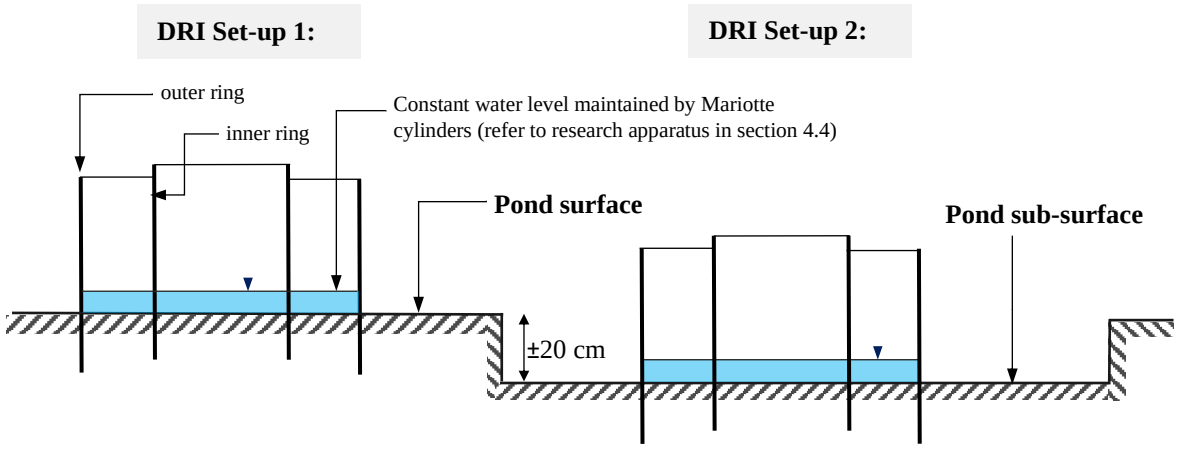

Figure 4-4: Schematic of two different DRI test set-ups on each location within a pond

4.3 Individual Investigated Ponds

The three investigated ponds and the positions of the DRI tests within each pond are shown in Figure 4-5 to Figure 4-7. Localised wetlands were observed in Ponds 1 and 3 thus restricting infiltration testing on those areas. Pond 2 was completely dry during the time of the investigation with the channelized Lotus River separating it from an adjacent wetland. Variations in vegetation and soil across each ponds' surface can also be seen from the figures including the proximity of the ponds to residences and surrounding developments.

Figure 4-5: Infiltration Test Locations within Pond 1

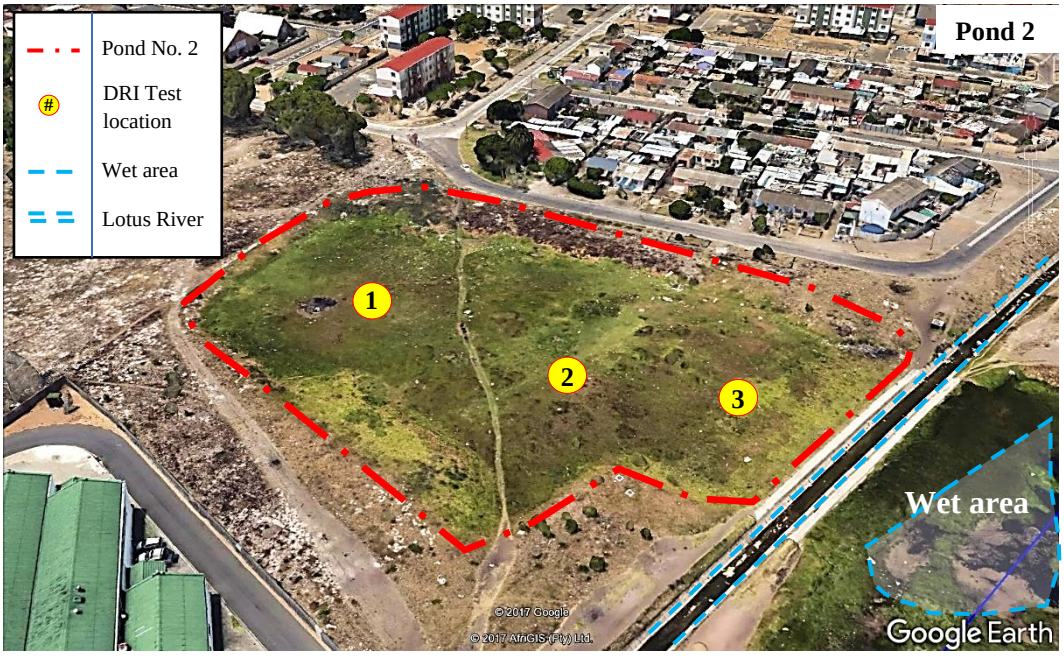

Figure 4-6: Infiltration Test Locations within Pond 2

Figure 4-7: Infiltration Test Locations within Pond 3

4.4 Research Apparatus

4.4.1 Double-Ring Infiltrometer

The Double-Ring Infiltrometer (DRI) in-situ test was adapted over other infiltration test methods due to its simplicity and extensive use in hydrogeologic investigations (ASTM, 2009). It allows for a relatively quick comparison of in-situ steady-state infiltration rates. Because many factors influence the infiltration rate, tests conducted at the same site are not likely to give the same results however the results are useful for comparative and index value determinations. Since this investigation involved conducting tests on numerous locations, the flexibility and portable nature of the apparatus was advantageous for ease of mobility. The partly vegetated sandy soil conditions in the investigated ponds were applicable for this test excluding local wet areas. The main components of the DRI apparatus and detail of dimensions are shown in Figure 4-8 and Figure 4-9 respectively.

Figure 4-8: Double-Ring Infiltrometer Apparatus

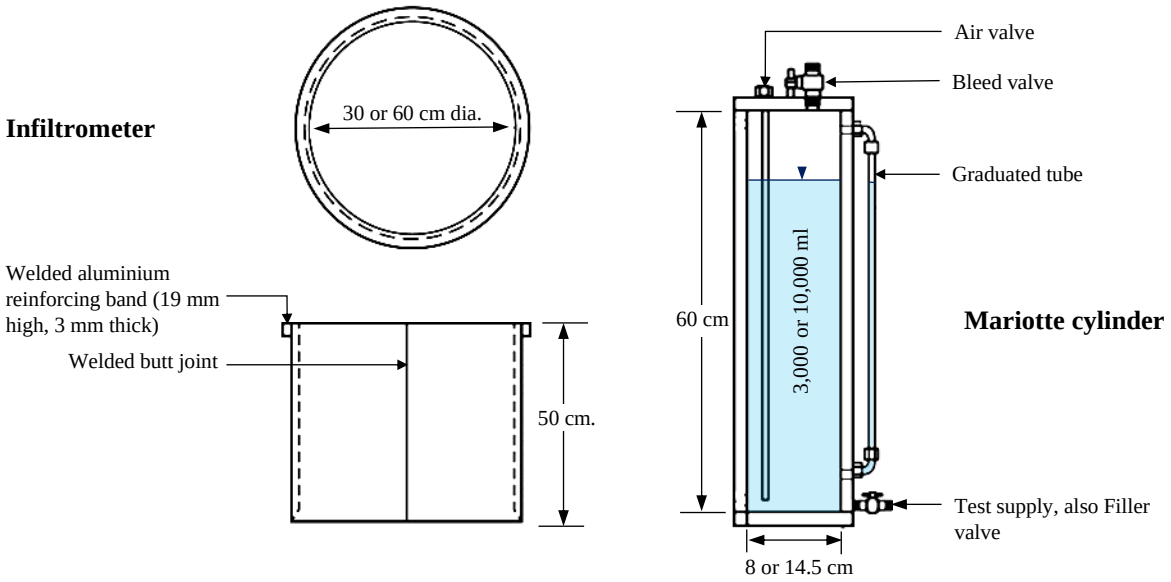

Figure 4-9: Double-Ring Infiltrometer and Mariotte cylinder dimensions

4.4.2 Other Apparatus

Additional apparatus used to carry out the infiltration investigation, in conjunction with the double-ring infiltrometer apparatus are illustrated in Figure 4-10; below is a description of these apparatus:

a) 200 mm long, 50 mm diameter steel soil sampling tubes;
b) 4-liter re-sealable plastic bags for soil sample collection;
c) 5.5-kg sledgehammer, a rubber hammer, 600 mm length of wood around 50 by 100 mm, shovel, spirit level, steel measuring tape, thermometer, stopwatch.
d) 1000-litre water supply tank.
e) A van with a minimum load capacity of 1000 kg.

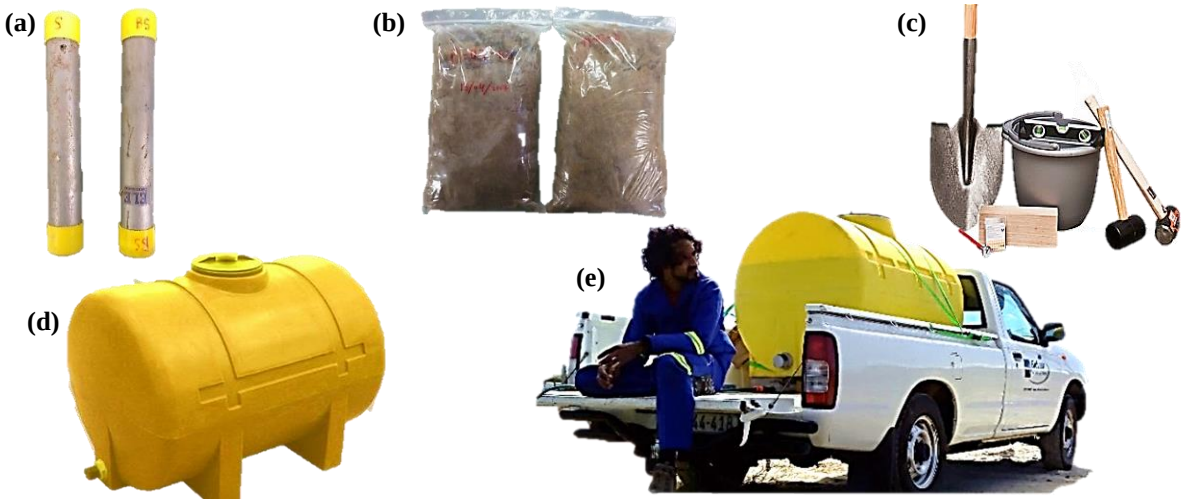

Figure 4-10: Additional apparatus used during infiltration experiment

4.5 Infiltration Test Program

In total, eighteen constant-head Double-Ring Infiltration tests were conducted in three selected stormwater ponds (i.e., six tests per pond), nine of which involved carrying out the test on the surface of the ponds whilst the other nine on the sub-surface (i.e., 200 mm below the surface). The complete test program is listed in Table 4-2. Notations used in the 'Test ID' column of the field test schedule are described in Figure 4-11:

Table 4-2: DRI experimental test program

Test no.	Test ID	Pond No.	Sample No.	DRI Set-up level	Test Date
1	P1-1-S	1	1.0	Surface	27/03/2017
2	P1-1-BS	1	1.1	Below surface	28/03/2017
3	P1-2-S	1	2.0	Surface	29/03/2017
4	P1-2-BS	1	2.1	Below surface	30/03/2017
5	P1-3-S	1	3.0	Surface	31/03/2017
6	P1-3-BS	1	3.1	Below surface	01/04/2017
7	P2-1-S	2	1.0	Surface	03/04/2017
8	P2-1-BS	2	1.1	Below surface	04/04/2017
9	P2-2-S	2	2.0	Surface	05/04/2017
10	P2-2-BS	2	2.1	Below surface	06/04/2017
11	P2-3-S	2	3.0	Surface	07/04/2017
12	P2-3-BS	2	3.1	Below surface	08/04/2017
13	P3-1-S	3	1.0	Surface	10/04/2017
14	P3-1-BS	3	1.1	Below surface	11/04/2017
15	P3-2-S	3	2.0	Surface	12/04/2017
16	P3-2-BS	3	2.1	Below surface	13/04/2017
17	P3-3-S	3	3.0	Surface	14/04/2017
18	P3-3-BS	3	3.1	Below surface	15/04/2017

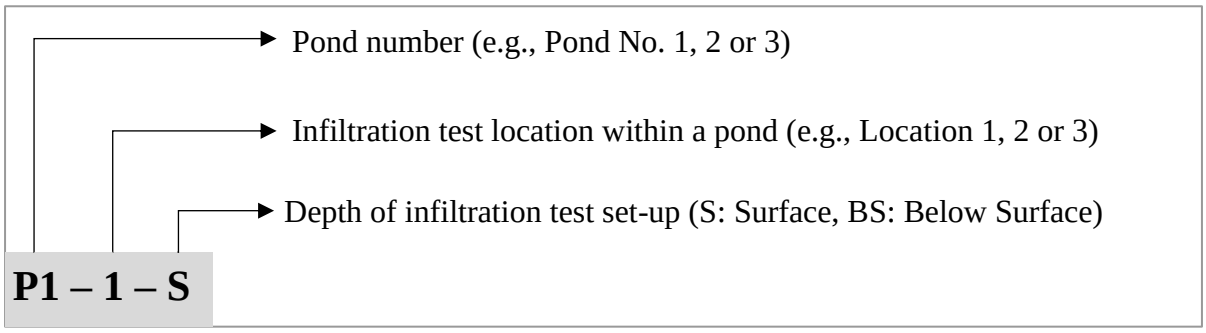

Figure 4-11: Description of notations used for test identification

4.6 Infiltration Investigation

4.6.1 Soil Sample Collection

Before each infiltration test, soil samples were collected adjacent to each DRI test location for further laboratory testing. Determining the effects of initial soil parameters helps in the prediction of more accurate soil hydraulic parameters. The soil samples were collected in two forms, disturbed and relatively undisturbed. The disturbed samples were stored in sealable plastic bags to prevent moisture loss whilst 200 cm high hollow cores were driven into the ground to retrieve intact soil specimens.

4.6.2 Calibration of Apparatus

Before the initial use and reuse of the DRI apparatus, it was calibrated to ensure that accuracy and consistency were maintained. Infiltration measurements were only recorded for water passing through the inner ring thus the surface area of the inner 30 cm ring was measured after each test to ensure that the area at the bottom of the ring was not altered during the installation process of the previous test. The surface area of the inner ring was crucial for calculating the volumetric flow of infiltrated water which is equal to the surface area multiplied by the change in height of the water within the inner ring. A steel rule was used to determine these measurements providing an overall accuracy of 1%.

For each of the Mariotte cylinders, a relationship between the change in elevation of the fluid level on the graduated tube and the change in volume of water dissipated was established. Three calibration trials were conducted for each Mariotte cylinder and the results of ΔVolume versus ΔHeight were plotted to observe a linear relationship with a general accuracy of 1%.

4.6.3 Double-Ring Infiltrometer Test

The infiltration test procedure was conducted following ASTM D3385 – 09: *Standard Test Method for Infiltration Rate of Soils in Field Using Double-Ring Infiltrometer*. As illustrated in Figure 4-12, the test consisted of two open cylinders (inner and outer) each manually driven into the ground before being partially filled with a constant head of water with the aid of two Mariotte cylinders. The infiltration rates were calculated by measuring the volume of liquid added to the inner ring to maintain the water at a constant liquid level until steady infiltration rates were achieved. A steady infiltration rate was assumed when the rate of discharge was below 0.5% over a 5-minute time interval.

The first step of the procedure involved the establishment and preparation of a test location which was relatively level with a clear surface area of approximately 3 by 3 m within the pond. For the case of a sub-surface infiltration test, about 200 mm of topsoil was excavated and the ground was cleared and levelled before driving the cylinders into the ground (Figure 4-13).

To drive the cylinders into the ground, a driving cap was first placed on the outer cylinder, then a wooden block was placed on the driving cap. A sledgehammer was then used to deliver heavy blows uniformly around the cylinder with a second person standing on top of the driving cap

to facilitate driving the rings uniformly until the desired depth was achieved. To prevent water in the inner from leaking to the ground surface surrounding the ring, the outer ring was driven to approximately 150 mm whilst the inner ring was driven to about 100 mm.

If the surface of the soil surrounding the walls of the rings was slightly disturbed by the driving process, the soil was tamped and recompacted until its original firmness was achieved. If, however, the soil surrounding the driven rings' walls was excessively disturbed, the apparatus was set up in a new location.

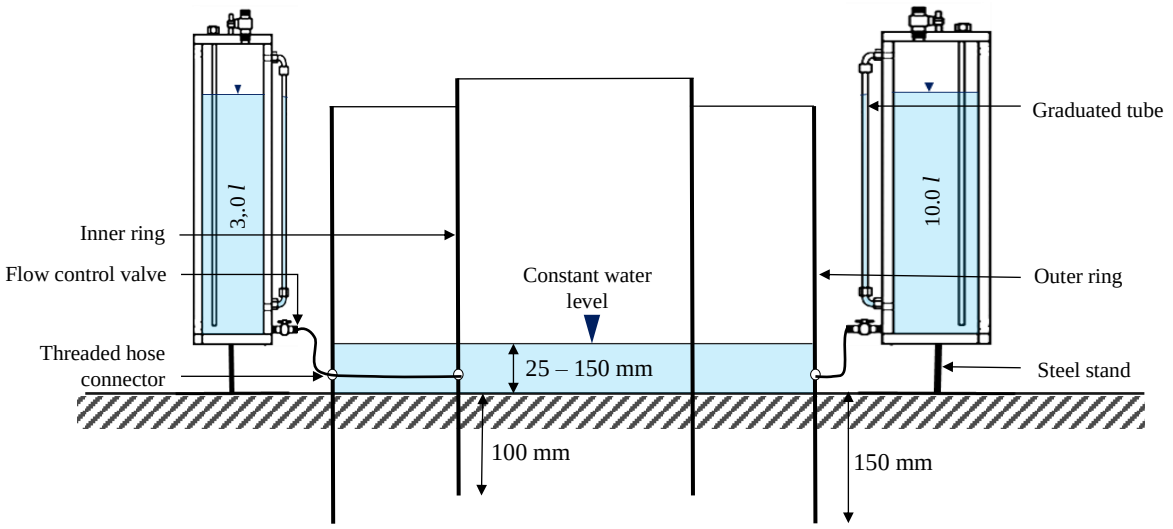

Figure 4-12:Detailed schematic of DRI test set-up

Figure 4-13: Preparation of sub-surface DRI test

Once the rings were driven and a spirit level was used to check the ring sides to be vertical, the pipe leading from the water supply tank was carefully connected and secured as shown in Figure 4-14-a. A pressure head above 2.0 m was available to supply the Mariotte cylinders throughout the tests owing to their height above the pond surfaces (Figure 4-14-b).

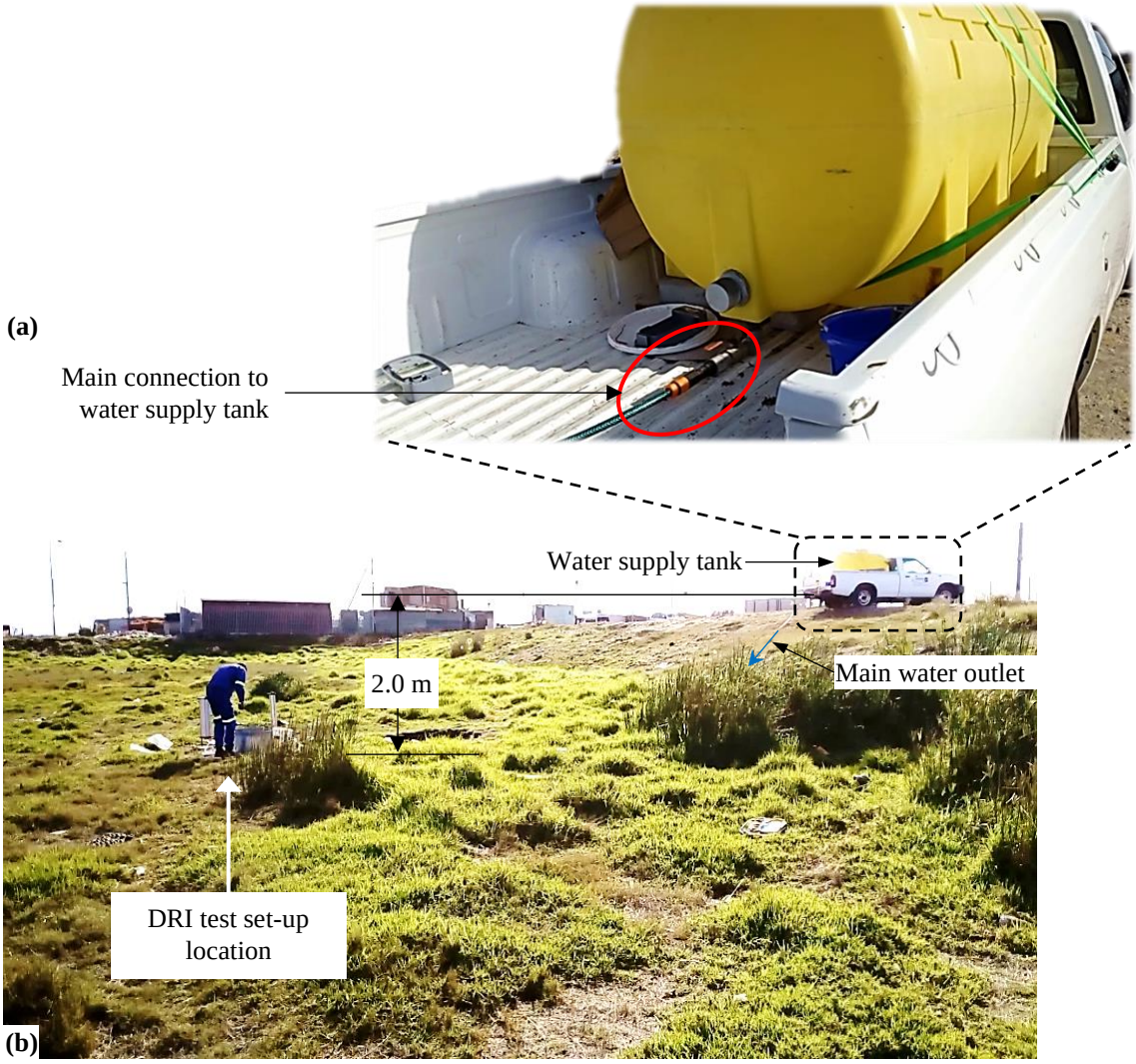

Figure 4-14: (a) Connection of DRI pipes to main water supply, (b) Relative position of test

The pipe network configuration of the apparatus was generally the same for each test however the pipe lengths varied according to the distance of the set-up locations relative to the main water supply. Figure 4-15 shows a complete set-up of a sub-surface DRI test with all components whilst a schematic in Figure 4-16 highlights the water flow connection.

Once the pipe network was connected across the system, the main outlet pipe from the 1000 *l* water supply tank was opened to supply the two Mariotte cylinders with water. Before pouring any water into the DRI, splash guards were placed on the surface within the annular space of both the inner and outer rings to prevent erosion of soil when water was initially supplied.

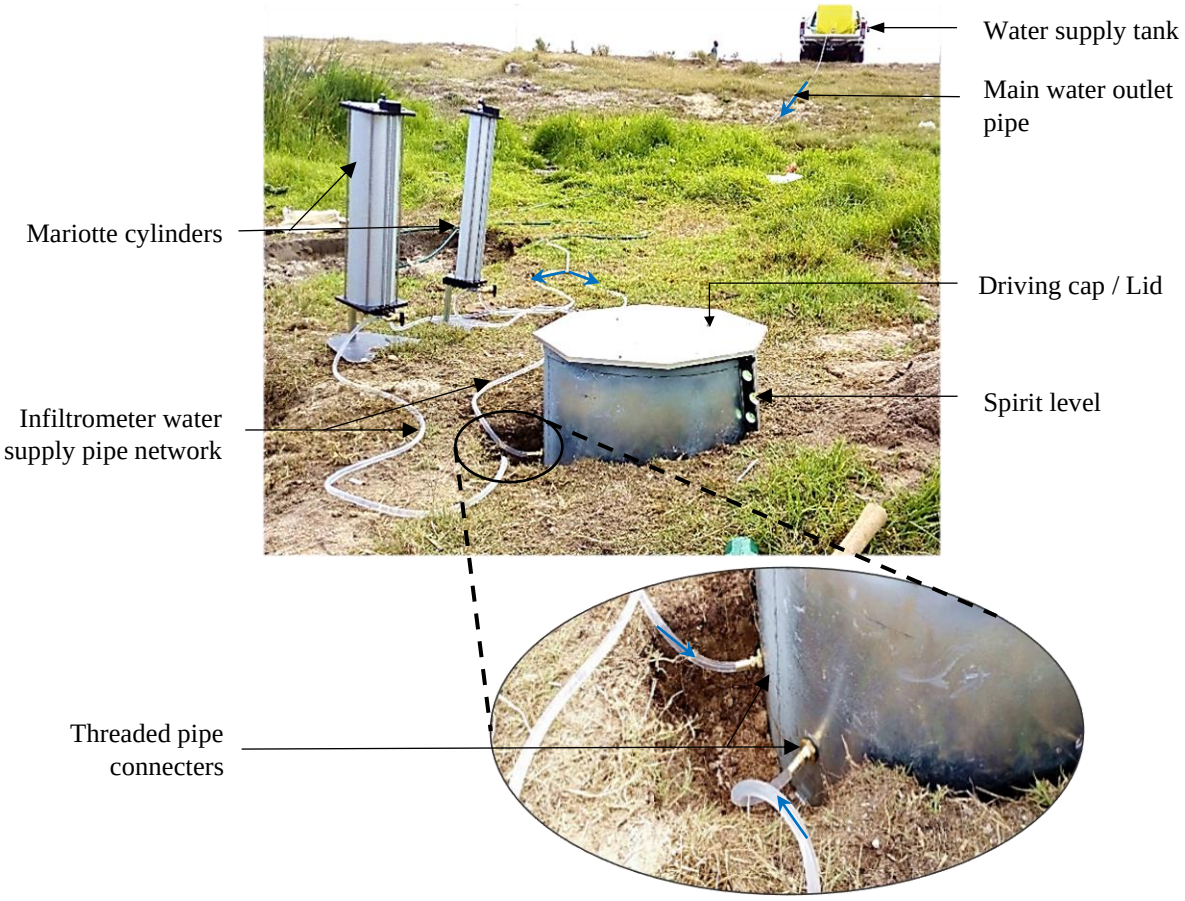

Figure 4-15: Complete sub-surface DRI test configuration

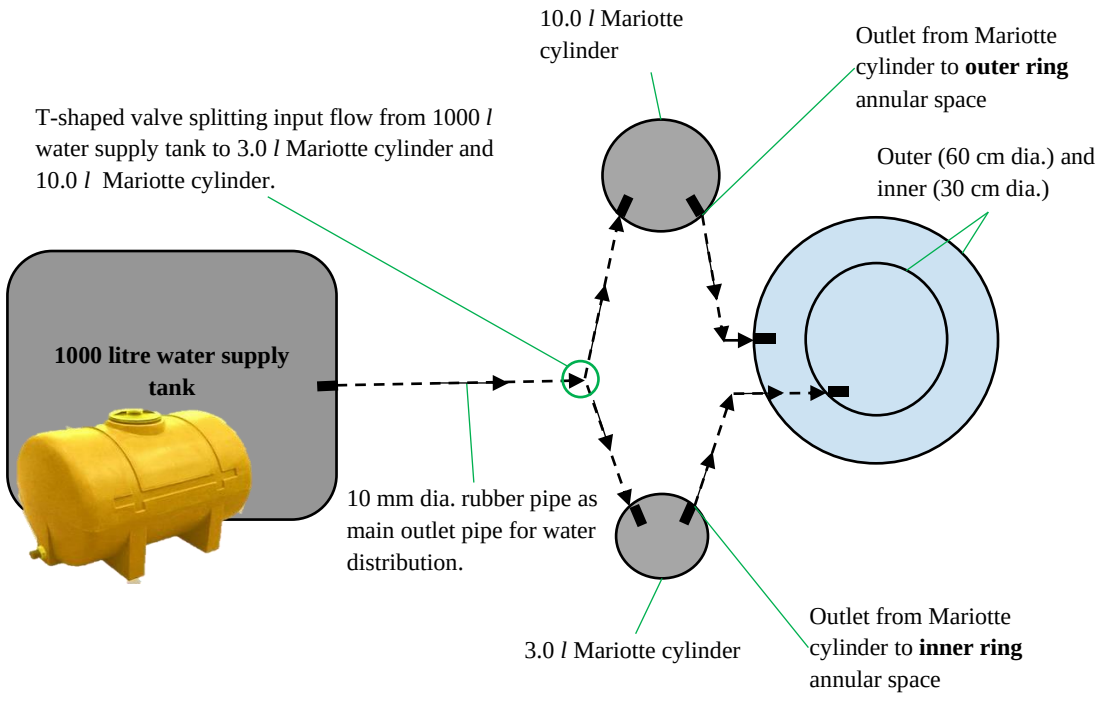

Figure 4-16: Double-Ring infiltrometer water-flow configuration

A bucket was used to initially pour water into both rings up to the desired level (between 25 – 150 mm) before removing the splash guards. The flow from the Mariotte cylinders was then initiated by opening the outlet valves to maintain the same water level in both rings at the selected head.

The following information was recorded during each test in the field-test data form:

1. Date of the test;
2. Location of test site;
3. Weather conditions;
4. Description of test site including shallow soil profile;
5. The area of the two rings, and the annual space between them;
6. The ground temperature to a depth of about 200 mm using a probing thermostat (Figure 4-17-a);
7. The temperature of water within the inner ring;
8. The constant depth of water maintained in the inner ring and annular space;
9. Depth to water table if available;
10. The volume of liquid added to maintain a constant head in the inner ring (whilst keeping the same water level in the annular space) at various time intervals by measuring the change in water level on the graduated tube of the inner ring's Mariotte cylinder (Figure 4-17-b).

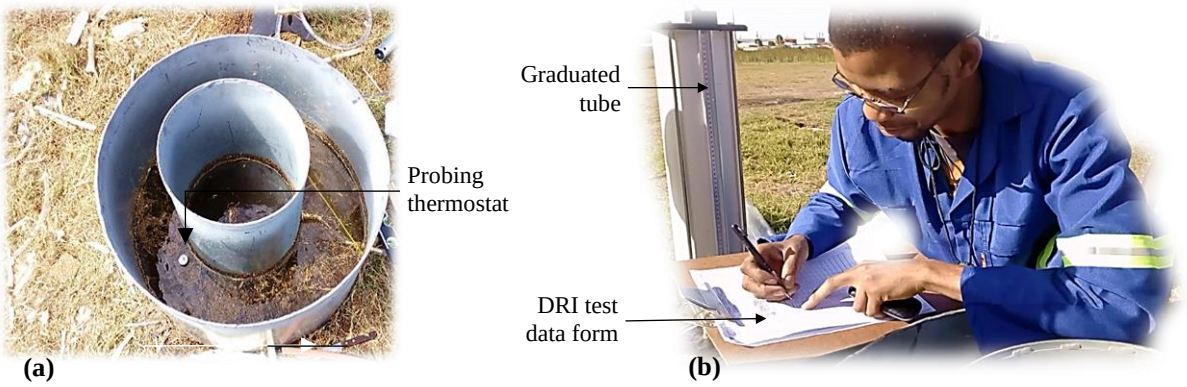

Figure 4-17: (a) Temperature measurement, (b) Recording test measurements

The data was recorded at increasing time intervals with each hour. For sites with more pervious soil material, readings were recorded more frequently than those with lower permeability. Each test continued until a relatively constant infiltration rate was obtained. To mitigate evaporation in the rings, the driving cap was placed as a lid over the two rings. Upon completion of the test, a rubber hammer was tamped along the sides of the rings to loosen them before removal.

In soils of very low permeability, low infiltration rates could be explained by dense underlying soils creating an almost impervious seal around the bottom of the rings Figure 4-18-a. Ponded

water was observed as shown in Figure 4-18-b after a test was conducted at a location within Pond 1 with very low permeability.

(a) **(b)**

Figure 4-18: (a) Very dense soil sealing ring (b) Completed DRI test on low permeability soil

4.7 Quality Concerns

Due to the variability in soils tested and the numerous factors related to soil and water which may affect the infiltration test results, the recorded infiltration rates were considered as index values. Notwithstanding the variable nature of this in-situ test, quality and consistency were maintained for factors that were controllable to limit any potential bias in the obtained results. Elaborated below are the measures which were adapted to ensure quality and consistency.

- Recording of information required to complete the field-test data form (Figure 4-19).
- The same apparatus was used throughout this investigation.
- The DRI apparatus was properly calibrated before the beginning of each test.
- Infiltration tests were monitored physically from start to end, even for test sites with very low infiltration rates. This was done to prevent any tempering of the apparatus by curious locals passing along or children playing nearby. Additionally, continued monitoring of the tests ensured that readings were recorded timeously.
- A lid was placed over the rings to prevent evaporation during the testing, particularly on areas that were found to be nearly impermeable.
- Subsurface tests were all conducted within 200 mm deep excavations below the stormwater ponds' surface beds. Additionally, the base of each subsurface test was cleared of all obstructions and levelled before the rings were driven into the ground.
- Infiltration tests were not conducted on surfaces that were extensively disturbed by the driving of the rings. Rather, the set-up process would be reset at alternative test locations.
- Rings were cleaned to remove any excess soil before conducting the next test.

UNIVERSITY OF CAPE TOWN
IYUNIVESITHI YASEKAPA • UNIVERSITEIT VAN KAAPSTAD

Infiltration Test Data Form

Date: __/04/2017
Tested by: Paul Mavundla
Project Identification:
Test Location:
Liquid Used:
Depth to water table (m):
pH
Liquid level maintained using Measuring tape
Penetration of outer ring (cm)
Penetration of inner ring (cm)

Constants	Area (cm^2)	Head of Liquid (cm)	Volume of liquid (cm^3)
Inner Ring	707		0
Annualar Space	2106		0

Inner ring diameter (cm): 30
Outer ring diameter (cm): 60
Thickness of ring (cm): 0,3

Trial No.		Time (hr:min)	Elapsed Time: Δ/total (min:ss)	Flow Readings				Liquid Temp (°C)	Incremental Infiltration Rate		Ground Temperature = _ °C at depth of __cm. Remarks conditions, etc
				Inner Reading		Annular Space					
				Reading (cm)	Flow (cm^3)	Reading (cm)	Flow (cm^3)		Inner (cm/h)	Annular (cm/h)	
1	S										
	E										
2	S										
	E										
3	S										
	E										
4	S										
	E										
5	S										
	E										
6	S										
	E										
7	S										
	E										
8	S										
	E										
9	S										
	E										
10	S										
	E										
11	S										
	E										
12	S										
	E										
13	S										
	E										
14	S										
	E										
15	S										
	E										
16	S										
	E										
17	S										
	E										
18	S										
	E										
19	S										
	E										
20	S										
	E										
21	S										
	E										
22	S										
	E										
23	S										
	E										

Test Standard:
ASTM D3385 - 09

Page__of__

Figure 4-19: Data recording form for infiltration test

4.8 Data Processing

Using the recorded infiltration test data, a plot of both the cumulative infiltration F_p and incremental infiltration f_p versus total elapsed time was plotted (Figure 4-20). The cumulative infiltration capacity $F_p(t)$ is defined as the accumulated infiltration volume of water over a period beginning from the start of the test process and can be expressed by the following equation:

$$F_p = \int_0^t f_p(t)dt \qquad 4.1$$

Hence, the curve $F_p(t)$ is the mass curve of infiltration. From Equation 4.1, it thus follows that the infiltration potential at any given time $f_p(t)$ can be expressed as:

$$f_p = \frac{dF_p(t)}{dt} \qquad 4.2$$

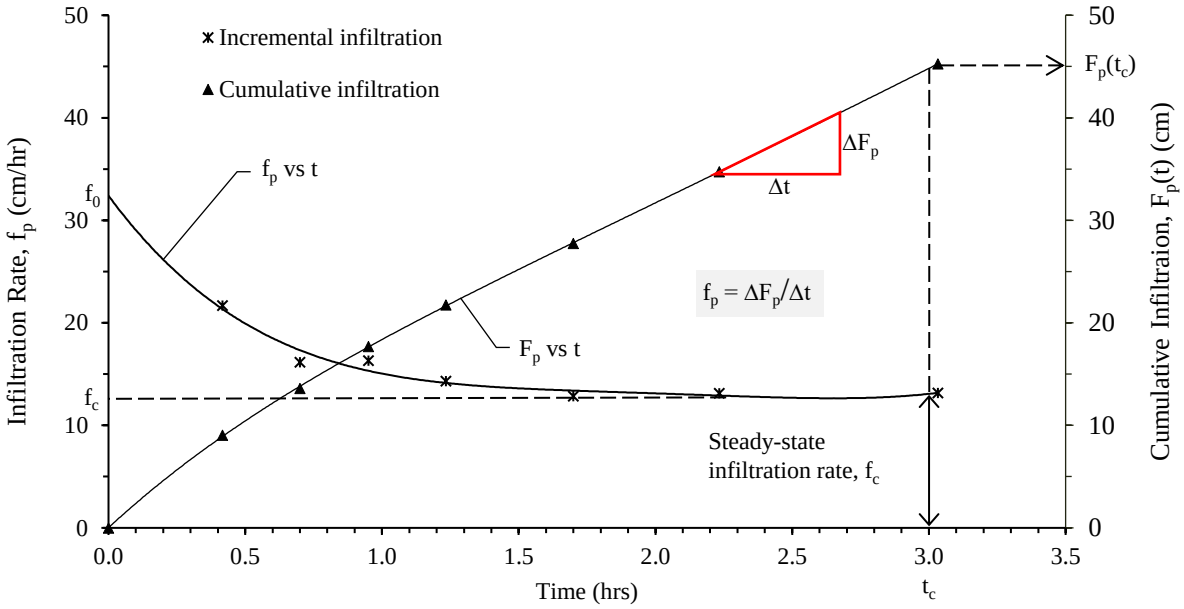

Figure 4-20: Plot of infiltration rate and cumulative infiltration rate versus time

It was observed from Figure 4-20 that the steady-state infiltration rate f_c is equal to the gradient of the linear portion of the $F_p(t)$ curve.

Two equations were adapted for the hydrological analysis of the DRI test results, namely: Horton's 1933 and Green-Ampt's 1911 Equations. These equations were selected because they aided in achieving the following:

a) Estimating the initial infiltration rate of water through the soil at $t = 0$, f_0;

b) Estimating Darcy's saturated hydraulic conductivity K of the soil; and

c) Expressing the obtained infiltration test results in the form of general curves considering the physical properties of the soil such as porosity ɳ and capillary suction S_c.

Horton's 1933 equation for infiltration capacity, $f_p = f_c + (f_0 - f_c)^{e^{-\lambda t}}$, was rearranged and expressed as follows:

$$(f_p - f_c) = (f_0 - f_c)^{e^{-\lambda t}} \quad 4.3$$

By taking logarithms on each side of Equation 5.1, i.e.

$$ln(f_p - f_c) = ln(f_0 - f_c)^{e^{-\lambda t}} \quad 4.4$$

The plot of $ln(f_0 - f_c)$ versus time was graphed with a linear best-fit line (Figure 4-21-a). The intercept value of the best-fit line was equated to $ln(f_0 - f_c)$, thus solving for f_0. The slope of the best-fit line was equated to Horton's infiltration decay coefficient λ.

The statistical descriptors for Horton's parameters in Equation 4.4 were determined and are presented in Table 4-3.

Table 4-3: Horton's infiltration parameters

Ponds	Parameters	Mean	Minimum	Maximum
Pond 1	λ	1.9	1.0	3.0
	f_o (cm/hr)	3.6	0.7	5.8
	f_c (cm/hr)	1.4	0.3	2.9
Pond 2	λ	0.6	0.1	1.3
	f_o (cm/hr)	25.8	9.3	31.8
	f_c (cm/hr)	20.6	3.8	28.2
Pond 3	λ	0.8	0.3	2.4
	f_o (cm/hr)	17.80	5.82	41.18
	f_c (cm/hr)	10.54	2.22	22.80

Green-Ampt's 1911 proposed equation for infiltration capacity, $f_p = K_s\left(1 + \frac{ɳ S_c}{F_p}\right)$, was based on Darcy's law and considered to be a linear equation as follows:

$$f_p = m + \frac{n}{F_p} \quad 4.5$$

where f_p = incremental infiltration capacity

S_c = capillary suction at the wetting front

η = porosity of the soil

F_p = cumulative infiltration capacity

m = Green-Ampt parameter of the infiltration model and

n = Green-Ampt parameter of the infiltration model.

The Green-Ampt parameters were determined from laboratory experiments as described in Chapter 5 and summarised in Table 4-4.

Table 4-4: Green-Ampt's infiltration parameters

Ponds	Parameters	Mean	Minimum	Maximum
Pond 1	K_S (cm/hr)	1.2	0.3	2.3
	n	2.4	0.1	7.4
	η *(%)*	31	30	33
	Sc (cm)	7.3	0.1	23.1
Pond 2	K_S (cm/hr)	22.1	3.8	32.6
	n	29.3	9.9	48.5
	η *(%)*	40	30	45
	Sc (cm)	31.4	22.7	36.8
Pond 3	K_S (cm/hr)	9.6	2.0	21.6
	n	3.9	0.6	9.7
	η *(%)*	38	32	50
	Sc (cm)	11.1	1.9	30.5

The values of f_p were plotted against those of $1/F_p$ and a linear best-fit line was drawn through the points (Figure 4-21-b). The slope of the best fit curve represented m the value of Darcy's hydraulic coefficient K. The intercept value n of the curve was equated to ηS_c, and with the knowledge of η obtained through laboratory testing of redeemed soil samples (Chapter 5), S_c was thus estimated.

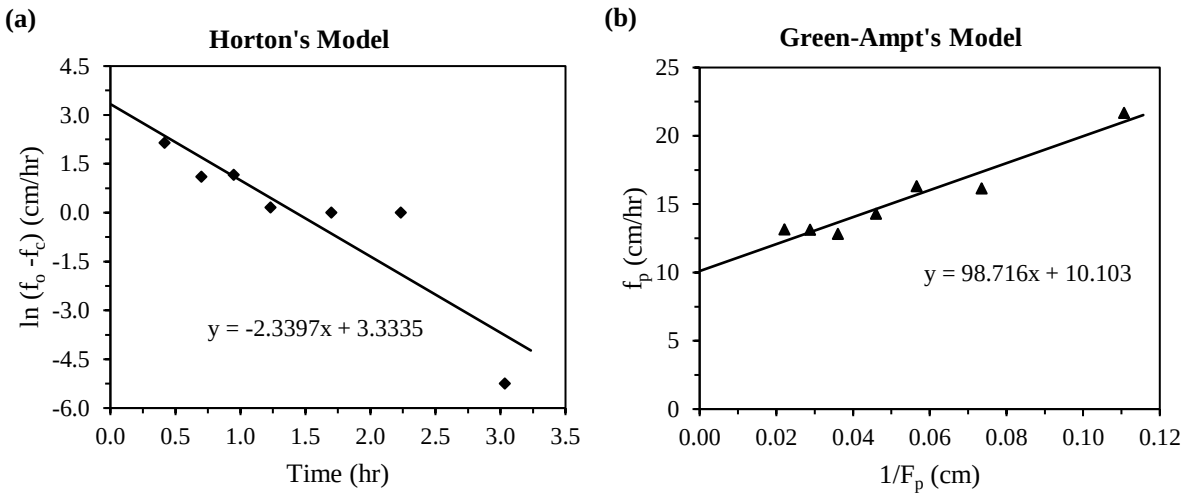

Figure 4-21: (a) Plot of $\ln(f_0-f_c)$ Versus time, and (b) f_p versus $(1/F_p)$

The field Double-Ring Infiltration (DRI) investigation revealed high variability in infiltration rates, and consequently hydraulic conductivity values, across the area of a single pond. The surface area of the ponds ranged between 0.9 – 3.2 ha, however, within those comparatively small areas, variations between the evaluated hydraulic conductivity values were noted to fluctuate by more than a single order of magnitude

When it comes to in-situ infiltration investigations, factors such as the type of soil, hydraulic gradient, boundary conditions, as well as the temperature of liquids used may affect infiltration test results. Because of this, ASTM (2009) has recommended for these results to be considered only as index values. Thus, conducting infiltration experiments at three different positions across each pond provided a better average representation of general soil properties and infiltration rates for reasonable design considerations. Detailed discussions of the field experimental results are presented in Chapter 6 .

5 Laboratory Infiltration Investigation

5.1 Introduction

To observe whether the hydraulic conductivity values obtained from the field Double-Ring Infiltrometer (DRI) tests described in Chapter 4 were consistent with those observed under laboratory conditions, constant-head permeability tests were conducted on soil samples retrieved from each of the field infiltration test locations.

This chapter discusses the materials, apparatus, sample preparation, and experimental procedures adapted in the laboratory permeability test investigation. It starts with a description of tests conducted to classify the physical properties of 18 soil samples retrieved from the three investigated stormwater ponds. The soil classification tests were conducted following American Standard for Testing and Materials (ASTM) International Standards. In the instance where no standards of practice were available (for example measuring the volume of core samples using water displacement method to determine the density), consistent procedures were adapted to warrant repeatability of results as reasonably as possible.

The chapter follows with a description of the constant-head permeameter apparatus and test method employed to determine the hydraulic conductivity of the various soil samples. The processing of permeability test results is explained before the chapter concludes with an outline of measures taken to ensure quality and accuracy were upheld throughout the experimental procedures.

Completely disturbed soil samples were attained from in situ infiltration test locations and stored in sealable plastic bags to mitigate moisture loss. Relatively undisturbed samples were also collected in 200 mm high hollow cores with internal diameters of approximately 50 mm. All samples were dated and labelled according to the DRI test locations and depths from which they were retrieved (Figure 5-1). This was done to ensure that the laboratory investigation results could be linked to the relevant field test.

A total of 18 soil sample bags and 18 core samples were retrieved from the field investigation. Physical classification tests listed in Table 5-1 as well as constant-head permeability tests were conducted using the disturbed soil samples. The core samples on the other hand were used to determine the density of the investigated in-situ soil layers.

Table 5-1: Soil physical properties test methods and standards

Soil Property	Test Method	Test Standard Code
Moisture content	Oven-drying	ASTM D2216-10
Particle grading	Dry sieve analysis	ASTM D6913-04
Specific gravity	Small pycnometer method	ASTM D854-14

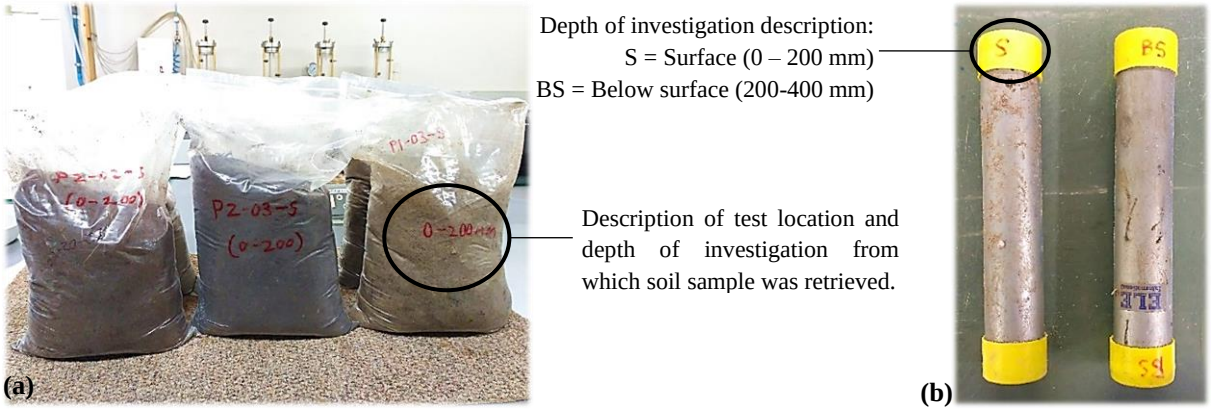

Figure 5-1: (a) Disturbed Soil samples and (b) cores from investigated stormwater ponds

5.1.1 Density

The bulk density ρ_b of in situ soil material was determined by dividing the mass m of each soil sample within the retrieved core by its estimated intact volume V (Equation 5.1). The volume was estimated using the water-displacement method elucidated in Figure 5-2. To avoid the dissociation of soil material within the core sampler, the cores were submerged in the graduated cylinders without removing the soil. The analysis accounted for the mass of the empty core to avoid overestimating the soil bulk density.

$$\rho_b = \frac{m}{V} \qquad 5.1$$

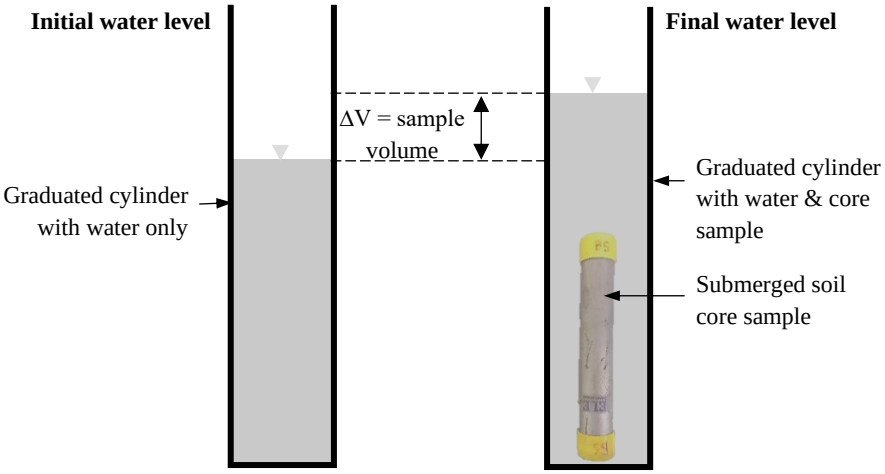

Figure 5-2: Schematic diagram of displacement method used to determine sample volume

5.1.2 Oven Dying

Before determining the various soil samples' particle grading and specific gravity, they were oven-dried at about 105°C for 24 hours and subsequently stored in sealed plastic bags to mitigate changes in moisture content (Figure 5-3). The oven-drying was carried to determine the natural moisture content *w* of the material, and to prepare the soil for dry sieve analysis and specific gravity tests which required the soil to be in a dry state. Because 18 different soil samples were handled during this drying process, cross-contamination of soils needed to be avoided, and careful measures were taken to label samples accordingly.

Laboratory oven used to dry soil samples at 105°C

Samples removed after 24 hrs to be used for sieve analysis and specific gravity test

Dry soil samples in sealed plastic bags to mitigate change in moisture content

Oven-dried samples in small tins for determination natural moisture content

Figure 5-3: Oven drying of soil samples

5.1.3 Soil Particle Grading

The determination of soil particle size distribution was carried out through dry sieve analysis as per ASTM D6913-04 guidelines while the soil classification was done following the Unified Soil Classification System (USCS). From the resultant grading curves of the 18 samples (Figure 5-4), the soils were all generally coarse-grained and sandy.

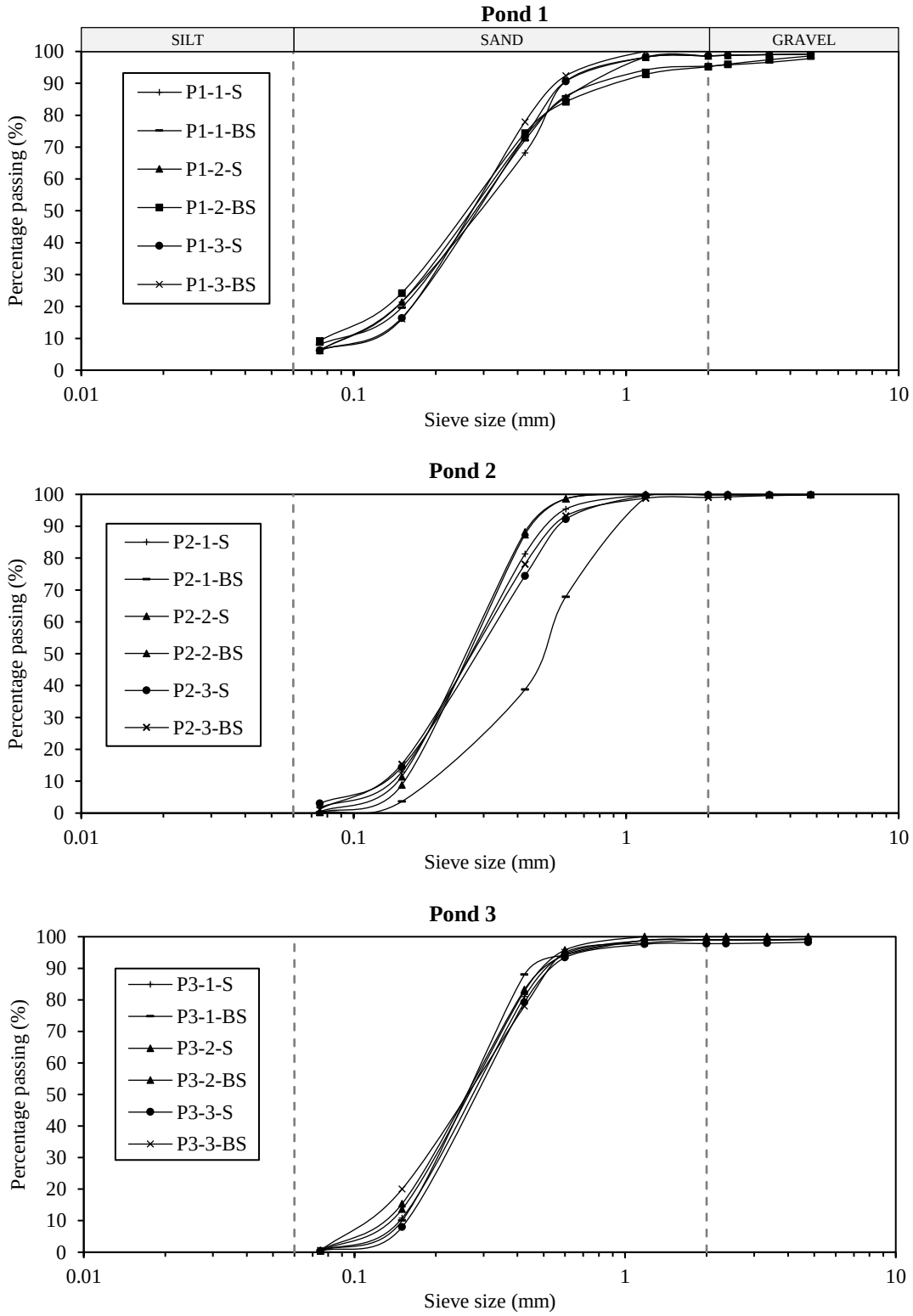

Figure 5-4:Grading curves of various soil samples from the investigated ponds

Coarse-grained soils are considered well-graded if the coefficient of uniformity (C_u) is greater than 6 and the coefficient of curvature (C_c) is between 1 and 3. These coefficients were

calculated using Equations 5.2 and 5.3 where D_{10}, D_{30} and D_{60} are, respectively, the soil particle diameters corresponding to the percentages finer than 10 %, 30%, and 60%.

$$C_u = \frac{D_{10}}{D_{60}} \quad 5.2$$

$$C_c = \frac{D_{30}^2}{D_{60} \times D_{10}} \quad 5.3$$

The six samples from Pond 1 were classified as poorly graded sand with silt (SP-SM) because between 5 and 10 % of the soil passed through the 0.075 mm aperture sieve and the C_u values were all generally below 6. Moreover, samples from Pond 2 and Pond 3 were all classified as poorly graded sand (SP) because less than 5 % of the soil particles were small enough to pass through the 0.075 mm sieve, and the C_u values ranged only between 1.3 and 2.3.

It should be noted that some of the tested samples were retrieved from stormwater ponds with vegetated topsoil comprising of impurities and litter from neighbouring residents. Consequently, before the sieve analysis organics, impurities, as well as cobbles, were omitted from the soil samples. Nevertheless, the results were considered valuable as the fraction of removed particles (Figure 5-5) was negligible (< 5%) relative to the overall samples sizes.

Figure 5-5: Organics, impurities, and cobbles removed from samples before sieve analysis

5.1.4 Specific Gravity

The soil particle density (also known as specific gravity G_s) of the samples was determined employing the small pycnometer test method illustrated in Figure 5-6. Gs is defined as the ratio between the density of soil solids only, and the density of water. It can also be expressed as:

$$G_s = \frac{W_S}{V_s \rho_w} \quad 5.4$$

where W_S is the mass of soil solids, V_s is the volume of soil solids, and ρ_w is the density of water.

Like the sieve analysis, soil samples were removed of impurities through sieving however only particles smaller than 4.75 mm were investigated as per ASTM D854-14 recommendations. G_s

values of samples from the three investigated ponds were found to be very close to one another as they ranged between 2.56 and 2.61. These values are typical for organic soils or sands with organic matter which can be owed to the presence of minor remnants of grassroots even after the clear majority had been removed.

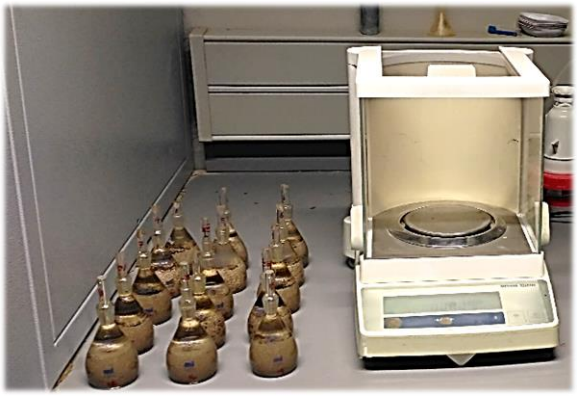

Small pycnometer bottles with soil and distilled water, weighed using sensitive enclosed electronic balance

Small pycnometer bottles with distilled water only.

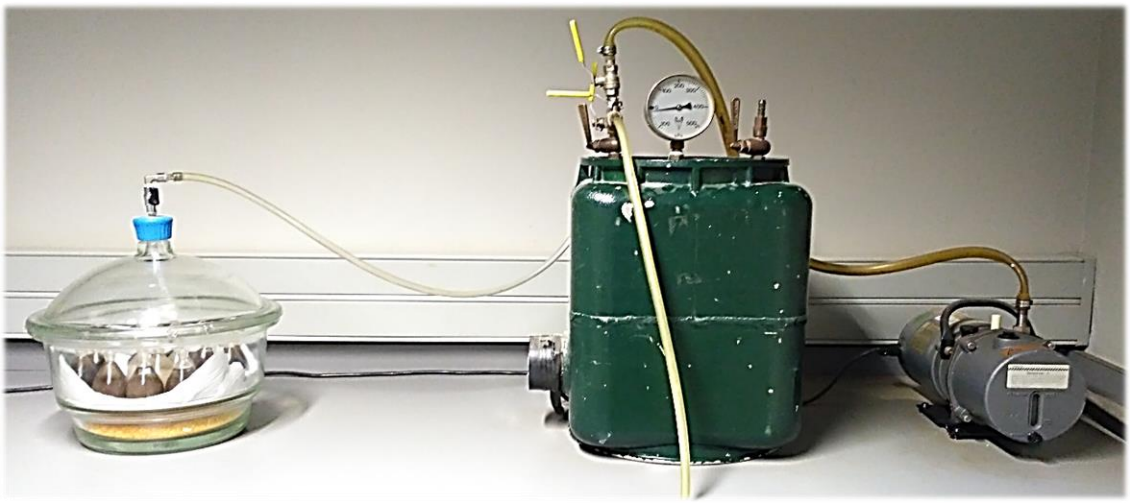

Entrapped air removed from small pycnometer bottles, with soil and water, using vacuum desiccator.

Figure 5-6: Specific Gravity test apparatus

5.1.5 Porosity

Using the recorded natural moisture contents w, bulk densities ρ_b and specific gravity G_s of the investigated soil samples, the average void ratios e were computed from the following relationship:

$$e = \left(\frac{G_s \times \rho_w}{\rho_d} - 1\right) 100 \qquad 5.5$$

where ρ_d is the dry density of the soil calculated as follows:

$$\rho_d = \frac{\rho_b}{1 - w} \quad 5.6$$

thus, the porosities n of each sample were computed using Equation 5.7.

$$n = \frac{e}{1 + e} \quad 5.7$$

The porosity values of the 18 investigated soil samples ranged between 0.27 and 0.51 with the highest corresponding to samples obtained from the surface (0 – 200 mm) of Pond 3 and the lowest from the subsurface (200 – 400 mm) of Pond 2. In general, the average porosities of the surface deposits of the three ponds were generally higher than those of the subsurface however this was not consistent for all cases.

5.1.6 Summary of Samples' Physical Properties

A summary of the average soil samples' physical properties obtained from laboratory tests and calculations, before permeability investigations, is presented in Table 5-2.

Table 5-2: Average physical properties of investigated soils

Property		Units	Pond 1		Pond 2		Pond 3	
			*Surface	**Below Surface	Surface	Below Surface	Surface	Below Surface
Soil Texture	Fines	%	6	8	2	1	1	1
	Sand		92	89	98	99	98	98
	Gravel		1	3	0	0	1	1
Effective Grain Size	d_{10}	mm	0,10	0,10	0,15	0,17	0,16	0,14
	d_{30}		0,19	0,19	0,20	0,25	0,21	0,19
	d_{60}		0,35	0,33	0,32	0,39	0,32	0,30
Coefficients of Uniformity and Curvature	C_u	-	3,53	3,57	2,15	2,32	1,30	1,36
	C_c	-	1,01	1,14	0,85	0,98	0,85	0,86
USCS Soil Group		-	SP-SM	SP-SM	SP	SP	SP	SP
Porosity		-	0.32	0.33	0.44	0.30	0.43	0.38
Void Ratio		%	47	49	78	43	77	61
Specific Gravity		-	2,61	2,60	2,49	2,60	2,56	2,58
Bulk Density		kg/m^3	1733	1889	1460	1917	1635	1930
Natural Moisture Content		%	6	8	5	5	13	17

*Sample from Surface (0 – 200 mm depth)
**Sample from Below Surface (200 – 400 mm depth)

5.2 Constant-Head Permeameter Investigation

5.2.1 Research Apparatus

The combination permeameter was the laboratory apparatus selected for determining the coefficient of permeability (also known as the hydraulic conductivity K) of the soil samples obtained from the field. This apparatus is designed to determine the permeability of either fine-grained or coarse-grained soils. Because the sieve analysis revealed that the 18 investigated soil samples were generally coarse-grained (i.e. more than 90 % of the particles were retained on the 0.075 mm aperture sieve tray), the specimens were thus tested using the constant-head assembly illustrated in Figure 5-7.

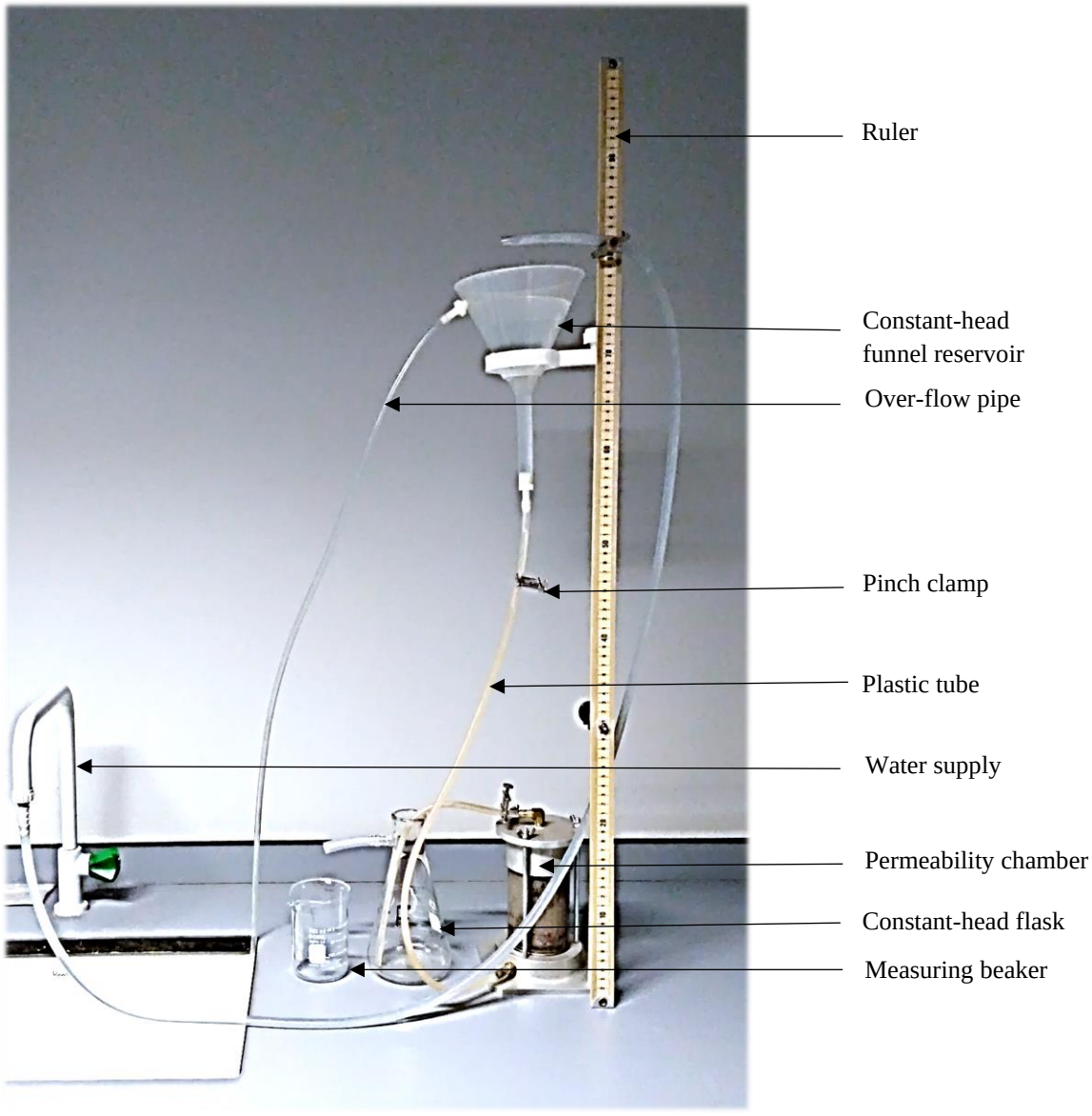

Figure 5-7: Constant-head permeability test apparatus

The testing apparatus' components were low-cost and easy to assemble. These included a plastic cylinder (or permeability chamber) for retaining the soil specimen, two porous stones, two rubber seals, two filter papers, a spring, a constant-head flask, a funnel, some pinch clamps, plastic tubes, a stand, and a long ruler. A detail of the components making up the permeability chamber is shown in Figure 5-8 with dimensions annotated on the schematic in Figure 5-9.

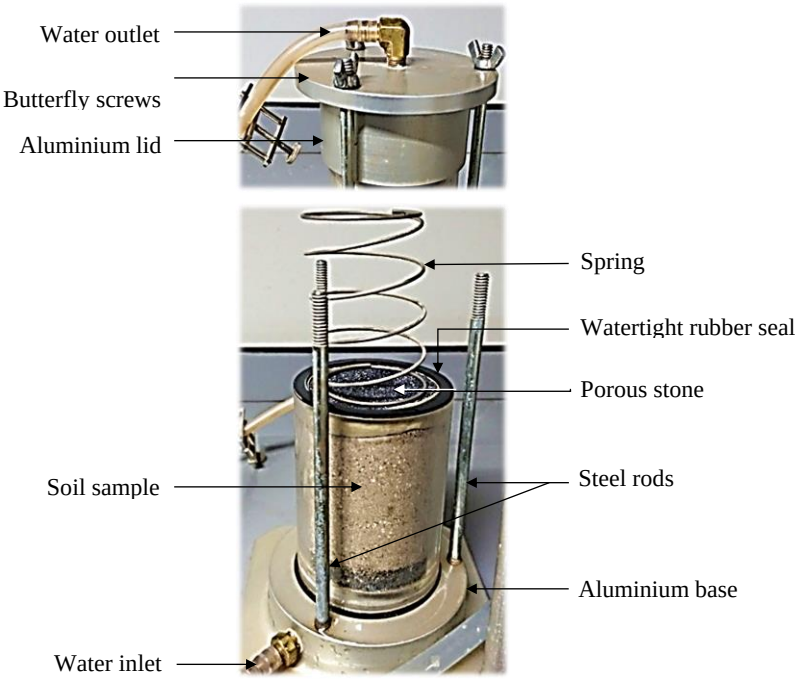

Figure 5-8: Permeability chamber components

The internal diameter of the plastic cylinder was measured to be 63 mm whilst the porous stones were marginally narrower in diameter by about 1 mm. The overall sample height between the top and bottom porous stones was maintained at 60 mm. The small gap between the top porous stone and the chamber was sealed with a rubber band to prevent fine particles from being washed out during the investigation.

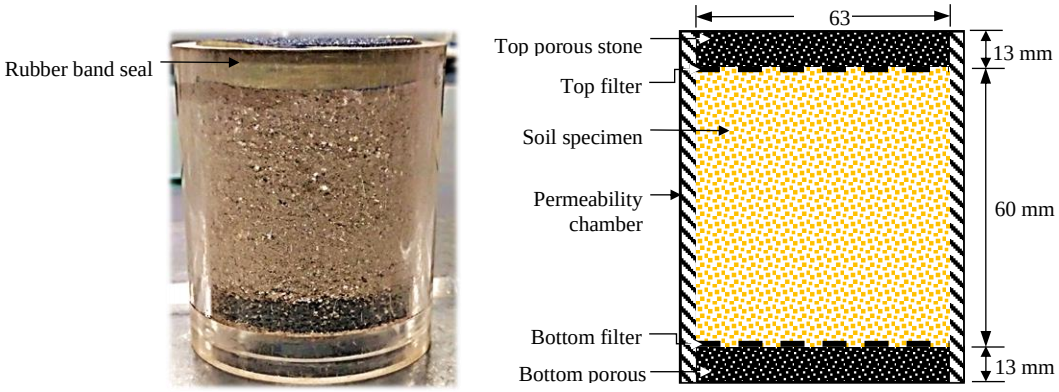

Figure 5-9: Permeability chamber image and schematic with dimensions

5.2.2 Permeability Test Schedule

A testing program developed for this permeability investigation is presented in Table 5-3. Each soil specimen was examined under three different pressure heads, consequently resulting in a total of 54 constant head permeability tests (i.e., 18 multiplied by 3).

Table 5-3: Permeability test program

Test No.	Pond No.	Sample No.	Sample Depth		Test Code	Bulk Density
-	-	-	S / BS	(mm)	-	kg/m^3
1	1	1	Surface	0 - 200	P1-1-S	1602
2		2			P1-2-S	1724
3		3			P1-3-S	1874
4		1	Below Surface	200 - 400	P1-1-BS	1767
5		2			P1-2-BS	2040
6		3			P1-3-BS	1859
7	2	1	Surface	0 - 200	P2-1-S	1460
8		2			P2-2-S	1464
9		3			P2-3-S	1456
10		1	Below Surface	200 - 400	P2-1-BS	1917
11		2			P2-2-BS	2046
12		3			P2-3-BS	1787
13	3	1	Surface	0 - 200	P3-1-S	1635
14		2			P3-2-S	1520
15		3			P3-3-S	1750
16		1	Below Surface	200 - 400	P3-1-BS	1930
17		2			P3-2-BS	1871
18		3			P3-3-BS	1990

5.2.3 Sample Preparation

Instead of using oven-dried samples, soil specimens retained in sealed plastic bags, at natural moisture content, were recompacted in the permeability chamber to achieve bulk densities associated with their respective in-situ densities. The specimen preparation procedure, before the permeability testing process, is illustrated in Figure 5-10 (a to h) and summarised below:

a) The required mass m of soil was weighed to obtain the necessary bulk density ρ_b using the relationship of $\rho = m/V$. The volume within the permeability chamber was maintained at a constant 187 cm^3 for all specimens.

b) The soil specimen was poured into the permeability chamber in small even layers.

c) The sample was compacted in incremental layers until obtaining the desired bulk density.

d) The top porous stone was wrapped with a rubber band to prevent loss of fines during testing

e) The top filter paper and porous stone were placed on top of the compacted sample.

f) The permeability chamber assembly was weighed on a digital scale before the sample length *L* was verified.

g) The chamber was placed on an aluminium base with a spring against the top porous stone to prevent the sample from expanding during testing.

h) An aluminium lid was placed on top of the chamber and fastened with butterfly screws, ensuring that a water-tight rubber seal was in place to prevent any leakage.

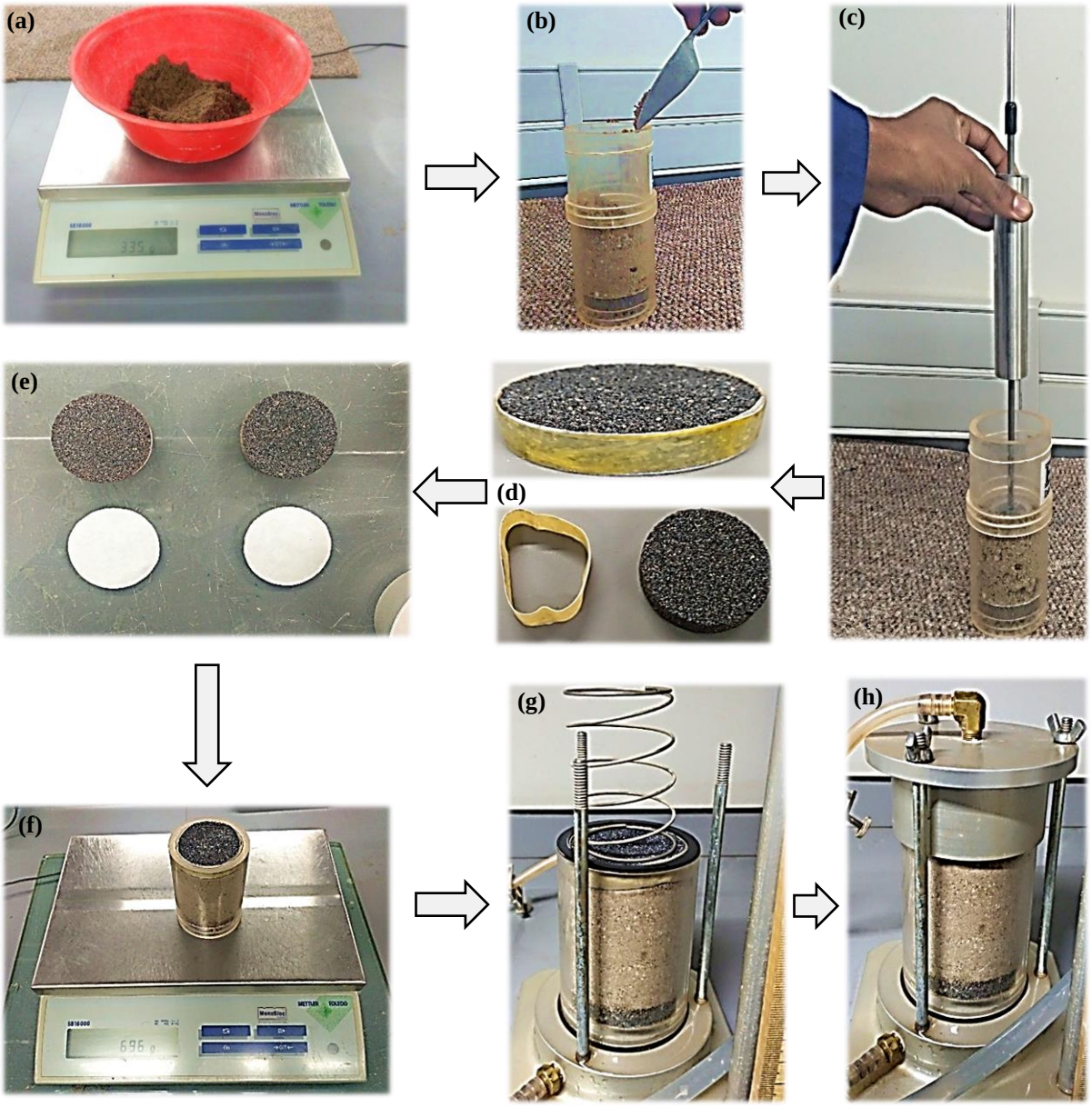

Figure 5-10: Permeability test sample preparation

5.2.4 Test Procedure

Once the sample was prepared, the constant-head funnel and meter stick (ruler) were assembled on a stand using clamps. Subsequently, the inflow and outflow pipes were connected, correspondingly, at the bottom and top of the permeability chamber (Figure 5-11).

Before running the test, a pinch clamp was used to seal the inflow pipe whilst a vacuum of approximately 50 kPa was applied for fifteen minutes through the outflow pipe to remove any trapped air within the sample. After the evacuation, the constant head funnel was filled with distilled water and the pinch clamp was gradually opened until the degree of saturation of the specimen under flow was close to 100%. At full saturation, the vacuum pump was disconnected, and the specimen was considered ready for testing.

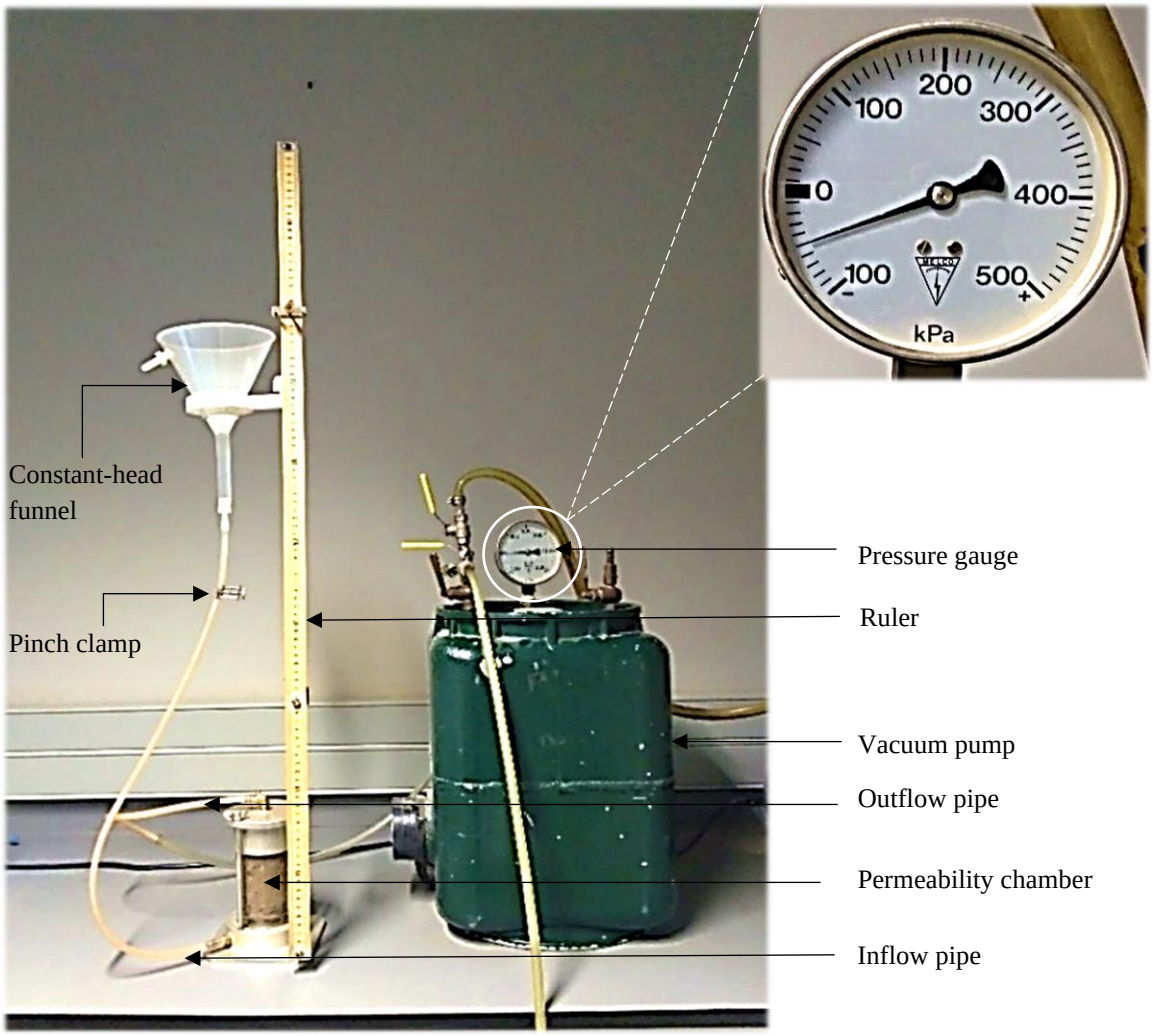

Figure 5-11: Removal of air voids from specimen at -50 kPa pressure

To determine the hydraulic conductivity K of the soil specimen, the schematic setup illustrated in Figure 5-12 was adapted for the testing process. In the Figure, the water-flow direction from the supply to the graduated cylinder is indicated by arrows.

With all pinch clamps fully opened, the water flow supplying the constant-head funnel was regulated so that the head difference h between the constant-head funnel and constant-head flask remained constant. Once equilibrium flow conditions were established, the water flowing out of the constant-head flask Q was collected in a graduated cylinder whilst the collection time t was recorded with a stopwatch. Because temperature T affects the viscosity of water and consequently the flow rate, a thermostat was used to measure the temperature of water collected in the graduated cylinder.

The procedure was repeated at three head-differences h so that a reasonable average was obtained when processing the data to determine K.

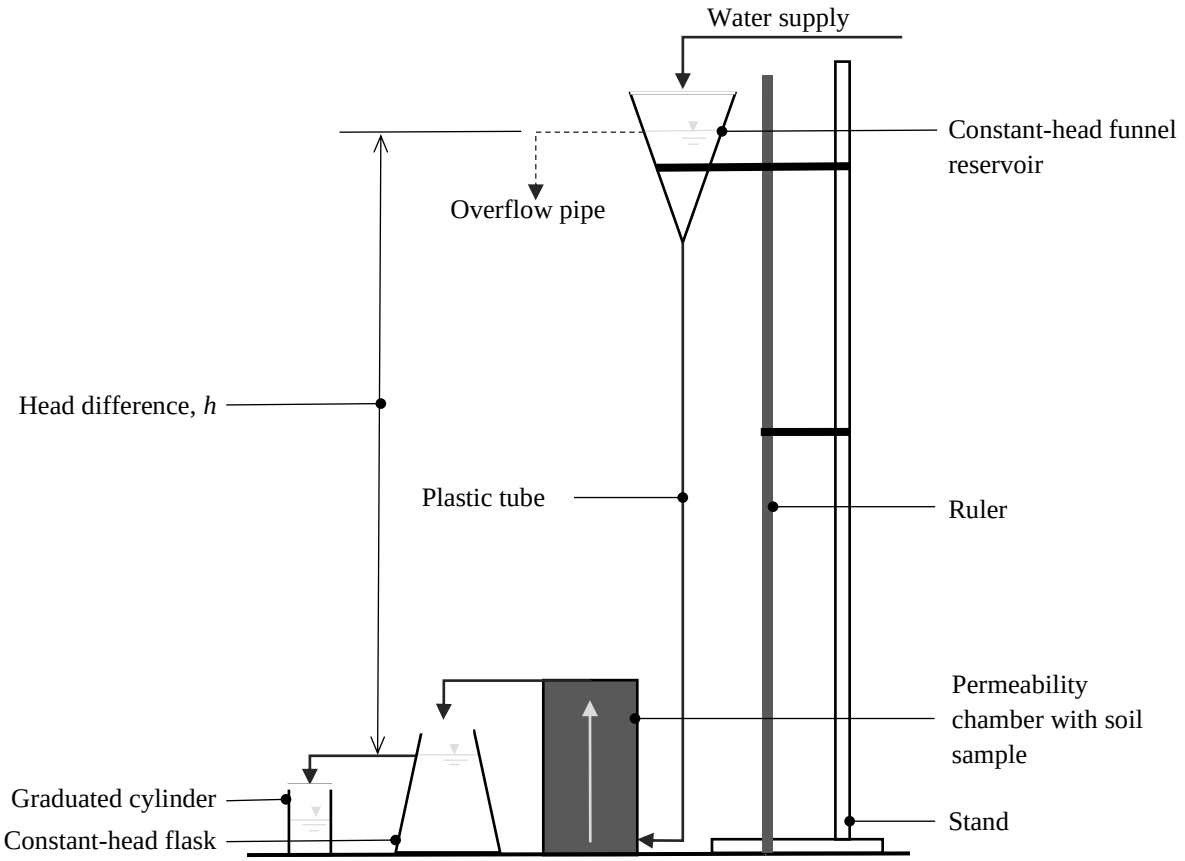

Figure 5-12: Schematic diagram of constant-head permeability test setup and flow direction

5.3 Data Processing

The hydraulic conductivity K (cm/s) was calculated as:

$$K = \frac{QL}{Aht} \tag{5.8}$$

with Q (ml) being the volume of water collected in the graduated cylinder, t (s) being the collection time, L (cm) being the vertical length of the soil specimen within the permeability chamber, A (cm^2) being the surface area of the chamber, and h (cm) being the vertical head

difference. In this investigation, L and A were kept constant for all tests at 60 cm, 31.2 cm^2 respectively. An average K value was used from the three varied head differences.

The value of K determined using Equation 5.8 is usually for water at a test temperature of 20°C. Because the temperatures measured during this investigation were approximately 25°C, modification factors were applied to account for the viscosity as follows:

$$K_{20°C} = K_{T°C} \frac{\eta_{T°C}}{\eta_{20°C}} \qquad 5.9$$

where $\eta_{T°C}$ and $\eta_{20°C}$ are viscosities of water at $T°C$ and $20°C$ accordingly. Figure 5-13 gives the values of $\eta_{T°C}/\eta_{20°C}$ for various water temperatures. It is apparent that an increase in water temperature results in a lower value for $\eta_{T°C}/\eta_{20°C}$ and correspondingly a lower hydraulic conductivity.

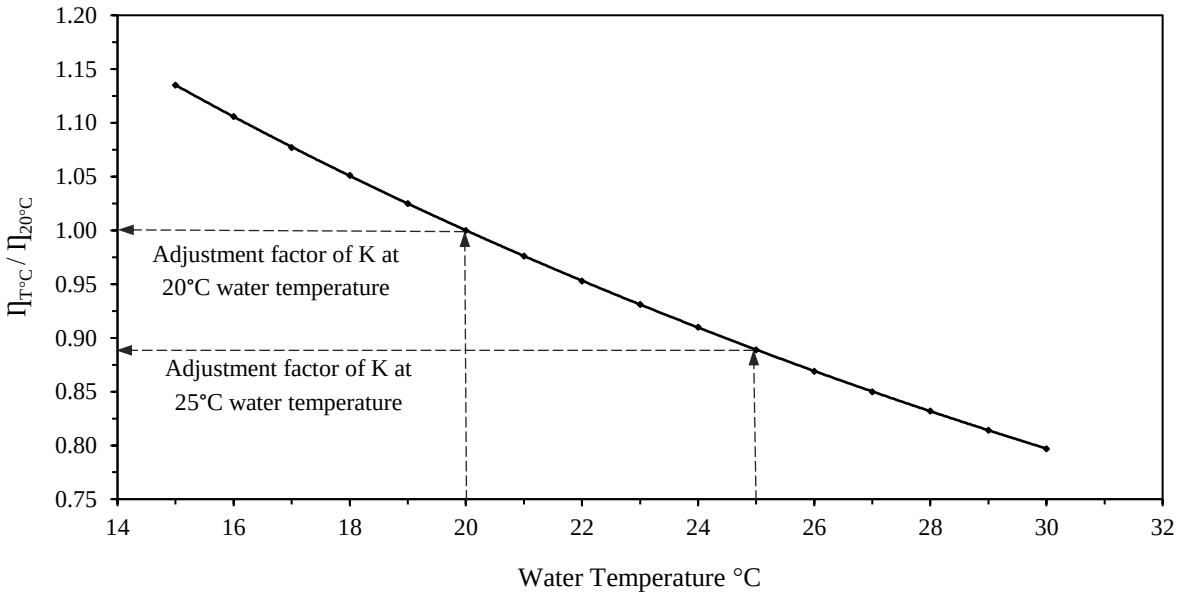

Figure 5-13: Variation of $\eta_{T°C} / \eta_{20°C}$ with water temperature
Adapted from: Braja (2002)

5.4 Accuracy and Quality Control

To ensure that quality and consistency was appreciated throughout the laboratory permeability investigation, the following measures were taken:

- The same apparatus was used for all the constant-head permeability tests.
- Soil specimen lengths and volumes were kept constant.
- Specimen densities were varied accordingly to replicate the associated in-situ bulk densities.

- The standard deviation of the averages between each set of three tests used to determine the average hydraulic conductivity of soil specimens was maintained at a maximum of 5%. analysed. Test sets that deviated beyond 5% from the average were repeated.
- Water temperature was measured to the nearest degree and effects of temperature and viscosity on K were accounted for with the appropriate correction factors.

Laboratory tests conducted on soil samples retrieved from the field test locations confirmed a significant percentage difference and an absence of any direct link between the investigated field and laboratory hydraulic conductivity values. The laboratory hydraulic conductivity was generally higher than the field hydraulic conductivity. The average difference between the laboratory method was subject to various disadvantages since the small sample area increased the possibility of large random errors, however, increased the likely repeatability because of the controlled environment. Detailed analysis and discussions of the laboratory experimental results are presented in Chapter 6 .

6 Analysis and Discussion of the Experimental Results

6.1 Introduction

All test results from the Double-Ring Infiltrometer (DRI) and Constant-Head Permeameter (CHP) tests conducted in the field and laboratory, respectively, are presented in this chapter. The chapter is divided into five main sections. The first section discusses the field DRI test results. The laboratory CHP test results and discussions appear in the second section. In the third section, a comparison between the field and laboratory results is presented. Before the chapter ends with a summary and conclusions of the experimental findings, the variability of the investigated soil's hydraulic conductivities is discussed in the fourth section.

6.2 Investigation of Field Infiltration Test Results

6.2.1 Surface Deposits of Investigated Ponds

Within each of the three investigated stormwater ponds, surface-strata observation pits were excavated to a depth of approximately 20 cm (Figure 6-1). This was done for two primary reasons, firstly to observe the extent to which the organic and loamy topsoil layers reached below the ponds' surfaces and secondly, to observe the underlying soil material which, in this investigation, was assumed to extend uniformly below the ground reaching depths greater than 10 m. These assumed uniform, continuous strata depths are based on borehole logs drilled within and around the study area.

Generally, the ponds' surfaces were mostly vegetated with naturally growing grass and weeds. Directly below the surfaces, dark brown (Pond 1 and Pond 3) and dark grey (Pond 2), loamy, organic, sandy layers were encountered to depths ranging between 6 cm (Pond 1 and Pond 3) and 11 cm (Pond 2). Underlying the loamy topsoil of Pond 1 and Pond 3 were light brown sands interbedded with greyish brown sand, particularly in Pond 3. On the other hand, Pond 2 consisted of uniform light grey sand below the 11 cm thick organic topsoil layer. In total, 18 DRI tests were conducted on these varying soil types within the stormwater ponds; both on the surface as well as 20 cm below the surface.

6.2.2 Double-Ring Infiltrometer Test Results

This section presents results from the field DRI tests in the typical form of cumulative infiltration versus time, as well as infiltration rate versus time diagrams. Further plots displaying the ranges within which the cumulative infiltration and infiltration rates fell within for each tested pond are presented and discussed. Furthermore, a summary indicating maximum and minimum infiltration values attained over a test period of three hours is presented. The results are discussed below for each of the three investigated ponds:

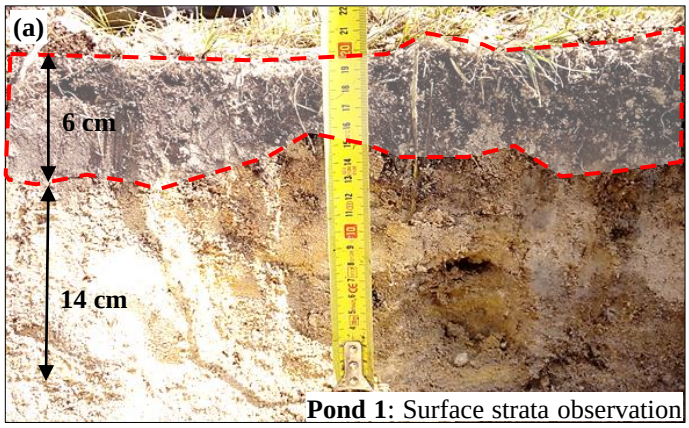

Pond 1: Surface strata observation

→ Dark brown, sandy, organic, loamy, top soil layer with grass (approximately 6 cm average thickness)

→ Light brown sand. Layer is assumed to extend to depths greater than 10 meters based on borehole log data presented in Chapter 5.

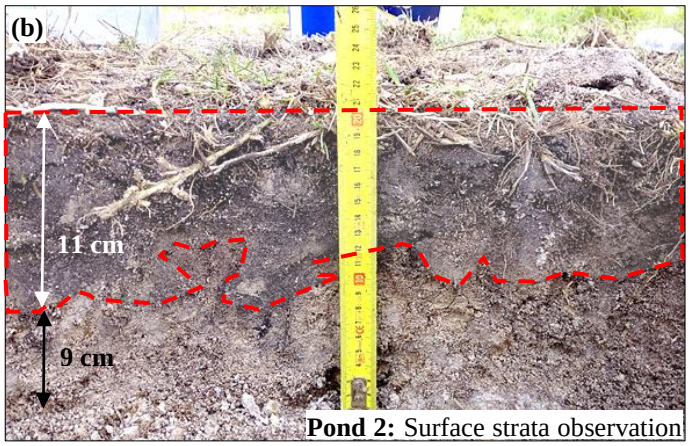

Pond 2: Surface strata observation

→ Dark grey, sandy, organic, loamy, top soil layer (approx. 11 cm average thickness)

→ Light grey sand. Layer is assumed to extend to depths greater than 10 meters based on borehole log data presented in Chapter 5.

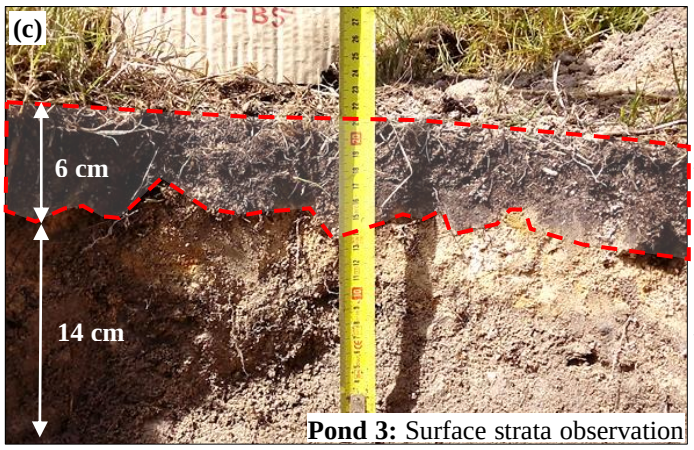

Pond 3: Surface strata observation

→ Dark brown, sandy, organic, loamy, top soil layer (approx. 11 cm average thickness)

→ Light brown to light grey sand. Layer is assumed to extend to depths greater than 10 meters based on borehole log data presented in Chapter 5.

Figure 6-1: General Surface deposits of (a) Pond 1, (b) Pond 2, and (c) Pond 3

6.2.2.1 Pond 1

The field infiltration results obtained from six DRI tests conducted within Pond 1 are presented in Figure 6-2 and Figure 6-3. For the three tests carried out at different locations on the pond's surface a common trend in the shape of the infiltration versus time curves was observed (Figure 6-2 a, c, and e). There was a general exponential reduction in the infiltration rate for the first hour followed by a relatively steady rate f_c until the test was concluded.

The initial infiltration rates f_o of the surface tests ranged between 6 and 33 cm/hr whilst the steady infiltration rates varied between 2.9 and 12.5 cm/hr. The associated cumulative infiltration F_p curves corresponded to the infiltration rate curves such that during the first hour of the test, the cumulative infiltration increased at a decreasing rate until steady-state was achieved from which the cumulative infiltration increased at a constant rate. Over a three-hour test period, the cumulative infiltration of the surface tests ranged between 8 and 45 cm.

Infiltration versus time curves of the three tests conducted below the surface displayed rather unconventional yet consistent trends and much lower infiltration rates than those of the surface tests (Figure 6-2 b, d, and f). From the beginning of the tests, the infiltration rates increased rapidly before reaching a peak after one hour. Following the peak infiltration rates were gradual reductions until steady infiltration rates were reached after approximately two and a half hours.

Initial infiltration rates of all three sub-surface tests were similarly low at approximately 0.10 cm/hr whilst the recorded steady infiltration rate ranged between 0.30 and 0.32 cm/hr. The corresponding cumulative infiltration curves increased in a linear manner with increasing time; negligible variations were observed through the course of the test period. All three sub-surface tests achieved maximum cumulative infiltrations of 1.0 cm.

On average, the measured initial infiltration rate f_o on the sub-surface of Pond 1 was 99% lower than that of the surface tests (Table 6-1). Similarly, the steady-state infiltration rate f_c was 95% lower when the top 20 cm topsoil layer was removed. A summary of the DRI test result values for each investigated location within the pond is presented in Table 6-2

Table 6-1: Percentage difference between initial and steady infiltration rates of surface and sub-surface tests in Pond 1

Surface		Below Surface	
Average Initial Infiltration Rate f_o	**Average Steady Infiltration Rate f_c**	**Average Initial Infiltration Rate f_o**	**Average Steady Infiltration Rate f_c**
cm/hr	**cm/hr**	**cm/hr**	**cm/hr**
17.33	5.97	0.10	0.31

f_o 99% decrease

f_c 95% decrease

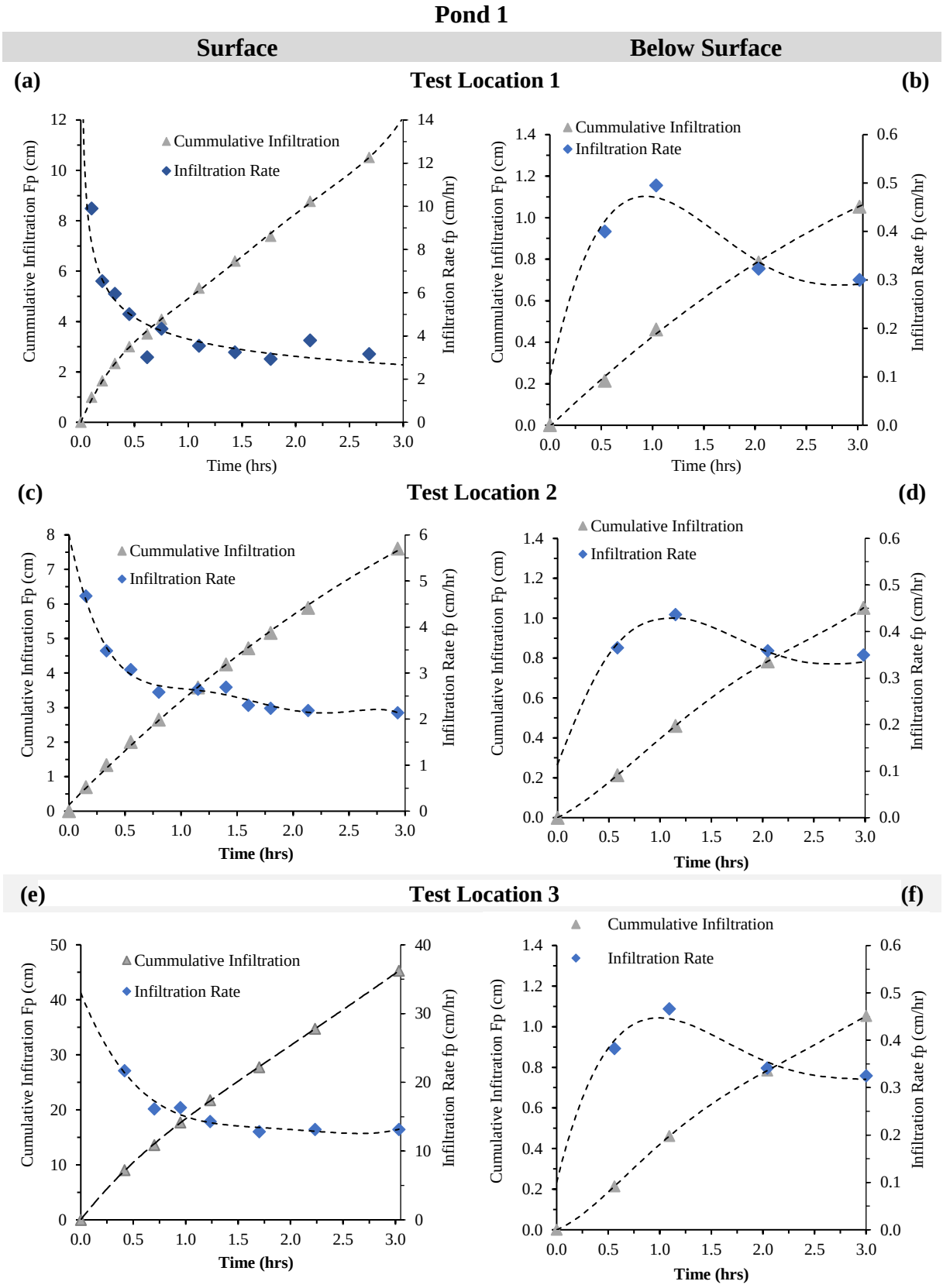

Figure 6-2: Pond 1 cumulative infiltration and infiltration rate versus time

Pond 1

Surface **Below Surface**

(a) **Cumulative Infiltration VS Time…** **……** **…** **……..(b)**

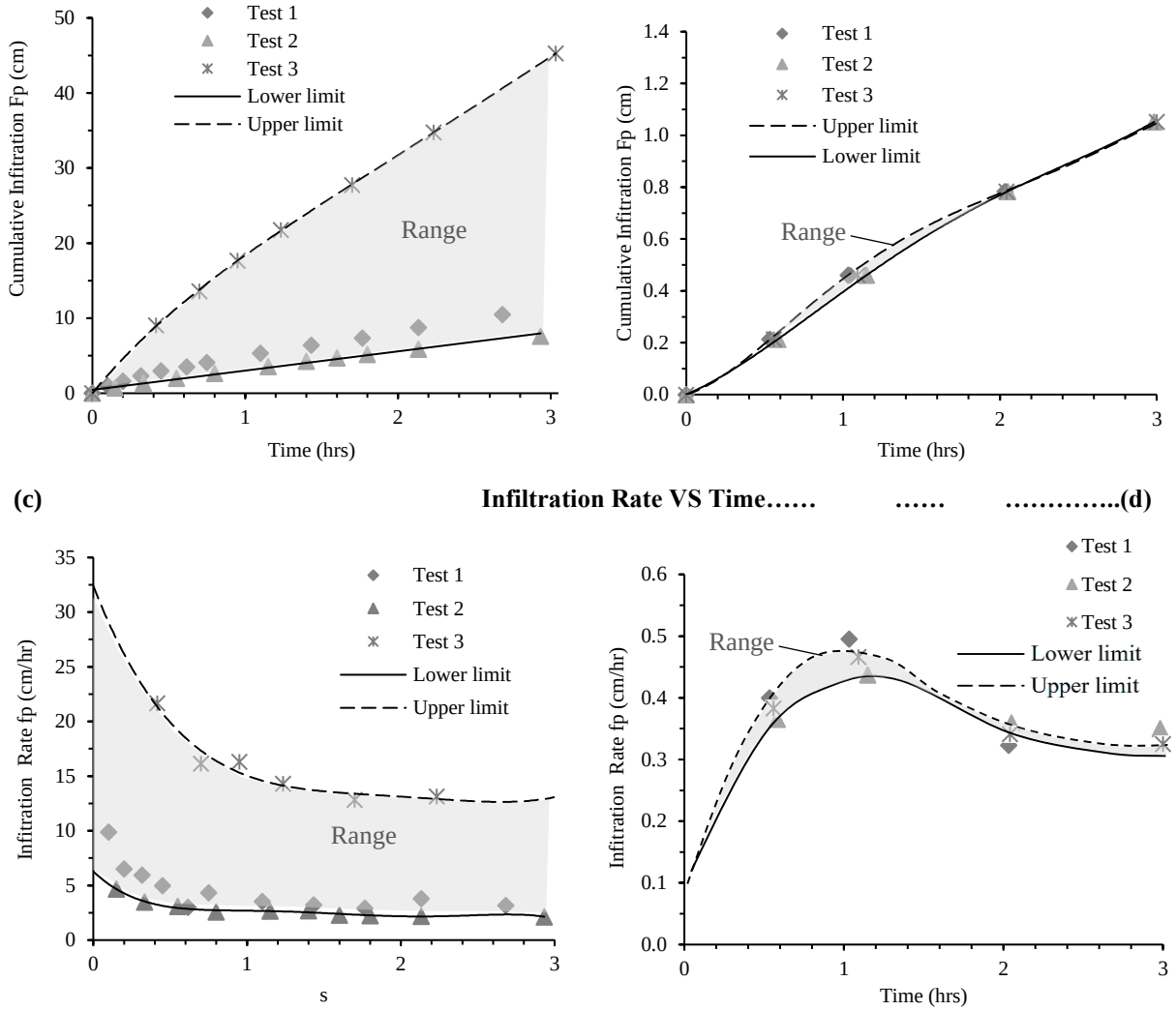

(c) **Infiltration Rate VS Time……** **……** **……..(d)**

Figure 6-3: Pond 1 Infiltration ranges from field DRI tests

Table 6-2: Summary of Pond 1 Field DRI Test Results

Surface					**Below Surface**				
Test location	F_p **t = 0**	F_p **t = 3hrs**	f_o **t = 0**	f_c **t = 3hrs**	**Test location**	F_p **t = 0**	F_p **t = 3hrs**	f_o **t = 0**	f_c **t = 3hrs**
-	cm	cm	cm/hr	cm/hr	-	cm	cm	cm/hr	cm/hr
1	0	10.5	13	2.9	1	0	1.1	0.1	0.30
2	0	8.0	6	2.5	2	0	1.1	0.1	0.32
3	0	45.0	33	12.5	3	0	1.1	0.1	0.31

6.2.2.2 Pond 2

Test results obtained from the inspected locations within Pond 2 are presented in Figure 6-4 and Figure 6-5. Unlike in Pond 1, the three infiltration rate curves obtained from surface tests did not demonstrate similar behaviour (Figure 6-4 a, c, e). Test Location 2 displayed a rapid reduction in the infiltration rate for the first two hours followed by a steady rate whilst Test Location 3 only displayed a rapid reduction in infiltration rate for the first 30 minutes after which a constant rate f_c was achieved with minor modulations gradually becoming steadier towards the end of the test. The infiltration rate of Test Location 1, on the other hand, generally fluctuated throughout the 3-hour test period, however, the fluxes became less rigorous in the final hour of the test.

The measured initial surface infiltration rates f_o ranged between 10 and 40 cm/hr whereas the steady-state rates varied between 5 and 31 cm/hr. Cumulatively, the respective infiltration over 3 hours ranged between 18 and 97 cm. The observed increase in the cumulative infiltration F_p was linear for Test Locations 1 and 3 however, Test Location 2 increased at a gradually decreasing rate before becoming linear ones steady-state rates were achieved from 2 hrs.

Analysis of the three infiltration rate curves of tests conducted below the surface of Pond 2 also revealed inconsistent patterns when compared to one another. Test Locations 1 and 3 displayed relatively constant infiltration rates for the entirety of the test period but the rates measured from Test Location 1 were significantly higher than those of Test Location 3. On the other hand, no measurable infiltration was observed below the surface of Test Location 2.

Initial infiltration rates below the surface varied from 0 to 31 cm/hr whilst the steady infiltration rates ranged between 0 and 28 cm/hr. A linear increase in the cumulative infiltration ranging between 0 and 88 cm after three hours was recorded below the pond's surface.

Generally, the field DRI tests conducted below the surface of the pond revealed lower infiltration rates than those conducted on the surface. The initial infiltration rate below the surface was found to be 54% less than that obtained on the surface. Comparatively, the average steady infiltration rate was 45% lower on the sub-surface of the pond (Table 6-3). Summarised in Table 6-4 are the infiltration values obtained from each experimental Test Location.

Table 6-3: Percentage difference between initial and steady infiltration rates of surface and sub-surface tests in Pond 2

Surface		**Below Surface**	
Average Initial Infiltration Rate f_o	**Average Steady Infiltration Rate f_c**	**Average Initial Infiltration Rate f_o**	**Average Steady Infiltration Rate f_c**
cm/hr	**cm/hr**	**cm/hr**	**cm/hr**
27.5	20.1	12.7	11

f_o 54% decrease

f_c 45% decrease

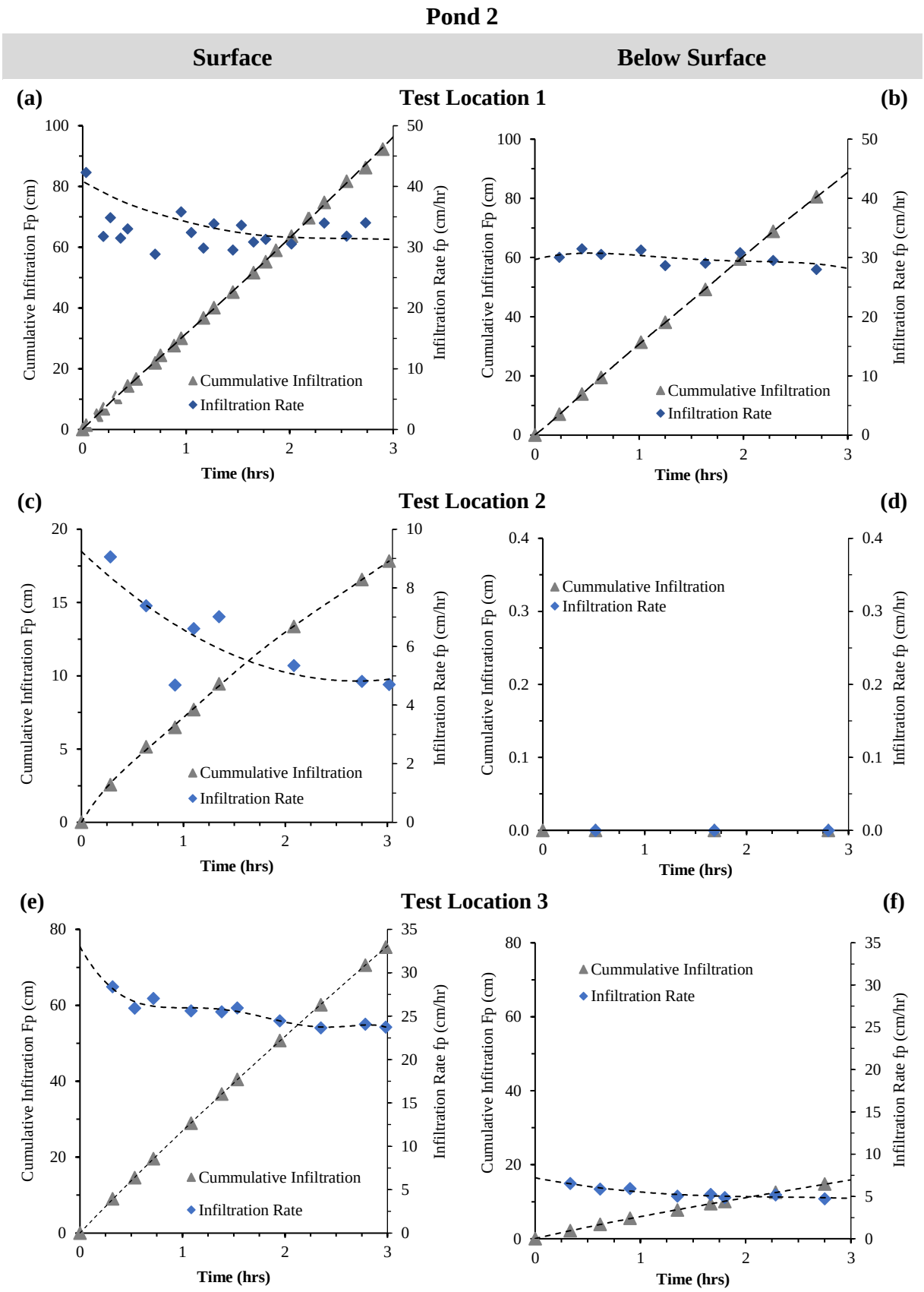

Figure 6-4: Pond 2 Cumulative infiltration and infiltration rate versus time

Pond 2

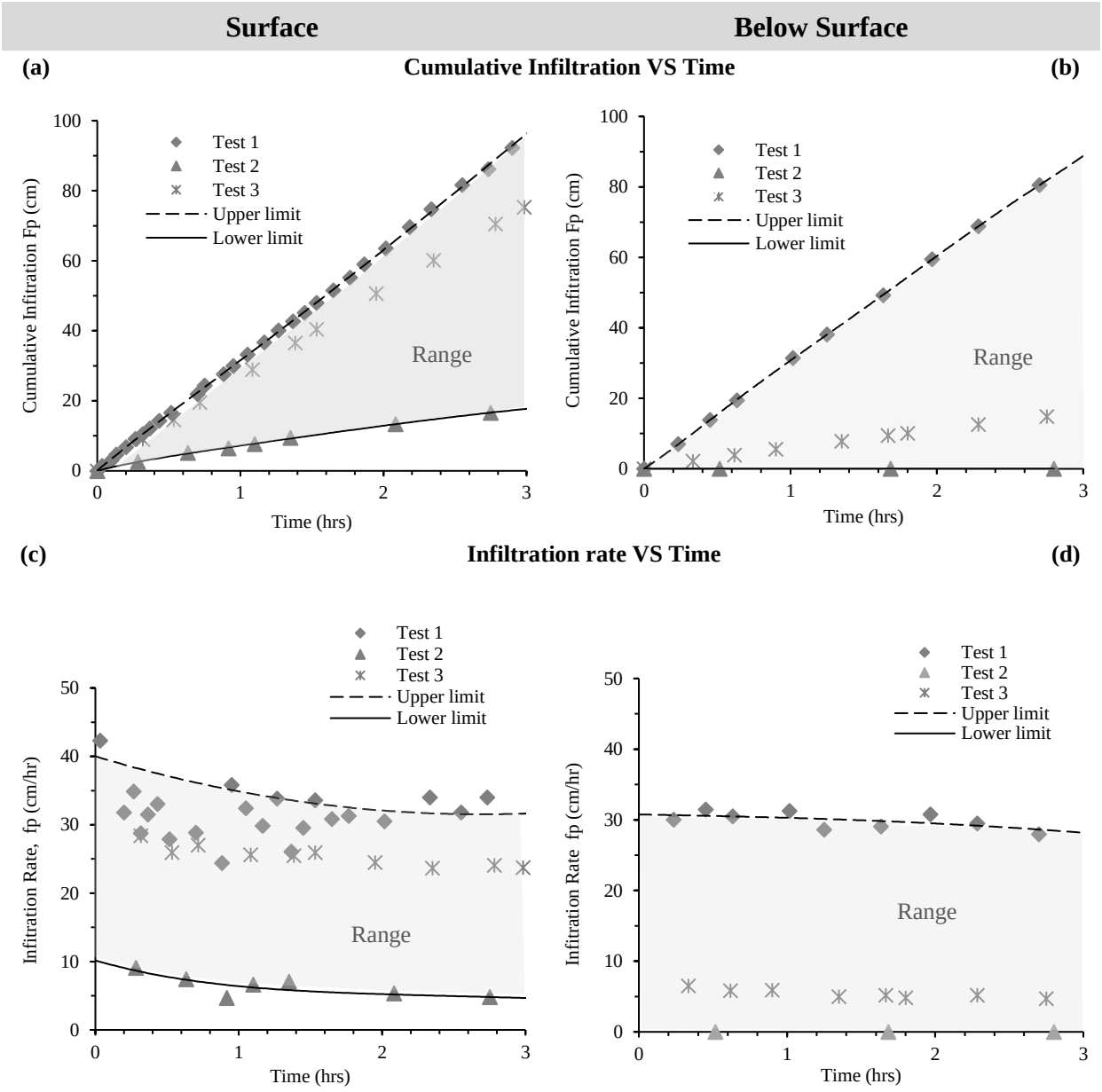

Figure 6-5: Pond 2 Cumulative and incremental infiltration versus time

Table 6-4: Summary of Pond 2 field DRI test results

Surface					Below Surface				
Test location	**F_p t = 0**	**F_p t = 3hrs**	**f_o t = 0**	**f_c t = 3hrs**	**Test location**	**F_p t = 0**	**F_p t = 3hrs**	**f_o t = 0**	**f_c t = 3hrs**
-	cm	cm	cm/hr	cm/hr	-	cm	cm	cm/hr	cm/hr
1	0	97	40	31.3	1	0	88	31	28
2	0	18	10	5	2	0	0	0	0
3	0	75	32.5	24	3	0	18	7	5

6.2.2.3 Pond 3

The third investigated pond's infiltration results are graphically represented in Figure 6-6 and Figure 6-7.

For infiltration tests conducted on the surface of Pond 3, the measured infiltration rates of the three test locations were generally constant over the 3-hour test period. Infiltration versus time plots obtained from Test Locations 1 and 2 were comparable in terms of their initial f_o and steady infiltration rates f_c, i.e., 6.2 and 5.0 cm/hr, respectively for both tests. On the other hand, Test Location 3 yielded significantly higher infiltration rates decreasing from an initial 25 cm/hr for the first 1.5 hours followed by a relatively constant rate of 23.5 cm/hr.

The cumulative infiltration F_p of the surface tests generally increased linearly, particularly at Test Locations 1 and 2. The plotted cumulative infiltration versus time curve of Test Location 3 however, exhibited slight reductions in the increasing infiltration which developed a linear trend from 1.5 hours until the test was concluded. An overall infiltration ranging between 14 and 64 cm was recorded after a test period of 3-hours for the surface tests.

Tests that were carried out below the surface revealed unconventional infiltration patterns. The observed infiltration rate versus time curves of the three inspected locations were linear, with gentle positive slopes such that the steady-state infiltration rates were greater than the initial infiltration rates. This trend was unlike any of the investigated ponds' locations, however, the increase in f_c from f_o was marginal. The initial infiltration rate of the sub-surface tests varied between 6 and 18.5 cm/hr whilst the corresponding steady infiltration rate ranged between 7.5 and 20 cm/hr.

Contrasting to the results obtained from Ponds 1 and 2, the average infiltration recorded on the sub-surface of Pond 3 was generally higher than that of the surface. The initial infiltration rate below the surface was 3 % higher than the surface infiltration (Table 6-3). Furthermore, the steady infiltration rate measured below the pond's surface was 23 % greater than the rate measured on the surface. The values obtained from the six in-situ infiltration tests within Pond 3 (i.e., three tests on the surface and three below the surface) are detailed in Table 6-6.

Table 6-5: Percentage Difference between initial and steady infiltration rates of surface and sub-Surface tests in Pond 3

Surface		**Below Surface**	
Average Initial Infiltration Rate f_o	**Average Steady Infiltration Rate f_c**	**Average Initial Infiltration Rate f_o**	**Average Steady Infiltration Rate f_c**
cm/hr	**cm/hr**	**cm/hr**	**cm/hr**
12.5	11.2	12.3	13.8

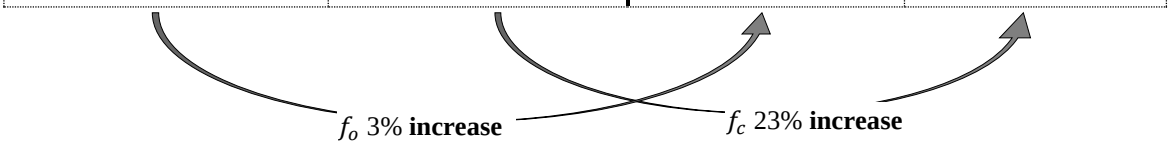

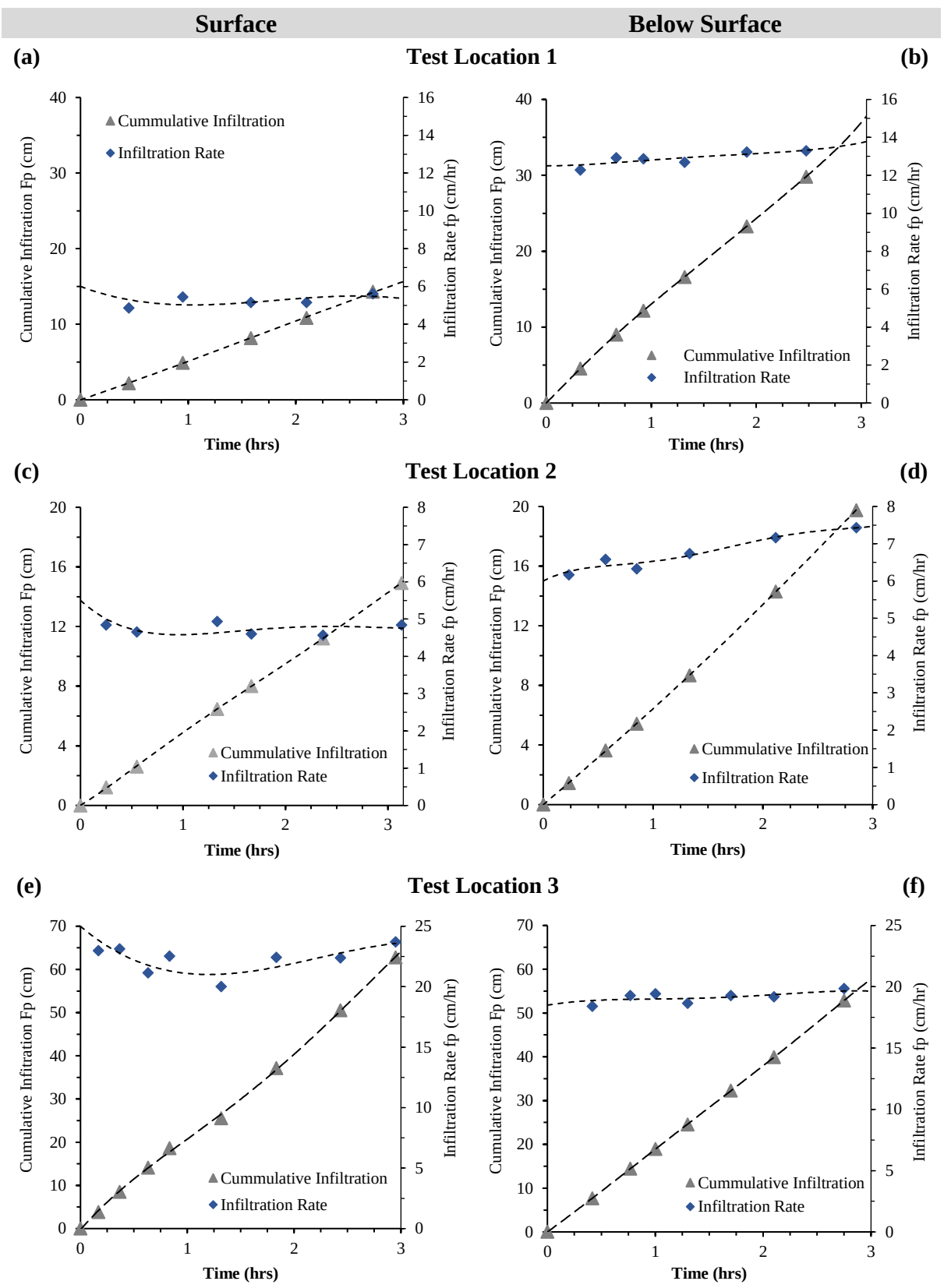

Figure 6-6: Pond 3 Cumulative infiltration and infiltration rate versus time

Pond 3

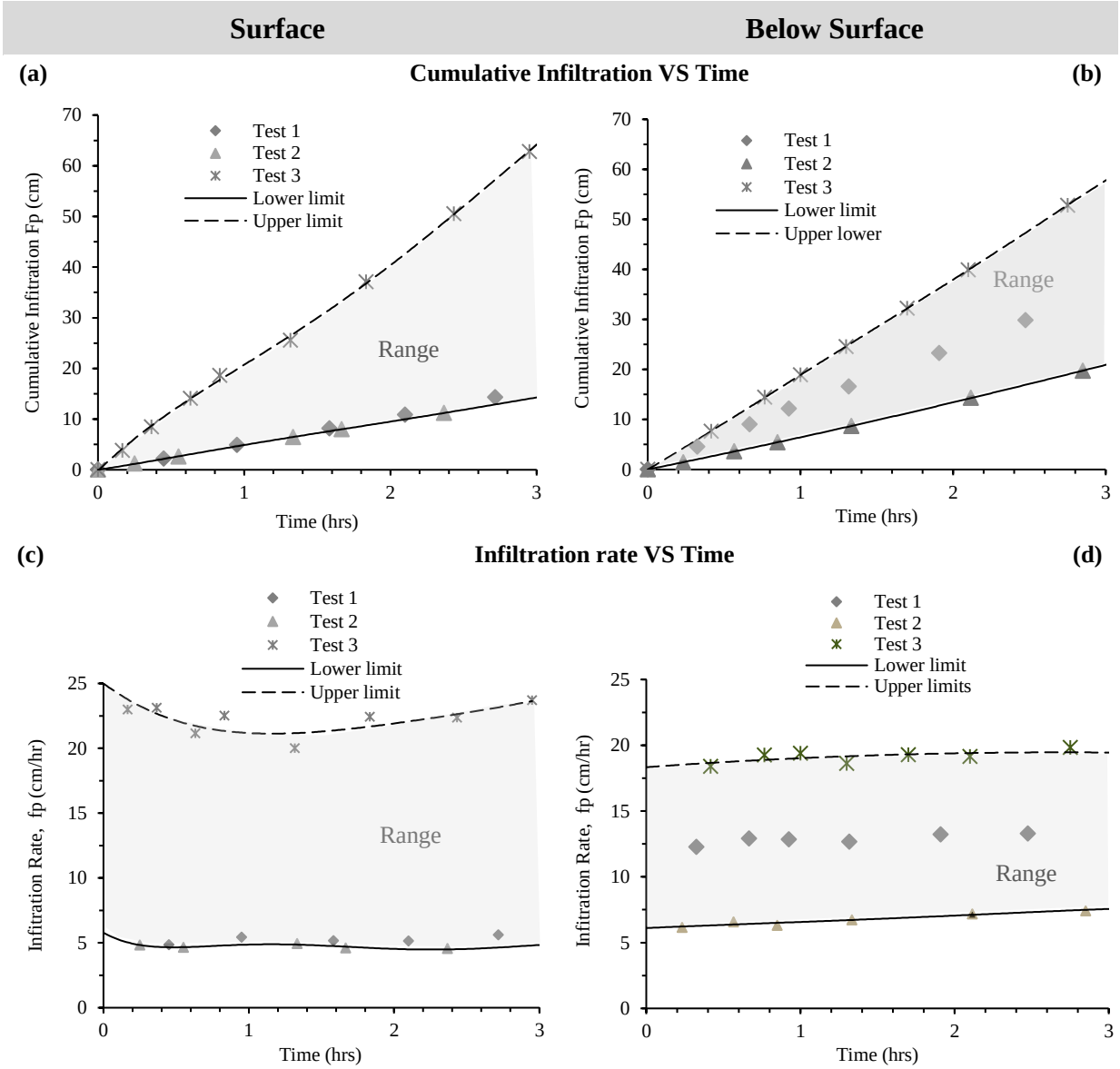

Figure 6-7: Cumulative and incremental infiltration versus time

Table 6-6: Summary of Pond 3 field DRI test results

Surface					Below Surface				
Test location	**F_p t = 0**	**F_p t = 3hrs**	**f_o t = 0**	**f_c t = 3hrs**	**Test location**	**F_p t = 0**	**F_p t = 3hrs**	**f_o t = 0**	**f_c t = 3hrs**
-	cm	cm	cm/hr	cm/hr	-	cm	cm	cm/hr	cm/hr
1	0	15	6.2	5.2	1	0	37.5	12.5	13.8
2	0	14	6.2	5.0	2	0	20.0	6.0	7.5
3	0	64	23.5	23.5	3	0	57.0	18.5	20.0

6.2.3 Evaluation of Hydraulic Conductivity Derived from Field DRI Test Results

With the aid of Green-Ampt's (1991) equation for infiltration capacity (Equation 2.5) the field DRI test data was used to determine the respective hydraulic conductivities K_s of each investigated location (Figure 6-8). Pond 1 was found to have the lowest mean K_s, with Pond 2 having the highest, and Pond 3's K_s values in between. The hydraulic conductivity perimeter was the governing material property regarding infiltration as it indicated the soil material's ability to transmit water when subjected to a hydraulic head (Fatehnia, 2015; Radcliffe *et. al*., 2010).

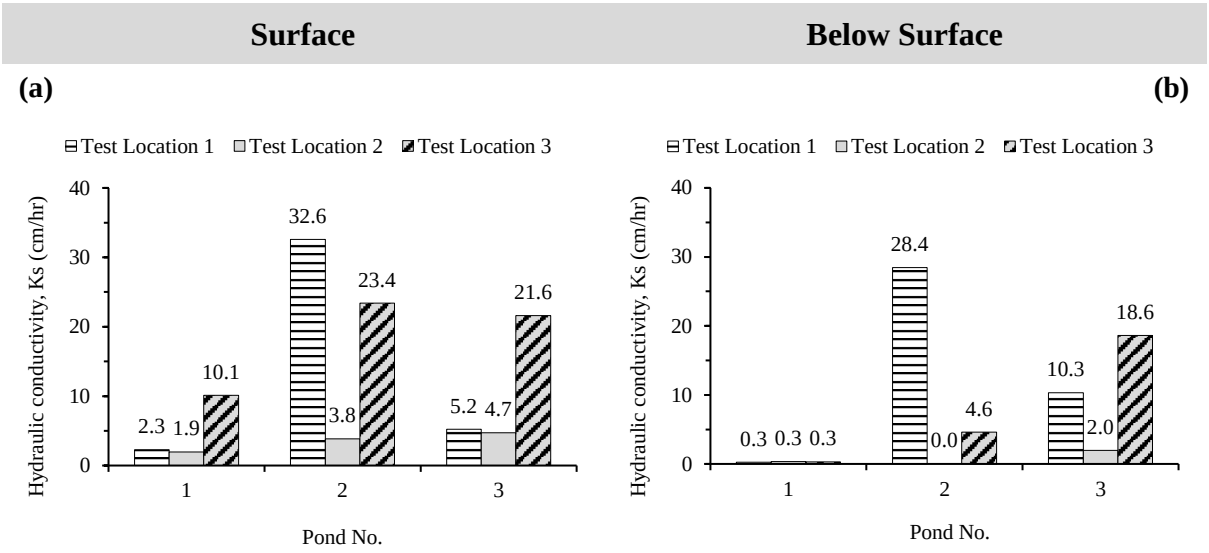

Figure 6-8: Hydraulic conductivities derived from field DRI test results

The variability in the obtained hydraulic conductivities was notable, for instance, three DRI tests conducted on the surface of Pond 1 yielded K_s values ranging between 3.8 and 32.6 cm/hr. Other factors which potentially contributed to this variability were the soil type, texture, structure, permeability, and drainage. Dissimilarities in the surface layer were evident within a single investigated pond. Parts of the pond's surface were well-vegetated, others had localized stagnant shallow water bodies, whilst others comprised solely of unconsolidated sands. Thus, from a design perspective, using the lowest obtained hydraulic properties would allow for a conservative design.

All investigated Test Locations within the three ponds displayed general reductions in the infiltration rates f_p which ultimately levelled off to some steady rate f_c. The only Test Locations which contradicted this behaviour were those on the sub-surface of Pond 3 as the steady infiltration rates f_c were measured to be marginally greater than the initial rates f_o. Furthermore, no measurable infiltration was observed over the entire duration of the DRI experiment on the sub-surface of Test Location 2 situated within Pond 2.

Three hours was found to be enough in allowing for steady-state conditions to be achieved on all investigated locations. Figure 6-9 summarises the minimum and maximum cumulative infiltrations, as well as steady-state infiltration rates obtained from the investigated ponds.

The four graphs in Figure 6-9 provide a visual comparison of the range of infiltration values measured in Ponds 1, 2, and 3. Note that f_o represents f_p at t = 0 hrs, and f_c represents f_p at t = 3 hrs. For infiltration tests conducted on the surface, the cumulative infiltrations correspond to the steady infiltration rates by a factor ranging between 2.7 and 3.6; this excludes the Test Location in Pond 2 which yielded no measurable infiltration.

The overall trend observed from the three considered ponds in this study was an increase in cumulative infiltration with increasing time. This behaviour was anticipated as it is typical for any porous medium exposed to a constant head of water.

When it comes to the three ponds' overall infiltration potential, based on measured f_c values, it was evident from Figure 6-9 (c) and (d) that during ponded conditions (i.e., stead-steady

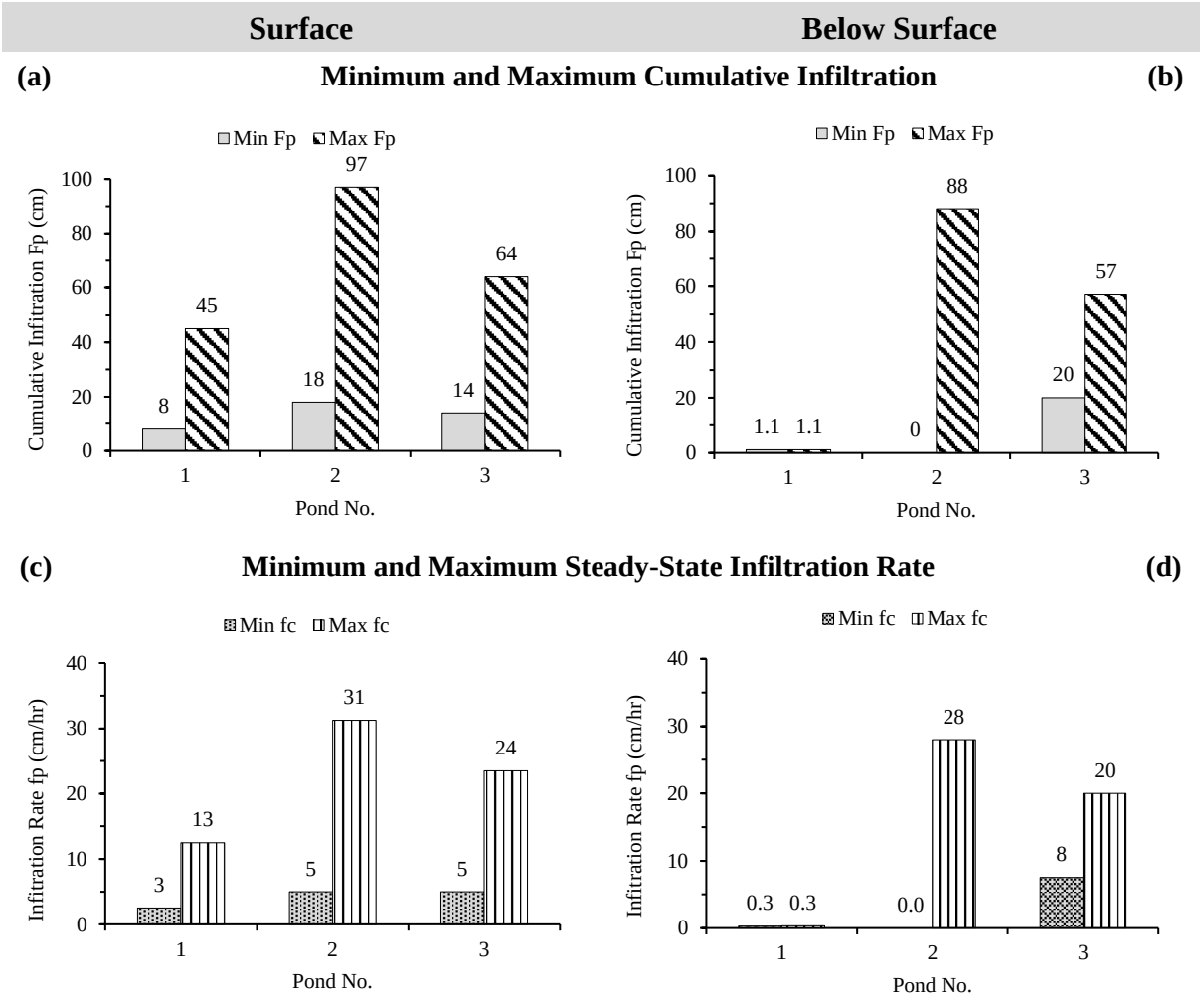

Figure 6-9: Minimum and maximum infiltrations of investigated ponds

infiltration rates) Pond 2 allowed for the greatest infiltration to occur during the DRI tests. Taking a closer look into these two ponds, it was concluded that using the maximum measured f_c values for the potential design of a stormwater management facility, or infiltration basin, would significantly over-estimate the practically obtainable infiltration rates of subsoils. The minimum measured steady infiltration rates would be a more reliable and conservative representative of the ponds' infiltration potential since variations within a single pond have been observed and noted to be rather significant in some instances. Pond 3 was the most suitable of the three ponds as it yielded the highest minimum infiltration rates when measured from both the surface and the sub-surface.

6.3 Investigation of Laboratory Infiltration Test Results

6.3.1 Hydraulic Gradient

The permeability of soil samples from each investigated field location was investigated in the laboratory using the Constant-Head Permeameter (CHP) apparatus described in Chapter 5. A vertical head difference h varying between 56 and 61 cm was maintained for each set of three tests. The associated average hydraulic gradients i for samples corresponding to each field Test Location are presented in Figure 6-10.

The hydraulic gradient i was defined by Equation 6.1 as the ratio between the vertical head difference h and the length L of a soil sample within the permeability chamber of the CHP apparatus.

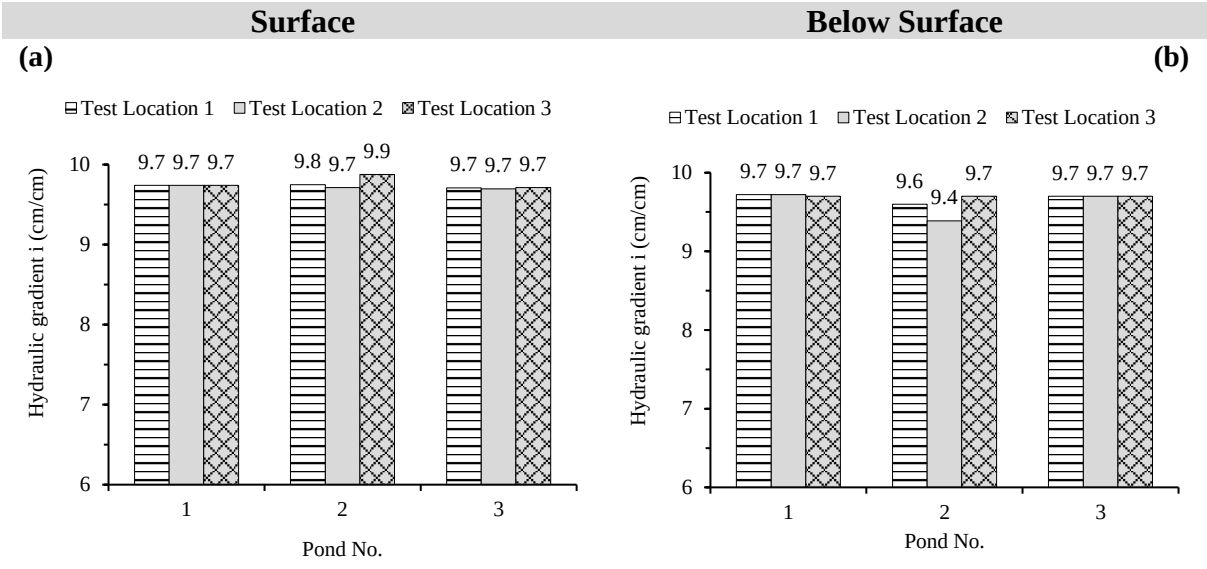

Figure 6-10: Hydraulic gradient obtained from laboratory CHP tests

$$i = \frac{h}{L} \qquad 6.1$$

It is apparent from the graphs in Figure 6-10 (a) and (b) that the hydraulic gradient was generally constant, averaging at 9.7, for samples obtained from both the surface and the sub-surface of the investigated ponds. This was owed to the constant sample length L (approx. 60 mm) maintained for all the CHP investigations, and the minor variations in the maintained head difference h during each set of tests.

6.3.2 Average Flowrate from CHP Tests

The volume of water V which flowed through the CHP test samples of fixed area A, after a specific time t, was measured to calculate an average flow rate q using Equation 6.2.

$$q = \frac{V}{At} \qquad 6.2$$

Because of the difference in soil physical characteristics and densities, the measured flow rates q varied for each tested sample (Figure 6-11). The densities of each recompacted soil sample corresponded to the respective bulk densities of the Test Locations. In general, samples retrieved from the ponds' surface (i.e., top 20 cm soil layer) yielded notably higher average flow rates than those obtained 20 to 40 cm below the surface.

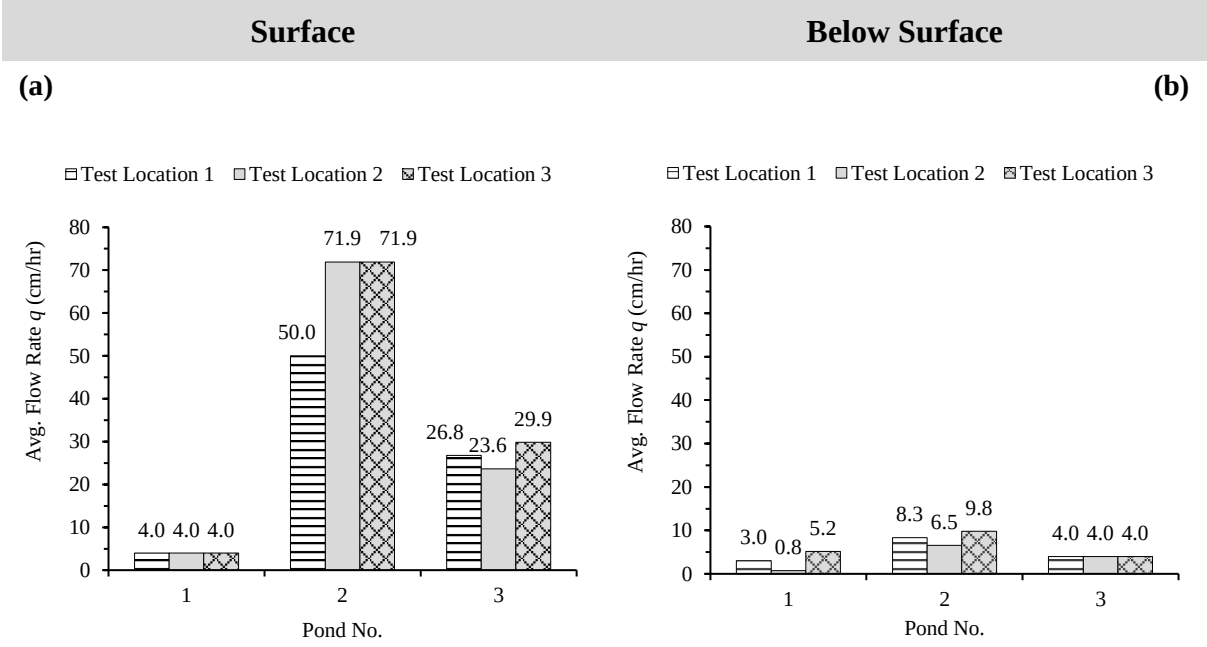

Figure 6-11: Average flow rate from laboratory CHP tests

Surface samples retrieved from the three inspected locations within Pond 1 had the lowest flow rates of around 4.0 cm/hr. Pond 3's samples had the second-highest flow rates ranging between 23.6 and 29.9 cm/hr, whereas Pond 2's samples achieved the greatest flow rates ranging between 50 and 71.9 cm/hr.

For samples obtained below the ponds' surface, Pond 1 and Pond 3 had similarly low average flow rates ranging from 0.8 to 5.2 cm/hr. On the other hand, samples from Pond 2's Test Locations exhibited marginally higher flow rates ranging between 6.5 and 9.8 cm/hr.

Generally, the average q values of samples acquired from the surfaces of the investigated ponds were higher than those of specimens acquired from the sub-surface. This was mainly due to the compacted nature of soils below the surface, which primarily reduced the flow of water due to a reduction in voids between soil particles.

6.3.3 Hydraulic Conductivity Derived from CHP Test Results

The average flow rates q measured from the laboratory Constant-Head Permeability CHP tests were used to calculate the respective hydraulic conductivities K_s of the soil samples acquired from the investigated ponds using Equation 5.8. The calculated K_s values of samples obtained from the ponds' surface, and below the surface, are presented in Figure 6-12. K_s is a measure of the soil material's ability to transmit water.

Comparing the two investigated depths, soil specimens obtained from the surfaces had noticeably higher hydraulic conductivities than those from the sub-surface. Samples from the surface of Pond 2 had the greatest hydraulic conductivity ranging between 23.5 and 65.8 cm/hr. Those from Pond 3 had intermediate K_s values ranging between 21.7 and 27.7 cm/hr, with Pond 1 yielding the lowest of 3.6 cm/hr.

Samples retrieved below the Ponds' surfaces yielded hydraulic conductivity values ranging from a low average of 2.7 cm/hr (Pond 1 samples), a midway average of 3.7 cm/hr (Pond 3 samples), with the highest being 6.2 cm/hr (Pond 2 samples).

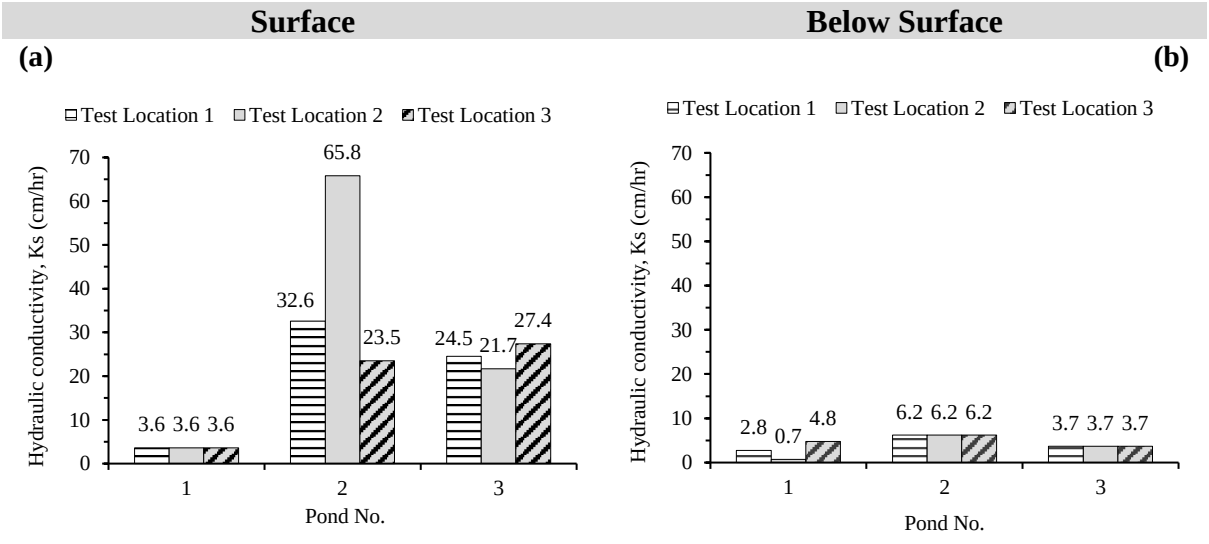

Figure 6-12: Hydraulic conductivities derived from laboratory CHP tests

6.4 Comparison Between Field and Laboratory Results

A comparative study of all research results was undertaken. In essence, it involved comparing the hydraulic conductivity values resulting from the field double-ring infiltration DRI tests $K_{S_{field}}$, and the laboratory constant-head permeability CHP tests $K_{S_{lab}}$, with one another to assess apparent trends and correlations between various measured soil properties. The sensitivity of the hydraulic conductivity to variable soil physical and hydraulic properties was investigated based on field and lab test results. The parameters which were evaluated were the hydraulic conductivity, the soil natural moisture contents NMC, bulk density ρ_b, porosity n, the field initial infiltration rates f_o, the field steady infiltration rate f_c, the soil effective grain size d_{10} and the laboratory average flow rate q.

The specific potential correlations which were investigated are enlisted below as follows:

i) Infiltration rate variation with natural moisture content
ii) Porosity variation with soil bulk density
iii) Field versus laboratory hydraulic conductivity
iv) Hydraulic conductivity variation with soil effect grain size
v) Hydraulic conductivity variation with soil bulk density
vi) Hydraulic conductivity variation with soil porosity
vii) Hydraulic conductivity variation with field steady infiltration rate
viii) Hydraulic conductivity variation with laboratory average flow rate

6.4.1 Infiltration Rate Variation with Natural Moisture Content of Soil

Presented in Figure 6-13 are graphical results of the observed relations between infiltration rate values with respect to the corresponding soils' natural moisture contents NMC.

Infiltration rates f_p measured in the field were suspected to be dependent on the actual moisture content of the soil (sorptivity). The sorptivity of soil generally increases as the boundary water content increases. It can be approximated as the slope of cumulative infiltration F_p versus the square root of time $\sqrt{t}$ Subranyama (2008).

Dry soils can generally absorb more water than those whose pores are already full. Thus, notwithstanding other factors which influence the infiltration rate, soils with lower natural moisture contents NMC were expected to yield higher initial infiltration rates f_o. Moreover, the difference between the steady-state infiltration rate f_c and f_o was expected to be greater for soils whose natural moisture content was relatively low.

The predicted relationship between f_p and the NMC was not observed across all the investigated sites. However, some of the assumed trends were evident. For instance, the average f_o was generally greater than the f_c in all the investigated ponds; confirming that none of the investigated soils were initially in a saturated state. Furthermore, soils in Pond 3 had the greatest moisture content and the difference between f_c and f_o was found to be very small.

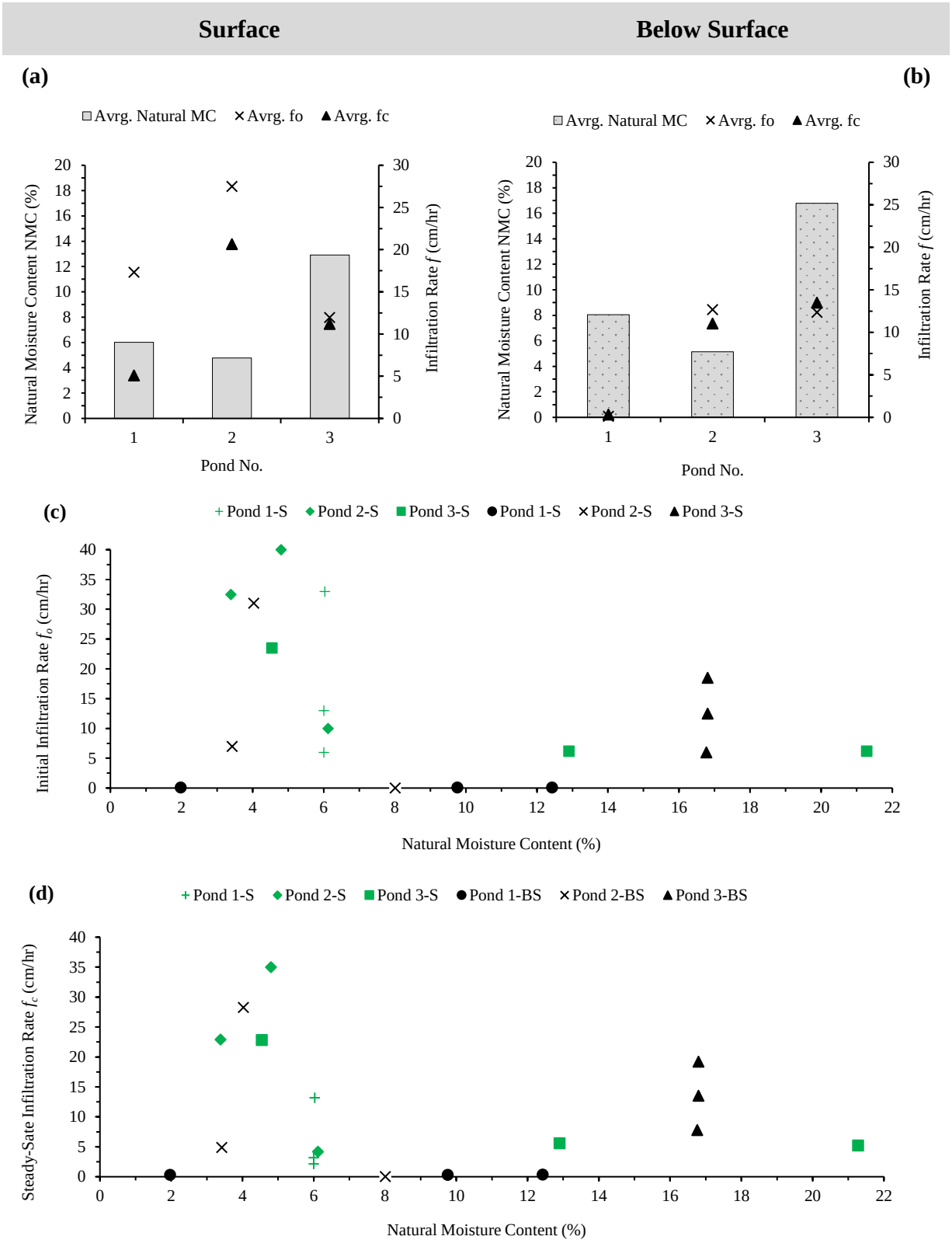

Figure 6-13: Average natural MC versus initial and steady infiltration rate

The natural moisture content of soils in Pond 2 was similar on the surface and below the surface, but the infiltration rates measured from the surface were greater. This can be owed to the denser sub-surface layer which made it more difficult for water to pass through the pore spaces of the soil.

Pond 1 on the other hand, was essentially impervious below the surface irrespective of the relatively intermediate natural moisture content. Again, this can be explained by a localized highly dense, almost impervious, sub-surface layer.

From the plots in Figure 6-13 (a) and (b), no direct correlation was observed between the infiltration rates (f_c and f_o) and the NMC of the soil. The plots of f_c and f_o versus NMC did however follow similar trends to one another. It was apparent that the majority of the investigated sites had natural moisture contents ranging between 3 and 7% whilst the NMC of other locations varied broadly between 8 and 22%.

6.4.2 Porosity Variation with Soil Bulk Density

Air voids within a specific soil sample are generally reduced when the material is subjected to compaction. This reduction in air voids due to compaction consequently increases the material's bulk density ρ_b. Thus, based on relationships between density, void ratio, and porosity (described in Equations 5.5, 5.6, and 5.7), an inverse relationship was distinguished between porosity n and bulk density ρ_b (Equation 6.3).

$$n \propto \frac{1}{\rho_b} \qquad 6.3$$

Since the soil materials investigated in this study were largely similar in their grain-size distribution and texture, an attempt was made to assess whether the general relationship described by Equation 6.3 could be observed from the measured bulk density ρ_b. and respective porosity n values (Figure 6-14).

The soil n values obtained from the investigated ponds' surfaces were generally greater than those of the sub-surface (Figure 6-14 (a) and (b)). The ρ_b values on the other hand, were higher below the surface. This was expected since the top 200 mm soil layers were loose and less compacted compared to the deeper sub-surface layers. Low ρ_b values associated with high porosities were observed on the surface of Ponds 2 and 3. Additionally, all the sub-surface soils showed low n values associated with higher bulk densities.

The average n values on the surface of Ponds 1, 2, and 3 were 0.32, 0.44, and 0.43 respectively, with corresponding ρ_b of 1733, 1460 and 1635 kg/m^3. Below the surface of Ponds 1, 2, and 3, average porosities of 0.33, 0.3, and 0.38 were measured with corresponding bulk density values of 1889, 1917, and 1930 kg/m^3 respectively. Overall, a general reduction in the porosity as the density increased was observed however, because soil specimens were acquired from different field test locations, the ideal inverse-relationship trend was not apparent from Figure 6-14 (c).

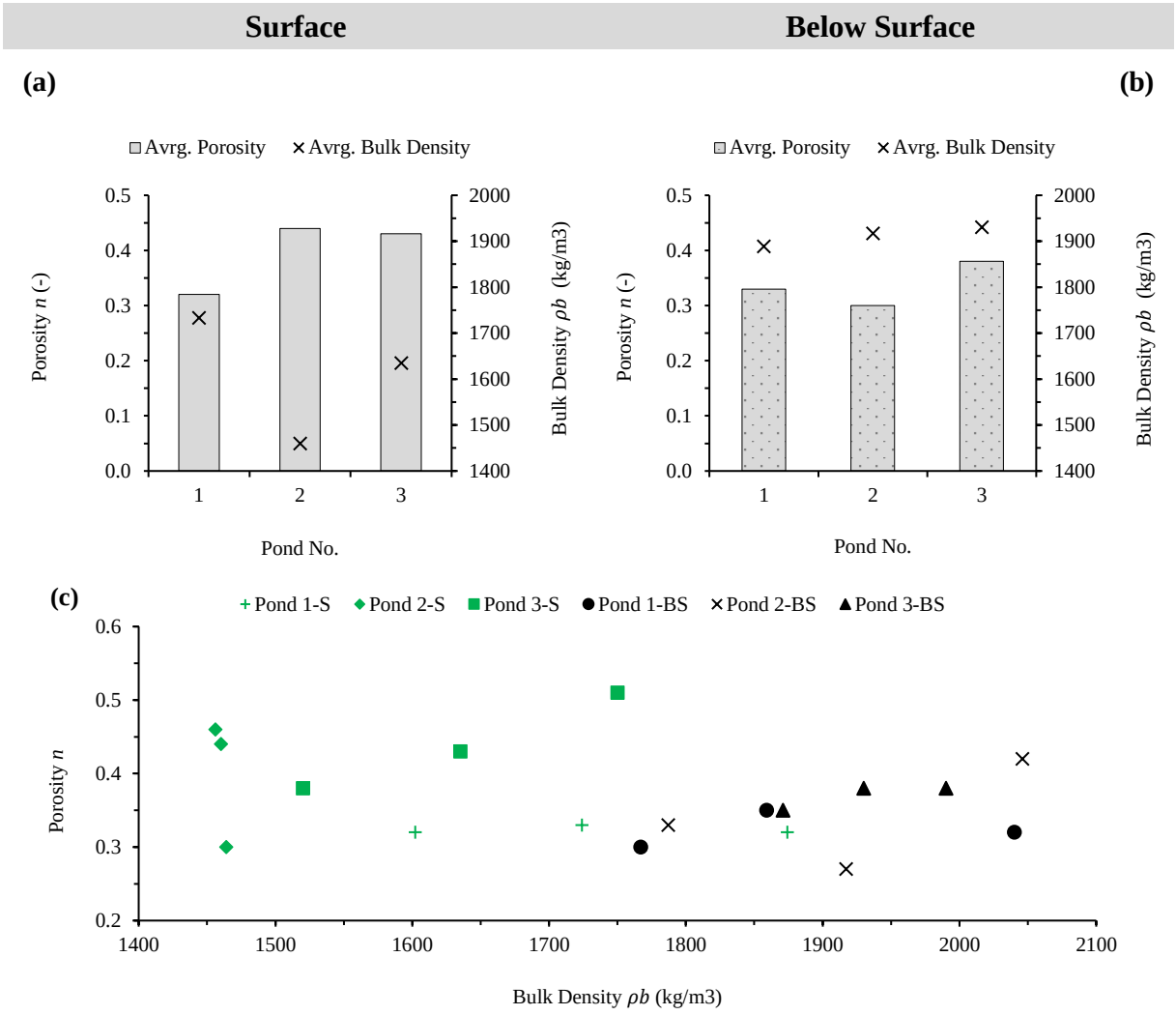

Figure 6-14: Average porosity versus bulk density

6.4.3 Field and Laboratory Hydraulic Conductivity

The relationship between hydraulic conductivity values derived from the field DRI tests $K_{S_{field}}$, and those calculated from the laboratory CHP test results $K_{S_{lab}}$ was investigated. Results from the two test methods are presented in Table 6-7 and Figure 6-15. Similar trends were observed between the results obtained from Pond 2 and Pond 3. Surface tests (i.e., 0 – 20 cm depth) of both ponds exhibited an average $K_{S_{lab}}$ greater than the $K_{S_{field}}$ by a factor of 2.25. Contrastingly, for tests conducted below the surface (i.e., 20 – 40 cm depth) the laboratory hydraulic conductivity was lower than the field hydraulic conductivities by a ratio of $K_{S_{lab}}/K_{S_{field}}$ equal to 0.6 for Pond 2 and 0.4 for Pond 3.

Pond 1, on the other hand, generally demonstrated characteristics of a low permeability soil as both the $K_{S_{lab}}$ and the $K_{S_{field}}$ were significantly lower than those obtained in Ponds 2 and 3, more particularly from the sub-surface tests. A consequence of this could be the relatively higher percentage of fine particles found in soil specimens from Pond 1. Unlike in Pond 2 and

Pond 3, the average $K_{S_{lab}}$ from surface tests was lower than the $K_{S_{field}}$ by a reduction factor of 0.8. However, below the surface, $K_{S_{lab}}$ was nine times greater than $K_{S_{field}}$.

Table 6-7: Comparison between average field and laboratory hydraulic conductivity values

Test Set-Up Description	Pond No.	Field Hydraulic Conductivity (cm/hr)	Laboratory Hydraulic Conductivity (cm/hr)	Percentage difference (%)	Average Percentage difference (%)
Surface	1	4.8	3.6	29	62
	2	19.9	44.7	77	
	3	10.5	24.5	80	
Below Surface	1	0.3	2.8	160	103
	2	11	6,2	56	
	3	10.3	3,7	94	

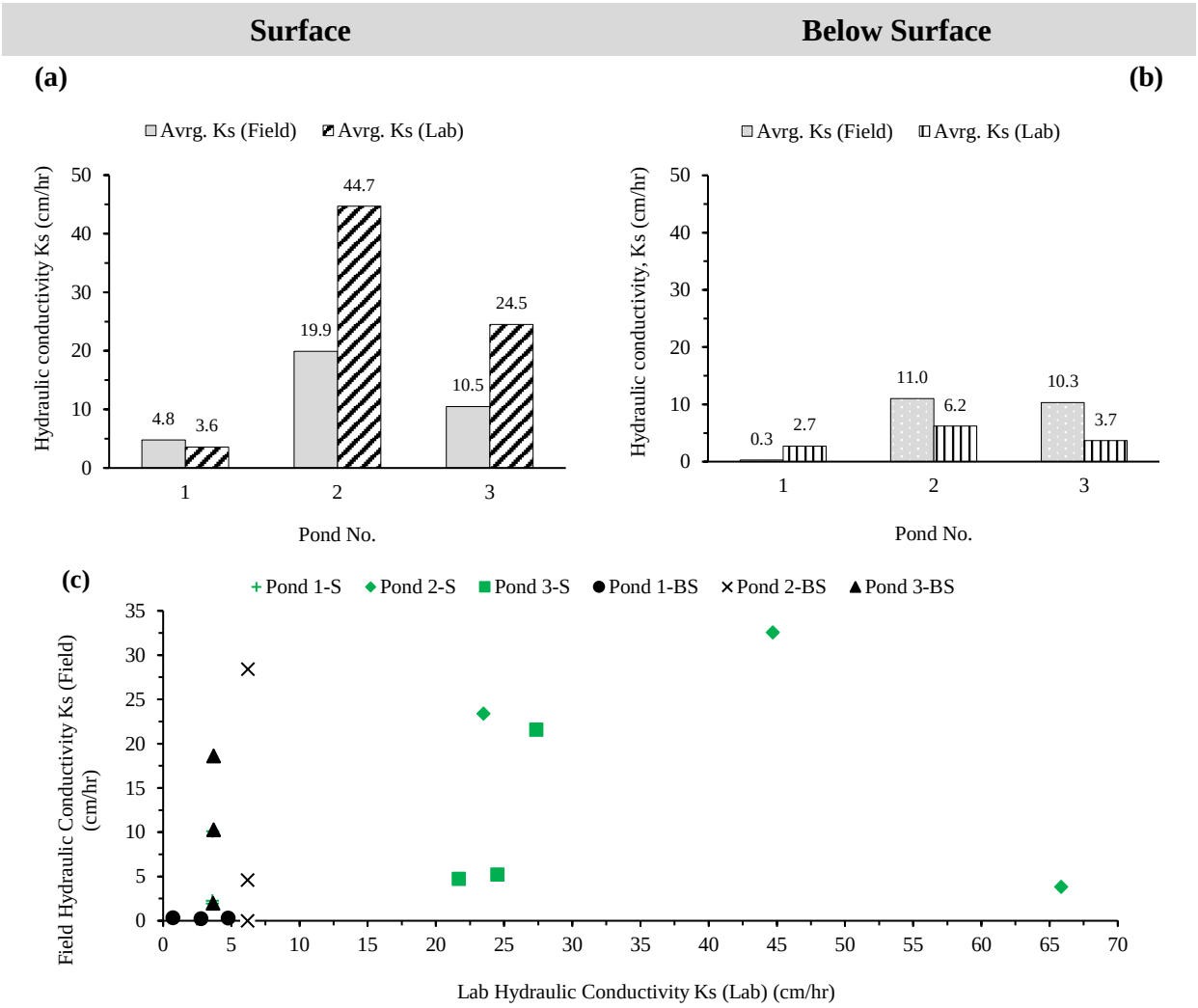

Figure 6-15: Comparison between average field and laboratory hydraulic conductivities

The plot in Figure 6-15 (c) highlights a loose correlation between the investigated $K_{S_{field}}$ and $K_{S_{lab}}$ values. Generally, when compared to each other, $K_{S_{field}}$ and $K_{S_{lab}}$ values differed by an average of 62% for tests conducted on the surface of the ponds, whilst those conducted 20 cm below the surface of the ponds diverged by 103%

6.4.4 Hydraulic Conductivity Variation with Soil Effective Grain Size

The textural class and particle size distributions of soils from the investigated ponds were comparable with one another. Soils from the surface of Pond 1 were classified, following the Unified Soil Classification System (USCS), as poorly graded sands with silt (SP-SM), whilst those from Pond 2 and Pond 3 were categorized as poorly graded sands (SP).

Despite similarities in textural classes of the assessed soil specimens, notable variations in the effective grain sizes D_{10} of the evaluated specimens were identified. The materials' effective grain size was determined from the particle-size distribution curves which represented the particle diameter corresponding to 10 % finer. Average D_{10} values of specimens obtained from the surface of Ponds 1, 2, and 3 were 0.10, 0.15, and 0.16 mm, respectively. For samples, retrieved from the ponds' sub-surfaces, D_{10} values were 0.10, 0.27 and 0.14 mm, correspondingly (Figure 6-16 (a) and (b)).

Empirical correlations between hydraulic conductivity K_s and effective grain size D_{10} for coarse-grained soils have been investigated by various authors with a common interest of reducing the effort in estimating hydraulic properties of sands over large areas. One of the oldest was suggested by Beyer (1964) and is expressed by Equation 6.4 where $K_{S_{Beyer,1964}}$ is the hydraulic conductivity in metres per second, C represents a dimensionless constant equal to $4.5 \times 10^{-3}\log(500/U)$, and U is the uniformity coefficient d_{60}/d_{10}. Analysis of Beyer's constant C, and associated hydraulic conductivity values, reviled no apparent correlation when compared to the measured $K_{S_{field}}$ and $K_{S_{lab}}$ values of this investigation (Table 6-8)

$$K_{S_{Beyer,1964}} = C \cdot (D_{10})^2 \qquad 6.4$$

Table 6-8: Ratios between hydraulic conductivities and soil effective grain sizes

Surface				
Pond No.	***C* Constant**	$K_{S_{Beyer,1964}}$	$K_{S_{field}}$	$K_{S_{lab}}$
-	-	**cm/hr**	**cm/hr**	**cm/hr**
Pond 1	9.7E-03	35.0	4.8	3.6
Pond 2	1.1E-02	86.4	19.9	44.7
Pond 3	1.1E-02	99.4	10.5	24.5
Below Surface				
Pond 1	9.7E-03	31.6	0.3	2.7
Pond 2	1.0E-02	104.8	11.0	6.2
Pond 3	1.1E-02	77.2	10.3	3.7

The K_s values estimated using Beyer's (1964) correlations significantly overestimated the measured K_s values by up to 100 times, thus considered unreliable for application in this study area. Assessment of the relationship between $(D_{10})^2$ and the measured field and laboratory K_s values showed a general increase in K_s with increasing D_{10}. The $K_{S_{field}}$ versus $(D_{10})^2$ plots exhibited a linear trend, which could be generalized as: $K_{S_{field}} = 920(D_{10})^2$ for $(0.075 \leq D_{10} \leq 0.19$ mm) (Figure 6-16 (c)). On the other hand, the $K_{S_{lab}}$ versus $(D_{10})^2$ plot in Figure 6-16 (d) illustrated a higher gradient trend with a positive slope.

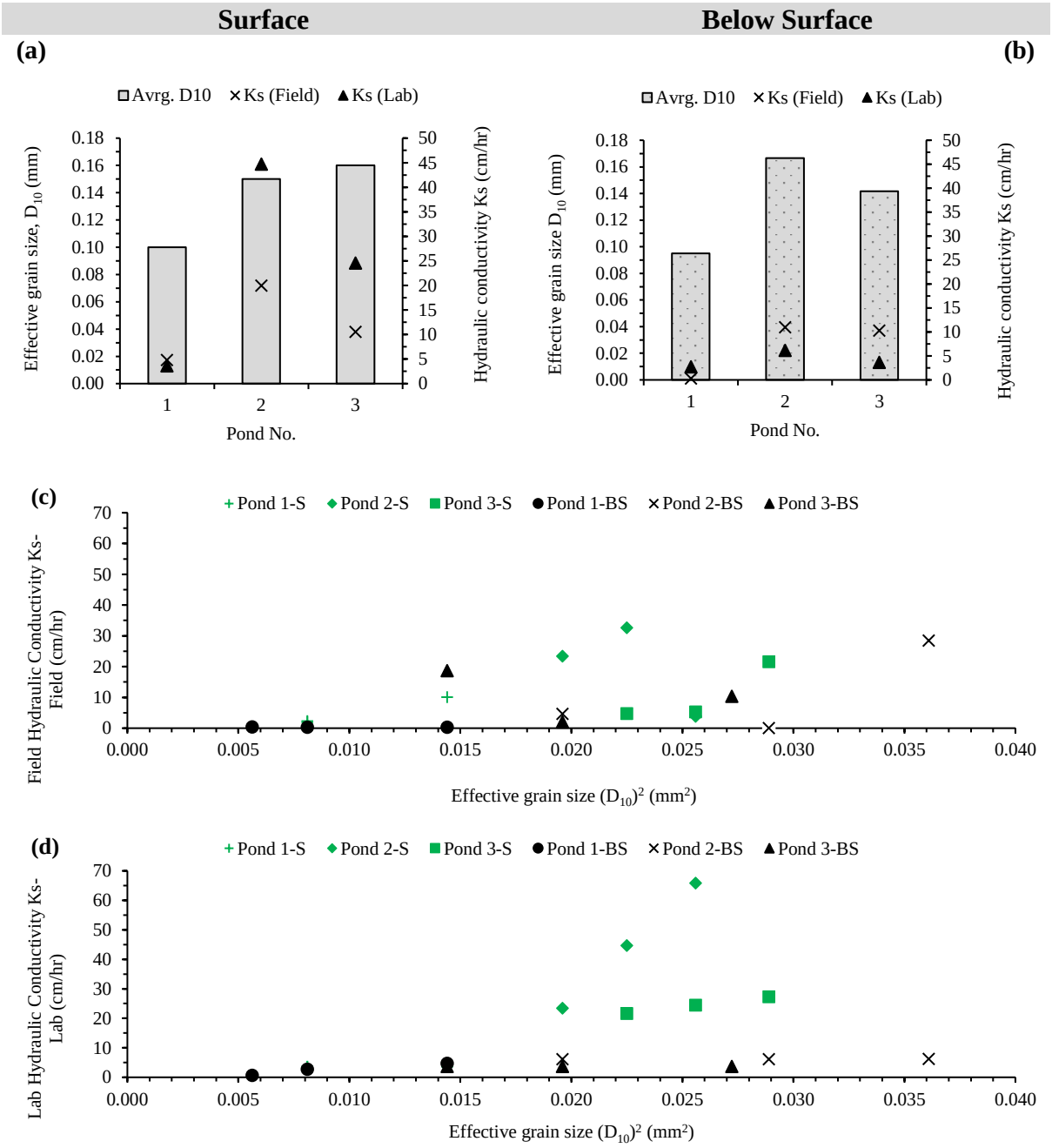

Figure 6-16: Average effective grain size versus field and laboratory hydraulic conductivity

6.4.5 Hydraulic Conductivity Variation with Soil Density

Illustrated in Figure 6-17 are results of the observed relationships between the soil materials' field and laboratory hydraulic conductivity values, and their corresponding bulk densities.

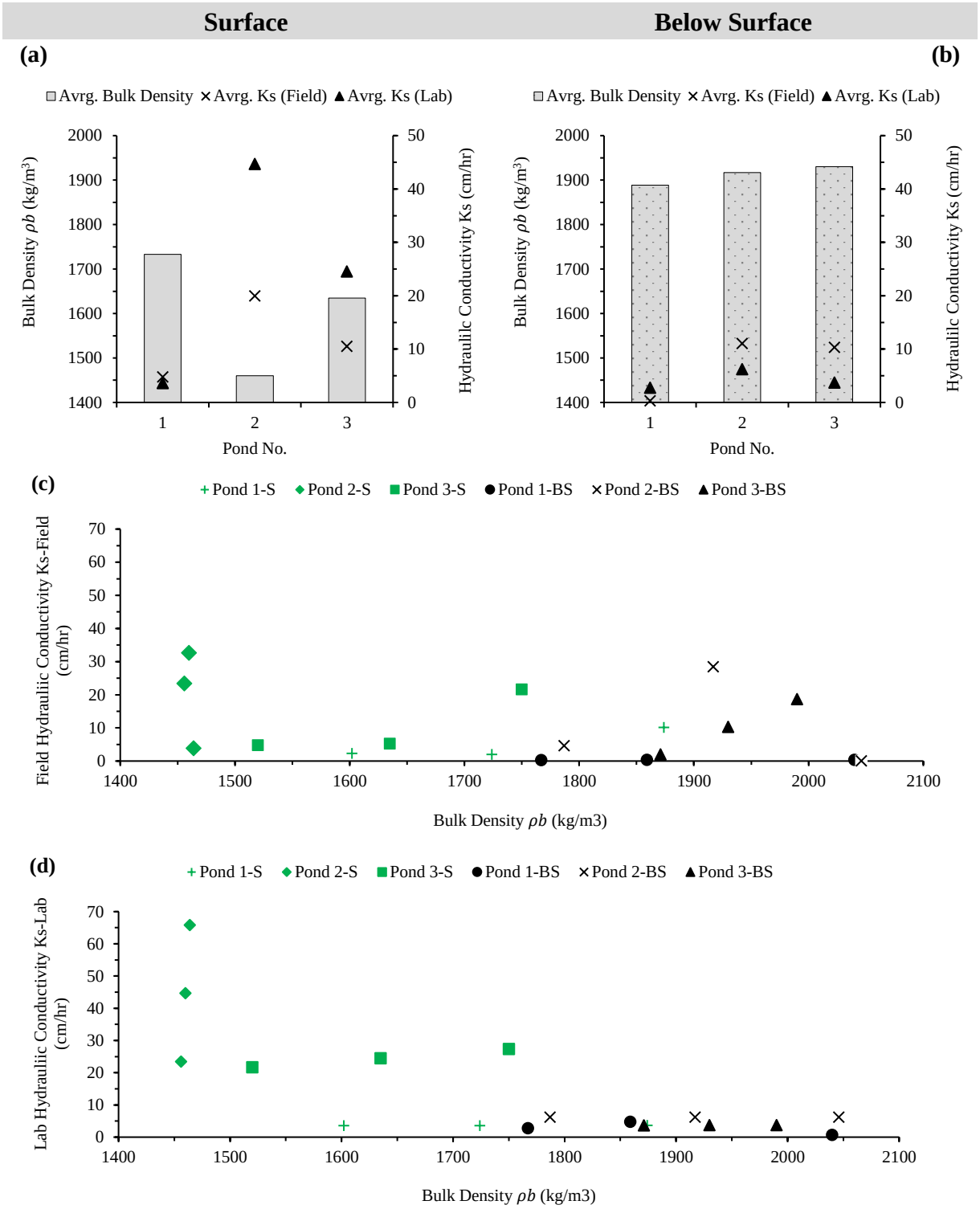

Figure 6-17: Average bulk density versus field and laboratory hydraulic conductivity

Section 6.4.2 elucidates the observed relationship between soil porosity and density; generally represented mathematically by Equation 6.3. A similar, inverse relationship was anticipated when assessing correlations between hydraulic conductivity and density (Figure 6-18). This correlation was expected from the experimental results because porosity is a function of density, and hydraulic conductivity is dependent on porosity as per Green-Ampt's 1911 proposed equation used to derive the field hydraulic conductivity $K_{S_{field}}$ values (Equation 2.5).

Assessment of soils from the considered ponds' surfaces generally revealed higher hydraulic conductivity values associated with lower bulk densities ρ_b, and vice versa. This correlation was more distinct for hydraulic conductivity values derived from the laboratory permeability tests $K_{S_{lab}}$ as opposed to those obtained from the field infiltration tests $K_{S_{field}}$ (Figure 6-18 (a)). The lowest bulk density was measured from surface core samples obtained in Pond 2, which corresponded to the highest average $K_{S_{field}}$ and $K_{S_{lab}}$ values of 19.9 and 44.7 cm/hr respectively.

Unlike with the surface tests, only minor variations in bulk density and hydraulic conductivity values were noted across the sub-surface of the three ponds (Figure 6-18 (b)). Soil specimens obtained from Pond 1 had the lowest ρ_b value (i.e. 1889 kg/m^3) in relation to samples obtained from the sub-surfaces of Ponds 2 and 3. Contrastingly, this lowest ρ_b value corresponded to the lowest $K_{S_{field}}$ and $K_{S_{lab}}$ values of 0.3 and 2.8 cm/hr. which was a contrasting, trend to that observed from surface samples.

From the plotted graph of hydraulic conductivity K_S versus bulk density ρ_b (Figure 6-18 (c) and (d)) a notable inverse correlation between $K_{S_{lab}}$ values and associated ρ_b values was evident, as compared to the relationship between $K_{S_{field}}$ against ρ_b. This, again, can be owed to the controlled nature and small scale of laboratory test settings compared to the variability of unfamiliar in-situ sub-surface conditions.

6.4.6 Hydraulic Conductivity Variation with Soil Porosity

Another distinct evaluated relationship was between hydraulic conductivity K_S and porosity n of soils within the three investigated ponds (Figure 6-18). Sections 6.4.2 and 6.4.5 verified inverse correlations between porosity n and density ρ_b values, as well as hydraulic conductivity and density values, respectively. Contrasting to the noted K_S versus n, and K_S vs ρ_b trends, a direct proportionality was anticipated between K_S and n. This was because an increased presence of voids, or pores, in soils generally promotes the entry and flow of water, thus a corresponding increase in hydraulic conductivity.

From Figure 8-17 (a) and (b), higher porosity values were observed in soil specimens obtained from the surfaces, as opposed to the sub-surfaces, of the three investigated ponds. A clear trend was not evident, however, upon focusing on the plots in Figure 6-18 (c) and (d), a linear increase in the hydraulic conductivity was observed as the porosity increased from 0.33 to 0.52. Below n values of 0.33, anomalies were observed as high hydraulic conductivity values

corresponded to low porosity values. On average, the general trend, based on experimental relations between the K_S values from the lab and field tests, was as follows: $K_S = 220n$ where $(0.33 \leq n \leq 0.52)$.

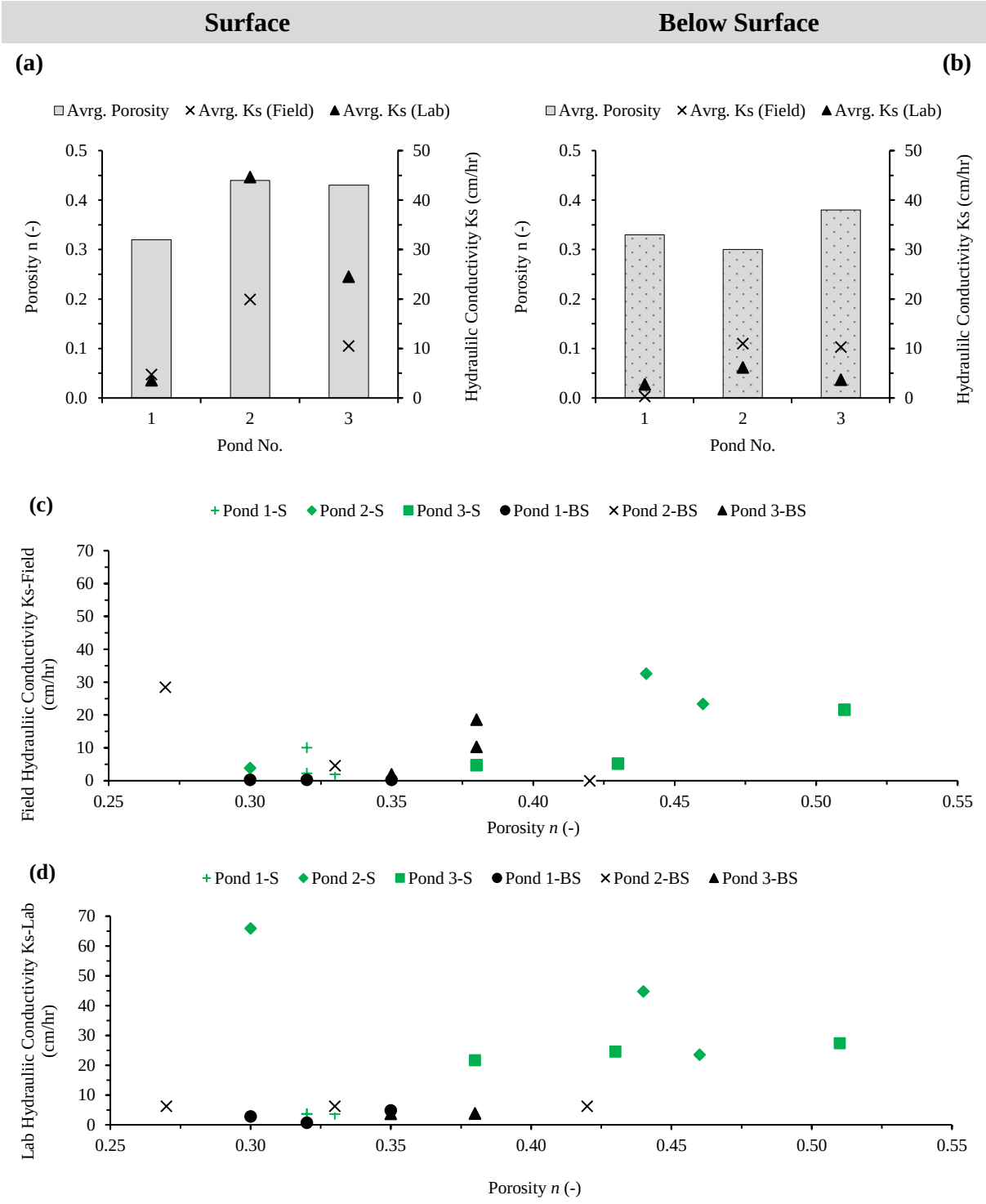

Figure 6-18: Average porosity versus field and laboratory hydraulic conductivity

6.4.7 Hydraulic Conductivity Variation with Steady-State Infiltration Rate

Figure 6-19 demonstrates results of the observed relationships between the assessed soils' field, and laboratory hydraulic conductivity values K_S, versus the field steady infiltration rates f_c.

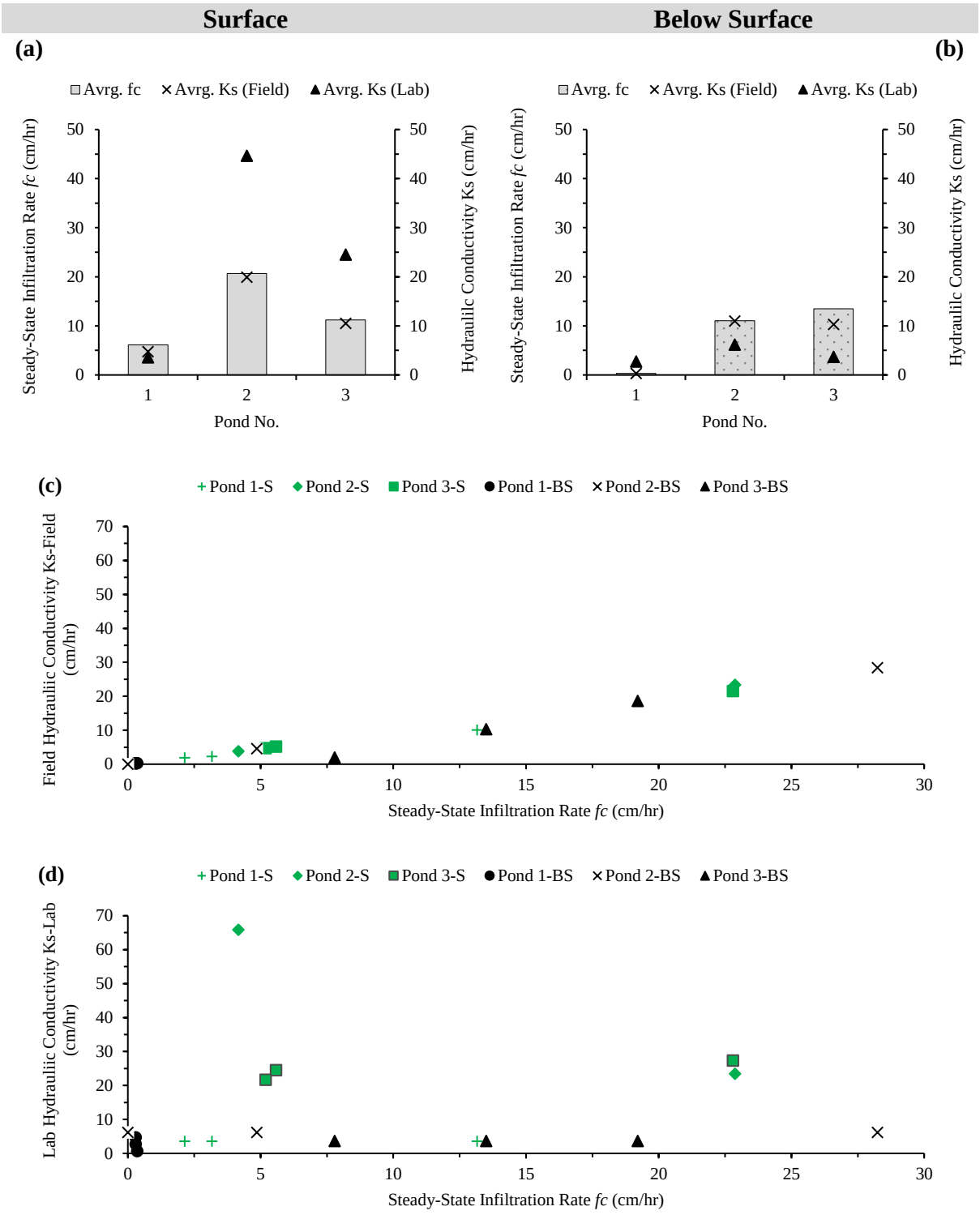

Figure 6-19: Average hydraulic conductivity vs field steady infiltration rate

The measured in-situ infiltration rates of the three investigated ponds were noted to decrease from the beginning of the tests to some steady rate f_c after a maximum test period of three hours. This decrease in infiltration rate, with increasing time, was associated with the subsoil becoming saturated.

The average steady infiltration rates f_c measured from the surfaces of the three ponds were 6.2, 20.6, and 11.2 cm/hr, correspondingly (Figure 6-19 (a)). When measured from the sub-surface, f_o values were generally lower within Ponds 1 and 2 (i.e. 0.3 and 11.0 cm/hr respectively) compared to Pond 3's average rate.of 13.5 cm/hr (Figure 6-19 (b)).

The field hydraulic conductivity values $K_{S_{field}}$ revealed distinct correlations. There was an overall agreement between the hydraulic conductivity values measured from the field and the steady infiltration rates. From Figure 6-19 (c), a positive linear trend was recognised such that the average ratio between $K_{S_{field}}$ and f_c was approximately 0.93. This empirical correlation could be expressed generally as follows: $K_{S_{field}} = 0.93 f_c$, for f_c values ranging between 0 and 29 cm/hr. From these results, the in-situ hydraulic conductivity was anticipated to approach the steady-state infiltration rate as the soil approached a fully saturated state. On the other hand, no apparent relationship was noted between the measured laboratory hydraulic conductivity values $K_{S_{lab}}$ and the field steady infiltration rates f_c (Figure 6-19 (d)).

6.4.8 Hydraulic Conductivity Variation with Average Laboratory Flowrate

The average flow rate q of water passing through samples assessed in the laboratory permeability investigation was compared to the corresponding hydraulic conductivity values obtained from the lab $K_{S_{lab}}$ and field $K_{S_{field}}$ investigations. Overall, the q values of specimens obtained from the surface of the ponds were higher than the rates measured from sub-surface samples (Figure 6-20 (a) and (b)).

The highest average flow rate q was measured from samples acquired on the surface of Pond 2 (i.e. 49.3 cm/hr) whilst the lowest was from soils obtained below the surface of Pond 1 (i.e., 3.0 cm/hr). This was a similar instance for the steady flow rates f_c measured in the field (Figure 6-19 (a) and (b)).

The plot in Figure 6-20 (c) does not show any distinct relationship between the $K_{S_{field}}$ and q values; again, highlighting the lack of correspondence between lab and field infiltration properties of the soil materials.

In contrast, a discernable linear relationship between the $K_{S_{lab}}$ and q values can be observed in Figure 6-20 (d). The gradient of this linear trend, based on the experimental results, allowed for the generalization of $K_{S_{lab}}$ values in terms of the measured q values as follows: $K_{S_{lab}} = 0.89q$, for q values ranging between 0 and 66 cm/hr. The ratio between $K_{S_{lab}}$ and q was expected to be closer to 1 because of the saturated nature of the lab permeability test samples,

however, this was not the case when compared to the K_{field} versus the in-situ steady infiltration rates described earlier in section 6.4.7.

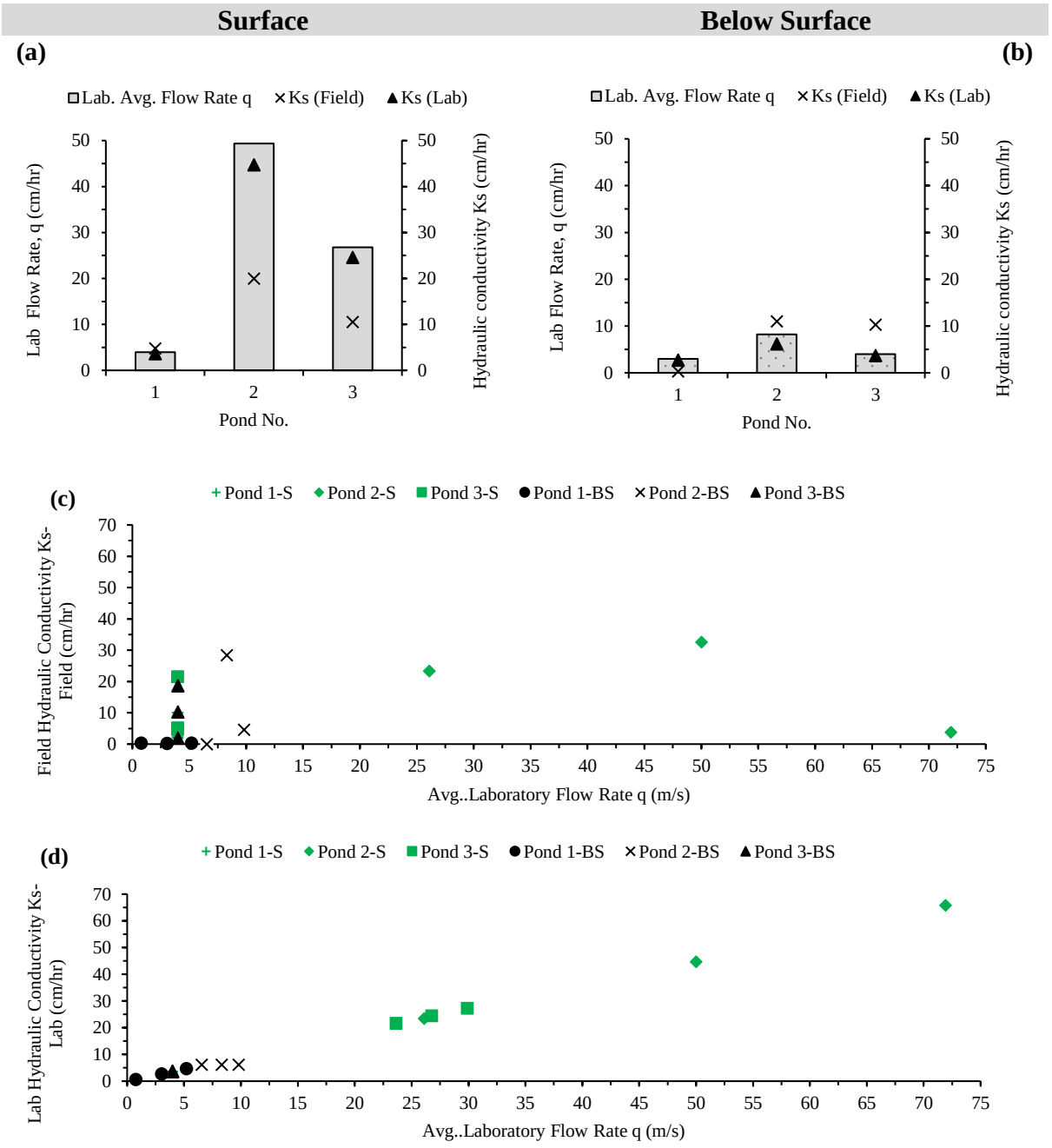

Figure 6-20: Average Laboratory Flow Rate vs Field and Lab Hydraulic Conductivity

6.5 Variability Soil of Hydraulic Conductivity

For the same type of soil material, variations between evaluated hydraulic conductivity values were noted to fluctuate by more than a single order of magnitude. For example, the hydraulic conductivity values obtained from measuring infiltration on the surface of Pond 1, at three test locations, ranged between 1.9 cm/hr. (i.e., 2.81×10^{-3} cm/s) and 10.1 cm/hr. (i.e., 5.28×10^{-4} cm/s).

Based on thorough reviews of all field infiltration, and lab permeability test results, evaluation methods, Moriasi et al. (2007), recommended that in addition to visual comparisons of observed hydraulic conductivity results, statistical techniques should be applied. A brief analysis was therefore conducted to assess the degree of variation of the average hydraulic conductivity values. Table 6-9 shows the hydraulic conductivity values obtained from the field and lab testing methods carried out in this investigation. The mean, standard deviation, and coefficient of variation CV of each set of tests were calculated.

Table 6-9: Statistical analysis of hydraulic conductivity values obtained from the field infiltration, and laboratory permeability investigations

Field (Surface)					
Pond no.	Test Loc.	K_S	Avg. K_S	Std. Dev.	CV
-	-	cm/hr	cm/hr	-	%
1	1	2.3	4.8	4.6	97.0
	2	1.9			
	3	10.1			
2	1	32.6	19.9	14.7	73.8
	2	3.8			
	3	23.4			
3	1	5.2	10.5	9.6	91.6
	2	4.7			
	3	21.6			

Field (Below Surface)					
Pond no.	Test Loc.	K_S	Avg. K_S	Std. Dev.	CV
-	-	cm/hr	cm/hr	-	%
1	1	0.3	0.3	0.0	0.0
	2	0.3			
	3	0.3			
2	1	28.4	11.0	15.2	138.6
	2	0			
	3	4.6			
3	1	10.3	10.3	8.3	80.6
	2	2			
	3	18.6			

Lab (Surface)					
Pond no.	Test Loc.	K_S	Avg. K_S	Std. Dev.	CV
-	-	cm/hr	cm/hr	-	%
1	1	3.6	3.6	0.0	0.0
	2	3.6			
	3	3.6			
2	1	32.6	40.6	22.3	54.8
	2	65.8			
	3	23.5			
3	1	24.5	24.5	2.9	11.6
	2	21.7			
	3	27.4			

Lab (Below Surface)					
Pond no.	Test Loc.	K_S	Avg. K_S	Std. Dev.	CV
-	-	cm/hr	cm/hr	-	%
1	1	2.8	2.8	2.1	74.1
	2	0.7			
	3	4.8			
2	1	6.2	6.2	0.0	0.0
	2	6.2			
	3	6.2			
3	1	3.7	3.7	0.0	0.0
	2	3.7			
	3	3.7			

The CV was computed as the ratio between the standard deviation and the mean. A higher CV corresponded to a greater level of dispersion around the mean. In this analysis, the CV was used to qualitatively determine the magnitude of spatial variability of soil hydraulic conductivity. A weak variability was defined by CV $\leq$ 10%, moderate when 10% $\leq$ CV $\leq$ 100%, and strong when CV $\geq$ 100% (Wei et. al., 2008).

Based on the analysis of variance, significant statistical differences were found between the hydraulic conductivity K_S values obtained from the field DRI and lab CHP test results. The variability of field K_S values were generally greater than those from the laboratory. The strongest variability was detected from field tests conducted on the sub-surface of Pond 2 (i.e. CV = 138.6%). This could be owed to the localized impervious soil layer encountered at Test Location 2 within Pond 2 which resulted in no observable infiltration for the duration of the DRI test. The bulk of the test results however fell within the moderate variation range of CV.

Notable variances were recognized broadly between the CV of the surface and sub-surface infiltration tests. Contrastingly, this difference was relatively minor when assessing Pond 3's field infiltration results which suggested that the vegetated sandy-loamy topsoil in the pond did not have a substantial influence on sub-surface soil's infiltration rates. Moreover, a uniform or homogeneous subsoil layer was expected based on these results. The average K_S value of Pond 3 was considered representative since the CV was comparable, for both the surface and sub-surface soil layers.

Even though soil samples tested in the laboratory were retrieved from the same locations as the field tests, as well as re-compacted to the same densities, boundary conditions appeared to be the governing influence of the spatial variance of hydraulic conductivity. Consequently, most hydrogeologists and geotechnical engineers today, maintain the practice of conducting in-situ tests before providing hydrogeological design recommendations for any given site, irrespective of existing correlations most often used to acquire crude estimates in the absence of actual field data.

When it comes to in-situ infiltration investigations, many factors related to the soil material, boundary conditions, as well as the liquids used may affect infiltration test results. Because of this, ASTM (2009) suggested for these results to be considered only as *index* values. Index properties in soil are physical characteristics that assist in the identification and classification of different soil materials. Examples of index properties include moisture content, specific gravity, in-situ bulk density, particle size distribution, etc.

6.6 Summary of Experimental Results

A summary of the average physical and hydraulic properties of soils within the investigated ponds is presented in Table 6-10. The average values presented are based on results from three separate locations within each pond to provide a better representation of general soil properties and infiltration rates. When compared to previous authors' findings (Gerber, 1980; Wessels & Greef, 1980; Tredoux et al., 1980; Henzen, 1973) results obtained in this study were comparable to proposed soil properties within the Zeekoe catchment area (Table 6-11).

Table 6-10: Summary of average physical and hydraulic properties of investigated soils

Property		Units	Pond 1		Pond 2		Pond 3	
			*Surface	**Below Surface	*Surface	**Below Surface	*Surface	**Below Surface
Natural Moisture Content	**NMC**	**%**	6	8	5	5	13	17
Porosity	***n***	**-**	0.32	0.33	0.44	0.3	0.43	0.38
Effective Grain Size	d_{10}	**mm**	0.10	0.10	0.15	0.17	0.16	0.14
Bulk Density	ρ_b	**kg/m^3**	1733	1889	1460	1917	1635	1930
Lab Hydraulic Gradient	***i***	**cm/cm**	9.7	9.7	9.8	9.6	9.7	9.7
Lab Average Flow Rate	***q***	**cm/hr**	4	3	49.3	8.2	26.8	4
Lab Hydraulic Conductivity	K_{Slab}	**cm/hr**	3.6	2.8	44.7	6.2	24.5	3.7
Field Hydraulic Conductivity	K_{Sfield}	**cm/hr**	4.8	0.3	19.9	11	10.5	10.3
Field Initial Infiltration Rate	f_o	**cm/hr**	17.3	0.1	27.5	12.7	12	12.3
Field Steady Infiltration Rate	f_c	**cm/hr**	6.2	0.3	20.7	11	11.2	13.5

*Sample from Surface (0 – 20 cm depth)
**Sample from Below Surface (20 – 40 cm depth)

Table 6-11: Hydraulic properties of Zeekoe catchment area proposed by various authors including this study

Parameter / Property	Units	Magnitude	Source / Author	Year
Hydraulic Conductivity	**cm/hr**	0.04 -4.2	Gerber	1980
		14.6 – 70.8	Wessels & Greeff	1980
		0.3 – 19.9	**This study**	
Porosity	**-**	0.10 – 0.15	Wessels & Greeff	1980
		0.02 – 0.25	Gerber	1980
		0.10 – 0.25	Tredoux et al.	1980
		0.20 – 0.25	Henzen	1973
		0.30 – 0.44	**This study**	
Effective grain size, D_{10}	**mm**	0.1 – 0.2	Tredoux et al.	1980
		0.1 – 0.17	**This study**	
Uniformity Coefficient, C_U	**-**	2.5 -4.0	Tredoux et al.	1980
		1.3 – 3.6	**This study**	

This investigation did not reveal a connection between the hydraulic conductivity values obtained from the field Double-Ring Infiltrometer (DRI) and the laboratory Constant-Head Permeability (CHP) tests. Experiments by previous authors (Radcliffe & Šimůnek, 2010), on the other hand, have shown that the in-situ saturated hydraulic conductivity is generally less than the saturated hydraulic conductivity measured on intact core samples in the laboratory. This has been attributed to the presence of entrapped air under field conditions which effectively reduces the cross-sectional area available for water to flow, and the water potential gradient. It is also possible that cored samples retrieved from the ponds' surfaces contained more sand than the underlying strata therefore increasing the measured permeability under laboratory test conditions.

Contrasting to findings described by Campbell, 2016 and Teague, 2010, the field hydraulic conductivities obtained from the surface alluvium of Ponds 2 and 3 were greater than those from the laboratory tests. This could be owed to the uncompacted nature of these soil layers. Moreover, the K_S values of the sub-surface soil layer within Pond 1 were also found to be greater than the associated laboratory K_S values, thus signifying possible low-permeability soil layers at greater depths within the pond.

For practical application and design purposes, it would be more reliable to consider the hydraulic conductivity values interpreted from the field tests using the Green-Ampt hydrological analysis method, as opposed to the laboratory tests. Based on the average soil hydraulic properties determined through the field infiltration tests, as well as borehole data from within and around the study area up to depths greater than 10 m, the recommended soil hydraulic properties were graphically summarised for each of the three investigated ponds (Figure 6-21 (a) to (c)).

The recommended soil properties are applied in infiltration simulations discussed in Chapter 7 Overall, soils within Pond 2 yielded the greatest infiltration potential with $K_{S_{field}}$ values ranging between 11.0 and 19.9 cm/hr. The hydraulic properties of soils within Pond 1 on the other hand, were found to be least favourable to promote water infiltration and potential groundwater recharge.

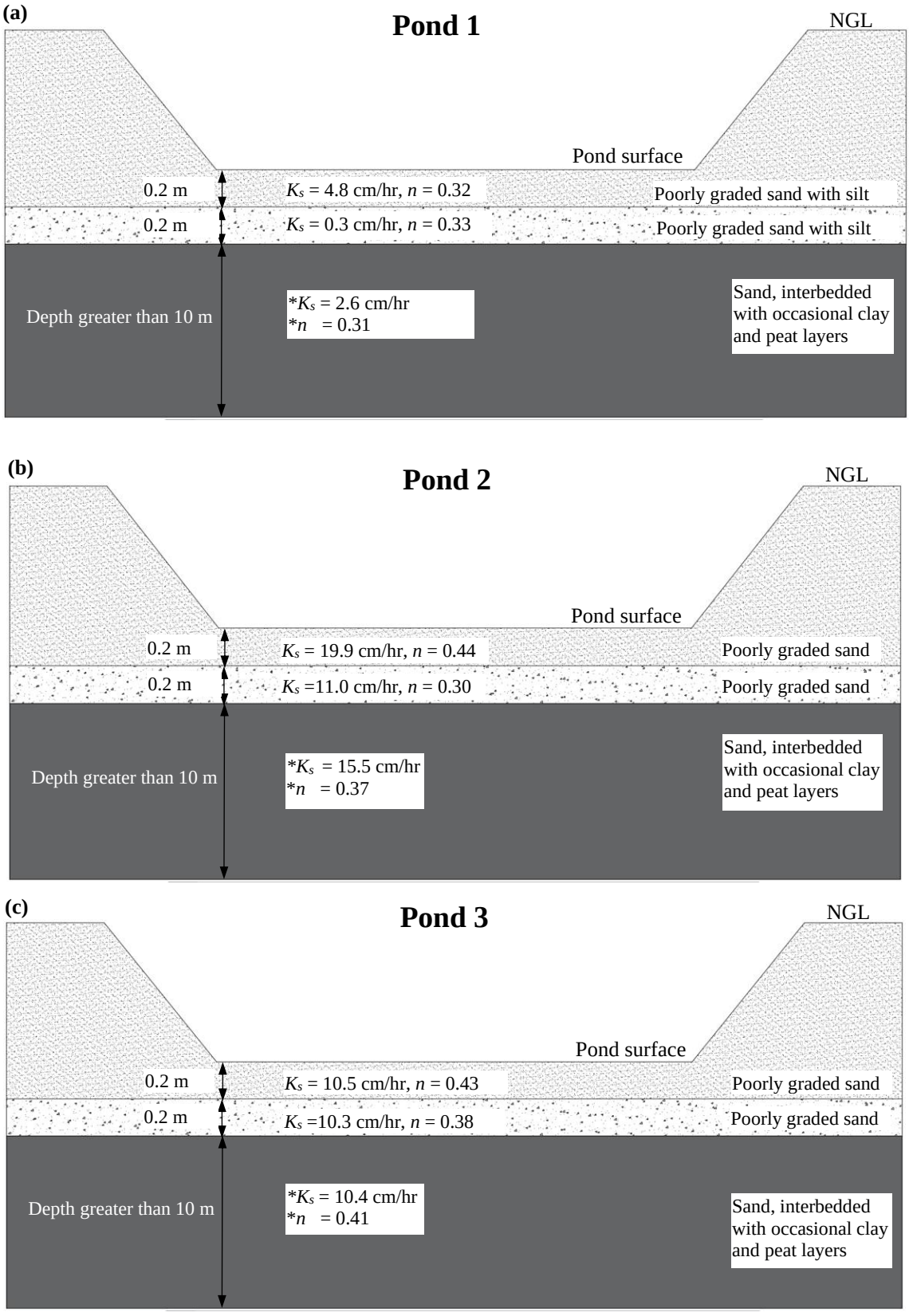

*Proposed values based on borehole log data and previous author's results and correlations (Chapter 3)

Figure 6-21: Graphical summary of average field hydraulic properties

7 Infiltration Simulations

7.1 Introduction

A numerical modelling computer software, HYDRUS 2-D, was utilized in conjunction with a built-in program, Rosetta-Lite, to infer groundwater flow characteristics in the deeper subsurface alluvium underlying the stormwater ponds investigated in this study.

The HYDRUS 2-D software used finite elements in space and finite differences in time to numerically solve and graphically simulate the movement of water through the unsaturated zone by combining equations for fluid flux and storage with conservation of mass equations (Radcliffe and Šimůnek, 2010).

The Rosetta-Lite software used five hierarchical pedotransfer functions (PTF's) to compute hydraulic conductivity values and water-retention information based primarily on soil particle size and density data measured in the laboratory.

This chapter begins with a description of the HYDRUS 2-D model solver, followed by an evaluation of various soil parameters estimated using the Rosetta-Lite software before the selection of appropriate input values for model simulations. The first simulations were small-scale 2-D models replicating the infiltration conditions of the field Double-Ring Infiltrometer (DRI) investigation. Large-scale models simulating water movement through a thicker unsaturated zone were subsequently developed to estimate the time it would take before the wetting front (interface between soil's initial state and newly wetted zone) would reach the water table located 5.5 m below the ponds' surfaces (Conrad, 2014). The effects of various surface crusts on the infiltration rate are explored before the chapter concludes with a description of the potential application and adaptation of groundwater recharge.

7.2 HYDRUS 2-D Model Solver

The program HYDRUS 2-D finite element (FE) software is capable of simulating both two and three-dimensional movement of water, heat, and solutes through soil media with variable degrees of saturation. A wide range of boundary conditions and finite element mash options are offered by the software and have been used by previous researchers to simulate infiltration through a single and Double-Ring Infiltrometer (DRI), (Fatehnia, 2015; Lai et al., 2010; Lazarovitch et al., 2007; Lai and Ren, 2007).

Through finite-difference approximations, the program applies Richard's (1931) equation (Equation 7.1) to simulate flow through the unsaturated zone:

$$\frac{\partial \theta}{\partial t} = \frac{\partial}{\partial x_i}\left[K\left(K_{ij}^{A}\frac{\partial \psi}{\partial x_j} + K_{iZ}^{A}\right)\right] - S \qquad 7.1$$

where S represents a sink term [m^{-1}], K_{ij}^{A} are components of a dimensionless anisotropy tensor K^{A}, x_i denotes spatial coordinates [m], θ is the volumetric water content, and K is the unsaturated hydraulic conductivity[m/s], given by Equation 7.2

$$K(\psi, x, y, z) = K_S(x, y, z) K_r(\psi, x, y, z) \tag{7.2}$$

where K_S is the saturated hydraulic conductivity and K_r is the relative hydraulic conductivity, or the ratio between unsaturated and saturated hydraulic conductivity, defined by van Genuchten (1980) using Equation 7.3.

$$K_r = \frac{\left\{1 - \left(\frac{h}{\alpha'}\right)^{(N\prime-1)} \left[1 + \left(\frac{h}{\alpha'}\right)^{N\prime}\right]^{(-\gamma)}\right\}^2}{\left[1 + \left(\frac{h}{\alpha'}\right)^{N\prime}\right]^{\frac{\gamma}{2}}} \tag{7.3}$$

where h is the pressure potential, and γ, N' and α' are constants defined by Equation 7.4 and Equation 7.5.

$$N' = \frac{1}{1 - \gamma} \tag{7.4}$$

$$\alpha' = \frac{\alpha}{\left(\frac{21}{\gamma - 1}\right)(1 - \gamma)} \tag{7.5}$$

7.3 Parameter Evaluation

The Rosetta-Lite program applied the van Genuchten (1980) expression for relative hydraulic conductivity in terms of pressure head. The software computed the van Genuchten empirical retention parameters (α and N) using the investigated soil's particle-size distribution and bulk density data of tested specimens retrieved from the field. Illustrated in Figure 7-1 is the software window highlighting the pertinent input and output variables.

The van Genuchten parameters computed by the Rosetta software displayed strong correlations to the correspondingly calculated hydraulic conductivities K_{S_R}. A positive linear-like relationship was observed between the van Genuchten parameter, N, and the hydraulic conductivity estimated by Rosetta, K_{S_R} (Figure 7-2 (a)). Soil specimens attained from sites with high hydraulic conductivities had higher N values, whilst those from low hydraulic conductivity sites yielded lower N values.

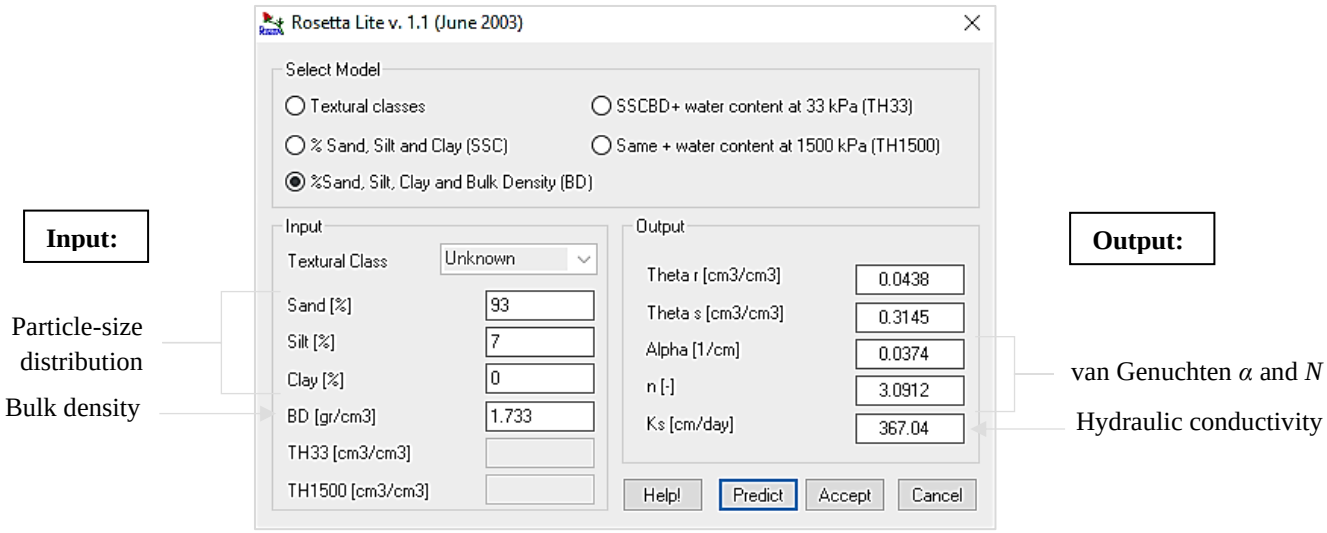

Figure 7-1: Rosetta-Lite Software Window

A contrasting relationship was observed between the hydraulic conductivities estimated by Rosetta, K_{S_R}, and the van Genuchten alpha, α, parameters. Higher hydraulic conductivity Test Locations yielded low α values and vice versa (Figure 7-2 (b)).

The trends observed from the two plots in Figure 7-2 were comparable to previous authors' findings such as Teague (2010) who conducted a similar study on silty sands near Joshua Tree in California, USA. In his findings, Teague also observed a positive linear-like relationship between Rosetta calculated van Genuchten parameters, N, and the corresponding computed hydraulic conductivities (Figure 7-3). The α parameter on the other hand, generally reduced with an increase in the hydraulic conductivity, similar to the findings of this study.

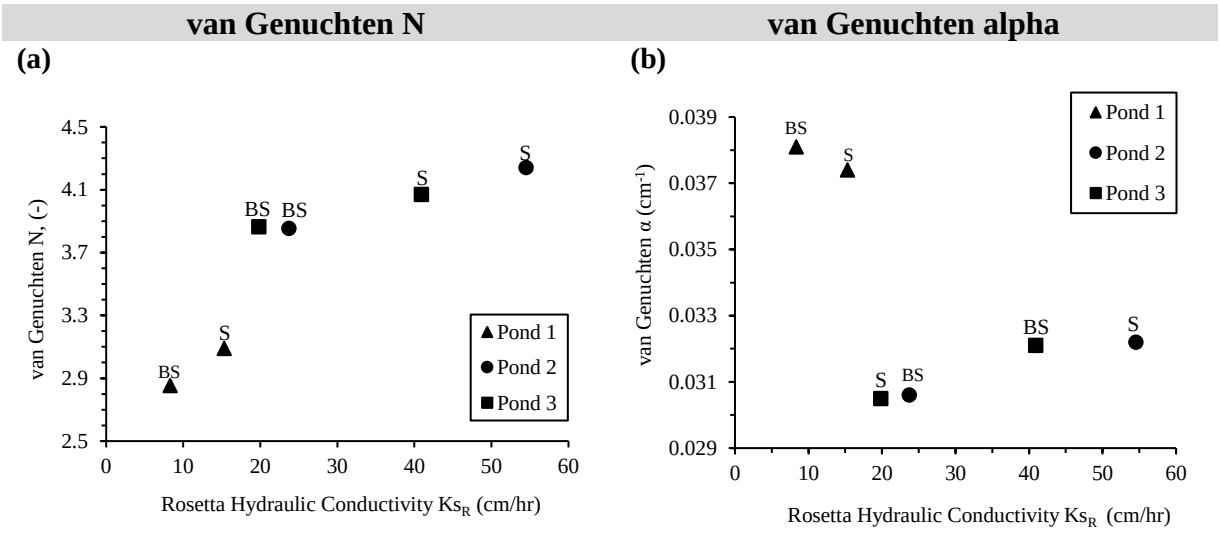

S: Surface (0 – 20cm); **BS**: Below Surface (20 – 40 cm)

Figure 7-2: Rosetta-Lite Estimated van Genuchten Parameters Compared to Rosetta Calculated Hydraulic Conductivities.

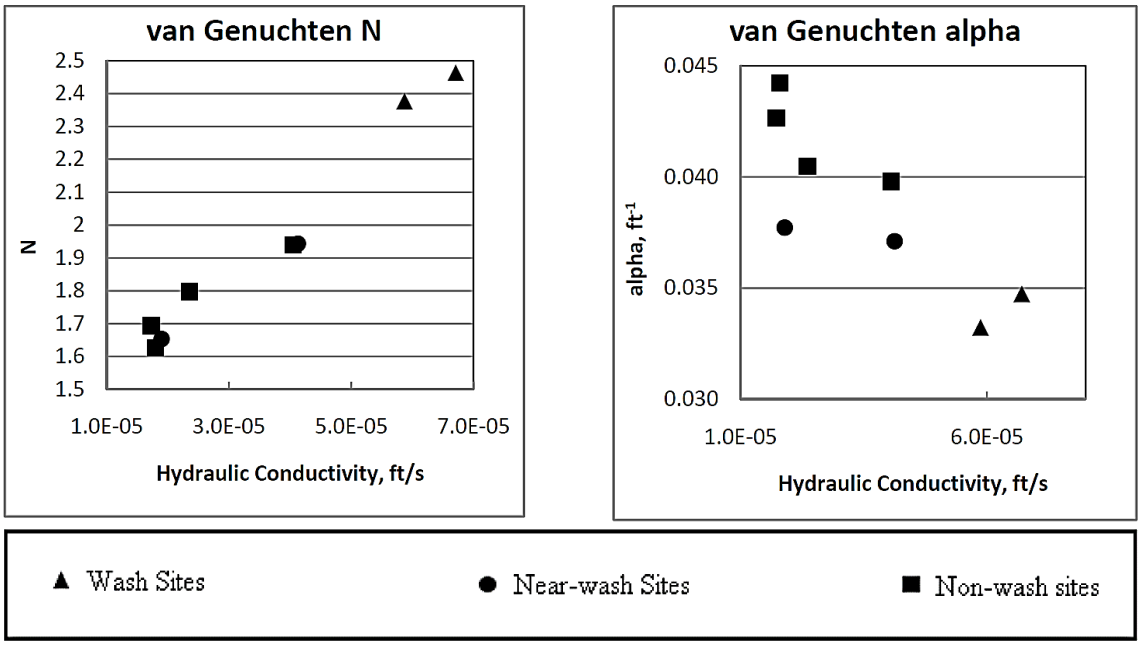

Figure 7-3: Rosetta estimated van Genuchten parameters compared to Rosetta calculated hydraulic conductivities, from data collected near Joshua Tree California, Jan. 2008
Adapted from: Teague (2010)

A comparison between the Rosetta calculated hydraulic conductivity values, K_{S_R} and the field hydraulic conductivities $K_{S_{field}}$ is shown in Figure 7-4 and Table 7-1. The saturated hydraulic conductivities estimated by the Rosetta software were within the characteristic range of fine sand to silty sands according to typical values shown in Table 7-2 (Campbell, 2016). Like the field and lab results, the K_{S_R} values of soils tested from the surface (0 – 0.2 m depth) of the ponds were overall greater than those tested from below the surface (0.2 – 0.4 m depth).

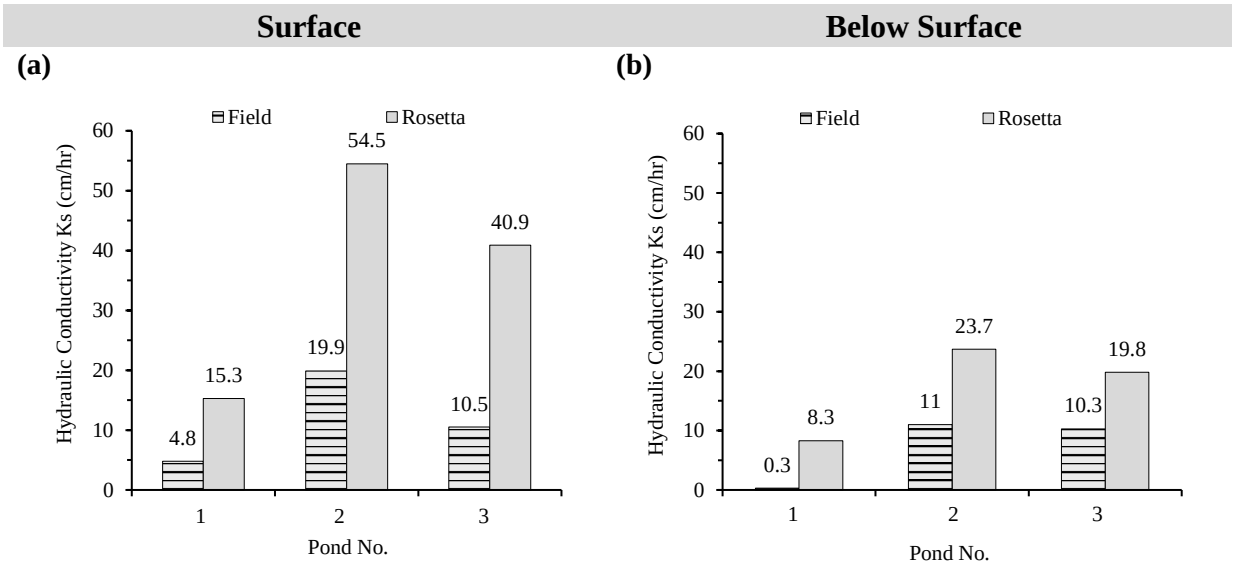

Figure 7-4: Average Field, Lab, and Rosetta Hydraulic Conductivities

Table 7-1: Comparison between average field and Rosetta hydraulic conductivity values

Test Set-Up Description	Pond No.	Field Hydraulic Conductivity (cm/hr)	Rosetta Hydraulic Conductivity (cm/hr)	Percentage Difference (%)	Average Percentage Difference (%)
Surface	1	4.8	15.3	104	105
	2	19.9	54.5	93	
	3	10.5	40.9	118	
Below Surface	1	0.3	8.3	186	107
	2	11	23.7	73	
	3	10.3	19.8	63	

Table 7-2: Typical values of hydraulic conductivity
Adapted from: Campbell (2016)

Soil Class	Saturated Hydraulic Conductivity, K_S (cm/hr)
Silty Sand	>11,78
Loamy Sand	2,99
Sandy Loam	1,09
Loam	0,34
Silt Loam	0,65
Sandy Clay Loam	0,15
Clay Loam	0,10
Silty Clay Loam	0,10
Sandy Clay	0,06
Silty Clay	0,05
Clay	0,03

The values obtained from Rosetta were all greater than those from the field by an average of 106%, however, a comparable trend was evident in respect of Ponds with high K_S values and those with low K_S values. The similarity in hydraulic conductivity values was closest between the laboratory and Rosetta sub-surface test results of Pond 3 with a difference of 63%. This similarity may be attributable to the continuous reworking of surface sediments of the pond forming a well-ordered soil surface structure. A closer correlation was anticipated between the hydraulic conductivity values estimated using Rosetta, and those from the lab, bearing in mind the Rosetta input figures were obtained directly from the lab analysis of in-situ soil samples.

The greatest difference in the hydraulic conductivities (i.e., 118%) was between the field and Rosetta values from Pond 3's surface-test results. The field hydraulic conductivity value

$K_{S_{field}}$, was 10.5 cm/hr whilst Rosetta's was 40.9 cm/hr. These figures were of different orders of magnitude, however, within the typical range for fine sand to silty sand.

The pedotransfer functions (PTF's) used by Rosetta-Lite were based on laboratory-derived data from general soil types (i.e., sand, loamy sand, loam, silt, sandy clay loam, silty clay, etc) which limited the degree of accuracy to reproduce field conditions in alluvium which lacks extensive soil information. Thus, the hydraulic conductivity values determined from field infiltration experiments were used in the models to better replicate in-situ conditions.

7.4 Model Setup

Axisymmetric models were developed such that the upper left corner of the model space represented the position of the vertical centreline. The first models simulated infiltration through a Double-Ring Infiltrometer (DRI), whilst the second set of models represented infiltration through the surface of a full-scaled pond.

Model domain sizes were selected to ensure that the outer boundaries did not affect the flow field within the domain. Domain spaces were separated into small, unstructured, triangular-shaped finite element (FE) mesh which varied in size.

Although the HYDRUS-2D software offered a wide range of simulation modules (i.e., heat movement, solute transport, evaporation, evapotranspiration, and root-water uptake), only water flow through the unsaturated zone of soil was simulated in this study. The cumulative infiltration of each simulated scenario was determined from the volumetric water flux across the inner-ring boundaries of the DRI apparatus, and the ponds' horizontal extent.

7.5 Hydraulic Parameters Used in Models

The soil hydraulic parameters used in the simulations are summarised in Table 7-3. The parameters θ_r and θ_s denote the residual and saturated moisture contents respectively.

Table 7-3: Experimental soil parameter values used in HYDRUS models

Pond	Soil Layer Descript.	Depth	θ_r	θ_s	α	N	$K_{S_{field}}$
#	-	m	cm^3/cm^3	cm^3/cm^3	1/cm	-	cm/hr
1	Surface	0 - 0.2	0,048	0,320	0,035	2,681	4,80
	Below-Surface	0.2 - 0.4	0,044	0,281	0,037	2,541	0,30
	Greater Depths	0.4 - 10	0,046	0,300	0,036	2,611	2,55
2	Surface	0 - 0.2	0,054	0,398	0,031	4,151	19,90
	Below-Surface	0.2 - 0.4	0,049	0,272	0,030	3,806	11,00
	Greater Depths	0.4 - 10	0,052	0,335	0,031	3,979	15,45
3	Surface	0 - 0.2	0,051	0,344	0,031	3,950	10,50
	Below-Surface	0.2 - 0.4	0,049	0,270	0,030	3,617	10,30
	Greater Depths	0.4 - 10	0,050	0,307	0,031	3,783	10,40

7.6 Simulation of Double-Ring Infiltrometer Field Test

The initial simulations' configurations represented the field Double-Ring Infiltrometer (DRI) test conditions. Figure 7-5 illustrates a schematic of the two different test set-ups which were adapted. The model arrangement and input parameters closely signified those of the field conditions to obtain a perspective of the wetting front variation with time. The hydraulic conductivity values used as model inputs for each simulated test were those measured from the field.

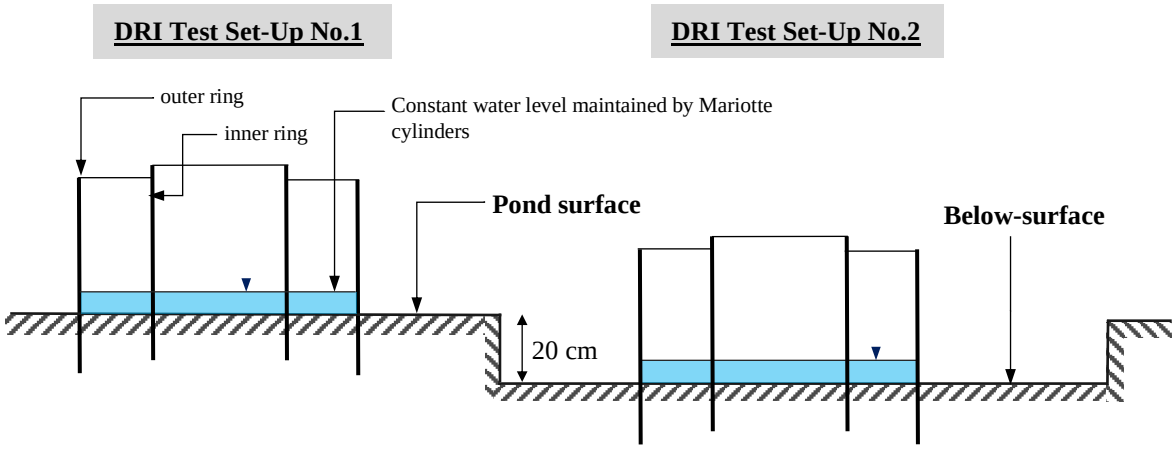

Figure 7-5: Schematic of two adapted DRI field test set-ups

7.6.1 Model Domain

The model domain was 2 m in the radial direction, r, and 1 m in the vertical, z. The upper left corner represented the location of the centre of the DRI apparatus with a 15 cm horizontal separation between the inner and outer rings. The rings were driven into the ground to a depth of 15 cm. The model geometry of the first test set-up represented the field DRI tests which were conducted directly on the ponds' surfaces (Figure 7-6). The second set-up represented the DRI test after the removal of a 20 cm of topsoil layer (Figure 7-7)

To simulate the unsaturated zone at equilibrium, the initial conditions for the hydrostatic pressure head were set to a minimum of -100 cm at all depths within the profile window. The water table depth was far beyond the depth of the domain and was thus not included in this initial set of simulations.

The primary time step of the simulation was set to 0.0024 hours with a minimum and maximum of 0.00024 hours and 3 hours, respectively. The simulation period was maintained at a constant 3 hours to match the duration of infiltration measured in the field-test data. The measured infiltration rates were noted to generally decrease from the beginning of the tests to some steady rate f_c after a maximum test period of 3 hours.

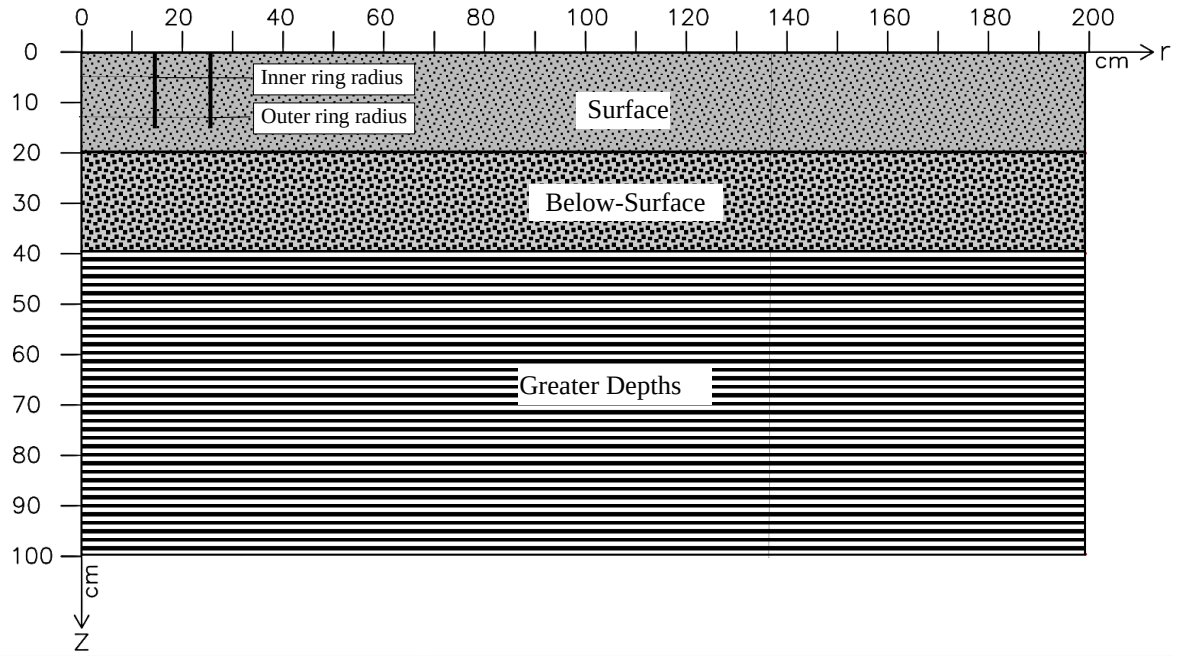

Figure 7-6: DRI Set-up 1 - Axisymmetric surface test model geometry

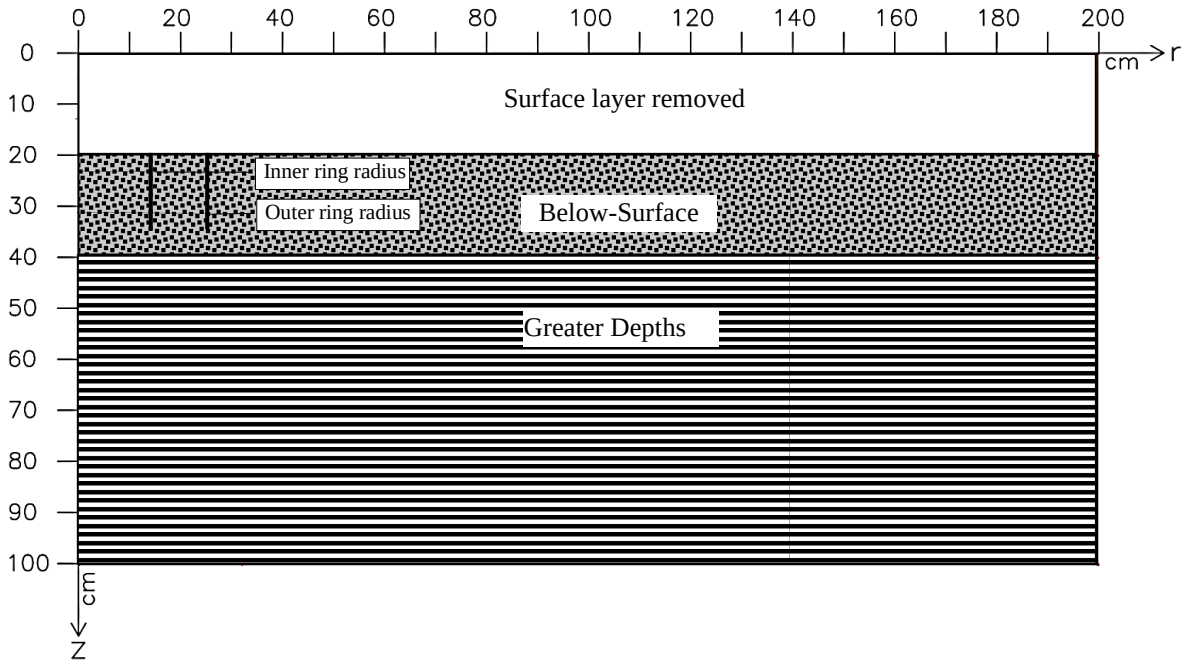

Figure 7-7: DRI Set-up 2 - Axisymmetric sub-surface test model geometry

7.6.2 Model Grid

The finite element (FE) mesh size immediately surrounding the DRI was modelled to be significantly smaller relative to the increasingly larger mesh size as the distance increased radially from the rings. Directly underneath the rings, the mesh size was 1.0 cm which increased radially to a maximum of 5 cm at the domain boundary to ensure that the cells describing the walls of the infiltrometer rings were no-flow boundaries.

A constant pressure head of 15 cm was simulated at the surface boundary representing the inner and outer rings of the DRI apparatus; all other boundaries were modelled as no-flux boundaries. Interaction of the model wetting front with the model boundaries was avoided over the simulated test period. Figure 7-8 illustrates the model domain with the boundary conditions.

Before running a numerical solution to generate results in HYDRUS-2D, a step-wise code was run in a separate window to verify the following parameters: horizontal plane flow, nodal information, geometric information, material information, time information, and seepage face information. The relevant parameters used in this study to simulate the DRI field test are presented in Table 7-4.

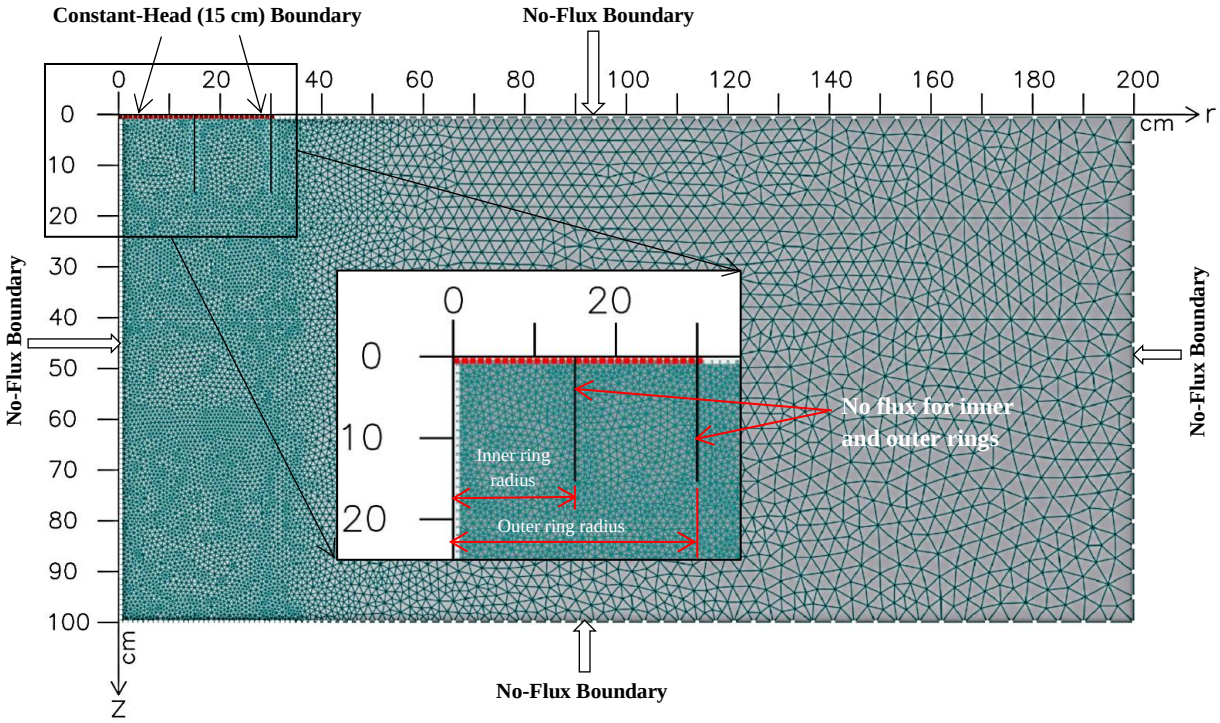

Figure 7-8: Two-Dimensional Axisymmetric Model Domain and Boundary Conditions used to Simulate Field DRI Test in HYDRUS 2-D

Table 7-4: Numerical model characteristics used in the simulation of Double-Ring Infiltrometer field test in HYDRUS 2-D

Description	Parameter	Unit	Magnitude
Time Discretization	Initial	hour	0
	Final	hour	3
	Initial time step	hour	0.0024
	Minimum time step	hour	0.00024
	Maximum time step	hour	120
	Number of print time	hour	10
Iteration	Maximum number of iterations	-	10
	Water content tolerance	-	0.001
	Pressure head tolerance	cm	1
Rectangular dimensions	Horizontal rectangular dimension	cm	200
	Vertical rectangular dimension	cm	100
	FE mesh size	cm	1 - 5
Boundary conditions	Top	-	Constant head and no-flux
	Bottom	-	No flux
	Right side	-	No flux
	Left side	-	No flux

7.6.3 Simulation Results

With the model domain set to an initial equilibrium pressure head of -100 cm, and the Double-Ring Infiltrometer DRI maintaining a constant 15 cm head of water in both the inner and outer rings (like in the field infiltration investigations), the variation in pressure head was observable at various time intervals using the HYDRUS 2-D graphic user interphase (GUI). Results after 3-hour simulation periods are presented in Figure 7-9.

The movement of water through the underlying soil strata of the modelled ponds was in both the vertical and horizontal directions from the centre of the DRI. The observed lateral flow was attributable to the water in the outer ring and the effects of capillarity which varies with soil texture and shape, whilst the vertical flow was a result of the water in the inner ring (Figure 7-10). Because the surface area between the outer ring and the inner ring was larger (2121 cm^2) compared to the surface area within the inner ring (706 cm^2), more water infiltrated laterally through the outer ring compared to vertically through the inner ring. The bi-directional flow pattern was more uniform in Pond 2 and Pond 3 which can be owed to the similarities between the two ponds' soil properties.

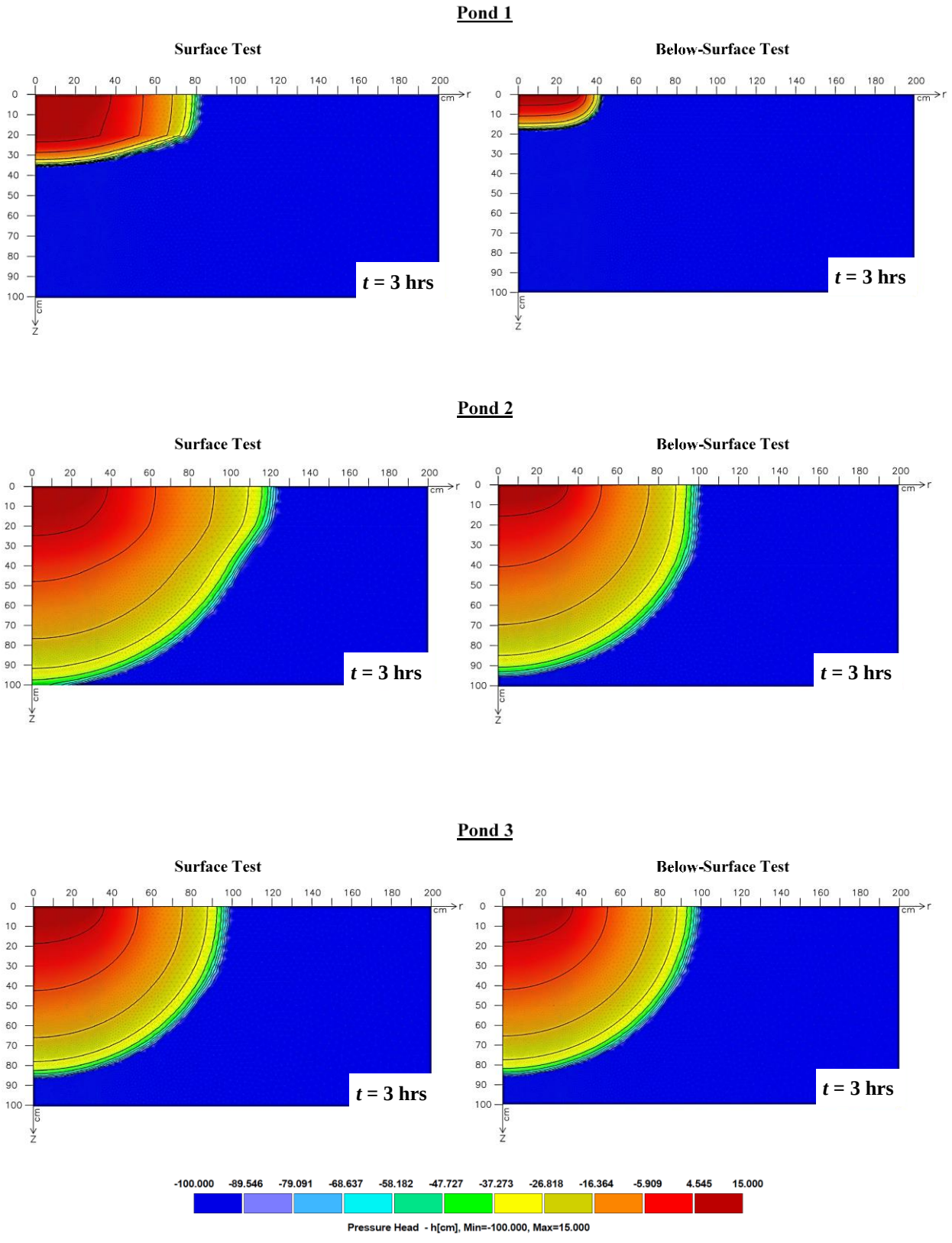

Figure 7-9: Axisymmetric pressure head distribution (cm) below the Double-Ring Infiltrometer at the three investigated ponds after a 3-hr test period. HYDRUS 2-D was used for the simulations.

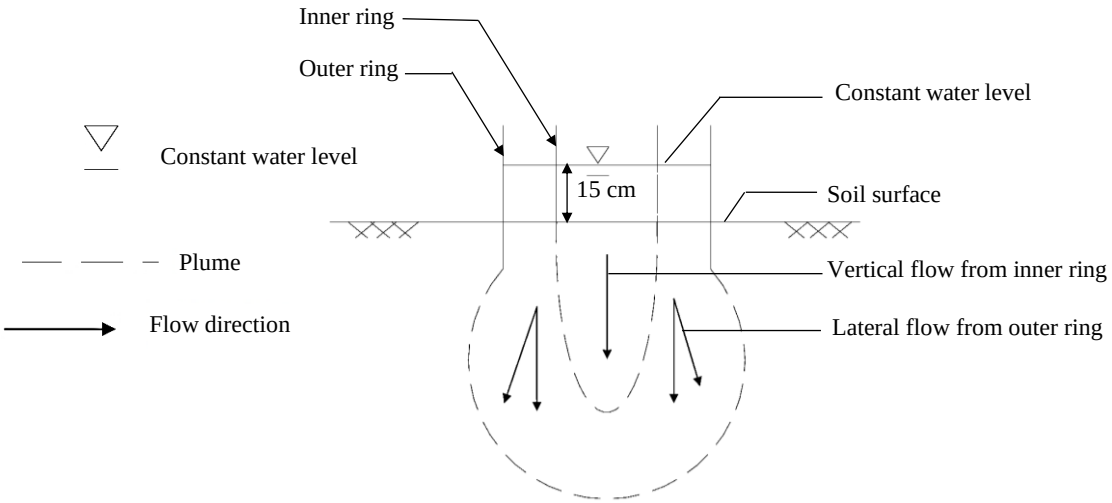

Figure 7-10: Steady infiltration of water from a Double-Ring Infiltrometer

Cross-sections taken along the centreline of each DRI simulation (i.e., vertically along the plane where r = 0 cm) illustrated the moisture distribution with increasing depth. Plots in Figure 7-11 display the depth of infiltration at pressure heads varying from a constant 15 cm at the surface, to an equilibrium pressure head of -100 cm.

The wetting front moved to greater depths in ponds with higher hydraulic conductivities. A general agreement between hydraulic conductivity and infiltration rate was recognised. Lower infiltration rates can be matched with lower hydraulic conductivity values. This is particularly notable when comparing the surface and below-surface plots for Pond 1 in Figure 7-11. The greatest depth reached by the wetting front after 3 hours was 100 cm in Pond 2 with preferential hydraulic properties across its various underlying soil layers.

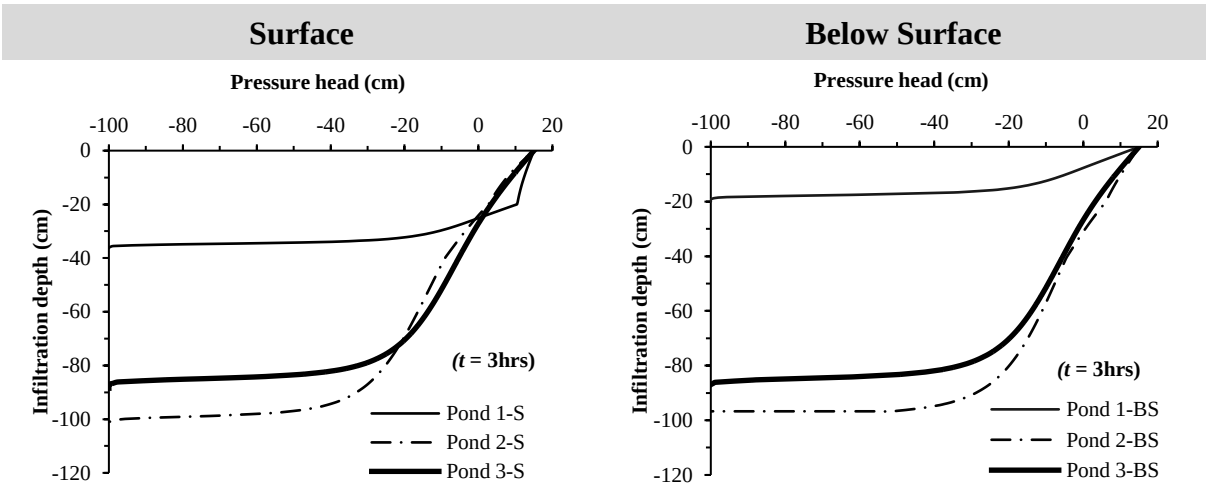

Figure 7-11: Simulated DRI Infiltration depth variation with pressure head at t = 3hrs

A comparison was made between the average infiltration rates measured from the field DRI tests and the infiltration rates obtained from the HYDRUS 2-D simulations. A summary of the results is presented in Table 7-5. The infiltration rates obtained from HYDRUS 2-D were generally higher than the field-measured rates. The percentage difference ranged from 67 – 182% which suggested sensitivity to near-surface heterogeneity, and the presence of a low permeability layer at greater depths below the pond surfaces. The variation in soil texture and permeability in subsurface soil layers can cause an impediment to the overall flow of water.

Table 7-5: Average field DRI and HYDRUS 2-D infiltration rates at *t* = 3hrs

Test Set-up Description	Pond No.	Average Field Infiltration Rate (cm/hr)	HYDRUS 2-D Infiltration Rate (cm/hr)	Percentage Difference	Average Percentage Difference
Surface	1	6.2	12.3	67	68
	2	20.7	33.6	48	
	3	11.2	29.0	89	
Below-Surface	1	0.3	6.7	182	118
	2	11.0	32.3	98	
	3	13.5	28.7	72	

Horton's (1933) method (described in section 4.9) was used to determine the infiltration decay coefficient λ expressed in the following exponential relationship: $f = f_c + (f_o - f_c)\, e^{-\lambda t}$. An inverse relationship was observed between the coefficient λ and the associated steady-state infiltration rate f_c. A high decay coefficient corresponded to a low infiltration rate and vice versa. Pond 2 (with the highest observed infiltration rate) corresponded to the lowest decay coefficient of 0.6 whilst Pond 1 (with the lowest infiltration rate) had the highest λ value of 1.9. A comparison between the infiltration decay coefficient and the steady-state infiltration rate of the three investigated ponds is summarised in Table 7-6. Knowledge of the infiltration decay rate of soils in stormwater ponds can aid in accounting for the gradual clogging of surface layers.

Table 7-6: Comparison between Horton's λ and the steady infiltration rate f_c

Pond	Horton's Infiltration Decay Coefficient λ	Average Steady Infiltration Rate f_c (cm/hr)
1	1.9	1.4
2	0.6	20.6
3	0.8	10.5

7.7 Simulation of Water Movement Through Pond Surface to Water Table

Large-scale models were subsequently developed to simulate water movement through a thick unsaturated zone to estimate the time required before the wetting front would reach the water table. A schematic cross-section across a typical circular spreading pond with a constant head of water is shown in Figure 7-12

To assess the influence of a surface crust layer of low permeability on infiltration, the hydraulic conductivity of the top 20 cm soil layer was varied between 0.1, 1.0, and 10 cm/hr. Infiltration rates determined from in-situ investigations were used as a benchmark and compared to the infiltration rates obtained after varying the hydraulic conductivity of the surface layer.

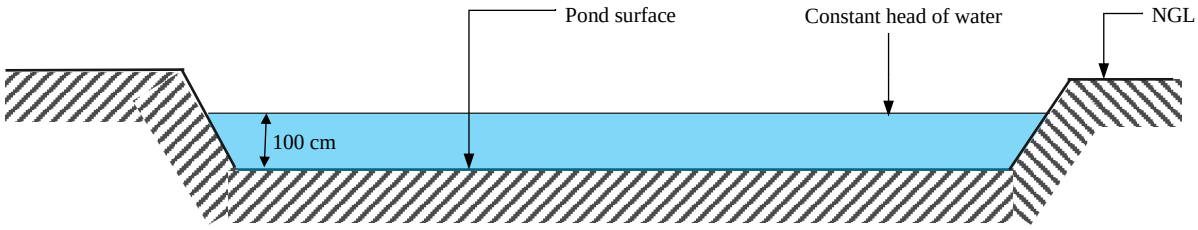

Figure 7-12: Schematic of a typical stormwater pond with 100 cm constant head of water

The large-scaled simulations were like the DRI field test simulations with the key differences being the applied constant head of water at the pond surfaces (from 15 cm to 100 cm), the domain sizes (from 200×100 cm; to 65×6.5 m), and simulation durations (from 3 up to 140 hours).

7.7.1 Model Domain

The model domain was enlarged to represent a radial cross-section through a circular pond with a surface area of 0.79 ha. The upper left corner of the model space represented the location of the centre of the pond. The domain extended 65 m in the radial direction *r* from the centre and 6.5 m in the vertical *z*-direction (Figure 7-13). The pond was simulated at the surface by active cells extending radially by 50 cm. Infiltration of water within the ponds was regulated by 100 cm constant head at the boundary representing the pond surface, which aimed to depict conservative yet realistic conditions during a rainy season. The soil strata were divided into three layers, each possessing soil properties summarised in Table 7-3.

To simulate a thick unsaturated zone, a minimum pressure head of -100 cm across the domain space represented the initial hydraulic conditions at equilibrium with the water table at 5.5 m below the surface. Each simulation ran until the wetting front moved through the unsaturated zone to the water table. To achieve this for each modelled pond, the simulation durations varied between 15 – 140 hours.

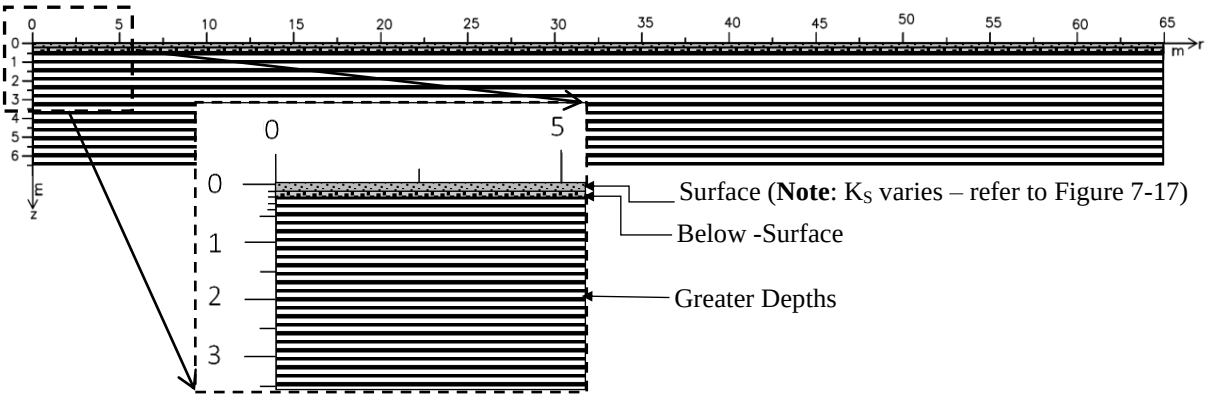

Figure 7-13: Stormwater pond surface infiltration model geometry

Interaction of the wetting front with the model boundaries was avoided. The primary time step of the simulation was set to 0.024 hours with a minimum and maximum of 0.0024 hours and 140 hours, respectively.

7.7.2 Model Grid

Due to the large-scale nature of the models, the FE mesh size was increased from 5 to 20 cm and maintained across the entire domain in both the vertical and horizontal directions (Figure 7-14).

A step-wise code was run to verify key parameters (i.e., horizontal plane flow, nodal information, geometric information, material information, time information, and seepage face information) before numerical solutions were processed to generate results.

The numeral model characteristics used to simulate water movement through the pond surface to the water table are presented in Table 7-7.

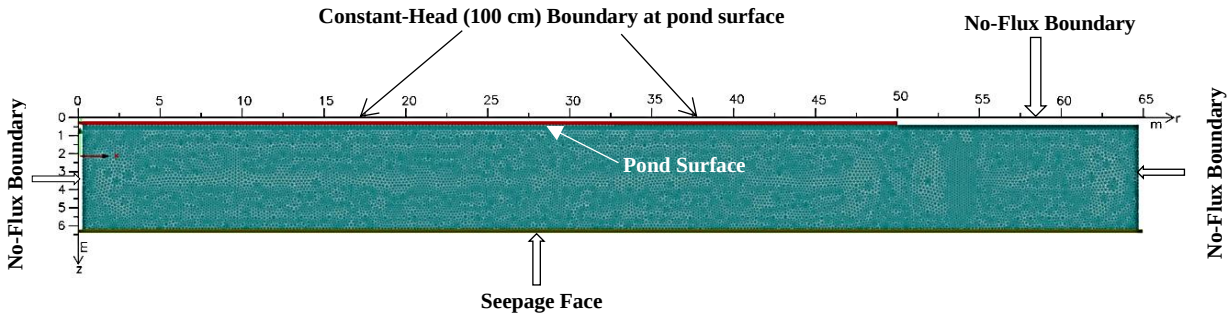

Figure 7-14: Two-Dimensional axisymmetric model domain and boundary conditions used to simulate water movement through pond surface in HYDRUS 2-D

Table 7-7: Numerical model characteristics used in the simulation of water movement through pond surface to water table in HYDRUS 2-D

Description	Parameter	Unit	Magnitude
Time Discretization	Initial	hour	0
	Final	hour	200
	Initial time step	hour	0.0024
	Minimum time step	hour	0.00024
	Maximum time step	hour	120
	Number of print time	hour	100
Iteration	Maximum number of iterations	-	10
	Water content tolerance	-	0.001
	Pressure head tolerance	cm	1
Rectangular dimensions	Horizontal rectangular dimension	cm	6500
	Vertical rectangular dimension	cm	650
	FE mesh size		20
Boundary conditions	Top	-	Constant head
	Bottom	-	Seepage face
	Right side	-	No flux
	Left side	-	No flux

7.7.3 Simulation Results

The HYDRUS 2-D graphic user interphase (GUI) was used to observe the wetting front movement from the ponds' surfaces at various time intervals, and to assess the time taken before the water table was reached 5.5 m below the surface (Figure 7-15).

Infiltration of water was modelled by adapting in-situ and laboratory-derived soil hydraulic and physical properties of the surface layer (0 – 20 cm) and below-surface layer (20 – 40 cm). Borehole log data from within and around the study area was used to infer soil properties at greater depths.

The time required for the wetting front movement from the pond surfaces to the water table was determined to be 140 hours in Pond 1, 15 hours in Pond 2, and 25 hours in Pond 3. The corresponding infiltration rates were 3.9 cm/hr for Pond 1, 36.7 cm/hr for Pond 2, and 22.0 cm/hr for Pond 3. These infiltration rate values were higher than what could be anticipated in reality because the HYDRUS 2-D model assumed uniform hydraulic properties in each soil layer and did not consider compaction, consolidation, or variations in the deeper subsurface geology.

Site-specific data about soil hydraulic properties at greater depths beyond 40 cm would aid in refining the models, however, the processes required would be rigorous and costly such as

well-pumping tests, and soil logging at each pond to depths of up to 6 m. The information used in this study was reasonable as it represented deeper soil layers at sites near the investigated ponds.

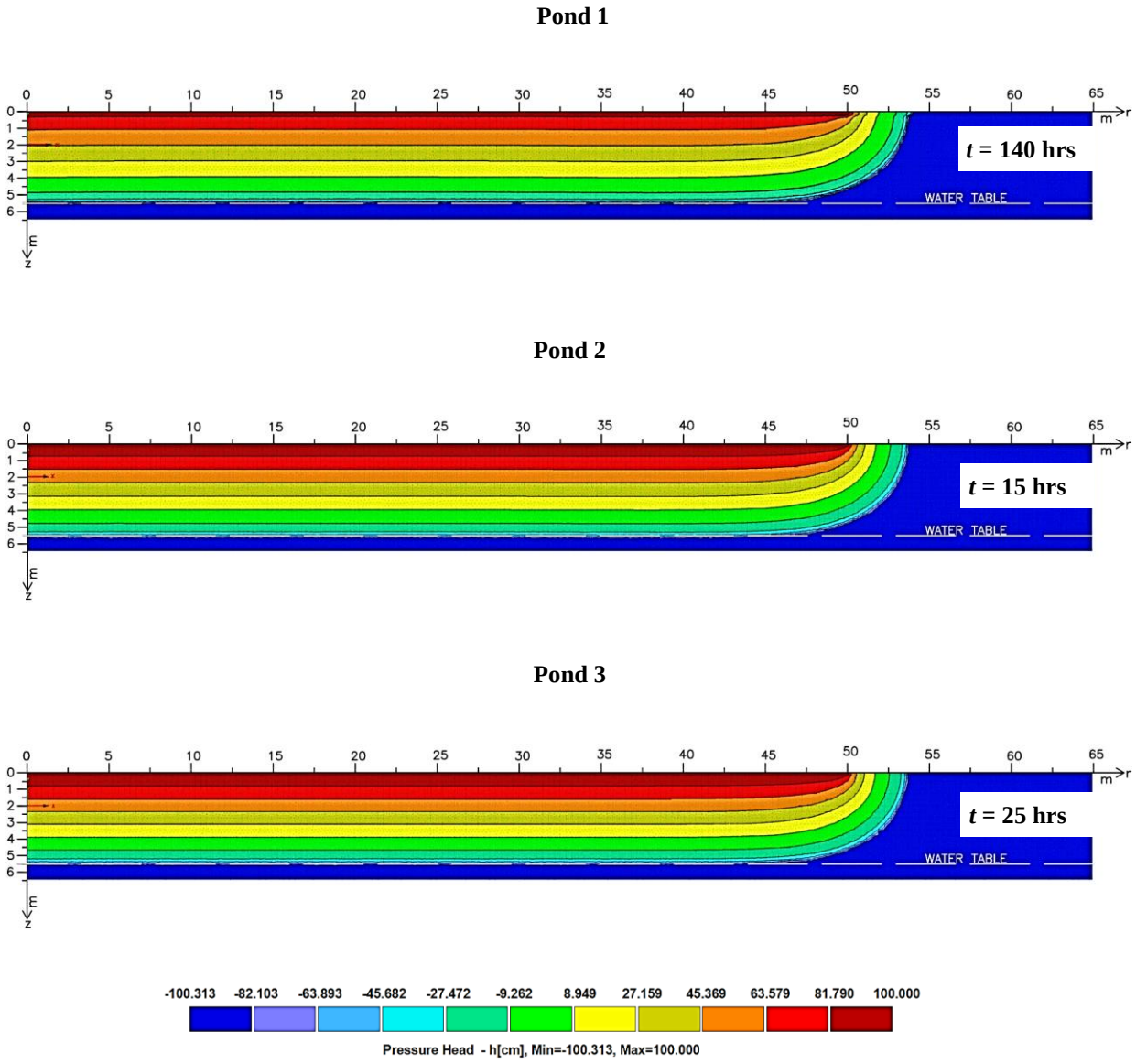

Figure 7-15: Pressure Head Distribution from HYDRUS 2-D Pond Infiltration Simulations

Despite the notable differences between the three ponds' infiltration rates, the horizontal movement of the wetting fronts within each pond was comparable, with Pond 2 and 3 displacing laterally by the same distance of 3.5 cm (i.e., from 50 to 53.5 cm) whilst Pond 1's wetting front moved by 3 cm (i.e., from 50 to 53 cm). The particularly lower infiltration rate in Pond 1 can be owed to dense underlying soils observed at numerous Test Locations within the pond at shallow depths (0 - ~40 cm). These dense layers created a low-permeability seal around the bottom of the DRI inner ring during the field infiltration investigations, thus lowering the infiltration rates.

Vertical cross-sections taken along the pond centre lines (i.e., at r = 0 m) illustrate the propagation of the wetting front in terms of pressure head (Figure 7-16). A strong agreement between the pressure head variation, at various depths, in Pond 2 and Pond 3 was observed when the wetting front reached the water table because of the similarity in soil properties of the two ponds.

Data showed a decrease in the infiltration rate in Pond 1 due to the presence of a layer of lower hydraulic conductivity on the surface which was evident at early times (5 – 10 hrs) in the simulation. At depths beyond 40 cm, this detected decrease in infiltration rate was not significant.

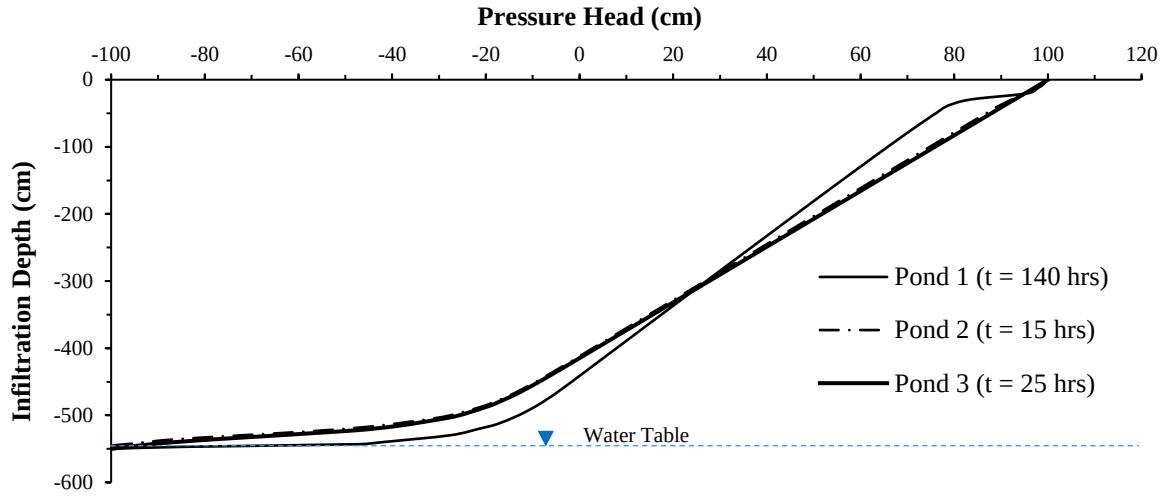

Figure 7-16: Simulated Position of the Wetting Front Below Stormwater Ponds to the Groundwater Table

7.7.4 Effects of Varying the Surface Layer's Hydraulic Conductivity

During major rainfall events, overland flow from stormwater runoff collects impurities and fine particles before entering stormwater ponds. Clogging of the surface layer, caused by bacteria or fine particle material, is one drawback to the use of ponds for surface infiltration (Baveye et al., 1998; Bouwer, 2002; Reddy, 2008).

To study the effect of the topsoil permeability on overall infiltration, the hydraulic conductivity K_S of the pond surface layers was varied from initial values obtained from the field investigations $K_{S_{field}}$, to three additional soil types (i.e., sandy clay with K_S = 0.1 cm/hr; sandy clay loam with K_S = 1.0 cm/hr; and silty sand with K_S = 10.0 cm/hr). By varying the hydraulic conductivity of the surface layer (i.e., the top 20 cm soil layer) within each pond, and maintaining the same simulation periods and conditions, the resultant effect on the overall infiltration rate, and accordingly the wetting front movement, was observable. Centreline cross-sections taken along the vertical plane (i.e., at r = 0 m) illustrate the varying effects of these changes (Figure 7-17).

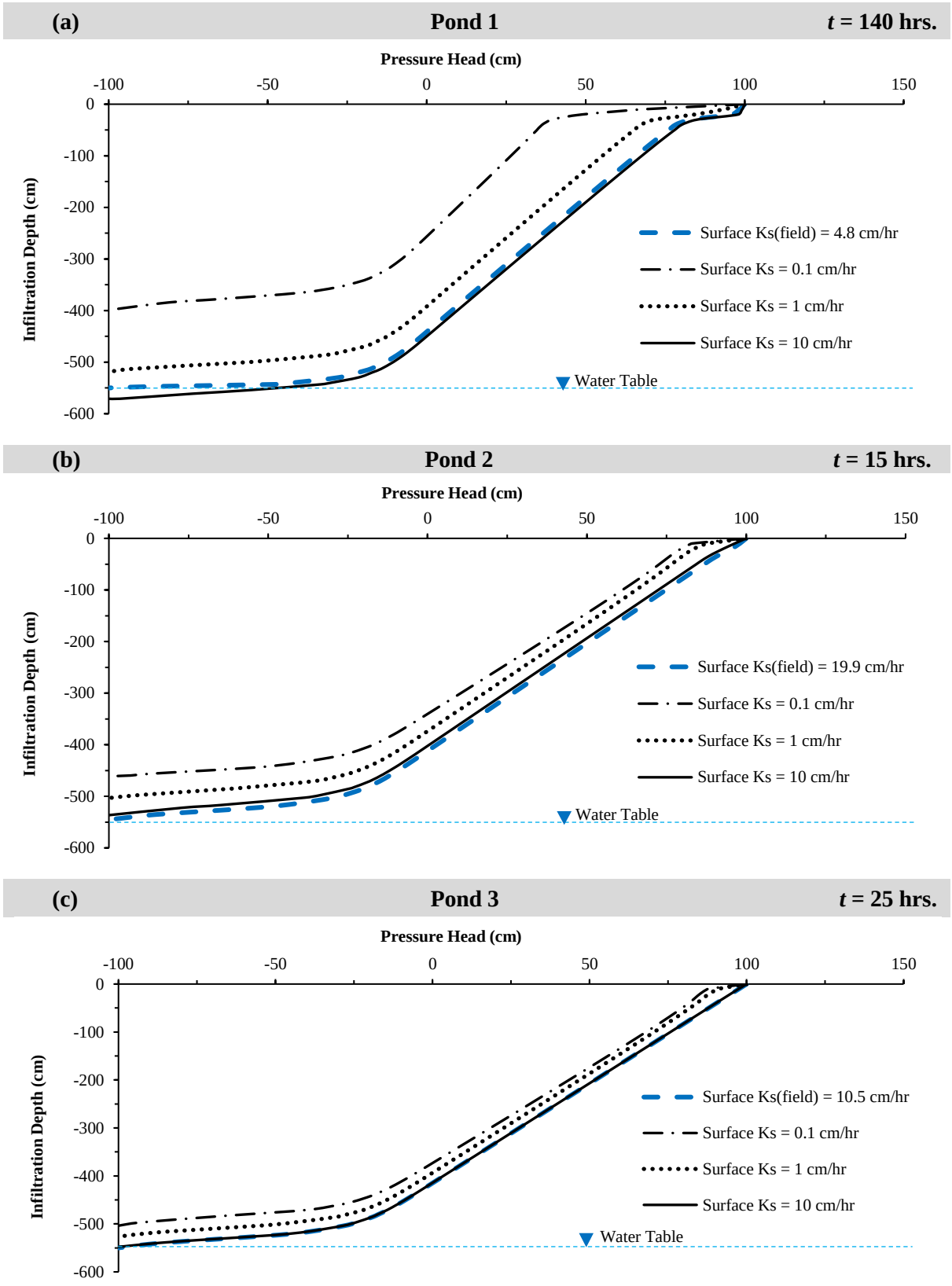

Figure 7-17: Modelled pressure head curves from varying hydraulic conductivities of 20 cm surface layer

By changing the hydraulic conductivity of the surface layer in Pond 1 from the in-situ determined 4.8 cm/hr to 0.1 cm/hr, the infiltration rate reduced from 3.9 cm/hr to 2.8 cm/hr, with the wetting front depth decreasing by 150 cm (i.e., from 550 cm to 400 cm) after a period of 140 hrs. A summary of the infiltration rates and wetting front depth associated with the various surface layers is presented in Table 7-8.

From the graphs Figure 7-17 it is evident that the varying hydraulic conductivities of the surface layer had the most influence on the infiltration rates in Pond 1 with distinct differences in the shape and depth of the wetting front in terms of pressure head. Pond 3 displayed the least sensitivity to the varying surface hydraulic conductivity values whilst Pond 2 displayed moderate variations. Surface layers of low permeability resulted in an initial reduction in infiltration rates at early times and consequently an increase in the time taken for the wetting front to reach the water table.

Findings from field infiltration investigations did not reveal an improvement in the measured infiltration rates when tests were conducted 20 cm below the pond surfaces. The surface soil was suspected to behave like a crust layer of low permeability caused by most likely a combination of runoff depositions and sieving surface creating a microstructure with three layers as exemplified in the time-step formations in Figure 7-18. Contrastingly, it was found that the infiltration rates determined from tests conducted directly on the pond surfaces were generally higher than those conducted 20 cm below the surface suggesting the existence of a layer of lower hydraulic conductivity at depths beyond 20 cm.

The most critical scenario for infiltration was represented by the 20 cm sandy clay surface crust layer with K_S = 0.10 cm/hr. The resultant increase in the time required for the wetting front to reach the water table was from 140 – 193 hrs (i.e., 53 hr increase) in Pond 1; from 15 – 18 hrs (i.e., 3 hr increase) in Pond 2; and from 25 – 27 (i.e., 2 hr increase) in Pond 3.

Table 7-8: Effect of varying hydraulic conductivity of 20 cm surface layer on infiltration

Pond	Simulation Duration (Hours)	Hydraulic Conductivity of 20 cm Surface Layer (cm/hr)	Wetting Front Depth Below Surface (cm)	HYDRUS 2-D Infiltration Rate (cm/hr)
Pond 1	140	**4.8**	**550**	**3.9**
		0.1	398	2.8
		1.0	519	3.7
		10.0	571	4.1
Pond 2	15	**19.9**	**550**	**36.7**
		0.1	461	30.7
		1.0	503	33.5
		10.0	536	35.7
*Pond 3	25	**10.5**	**550**	**22.0**
		0.1	503	20.1
		1.0	523	20.9
		10.0	548	21.9

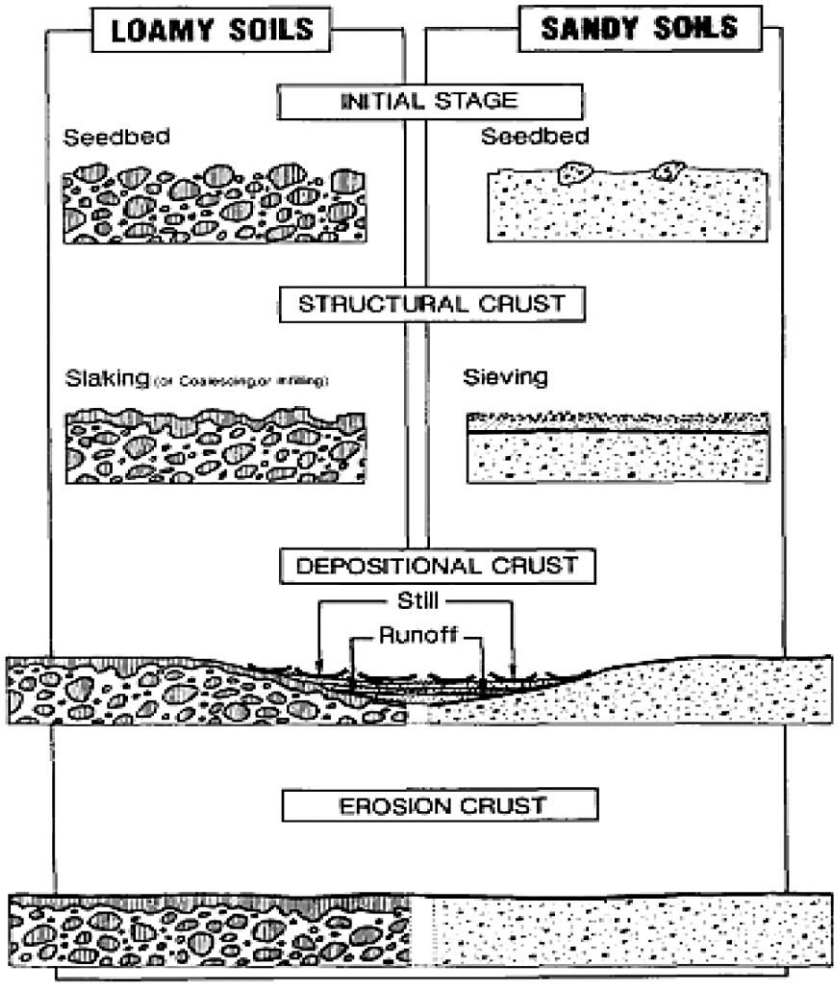

Figure 7-18: Time-step formation of crusts in loamy and sandy soils
Source: Valentin and Bresson (1992)

7.8 Potential Application

The three investigated ponds were selected based on their distribution across the Zeekoe catchment area. Each pond represented a group of ponds within a region of the catchment area. Findings from in-situ and laboratory infiltration experiments, as well as computer simulations, were in general agreement. Pond 1 was found to have the lowest infiltration potential, whilst Pond 2 and Pond 3 had similar infiltration rates with Pond 2 being moderately higher than Pond 3. In practice, the recharge times can be expected to be slightly lower than the results from the simulations.

A connection between the potential infiltration depth and the infiltration rate was recognised. Generally, regions with high potential infiltration depths were noted to possess good infiltration characteristics (Figure 7-19). Pond 1, with the lowest infiltration rate, is situated in a region that has the lowest potential infiltration depth. Correspondingly, Pond 2, with the highest infiltration rates, is in a region with the greatest potential infiltration depth.

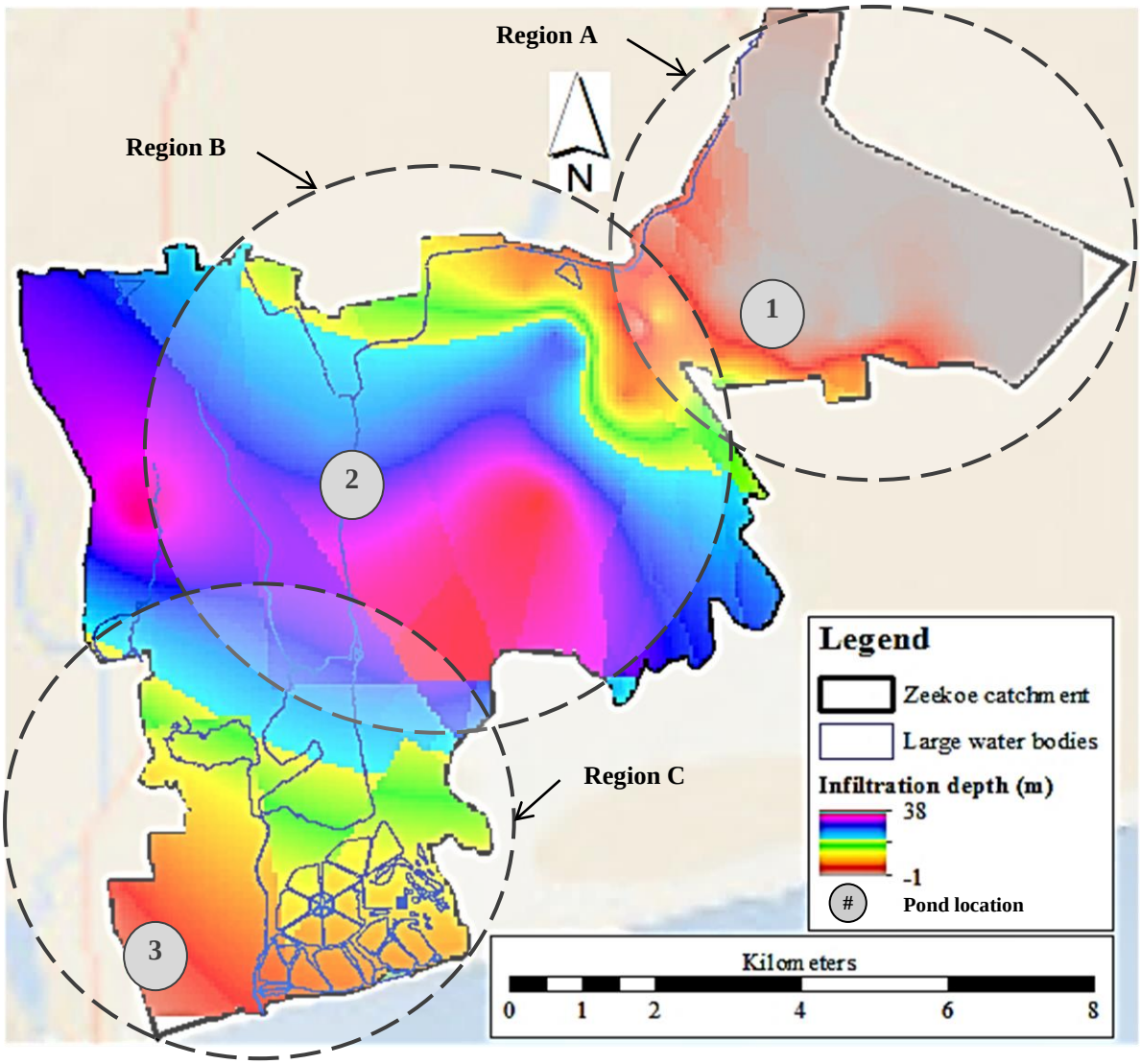

Figure 7-19: Potential infiltration depth across the Zeekoe catchment
Adapted from: Okedi (2017)

To further verify the appropriateness of adapting existing stormwater detention ponds in Region B as infiltration basins, results from an existing successful recharge facility in Atlantis (a township situated 50 km north of Cape Town) revealed recharge rates from 0.04 – 0.46 cm/hr in three of the facility's main infiltration ponds which can be classified as a low to very low Infiltration Class (Table 7-9). These infiltration rates were much lower than the average 20.6 cm/hr rate from in-situ DRI test data of Pond 2.

For good health and safety practices, prolonged stagnant water bodies in a public area need to be avoided. Unlike in Atlantis where the infiltration facility is barricaded, the investigated stormwater ponds are situated in residential areas – accessible to the public. It is thus essential for the ponds to have high infiltration rates to avoid ponding of water which can create a good breeding ground for mosquitoes and a drowning hazard for the public. With an average infiltration rate of 20.6 cm/hr (a 'very high' infiltration class according to Table 7-9) the ponds

located in Region B would be most suitable for artificial recharge. A simplified concept showing the recharge and recovery components of an artificial recharge strategy is shown in Figure 7-20.

Table 7-9: Classification of infiltration capacities
Adapted from: Subramanya (2008)

Infiltration Class	Infiltration Capacity (cm/hr)	Remarks
Very Low	<0.25	Highly clayey soil
Low	0.25 to 2.5	Shallow soils, Clay soils, Soils low in organic matter
Medium	1.25 to 2.5	Sandy Loam, Silt
High	>2.5	Deep sands, well drained aggregated soils.

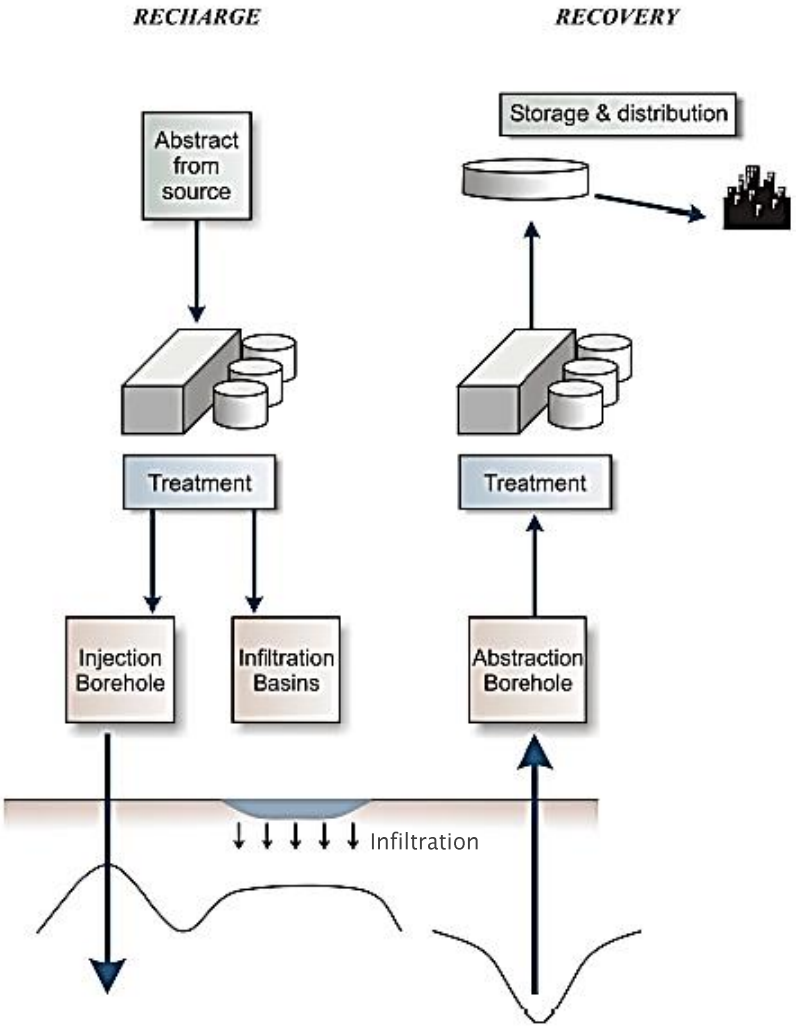

Figure 7-20: Artificial recharge strategy
Source: Murray *et al*. (2007)

8 Conclusions

8.1 Introduction

The general objective of this study was to evaluate the infiltration rate and hydraulic properties of three representative stormwater ponds across the Zeekoe catchment area to determine the feasibility of adapting these ponds to function as recharge basins that could potentially transfer detained stormwater runoff into the underlying aquifer for groundwater augmentation. To achieve this objective, a series of in-situ infiltration tests were carried out, laboratory permeability investigations and material classification experiments were conducted, and finally, numerical model simulations of water flow through the unsaturated zone were developed. The following sections present a summary of the main findings materializing from this study as well as recommendations for future research work.

8.2 Summary of Findings

The field Double-Ring Infiltration (DRI) investigation revealed high variability in infiltration rates, and consequently hydraulic conductivity values, across the area of a single pond. The surface area of the ponds ranged between 0.9 – 3.2 ha, however, within those comparatively small areas, variations between the evaluated hydraulic conductivity values were noted to fluctuate by more than a single order of magnitude. Because of this, ASTM (2009) has recommended for these results to be considered only as index values. Thus, conducting infiltration experiments at three different positions across each pond provided a better average representation of general soil properties and infiltration rates for reasonable design considerations.

Findings from field infiltration investigations did not reveal an improvement in the measured infiltration rates when tests were conducted 20 cm below the pond surfaces. The surface soil was suspected to behave like a crust layer of low permeability caused by a combination of runoff depositions. Contrastingly, it was found that the infiltration rates determined from tests conducted directly on the pond surfaces were generally higher than those conducted 20 cm below the surface suggesting the existence of a layer of lower hydraulic conductivity at depths beyond 20 cm.

The relationship between hydraulic conductivity values derived from the field infiltration experiments $K_{S_{field}}$, and those obtained from the laboratory permeability test results $K_{S_{lab}}$, was investigated. Results confirmed a significant difference and an absence of any direct link between the investigated $K_{S_{field}}$ and $K_{S_{lab}}$ values. The average difference between the laboratory method was subject to various disadvantages since the small sample area increased the possibility of large random errors, however, increased the likely repeatability because of the controlled environment.

The analysis of variance revealed significant statistical differences between the hydraulic conductivity values obtained from the field compared to those from laboratory test results. CV values from the in-situ infiltration experiments ranged between 0% and 138.6% whilst those from laboratory permeability tests ranged between 0% and 74.1%.

The hydraulic conductivity values obtained from the field and laboratory investigations were expected to diverge by some common factor. This factor would potentially aid in approximating in-situ infiltration potentials by testing soil samples in the laboratory as opposed to conducting rigorous and lengthy field tests. Plots of field hydraulic conductivity $K_{S_{field}}$ versus laboratory hydraulic conductivity $K_{S_{lab}}$ displayed no general correlation between the obtained values.

The hydraulic conductivity values estimated using Beyer's (1964) correlations significantly overestimated the measured field and lab hydraulic conductivity values by up to 100 times, thus deemed unreliable to estimate the hydraulic conductivity for soil types in this study area. Permeability estimates developed using grain-size correlations should thus be used with discretion to avoid significant miscalculations in designs.

A linear increase in the hydraulic conductivity values from the field and lab investigations was observed as the investigated soil porosity increased from 0.33 to 0.52. Overall, based on average values within each investigated stormwater pond, the hydraulic conductivity increased with increasing soil porosity.

No apparent relationship was noticed between the field hydraulic conductivity $K_{S_{field}}$ and the lab average flow rate q, however, a distinct positive linear correlation between the laboratory hydraulic conductivity $K_{S_{lab}}$ and the associated average flow rates q was recognised.

A comparison between the hydraulic conductivity values estimated by Rosetta-Lite K_{S_R}, and those determined from the field infiltration experiments $K_{S_{field}}$ revealed a general overestimation of the software's hydraulic conductivity by an average of 106%. Despite this difference in the hydraulic conductivities, both values were within the typical range for silty sands. To better replicate in-situ conditions for infiltration simulations, it was therefore considered a better representative to adapt actual physical properties and hydraulic conductivity values from field and laboratory classification experiments. Simulations proved to have the added benefit of adjusting required parameters to observe their respective effects on measured infiltration rates.

Pond 2, with the highest average infiltration rate (i.e., 20.6 cm/hr), corresponded to the lowest decay coefficient λ of 0.6. Pond 1, with the lowest average infiltration rate (i.e., 1.4 cm/hr), had the highest λ value of 1.9. Knowledge of the infiltration decay rate can aid in the prediction of gradual clogging for pond maintenance planning.

The time required for the wetting front movement from the pond surfaces to the water table was determined to be 140 hours in Pond 1, 15 hours in Pond 2, and 25 hours in Pond 3. The

corresponding infiltration rates were 3.9 cm/hr for Pond 1, 36.7 cm/hr for Pond 2, and 22.0 cm/hr for Pond 3. For an actual test pond, the infiltration rates would be expected to be slower, and recharge times would be greater because the HYDRUS 2-D model did not consider compaction, consolidation, or variations in the deeper subsurface geology.

When comparing the steady-infiltration rates obtained from this study (i.e., between 1.4 – 20.6 cm/hr) to those from the Atlantis recharge facility, it was apparent that the soil characteristics of the stormwater ponds in the Zeekoe catchment were suitable for the ponds to be adapted as infiltration basins for artificial recharge. Instead of allowing detained stormwater to flow through the pond outlet structures, the outlets could be controlled to promote infiltration.

A connection between the potential infiltration depth and the infiltration rate was recognised. Regions with high potential infiltration depths were noted to possess good infiltration characteristics. Ponds located within the central region of the Zeekoe catchment were found to have the greatest potential infiltration depth and the highest infiltration rate – represented by Pond 2 with an average infiltration rate of 20.6 cm/hr. Based on field infiltration data, laboratory data, and model simulations, ponds in the central section of the catchment area were considered suitable for artificial recharge. Although recharge times can be expected to be greater than the results from the simulations which had limited information about the subsurface geology, the durations should be comparable to ponds in the surrounding area.

8.3 Recommendations for Further Research

The following are recommendations for future research:

1) Implementation of a pilot project adapting the representative pond of Region B (Pond 2) located in the central area of the Zeekoe catchment. Instead of the pond being used as a detention pond, the outlet can be controlled to promote infiltration and groundwater recharge. Modification of the surface layer may be done, however, is not necessary because of preferential hydraulic properties which were determined at the site.

2) Further testing of soil in the study area to develop reliable empirical correlations.

3) A study on the effects of surface vegetation in a recharge basin.

4) A more extensive survey of the subsurface geology and soil hydraulic properties at greater depths beyond 40 cm would aid in refining the HYRDUS software models and assessing the subsurface conditions that would impede the flow of water.

5) Additional measured soil information such as soil-water retention points could cause Rosetta-Lite software to produce output data that better represents the vertical variability of soil hydraulic characteristics.

List of References

1. Adelana, S.M.A. and Xu, Y. (2006). Contamination and protection of the Cape Flats Aquifer, South Africa. Department of Earth Sciences, University of the Western Cape, Bellville, South Africa.
2. Adelana, S.M.A., and Xu, Y. (2008). Impacts of land-use changes on a shallow coastal aquifer, South-Western Cape, South Africa. Proc. XXXVI Congress of the International Association of Hydrogeologists (IAH), 28 October - 2 November 2008, Toyama, Japan.
3. Adelana, S.M.A., Xu, Y., and Vrbka, P. (2010). A conceptual model for the development and management of the Cape Flats, South Africa. Water SA, 36(4).
4. Amoozegar, A., and Wilson, G.V., (1999): Methods for measuring hydraulic conductivity and drainable porosity. p. 1149-1205. In R. W. Skaggs and J. van Schilfgaarde (ed.) Agricultural Drainage. Monograph No. 38, ASA-CSSA-SSSA, Madison, WI.
5. Armitage, N., Vice, M., Fisher-Jeffes, L., Winter, K., Spiegel, A., & Dunstan, J. (2013). South African Guidelines for Sustainable Drainage Systems. ISBN: ISBN 978-1-4312-0413-7.
6. Åstebøl, S. O., Hvitved-Jacobsen, T., & Simonsen, Ø. (2004). Sustainable stormwater management at Fornebu - From an airport to an industrial and residential area of the city of Oslo, Norway. Science of the Total Environment, 334-335, 239–249. doi: 10.1016/j.scitotenv.2004.04.042. ISBN: 0048-9697. ISSN:00489697.
7. ASTM (2009). Standard Test Method for Infiltration Rate of Soils in Field Using Double-Ring Infiltrometer. ASTM Standard Test Method. D3385-09. p.pp. 1–7.
8. Begum, S., Rasul, M. G., & Brown, R. J. (2008). Stormwater treatment and reuse techniques: A review. 2nd International Conference on Waste Management, Water Pollution, Air Pollution, Indoor Climate, 144–149. ISBN: 9789604740178.
9. Beyer, W. (1964) Zur Bestimmung der Wasserdurchlassigkeit von Kieson und Sanduen ausderKornverteilung. Wasserwirtsch.-Wassertech. 14. 165–169. (In German)
10. Bickerton, I.B., (1982). Estuaries of the Cape: Part II: Synopsis of Available Information on Individual Systems. Report No. 15: Zeekoe (CSW5). CSIR Research Report 414. Stellenbosch, South Africa.
11. Bouwer, H. (1969). Infiltration of water into nonuniform soil. Journal of the Irrigation and Drainage Division, 95(4), pp.451-462.

12. Bouwer, H. (2002). Artificial recharge of groundwater: Hydrogeology and engineering. Hydrogeology Journal. 10 (1). p.pp. 121–142.
13. Braja M.D. (2008). Advanced Soil Mechanics. 3rd ed. Taylor & Francis, 270 Madison Ave, New York. ISBN 0-203-93584-5.
14. Braja M.D. (2013). Principles of Geotechnical Engineering. 7th ed. Cengage Learning 200 First Stamford Place, Suite 400, Stamford, CT 06902, USA. ISBN: 9788131518793, 8131518795.
15. Braja, M.D. (2002). Soil Mechanics Laboratory Manual. 6th ed. New York Oxford. Oxford University Press.
16. Brown, C., & Dallas, H. (1995). Eerste River, Western Cape: Situation assessment of the riverine ecosystem. Final report, June 1995. Stellenbosch.
17. Brummer, T.B. (1981). A Development Plan for the Zeekoevlei Complex. M.Sc. Thesis. Town and Regional Planning. University of Stellenbosch. 72pp.
18. Bugan, R. D. H., Jovanovic, N., Israel, S., Tredoux, G., Genthe, B., Steyn, M., Allpass, D., Bishop, R., & Marinus, V. (2016). Four decades of water recycling in Atlantis (Western Cape, South Africa): Past, present, and future. Water SA, 42(4), 577–594. ISSN:03784738.
19. Burman, J. (1962). Safe to the sea. Cape Town. Human & Rousseau.167pp.
20. Burns, M. J., Fletcher, T. D., Walsh, C. J., Ladson, A. R., & Hatt, B. E. (2012). Hydrologic shortcomings of conventional urban stormwater management and opportunities for reform. Landscape and Urban Planning, 105(3), 230–240. doi: 10.1016/j.landurbplan.2011.12.012. ISBN: 0169-2046. ISSN:01692046. Retrieved from http://dx.doi.org/10.1016/j.landurbplan.2011.12.012.
21. Campbell. C. (2016). Water Potential: The Science Behind the Measurement (Part II). Environmental Biophysics. http://www.environmentalbiophysics.org/water-matric-potential-measurement-2/. Accessed on 29.09.2018.
22. Campbell. C. (2016). Water Potential: The Science Behind the Measurement (Part II). Environmental Biophysics. http://www.environmentalbiophysics.org/water-matric-potential-measurement-2/. Accessed on 29.09.2018.
23. Chow, V.T., Maidment, D. R., Mays, L.W. (1988). Applied Hydrology. McGraw-Hill International Editions. Civil Engineering Series. 572 pp.
24. City of Cape Town. Weekly Water Dashboard. (2021). https://resource.capetown.gov.za/documentcentre/Documents/City%20research%20reports%20and%20review/damlevels.pdf. Accessed on 19.08.2021.

25. Clar, M. L., Barfield, B. J., & O'Connor, T. P. (2004). Stormwater Best Management Practice Design Guide (Vol. 3: Basin B).
26. CoCT. (2012). City of Cape Town GIS Database: General Land use Layer Shapefile. Strategic Information Department. City of Cape Town, South Africa. Cape Town, South Africa.
27. Coombes, P. & Barry, M.. (2007). The effect of selection of time steps and average assumptions on the continuous simulation of rainwater harvesting strategies. Water Science and Technology, 55(4), 125–133.
28. Conrad, J.E. (2014). Groundwater Specialist Study – Cape Town International Airport Runway Re-alignment and Associated Infrastructure Project. GEOSS Report No: 2014/06-10. Stellenbosch, South Africa.
29. Deletic, A., Mccarthy, D., Chandrasena, G., Li, Y., Hatt, B., & Payne, E. (2014). Biofilters and wetlands for stormwater treatment and harvesting. ISBN: 9781921912221.
30. Department of Water Affairs (DWA). (2010). Strategy and Guideline Development for National Groundwater Planning Requirements. The Atlantis Water Resource Management Scheme: 30 years of Artificial Groundwater Recharge. PRSA 000/00/11609/10 Activity 17 (AR5.1), dated August 2010.
31. Department of Water Affairs (DWA). (2010). The Atlantis Water Resource Management Scheme: 30 years of Artificial Groundwater Recharge. Department of Water Affairs and Forestry. Pretoria, South Africa.
32. Department of Water Affairs (DWA). (2017) Groundwater Dictionary Index. www.dwa.gov.za/Groundwater/Groundwater_Dictionary/index.html?introduction_paleo_chanel.htm. Accessed 12.11.2017.
33. Department of Water Affairs and Forestry (DWAF). (2004). Overview of the South African Water Sector. National water resource strategy (Vol. 1).
34. Department of Water Affairs and Forestry. (2005). Groundwater Resource Assessment Phase II. Methodology for Groundwater Quantification. Project 1, Report 1B & 1C (draft).
35. Dillon P. (2005). Draft Code of Practice for Aquifer Storage Recovery. CSIRO Land and Water, Australia.
36. Dillon P. (2005). Future Management of Aquifer Recharge. Hydrogeology Journal, 13 (1): 313316.
37. Dillon, P., Pavelic, P., Page, D., Beringen, H., & Ward, J. (2009). Managed aquifer recharge: An Introduction. ISBN: 9781921107719.

38. Dixon, R.M., (1975): Design and use of closed-top infiltrometers. Soil Sci. Soc. Am. Proceedings, 39, 755-763.
39. DWS. (2014). WC WSS Reconciliation Strategy Status Report October 2013. Cape Town, South Africa. Retrieved from https://www.dwa.gov.za/Projects/RS_WC_WSS/Docs/WCWSS Status Report Oct2014 Final.pdf.
40. DWS. (2015). Department of Water and Sanitation - Hydrological Services - surface water data monitoring. Pretoria, South Africa.
41. Fatehnia, M. (2015). Automated Method for Determining Infiltration Rate in Soils Automated Method for Determining Infiltration Rate in Soils. PhD. Dissertation. Florida State University. Department of Civil and Environmental Engineering.
42. Fetter, C.W. (1988). Applied hydrogeology. 4th Ed. Waveland Press.
43. Fisher-Jeffes, L., Carden, K., Armitage, N., & Winter, K. (2017). Stormwater harvesting: Improving water security in South Africa's urban areas. South African Journal of Science, 113(1–2), 2–5. doi:10.17159/sajs.2017/20160153. ISSN:19967489.
44. Fletcher, T. D., Mitchell, V., Deletic, A., & Seven, A. (2007). Is stormwater harvesting beneficial to urban waterway environmental flows? Water Science and Technology, 55(4), 265–272.
45. Geology.com (2017) Geological terms beginning with "F". https://geology.com/dictionary/glossary-f.shtml. Accessed on 16.06.2017.
46. GEOSS, (2013). Geohydrological assessment of a proposed Belhar residential development. GEOSS Report Number: 2013/07-18. GEOSS - Geohydrological and Spatial Solutions International (Pty) Ltd. Stellenbosch, South Africa.
47. Gerber, A. (1976). An Investigation of the Hydraulic Properties of the Ground Water Resources in the Cape Flats (in Afrikaans). M.Sc. Thesis (unpubl.) Univ. Orange Free State. Bloemfontein, South Africa.
48. Gerber, A. (1981). A digital model of groundwater flow in the Cape Flats. CSIR Contract Report C WAT 46. CSIR, Pretoria, South Africa.
49. Gleick, P. H. (1998). Water in Crisis: Paths to Sustainable Water Use. Ecological Applications, 8(3), 571–579.
50. Green, W.H., and Ampt, G.A., (1911): Studies on soil physics. J. Agric. Sci., 4(1): 1-2

51. Hancock, G. S., Holley, J. W., & Chambers, R. M. (2010). A Field-Based Evaluation of Wet Retention Ponds: How Effective Are Ponds at Water Quantity Control? Journal of the American Water Resources Association, 46(6), 1145–1158. doi:10.1111/j.1752-1688.2010.00481.x. ISBN: 1093-474X. ISSN:1093474X.
52. Hartnady, C.J.H., and Rogers, J. (1990): The scenery and geology of the Cape Peninsular. Guidebook Geocongress '90 Geological Society South Africa, M 1: 1-67.
53. Hatt, B., Deletic, A., & Fletcher, T. (2006). Integrated treatment and recycling of stormwater: a review of Australian practice. Journal of Environmental Management, 79(1), 102–13. doi: 10.1016/j.jenvman.2005.06.003. ISSN:0301-4797.
54. Hawker, D. (2015). SA water crisis map: What you need to know. eNCA. Retrieved February 8, 2016, from https://www.enca.com/south-africa/sa-water-crisis-map-what-you-need-know.
55. Hay, R., McGibbon, D., Botha, F. and Riemann, K. (2015). Cape Flats Aquifer and False Bay – Opportunities to Change. 79th IMESA Conference. Cape Town, South Africa.
56. Hedden, S., & Cilliers, J. (2014). Parched prospects. Institute of Security Studies, (September), 16.
57. Henzen, M. (1973). The reclamation, storage, and abstraction of purified sewage effluents in the Cape Peninsula (in Afrikaans). M.Sc. Thesis, University of the Orange Free State, Bloemfontein. South Africa.
58. Heydorn, A.E.F. and Grindley, J.R. (1982). Estuaries of the Cape. Part II: Synopsis of Available Information on Individual Systems. Report No. 15: Zeekoe (CSW 5). National Research Institute for Oceanology. Council for Scientific and Industrial Research. Stellenbosch, South Africa.
59. Horton, R.E. (1933). The role of infiltration in the hydrologic cycle. Trans. Am. Geophys. Un., 4th Ann. Mtg. 446–460.
60. Hu, W., Saho, M.A., Wang, Q. J., Fan, J., Reichardt, K. (2008). Spatial Variability of Soil Hydraulic Properties on a Steep Slope in the Loess Plateau of China. Sci. Agric. (Piracicaba, Braz.), v.65, n.3, p.268-276.
61. Hyman, A. (2018). 505 gunshots in nine days in the heart of Cape Town gangland. Times Live. https://www.timeslive.co.za/amp/news/south-africa/2018-04-12-505-gunshots-in-nine-days-in-heart-of-cape-town-gangland/. Accessed 23.06.2018.

62. Lappala, E.G. (1981). Modelling of water and solute transport under variably saturated conditions State of the art: Modelling and Low-Level Waste Management--An Interagency Workshop, Denver, Colorado, December 1980, Proceedings, p. 81-137.
63. Mahed, G. (2018). Explainer: what there is to know about South Africa's aquifers. The Conversation. https://theconversation.com/explainer-what-there-is-to-know-about-south-africas-aquifers-102660. Accessed on 09th January 2022.
64. Matula, S. and Kozáková, H. (1997). A simple pressure infiltrometer for determination of soil hydraulic properties by in situ infiltration measurements. Rostlinna Vyroba-UZPI (Czech Republic). McArdle, P., Gleesen, J., Hammond, T., Heslop, E., Holden, R., & Kuczera, G. (2011). Centralised urban stormwater harvesting for potable reuse. Water Science and Technology, 63(1), 16–24.
65. Mitchell, V. G., Deletic, A., Fletcher, T. D., Hatt, B. E., & McCarthy, D. T. (2007). Achieving multiples benefits from stormwater harvesting. Water Science and Technology, 55(4), 135–144.
66. Moriasi, D. N., Arnold, J. G., Liew, M. W. Van, Bingner, R. L., Harmel, R. D., & Veith, T. L. (2007). Model Evaluation Guidelines for Systematic Quantification of Accuracy in WatershedMoriasi, D.N., Arnold, J.G., Liew, M.W. Van, Bingner, R.L., Harmel, R.D. & Veith, T.L. 2007. Model Evaluation Guidelines for Systematic Quantification of Accuracy in Watersh. American Society of Agricultural and Biological Engineers, St. Joseph, Michigan, 50(3), 885–900. doi:10.13031/2013.23153) @. Retrieved from www.asabe.org.
67. Muller, M., Schreiner, B., Smith, L., Koppen, B. Van, Sally, H., Aliber, M., Cousins, B., Tapela, B., Merwe-botha, M. Van Der, Karar, E., & Pietersen, K. (2009). Water security in South Africa. Development Planning Division Working Paper Series, 12(12), 40.
68. Murray, R., Tredoux G., Ravenscroft, P., Botha, F. (2007). Artificial Recharge Strategy. Version 1.3. Strategy Development: A National Approach to Implement Artificial Recharge as Part of Water Resource Planning. Department of Water Affairs and Forestry, South Africa.
69. Nascimento, N. O., Ellis, J. B., Baptista, M. B., & Deutsch, J.-C. (1999). Using detention basins: operational experience and lessons. Urban Water, 1(1999), 113–124. doi:10.1016/S1462-0758(00)00009-1. ISSN:14620758.
70. Ngoepe, K. (2015). 5 provinces declared drought disaster areas. News24. Retrieved February 8, 2016, from http://www.news24.com/SouthAfrica/News/5-provinces-declared-drought-disaster-areas-20151113.

71. Noemdoe, S., Jonker, L., & Swatuk, L. A. (2006). Perceptions of water scarcity: The case of Genadendal and outstations. Physics and Chemistry of the Earth, 31(15-16), 771–778. doi: 10.1016/j.pce.2006.08.003. ISBN: 1474-7065. ISSN:14747065.
72. Okedi, J. (2017). Water Research Commission Project K5/2526 Report – Viability of stormwater ponds in the Zeekoe catchment as water resources for Cape Town, South Africa University of Cape Town.
73. Okedi, J. (2019). The prospects for stormwater harvesting in Cape Town, South Africa using the Zeekoe Catchment as a case study. Engineering and the Built Environment, Department of Civil Engineering. http://hdl.handle.net/11427/30453.
74. Oki, T., & Kanae, S. (2006). Global hydrological cycles and world water resources. Science (New York, N.Y.), 313(5790), 1068–1072. doi:10.1126/science.1128845. ISBN: 0036-8075. ISSN:0036-8075.
75. Parsons, RP. (2000). Zeekoevlei and Rondevlei restoration study. Geohydrological specialist report. Report 060/SWA T -F 1 prepared for the south peninsular municipality and southern waters ecological research and consulting. Parsons and associates.
76. Philp, M., Mcmahon, J., Heyenga, S., Marinoni, O., Jenkins, G., Maheepala, S., & Greenway, M. (2008). Review of Stormwater Harvesting Practices Urban Water Security Research Alliance Technical Report No. 9, (9). ISSN:1836-5566.Radcliffe, D. and Šimůnek, J. (2010). Soil Physics with HYDRUS: Modelling and Applications. CRC Press. Taylor and Francis Group. 6000 Broken Sound Parkway NW, Suite 300. Boca Raton, FL 33487-2742.
77. Pitman, W. V. (2011). Overview of water resource assessment in South Africa: Current state and future challenges. Water SA, 37(5), 659–664. doi:10.4314/wsa.v37i5.3. ISBN: 0378-4738. ISSN:18167950.
78. Quayle, T. (2012). Recycling wastewater to bolster ground water supply: the story of Atlantis, South Africa. Cape Town, South Africa.
79. Radcliffe, D. and Šimůnek, J. (2010). Soil Physics with HYDRUS: Modelling and Applications. CRC Press. Taylor and Francis Group. 6000 Broken Sound Parkway NW, Suite 300. Boca Raton, FL 33487-2742
80. Reynolds W.D., and Elrick D.E. (1985): Measurement of field-saturated hydraulic conductivity, sorptivity and the conductivity-pressure head relationship using the “Guelph Permeameter,” paper presented at Conference on Characterization and Monitoring of the Vadose (Unsaturated) Zone, Soil Sci., 140, 292–302.

81. Rezende, O. M., Carneiro, P. R., & Miguez, M. G. (2011). Sustainable Stormwater Management: use of multifunctional landscapes in urban drainage for flood control. 12nd International Conference on Urban Drainage, (September), 11–16.
82. Richman, M.B., Leslie, L.M. (2018). The 2015-2017 Cape Town Drought: Attribution and Prediction Using Machine Learning. Procedia Computer Science, 140, 248-257. https://doi.org/10.1016/j.procs.2018.10.323.
83. Rockström, J., Falkenmark, M., Allan, T., Folke, C., Gordon, L., Jägerskog, A., Kummu, M., Lannerstad, M., Meybeck, M., Molden, D., Postel, S., Savenije, H., Svedin, U., Turton, A., & Varis, O. (2014). The unfolding water drama in the Anthropocene: towards a resilience-based perspective on water for global sustainability. Ecohydrology, 7, 1249–1261. doi:10.1002/eco.1562. ISSN:19360584. Retrieved from http://doi.wiley.com/10.1002/eco.1562.
84. Rohrer, A. (2014). Cape Town's Ponds. B.Sc. Dissertation. University of Cape Town. South Africa.
85. Rohrer, A. (2017). The viability of using the stormwater ponds on the Diep River in the Constantia Valley for stormwater harvesting. Thesis. University of Cape Town, Faculty of Engineering & the Built Environment, Urban Water Management. http://hdl.handle.net/11427/24918.
86. Schaap, M.G., F.J. Leij, and M. Th. van Genuchten. (2001). Rosetta: a computer program for estimating soil hydraulic parameters with hierarchical pedotransfer functions. Journal of Hydrology, 251:163-176.
87. Schreurs, J. (2001) Northern Huqf Geology. https://home.kpn.nl/lilian_jan_schreurs/oman. Accessed on 06 June 2018.
88. Schulze R.E., Maharaj M., Warburton M.L., Gers C.J., Horan M.J.C., Kunz R.P., and Clark D.J. (2008). South African Atlas of Climatology and Agrohydrology. Water Research Commission 1489/1/08.
89. Shamsudin, S., Dan, S., Aris, A., & Yusop, Z. (2014). Optimum combination of pond volume and outlet capacity of a stormwater detention pond using particle swarm optimization. Urban Water Journal, 11(2), 127 – 136. doi:10.1080/1573062X.2013.768680. ISSN:1573-062X. Retrieved from http://dx.doi.org/10.1080/1573062X.2013.768680.

90. Shan, H.(n.d.). Hydraulic Conductivity Tests for Soils. Presentation. Department of Civil Engineering. National Chiao Tung University. Retrieved February 5, 2021, from https://docplayer.net/20940841-Hydraulic-conductivity-tests-for-soils-hsin-yu-shan-dept-of-civil-engineering-national-chiao-tung-university.html.
91. Singh, K. (2015). Water crisis in SA reaches a breaking point. News24. Retrieved February 8, 2016, from http://www.news24.com/SouthAfrica/News/Water-crisis-in-SA-reaches-breaking-point-20151029.
92. Steduto, P., Faurès, J., Hoogeveen, J., Winpenny, J., & Burke, J. (2012). Coping with water scarcity: An action framework for agriculture and food security. ISBN: 978-92-5-107304-9. ISSN:1020-1203.
93. Subramanya, K. (2008). Engineering Hydrology. 3rd ed. Tata McGraw-Hill Publishing Company Limited. 7 West Patel Nagar, New Delhi.
94. Swarzenski, P.W., Martin, J.B. & Cable J.C. (2001). Submarine groundwater discharge in Upper Indian River Lagoon, Florida. U.S. Geological Survey Karst Interest Group Proceedings, Water-Resources Investigations. Report 01-4011. pg 194 - 197.
95. Tadross, M.; Johnson, P. (2012). Climate Change Projections for Cape Town: Adding value through downscaling. Sub-Saharan African Cities: A five-city Network to Pioneer Climate. Adaptation through Participatory Research & Local Action. ICLEI - Local Government for Sustainability – Africa. ISBN: 978-0-9921794-8-9.
96. Teague. N.F. (2010). Near-surface infiltration measurements and the implications for artificial recharge. Master thesis. San Diego State University. Department of Civil and Environmental Engineering. San Diego. California.
97. Theron, J.N.; Gresse, P.G.; Siegfried, H.P.; and Rogers, J. (1992). The geology of the Cape Town area. Explanation on Sheet 3318, Geological Survey, South Africa. 140 pp.
98. Tredoux, G.; Ross, R.; Gerber, A. (1980) The potential of the Cape Flats Aquifer for the Storage and Abstraction of Reclaimed Effluents (South Africa). Presented at the International Symposium on Artificial Groundwater Recharge, Dortmund, Germany, 14 to 18 May 1979. Z. dt. Geol. Ges.
99. UNESCO. (1978). World Water Balance and Water Resources of the Earth. Studies and Reports in Hydrology. Paris, France.
100. Valentin, C., Bresson, L.M. (1992). Morphology, genesis, and classification of surface crusts in loamy and sandy soils. Geoderma. 55: 225–245.

101. Vandoolaeghe, M.AC. (1984): Exploration of Coastal Primary Aquifers in the South-Western Cape. Division of Geohydrology. Department of Water Affairs. Cape Town.

102. Vandoolaeghe, M.AC. (1989). The Cape Flats ground water development pilot abstraction scheme; technical report GH3655, Directorate of geohydrology, DWAF.

103. Walsh, C. J., Fletcher, T. D., & Burns, M. J. (2012). Urban Stormwater Runoff: A New Class of Environmental Flow Problem. PLoS ONE, 7(9). doi: 10.1371/journal.pone.0045814. ISBN: 19326203. ISSN:19326203.

104. Windfinder (2017). Wind and Weather Statistics. Cape Town Airport. https://www.windfinder.com/windstatistics/cape_town_airport. Accessed on 26. 10. 2017

105. Wong, T., Breen, P., & Somes, N. (1999). Ponds vs wetlands–performance considerations in stormwater quality management. … Ecosystem Management, 1–10. Retrieved from http://www.northinlet.sc.edu/training/media/resources/Ponds V Wetlands SW Quality Mgmt.pdf

106. Woods-Ballard, B., Kellagher, R., Martin, P., Jefferies, C., Bray, R., & Shaffer, P. (2007). The SUDS manual (C697). doi:London C697. ISBN: 9780860176978. Retrieved from http://hdl.handle.net/10373/994

107. World Weather Online (2017). Historical Average Weather. https://www.worldweatheronline.com/cape-town-weather-averages/western-cape/za.aspx. Accessed on 15. 10. 2017.

108. Wright, A. & Conrad, J.E. 1995: The cape flats aquifer current status; Report no. 11/95, Groundwater program.

109. Youngs, E.G. 1991. Infiltration measurements – a review. Hydrological Processes 5: 309– 320amme, Watertek, CSIR

110. Ziervogel, G., & Smit, W. (2009). Learning to swim: Strengthening flooding governance in the City of Cape Town. In 2009 Amsterdam Conference on the Human Dimensions of Global Environmental Change “Earth System Governance: People, Places and the Planet”, 2-4 December 2009, Amsterdam (pp. 1–16). Amsterdam.